US Army Corps
of Engineers
Philadelphia District

Philadelphia District
North Atlantic Division

Delaware River Main Channel Deepening Project

Appendix B

Modeling Efforts / Hydraulic Analysis

May 1996

DELAWARE RIVER MAIN CHANNEL DEEPENING PROJECT

DESIGN MEMORANDUM

APPENDIX B

MODELLING EFFORTS/HYDRAULIC STUDIES

U.S. Army Corps of Engineers, Philadelphia District

May 1996

APPENDIX B

TABLE OF CONTENTS

ITEM	TITLE	SECTION
1. (A)	Navigation (Ship Simulation) Study.	B-1A
(B)	Memorandum for Record, 15 July 1994, "Feasibility of Asymmetric Channel Deepening of the Delaware River Navigation Channel."	B-1B
(C)	A 2-D Hydrodynamic Model of Delaware Bay.	B-1C
2.	Quantity Computations/Utility Relocations	B-2
3.	Shoaling and Maintenance Dredging.	B-3
4.	Shoreline Erosion Investigation.	B-4
5.(A)	Fine Scale Modeling of Potential Impacts of Four Proposed Dredged Material Disposal Sites (Sedimentation and Shellfish Survivability Studies).	B-5A
5.(B)	Empirical Assessment of Delaware Bay (Sand) Stockpiles.	B-5B

Delaware River Deepening
Hydraulics Appendices

APPENDIX B-5A

FINE SCALE MODELING OF POTENTIAL IMPACTS OF FOUR PROPOSED DREDGED MATERIAL DISPOSAL SITES (SEDIMENTATION AND SHELLFISH SURVIVABILITY STUDIES).

591

FINE SCALE MODELING OF POTENTIAL IMPACTS OF FOUR PROPOSED DREDGED MATERIAL DISPOSAL SITES
Sedimentation and Shellfish Survivability Studies

Final Report

30 November 1995

by

Offshore & Coastal Technologies, Inc. - East Coast
500 Spencer Road
Avondale, PA 19311
Tel: (610) 268-0410

for

U.S. ARMY CORPS OF ENGINEERS
Philadelphia District
Wanamaker Building
100 Penn Square East
Philadelphia, PA 19107-3390

593

TABLE OF CONTENTS

1. INTRODUCTION 1

2. SEDIMENT TRANSPORT/OYSTER IMPACT INVESTIGATIONS 1

2.1. Model Development/Description 1

2.1.1 Current, Wave and Sediment Transport Modeling . 1

2.1.2 Shellfish Survivability Modeling 5

3. SELECTION OF MODELING SCENARIOS 16

4. MODEL RESULTS 16

4.1 Egg Island Point, NJ, Wetland Restoration Site 16

4.2 Kelly Island, DE, Wetland Restoration Site 20

4.3 LC-5 and MS-19 Stockpile Sites 26

5. CONCLUSIONS AND RECOMMENDATIONS 29

Fine Scale Modeling of Potential Impacts of
Four Proposed Dredged Material Disposal Sites
on the Delaware Bay
30 November 1995

1. INTRODUCTION

The Philadelphia District is considering placement of dredged material at several sites in and along the Delaware Bay as part of its channel deepening study. The sites under consideration include two shoreline restoration sites, Egg Island Point, NJ, and Kelly Island, DE. Two nearshore stockpile sites are also being considered: Slaughter Beach, DE (site MS-19) and Lewes, DE (site LC-5). In evaluating the placement sites, it is necessary to examine the rates and pathways of sediment transport that may take place as a result of the placement. This report presents a fine scale numerical modeling study performed to examine potential sediment transport and a prototype data collection effort utilized to validate aspects of the numerical modeling.

2. SEDIMENT TRANSPORT/OYSTER IMPACT INVESTIGATIONS

2.1. Model Development/Description

In order to determine sediment transport characteristics at the four disposal sites, numerical models were configured to determine the characteristics of waves and currents which were then used to estimate rates and pathways of sediment transport.

2.1.1 Current, Wave and Sediment Transport Modeling

Currents were simulated using a two-dimensional flow model that was driven by boundary conditions at the ocean boundary of the Delaware Bay. Normal astronomical tide conditions and historical severe storm conditions (15 northeasters and 15 hurricanes) were simulated after calibrating the computer model to prototype data described later in this report. The results of the 10 most severe current-generating storms were retained for analysis of potential sediment transport. The effects of astronomical tide, wind-driven storm surge, bottom stresses due to shallow water bathymetry, and land boundaries were included in the model. Numerical modeling of currents was performed on a finite difference grid that covered the entire bay

595

on a 0.25 minute resolution in both latitude and longitude.

Fine-scale wave modeling was performed using a directional spectral steady state model, STWAVE. Boundary conditions were developed from a larger-scale hindcast of normal and storm conditions of the Delaware Bay. Six years of normal-condition waves (1987-1993) and historical severe storm waves were developed at the boundary of three fine-scale finite difference grids covering the Egg Island Point area, the Kelly Island area, and the stockpile site area, respectively. The fine-scale grids had a resolution of 0.25 minutes in both latitude and longitude. The locations of the study grids are illustrated in Figure 1.

Wave and current computer model runs were performed to produce a basis for determining the directions (pathways) and rates of sediment transport in the project areas.

Currents generated by tides and storm conditions create a shear stress along the seafloor. In turn, the sediment begins to move when the stress is sufficient. Waves tend to mobilize and transport sediment in a variety of ways. Wave-induced bottom velocities tend to transport bottom material in the onshore-offshore direction, creating an active beach profile in areas shallower than the depth of closure (otherwise known as the seaward limit of sediment transport). Second, waves also generate a residual current in the direction of wave propagation. This current will transport sediment if the associated bottom shear stress is of sufficient magnitude. Third, waves generate a longshore current and associated longshore transport of sediment along the shoreline.

Sediment transport pathways and rates due to currents (wave mass transport plus tidal/storm currents) were calculated by evaluating the associated bottom shear stress against the required shear stress to initiate sediment motion. Once initiation of motion was determined to be possible, the current speed was again evaluated against that needed to maintain transport and that needed to cause deposition. Incipient motion criteria were determined using a Shields curve as presented by Graf (1971). The sediment transport rates due to current were calculated using two relationships: for total load (suspended plus bed load), a relationship based on Albertson and Garde (1958) was employed. It is demonstrated by Graf (1971) that, in general, virtually all of the sediment is in suspension for the range of

Figure 1

Delaware Bay study grids.
Depths in feet

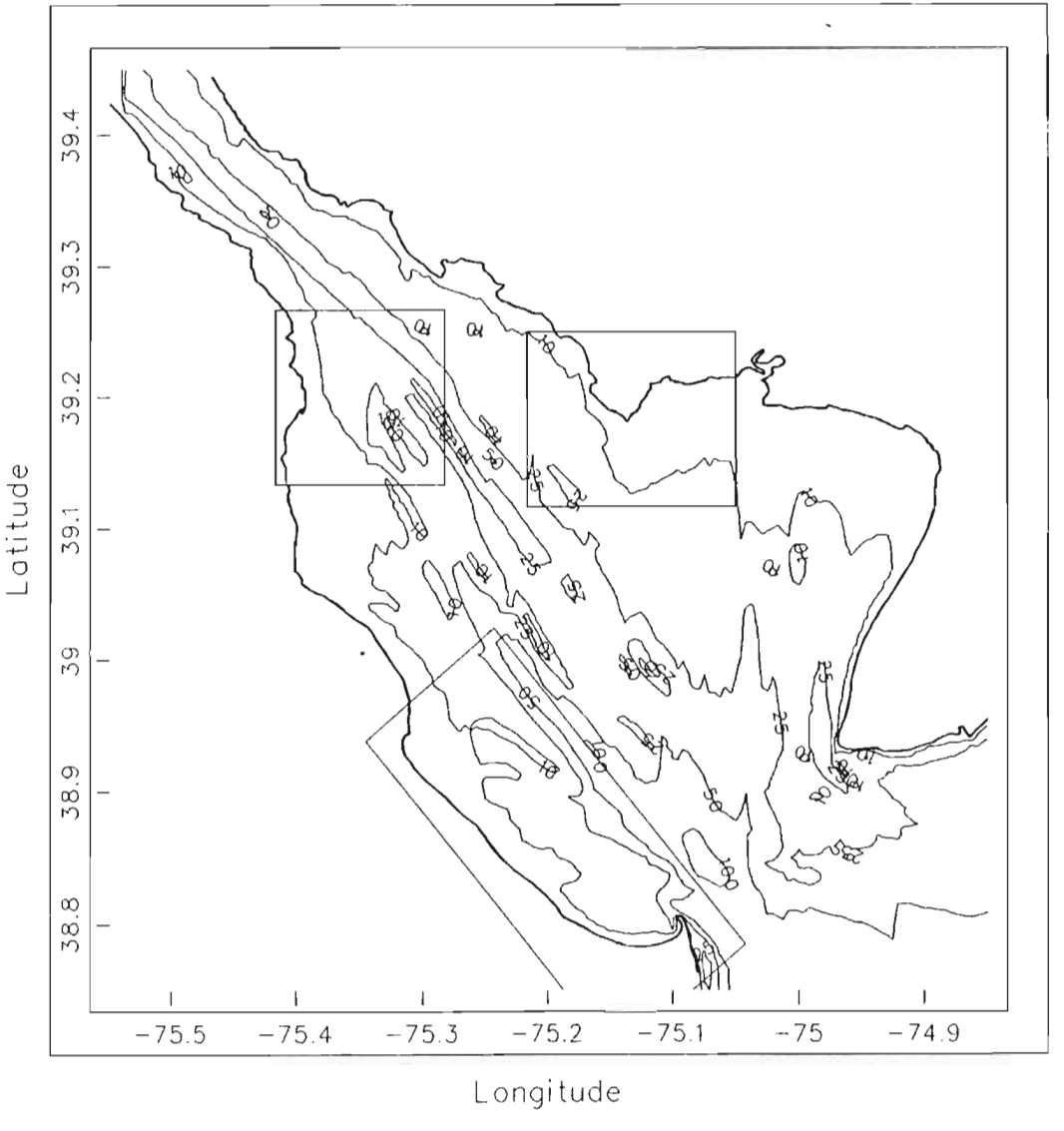

material sizes considered in this study. These values generally compared to total loads provided by Ackers and White (1973).

A sediment size of 0.30mm was generally used for the calculations of sand transport rates, as recommended by the Philadelphia District. A sediment size of 0.05mm was generally used for the calculations of silt transport characteristics.

Nearshore wave-driven longshore transport rates were derived using the Shore Protection Manual (1984) method. Waves transformed through the nearshore modeling grid were used so as to account for fine-scale refraction and sheltering due to stockpiles.

In order to provide a general knowledge of existing conditions under typical tidal forcing, and to provide a mechanism for calibrating the numerical current model, a series of tidal current measurements were made. At each site, six current measurement stations were occupied at approximately one hour intervals over a complete tidal cycle. Measurements were made with an acoustic doppler profiler (ADP), which measures currents over the entire profile from near the surface to near the bottom.

Current profile measurements were made with a 1.5 megaHertz Sontek Acoustic Doppler Profiler (ADP), which measures three dimensional velocity fields in a user-specified number of vertical cells with a resolution as fine as 0.25 meters. The ADP was deployed from a boat which shuttled between profiling stations, and then held a stationary position by a buoy while collecting time averaged data for one minute. Each measurement station was sampled at approximately one hour intervals. Horizontal current data were referenced to magnetic north by use of an internal compass and tilt compensator. The directions were later converted to true north using magnetic declinations published in NOAA navigational charts of the Delaware Bay.

Data were collected in a desktop personal computer and stored on the computer hard disk and floppy disk. Measurement station locations were determined with a Differential Global Positioning System (DGPS), with an accuracy of approximately +/- 4 meters.

Data were collected at four sites specified by the Philadelphia District Corps of Engineers. For each site, six measurement stations were established to cover the site in terms of area, water depth, and bathymetric features. Measurement stations were marked with buoys,

598

and the locations were measured with DGPS in case the a buoy was disturbed, and as a permanent record of the measurement locations. Each site was measured over a tidal cycle, with measurements at each station taken at approximately one hour intervals by shuttling sequentially between stations.

Water temperatures and salinities were measured periodically over the measurement sites to accurately determine the speed of sound, which is used by the ADP for calculating current velocities. Both water temperatures and salinities tended to remain relatively constant over the measurement site and throughout the tidal cycle.

The locations of the measurement sites are shown in Figures 2-5. Site A, Broadkill Beach Site, was the most southerly site, near Lewes, Delaware. Site C, Egg Island Point, is the most northeasterly site, near the mouth of the Maurice River, New Jersey. Site D, Kelly Island is the most northwesterly site, just north of the mouth of the Mahon River, Delaware. Site E, Slaughter Beach, is located in between sites A and C, just south of the mouth of the Mispillion River, Delaware. Coordinates of each measurement location at the four sites are presented in Appendix A.

The numerical current model was validated against the field data collected at each site by forcing the ocean boundary of the Delaware Bay with measured tides at Lewes, DE and Cape May, NJ. The model calibrated favorably at each site, as indicated in Figures 6-9. Vector plots of the entire bay on a flood tide and ebb tide are shown for illustration in Figures 10 and 11.

2.1.2 Shellfish Survivability Modeling

A shellfish survivability model was applied to the offshore Egg Island Point and Kelly Island sites in order to assess the impacts of potential current and turbidity conditions. The model simulates post-settlement oyster population dynamics. The model components are coupled by relationships that describe the removal of oyster energy by a parasite, relationships that relate the rate of parasite growth and oyster mortality and relationships that produce mortality in the oysters by the parasite.

The oyster model requires environmental time series input for food, salinity, temperature, turbidity and flow speed. Data for temperature, salinity, chlorophyll and turbidity were obtained from

599

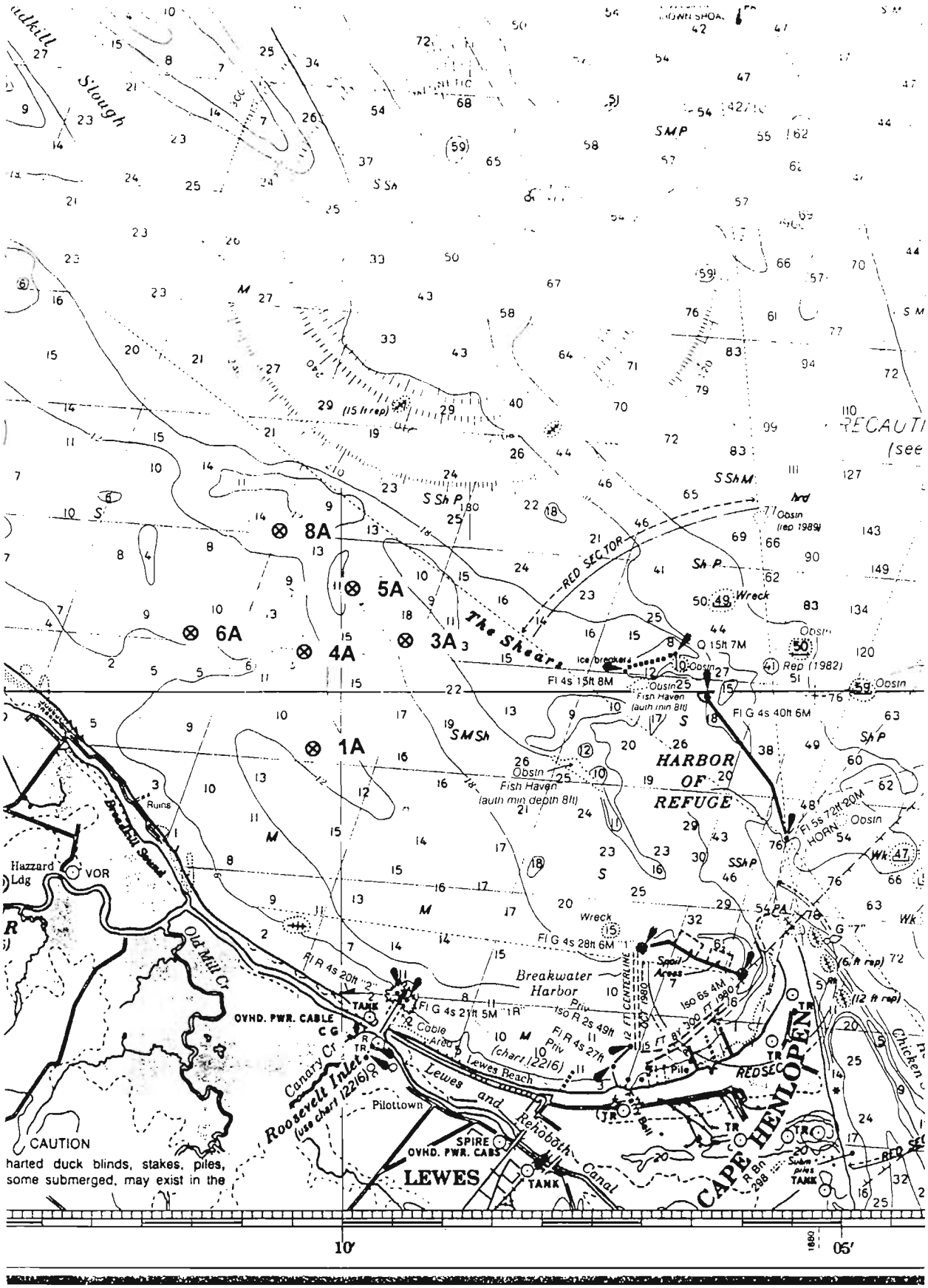

Figure 2: Current Measurement Sites, Broadkill Beach

600

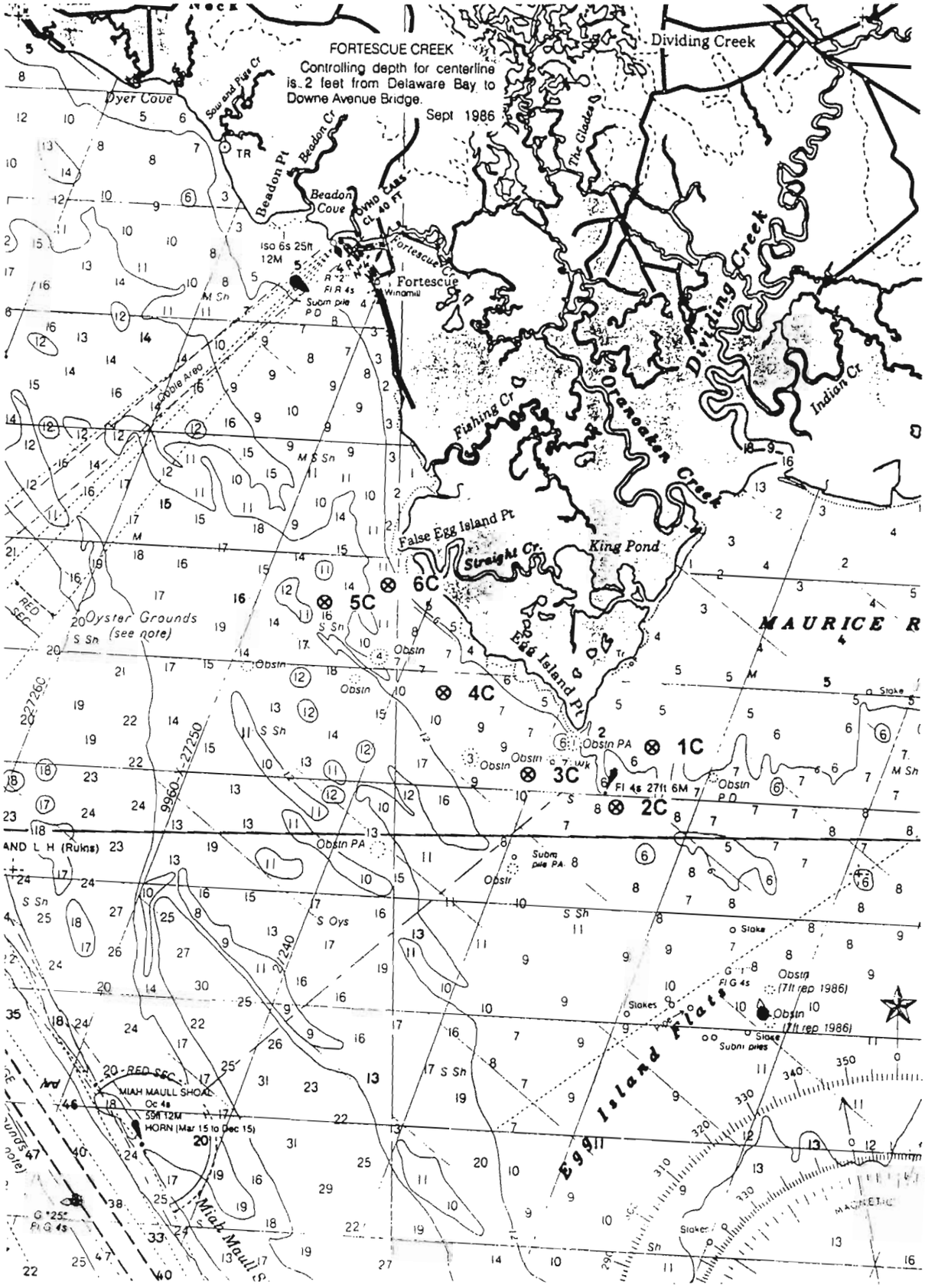

Figure 3: Current Measurement Sites, Egg Island Point

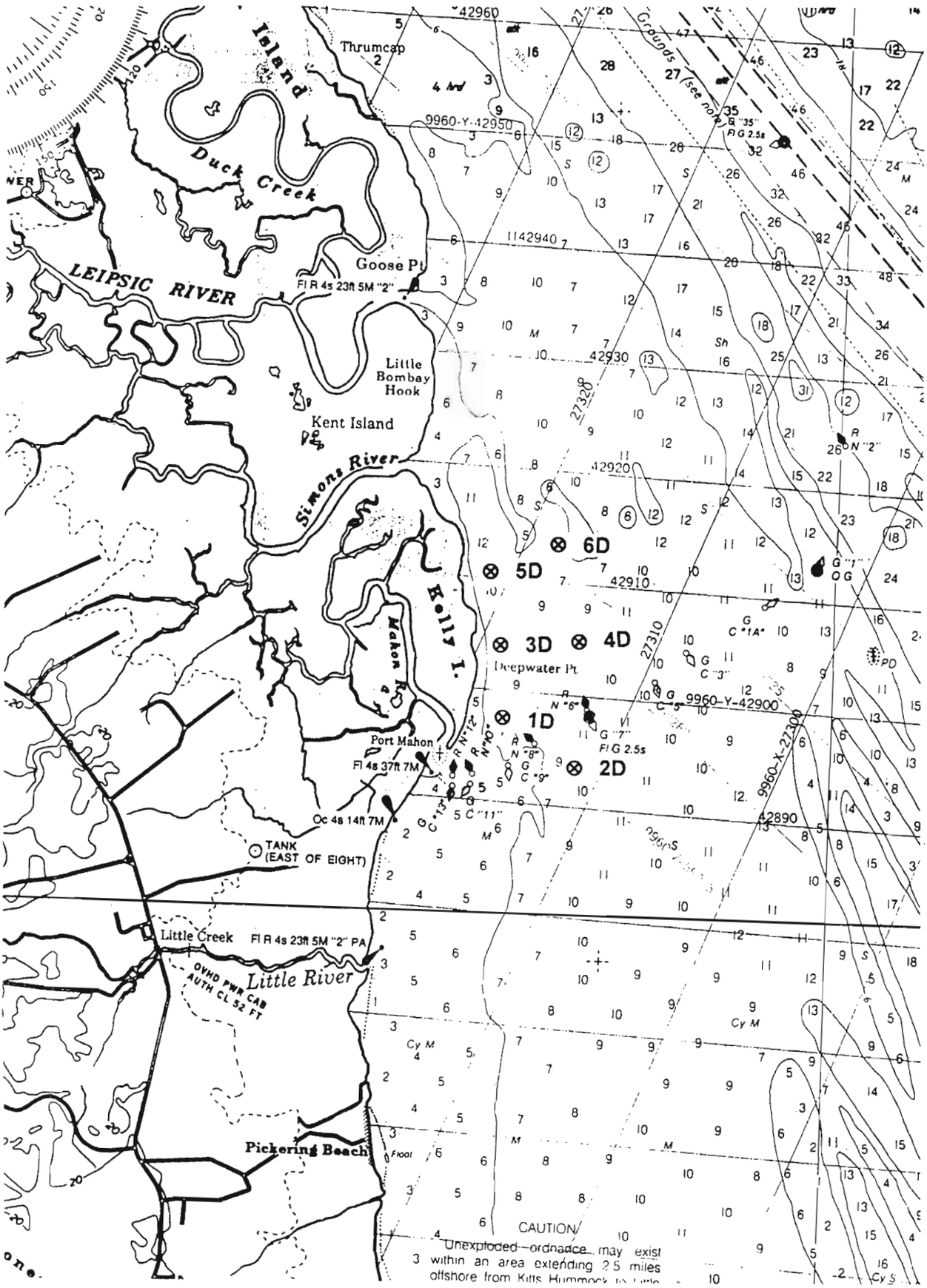

Figure 4: Current Measurement Sites, Kelly Island

602

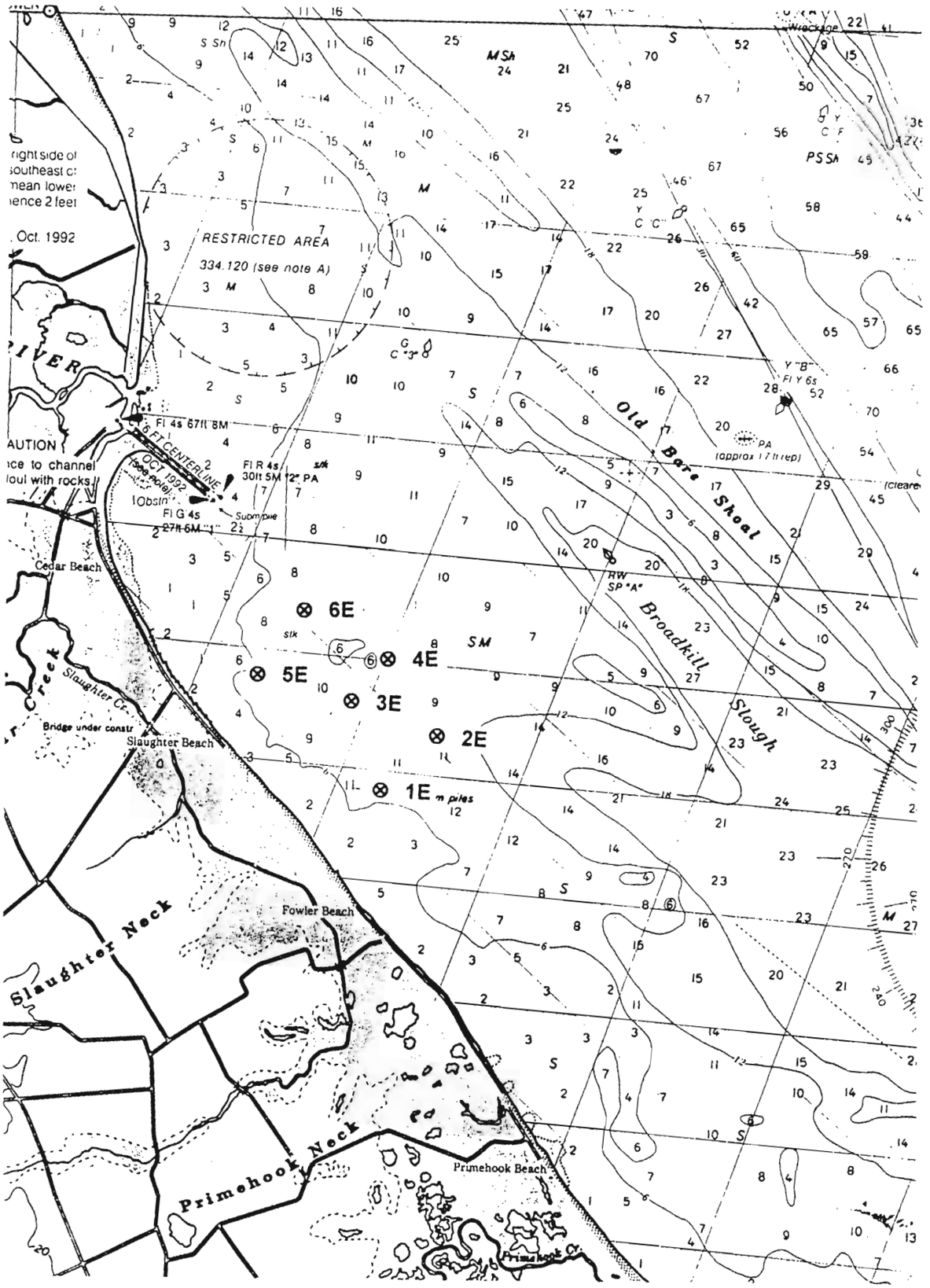

Figure 5: Current Measurement Sites, Slaughter Beach

Figure 6

Time-series of measured and modeled currents

Site: 5C (39 - 11.782 N 75 - 10.605 W)

Egg Island west

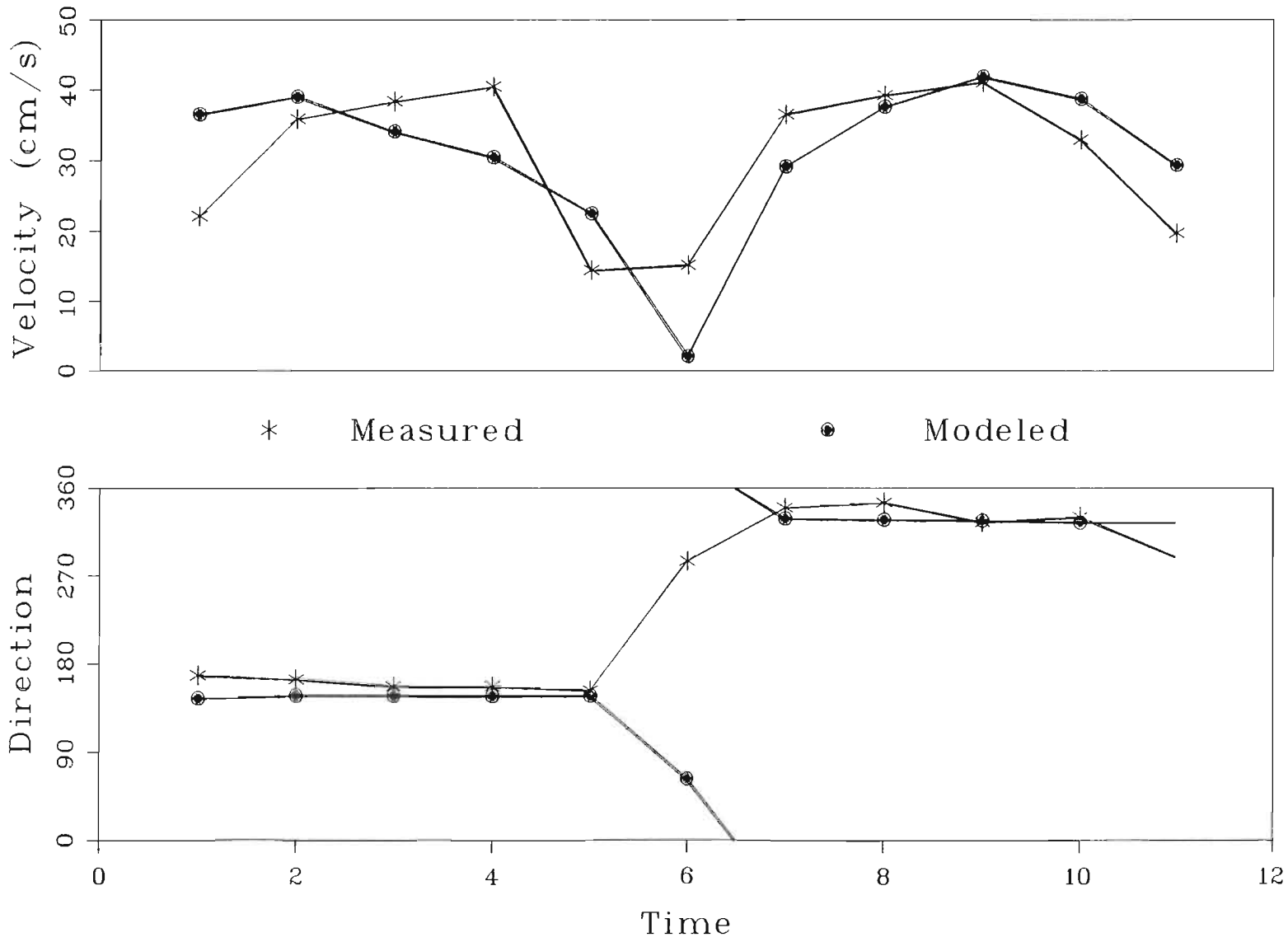

204

605

Figure 7

Time-series of measured and modeled currents

Site: 2D (39 - 11.072 N 75 - 22.465 W)

Kelly Island south

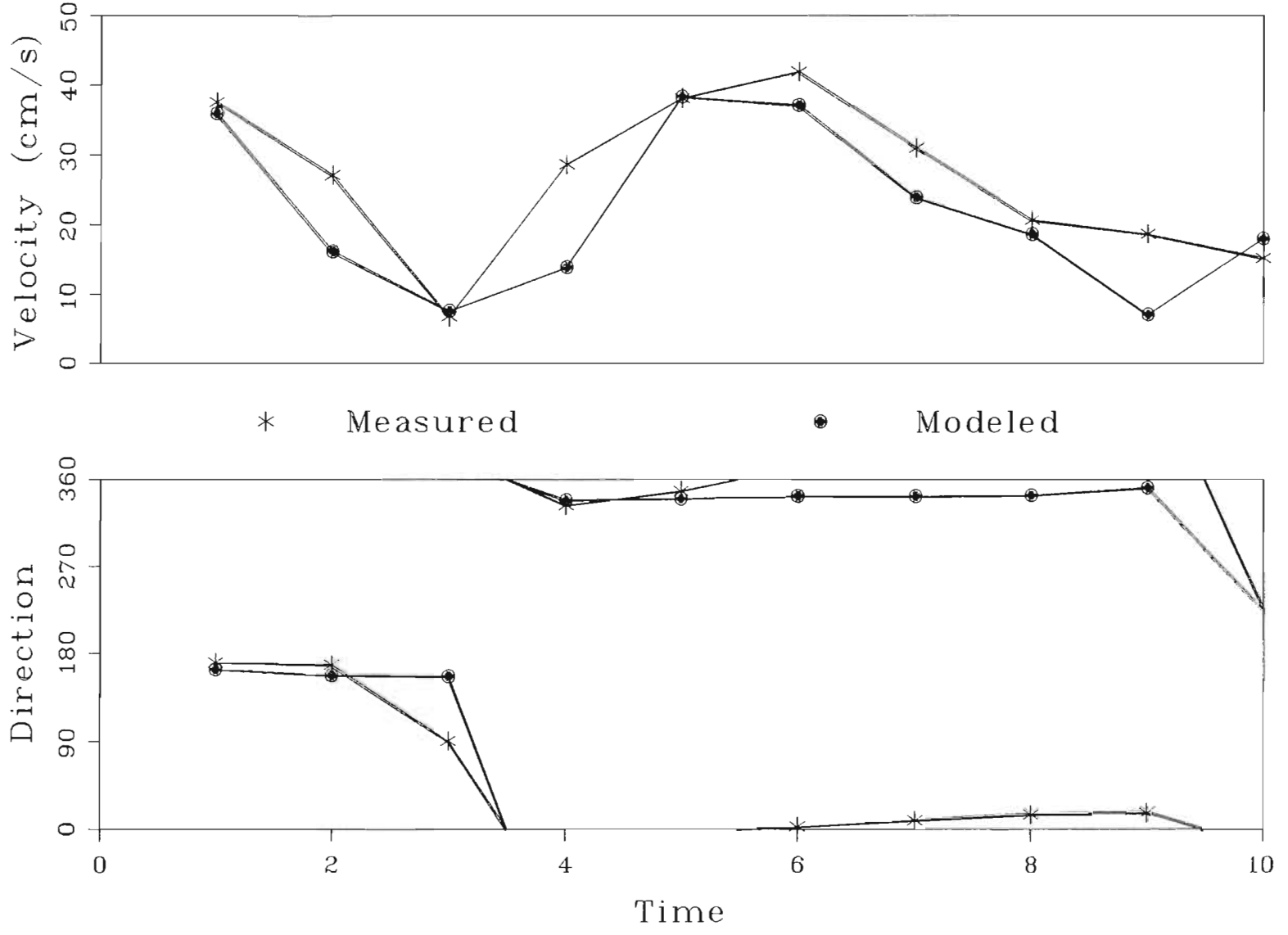

Figure 8

Time-series of measured and modeled currents

Site: 4E (38 - 54.921 N 75 - 16.080 W)

Slaughter Beach

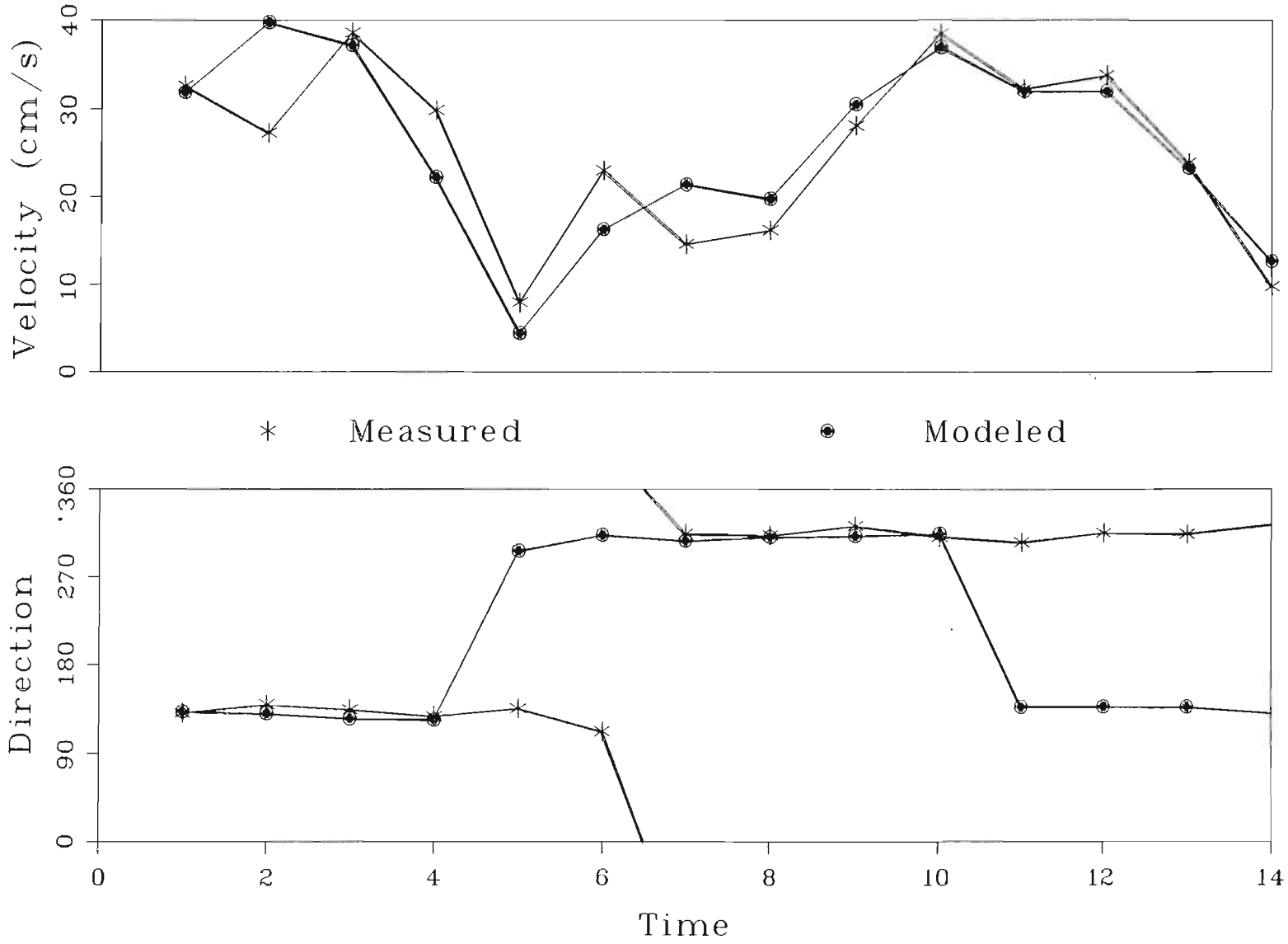

606

Figure 9

Time-series of measured and modeled currents

Site: 5A (38 - 50.746 N 75 - 10.043 W)

Broadkill Beach

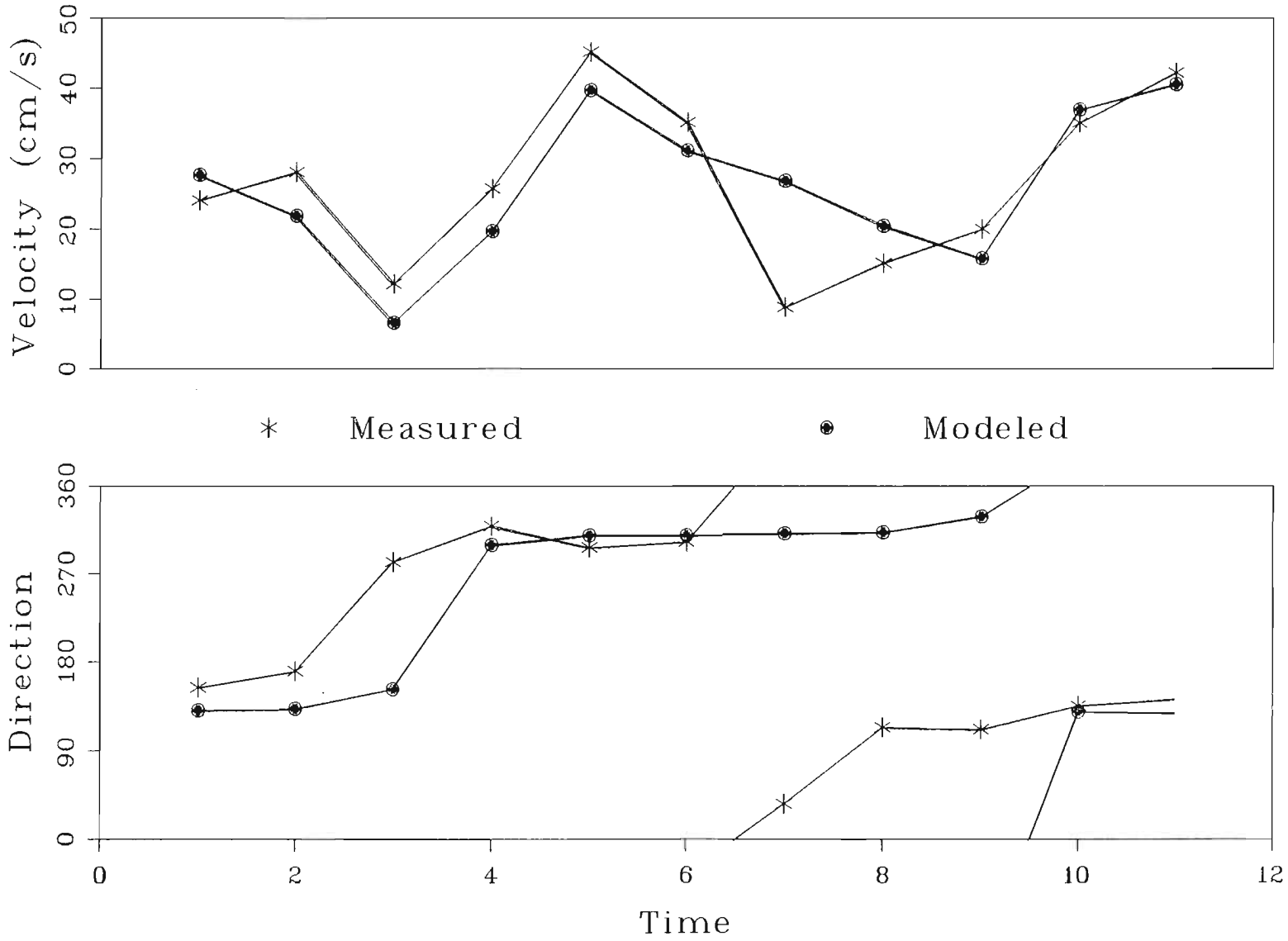

Figure 10

Delaware Bay Currents in cm/sec
Normal tide conditions
July 6, 1995 0000 EST

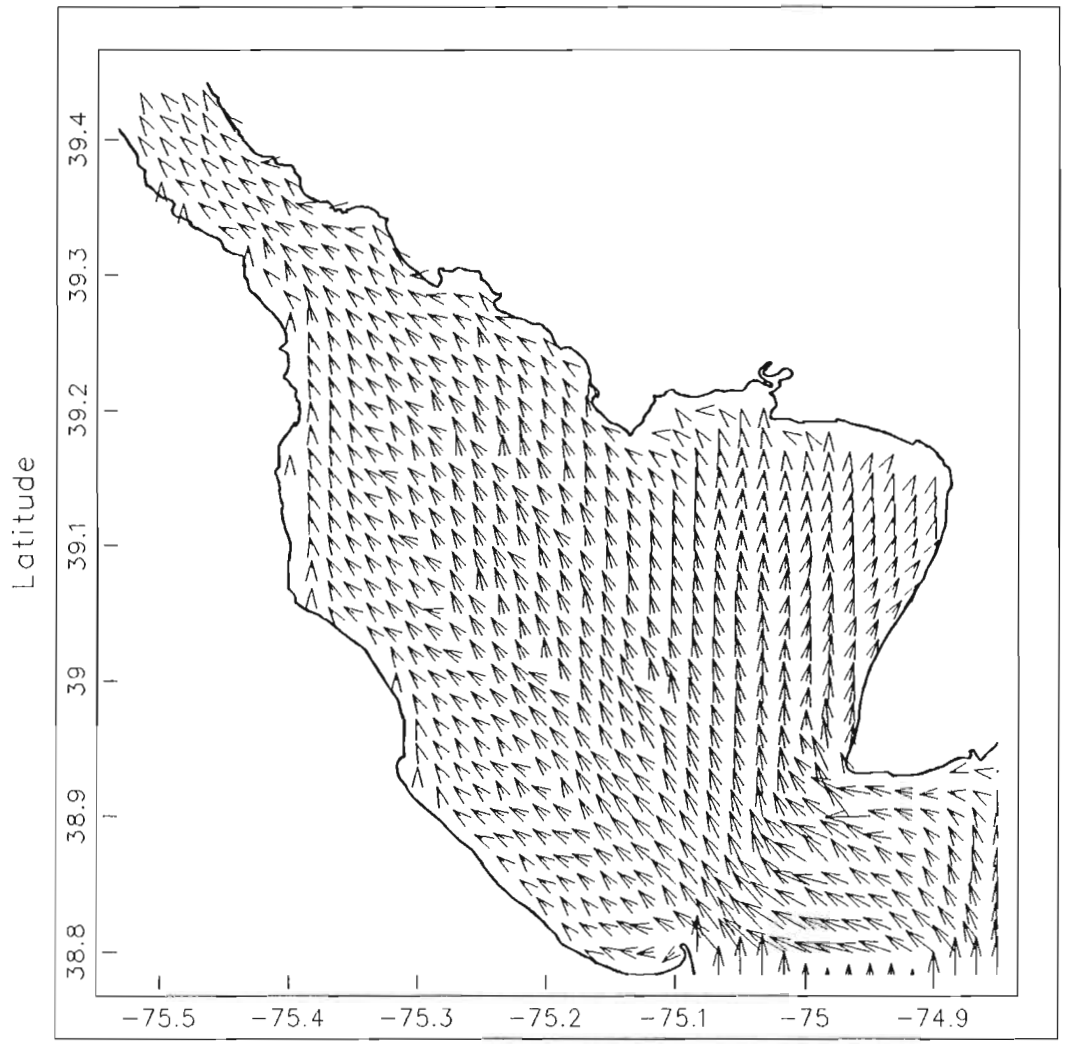

Reference Vectors

25 → 50 → 75 → 100 → 125 →

808

Figure 11

Delaware Bay Currents in cm/sec
Normal tide conditions
July 6, 1995 0007 EST

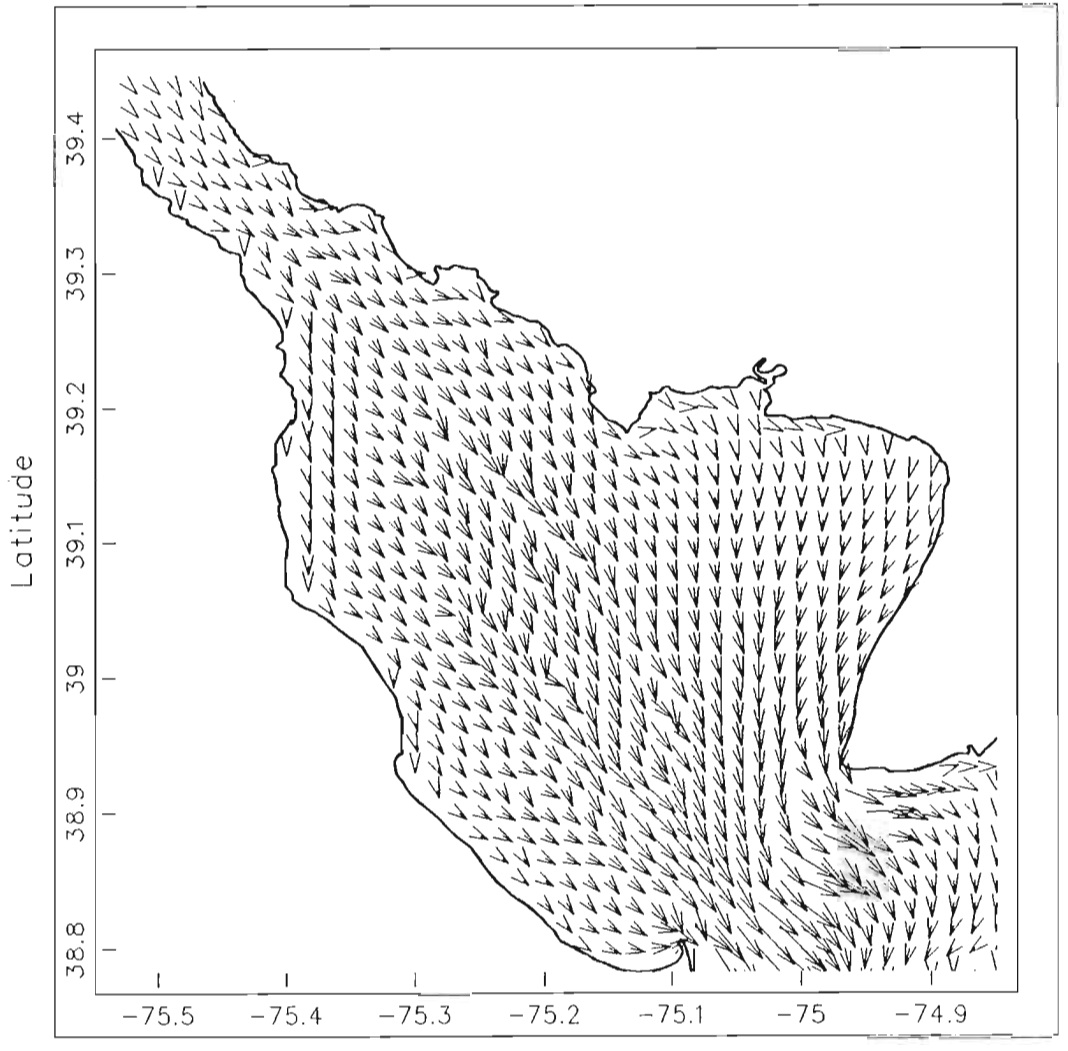

Reference Vectors

25 → 50 → 75 → 100 → 125 →

data collected by Haskins Shellfish Research Laboratory in the 1980's. In order to minimize the number of computer runs, the turbidity and flow speeds were parameterically varied in order to determine levels at which the oysters would be adversely impacted. Those results were then related to hindcasted turbidity and current speeds at the sites of interest. A more complete description of the model implemented is provided in a separate report produced by the Haskins Laboratory and included as Appendix E.

3. SELECTION OF MODELING SCENARIOS

The numerical models were used to generate conditions under which sediment is expected to be transported at each of the project disposal sites. At Egg Island Point and Kelly Island, the models were used to develop potential pathways of sediment that may move along the foundation of the geotubes or along the project area if the containment tubes were to be compromised. The sediment will be transported under normal tide and wave conditions at a long term rate, and will be transported under storm tide and wave conditions at more extreme rates that could be of concern to shellfish grounds. In addition, the Kelly Island area will contain a large amount of silt material that may move out into the bay under a catastrophic failure of the containment system. That case is assumed to be long term leaching of material into the bay under primarily normal tidal conditions.

At the stockpile sites LC-5 and MS-19, long term transport rates are of primary concern, in addition to the potential pathways of sediment toward and along adjacent shorelines.

4. MODEL RESULTS

4.1 Egg Island Point, NJ, Wetland Restoration Site

Based upon the results of the wave and current simulations for Egg Island Point and adjacent areas, sedimentation rates and pathways were delineated. Figure 12 presents the sediment pathways determined for the area.

To the **west of the point**, transport along the shoreline and the immediate offshore area was found to be dominated by tidal currents with the net tidal and storm transport directed to the north. Wave-driven sediment transport is generally onshore. The models do not

610

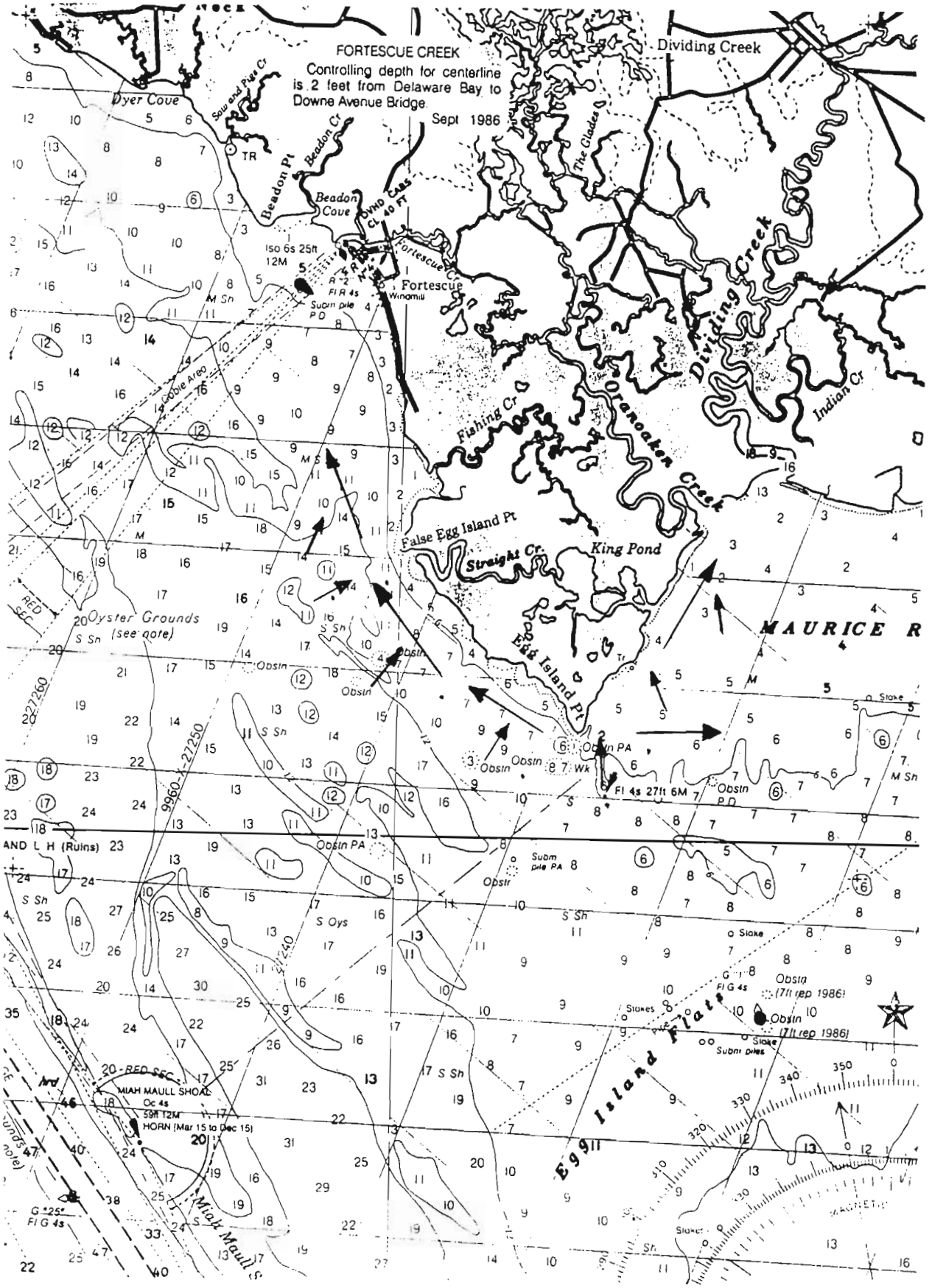

Figure 12: Sediment Pathways, Egg Island Point

611

indicate a significant mechanism that would transport sediment toward the shellfish areas to the west. With current speeds peaking at 40-45 cm/s during typical tidal conditions and 80 cm/s during extreme storm conditions, scour of sand similar in size to that planned for placement here can occur and current-driven longshore transport potential is calculated to be on the order of 5000 cubic yards per year (net). In an extreme storm (2-year and higher), current-driven transport potential along the shoreline is calculated to be on the order of 500 cubic yards per day of storm, and approximately 36,000 cubic yards of material per year potentially transported along the project's perimeter and from its external foundation to the northwest due to storms.

At locations to the east of the point, lower typical and storm current speeds of 30-40 cm/s and 85 cm/s, respectively, induce slightly lower sediment transport potential rates. Current-driven transport along the shoreline is directed along shore toward the NE at a rate of approximately 3500 cubic yards per year (net), including toward the east and possibly southeast of Egg Island Point. Annually, approximately 32,000 cubic yards of material can be potentially transported by currents in these same directions due to storms. Wave-driven transport is directed onshore. Wave-driven longshore transport potential rates are calculated to be 75,000-150,000 cubic yards (net) to the northeast on the eastern side of the point and the northwest on the western side of the point. Storm erosion analysis indicates that offshore-directed sediment transport is not likely due to the extremely flat offshore bottom slopes. The simulations do indicate, however, a potential material pathway is toward the east and possible toward the southeast where shellfish lease areas exist.

Potential transport rates are an indication of possible rates of natural removal of placed material from the area. With containment systems in place, only exposed sand will be subject to scouring at approximately the rates given above. However, if containment systems fail, transport to the NE, E, and NW will proceed at approximately those rates and shoreline recession will also proceed at rates similar to or slightly faster than recent historical shoreline recession.

Impacts on Shellfish

The sedimentation rates induced by sand placement in the Egg

617

Island Point area could have an impact on neighboring shellfish beds. Impacts are primarily due to an interruption in filter-feeding by the shellfish, which could cause a long-term reduction in health or population depending upon the length and severity of the interruption. Interruption in this project is considered to be due to an increase in suspended sediment concentration in the water column over the shellfish areas due the newly-available sediment material in the containment site.

The primary effect on shellfish will take place during storms when the greatest potential mobilization of sediment occurs. At Egg Island Point, a review of the hindcasted storm simulations and calculations of transport rates yields the following:

Recurrence	Peak Bottom Current(cm/s)	Duration (hours)	Potential Transport Conc.(mg/l) Ambient (Silt)	Proposed Fill (Sand)
1yr	50	36-48	250	15
10yr	60	48-60	500	30
20yr	65	48-60	700	45
50yr	75	24-72	1200	75
100yr	85	24-48	2000	125

In the table provided above, an estimate of extreme peak hourly storm bottom current speeds was estimated from the hindcasted population of storms which yielded 10 events exhibiting a storm-generated component over and above the normal astronomical tidal current. Also provided is a storm duration associated with each particular storm frequency which indicates that storms of the 1yr to 50yr range are northeasters while hurricanes become significant at the 50yr-100yr level. Ambient sediment transport concentrations are presented for each storm frequency based upon a review of typical and annual sediment loadings provided by Haskins Shellfish Laboratory taken continually over a year's time (see Appendix E). Based upon a general mean sediment transport rate of 40 mg/l in normal tidal currents peaking at 40 cm/s, storm values were determined by scaling to more extreme conditions based upon a velocity to the fourth power ratio, the accepted functionality for total sediment load. This is likely a conservative assumption given that the supply of sediment to the water column is not unlimited. Finally, an estimate of <u>potential</u> sediment transport concentrations is provided given an unlimited supply of material from the Egg Island Point fill.

The table provided above indicates that storm-induced sediment

613

transport of new material potentially is much less than the ambient sediment loading in the water column during most storm events. The Haskins Shellfish Laboratory investigation of the conditions required for impact on oyster survivability indicates that any 4-day event with the combined effect of ambient material plus the new source of material will have no observable effect on the shellfish. The longest extreme storm event found in the historical record and included in the hindcast was the March 1962 storm which lasted approximately 60 hours but caused relatively low current speed increases at Egg Island Point (about 50 cm/s). The peak current speed event was found to be the 1944 hurricane but that event caused increased current speeds for less that 24 hours which is typical of a summer/fall hurricane. The shellfish survivability model indicated that an August storm event of greater than 4 days and less than 30 days duration would be required for a significant impact on the population. Again, extreme events of record in that time of year are rare hurricanes which typically last no longer than 48 hours.

4.2 Kelly Island, DE, Wetland Restoration Site

Based upon the results of the wave and current simulations for Kelly Island and adjacent areas, sedimentation rates and pathways were delineated. Figure 13 presents the sediment pathways determined for the area.

Numerical flow modeling indicates that typical tidal current speeds decrease from south-to-north along the Kelly Island area, peaking at 50 cm/s at the southern end (Port Mahon), to 40 cm/s along the central section of the island, and 35 (ebb)- 55 (flood) cm/s at the northern end. The storm currents peak at approximately 80 cm/s along the entire area. Typical current-driven transport rates are on the order of 5000 cubic yards per year alongshore (net to south). In an extreme storm (2-year and higher), current-driven transport along the shoreline is calculated to be potentially on the order of 500 cubic yards per day during a 2-year event, and potentially approximately 29,000 cubic yards of material per year transported annually along the project's perimeter and potentially from its external foundation to the north and south due to storms. All model runs indicate a strong sediment pathway in the north-south direction along all of Kelly Island and sand transport should feed neighboring

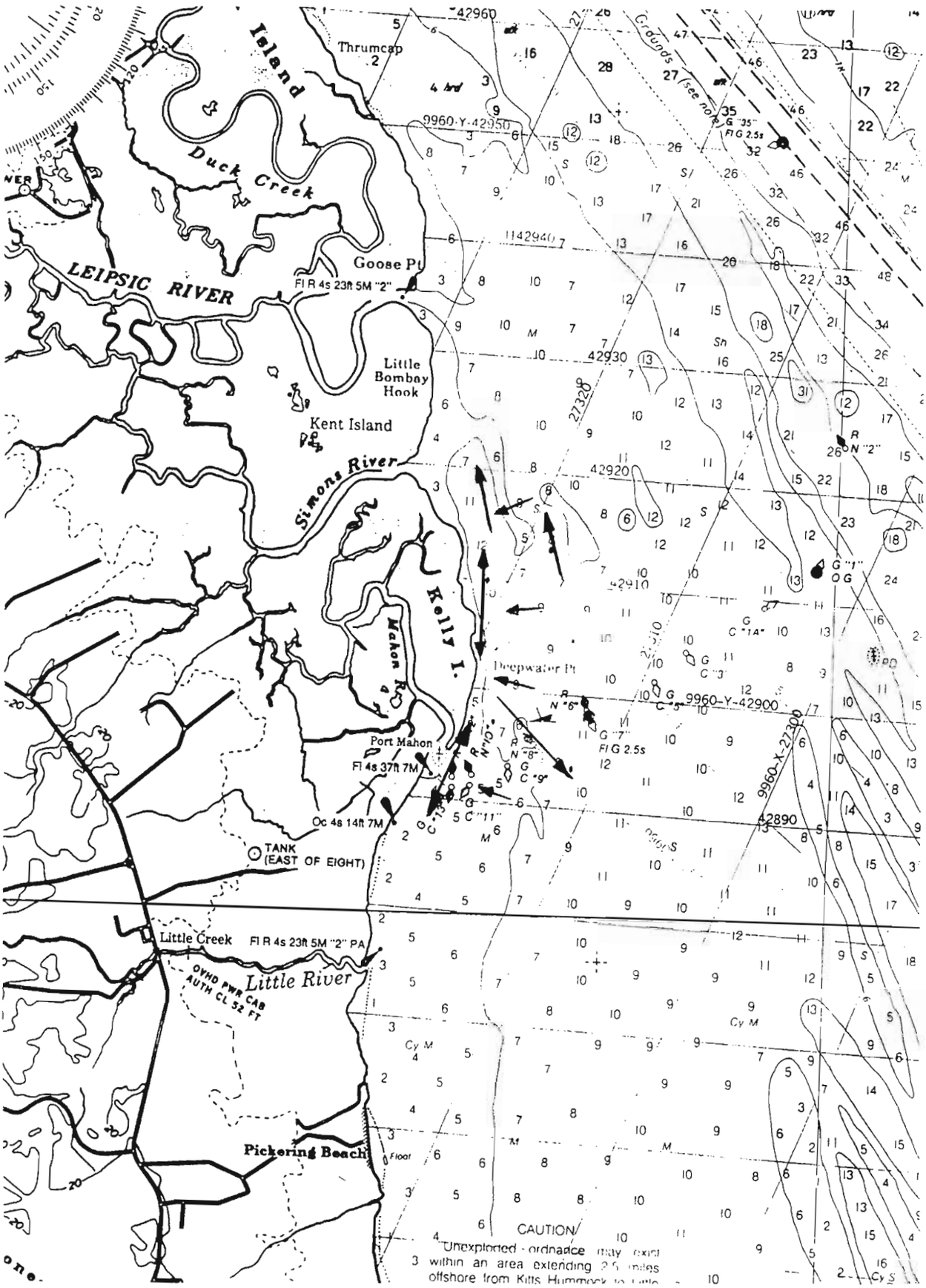

Figure 13: Sediment Pathways, Kelly Island

beaches or shoal the Port Mahon channel unless measures are taken to prevent shoaling. Wave transport is primarily onshore and alongshore at a potential annual rate of approximately 25,000-50,000 cubic yards (net) to the north. The sediment pathways discerned from the model results indicate that shellfish lease areas to the east should not be significantly impacted by sand placed at this project site. Although predominant winds are directed to the east during normal conditions, the corresponding wind-driven currents are not calculated to be sufficient to carry material offshore nor to significantly change the north-south direction of tidal currents. Storm wind-driven currents during both hurricanes and northeasters are onshore-directed (i.e. from the easterly quadrants), and are thereby expected to keep sediments moving close to the shoreline. Strong winter northwesterly winds may induce some offshore-directed sediment motion; however, this generally occurs during the months when shellfish are virtually dormant.

As in the Egg Island Point case and barring erosion of upland silt disposal areas, the rates of sediment transport potential will remain the same but the amount of readily available material for transport could increase if containment systems fail.

Kelly Island Silt Dispersion

Possible release of silt from the Kelly Island upland containment area is analyzed by assessing the fall velocity of 0.05mm material and its transport characteristics. Silt will generally be eroded from an area when flow velocities exceed approximately 30 cm/s and deposit only at slack tide. During a typical tidal cycle, silt material is calculated to have the potential to travel a maximum of approximately 3.6 nautical miles to the northern quadrant and southern quadrant from Kelly Island. Assuming that material will be transported along Kelly Island in a 100-foot wide swath (about 1/2 a normal-condition wavelength), the potential total sediment loading (or erosion) rate is calculated to be about 45 cubic yards per hour of normal-condition tide.

A more catastrophic assumption would be failure of containment structures and release of material during a storm. Following the same reasoning during an extreme storm, the material would travel approximately 7 nautical miles toward the northerly and southerly

quadrants. In the storm case, potential average total sediment loading (or erosion) rate is calculated to be approximately 1500 cubic yards per hour of storm tide condition, with rates peaking at 3500 cubic yards per hour at the peak of a major storm event. During a 100-year event, storm flows are estimated to have the approximate potential to transport a total of 100,000 cubic yards of silt material from the site split to the northerly and southerly quadrants. This approximately equates to 66 hours of erosive currents during the event. Conservatively assuming this material to cover 7 square nautical miles of seafloor, this equates to an average covering of approximately 1/8 inch of silt. The projected area of coverage based upon this analysis just barely overlaps the western edge of leased oyster bottoms to the southeast of Kelly Island. The anticipated silt dispersion is conservatively shown in Figure 14. The offshore extent of the sediment coverage area shown in the figure is considered to be a most-likely boundary for sediment deposition based upon the modeling results but could easily vary by 25-50% due to variability in specific storm characteristics and site-specific details of the bathymetry.

Impacts on Shellfish

The sedimentation rates induced by sand placement in the Kelly Island could have an impact on neighboring shellfish beds. Impacts are again primarily due to an interruption in filter-feeding by the shellfish, which could cause a long-term reduction in health or population depending upon the length and severity of the interruption. Interruption in this project is considered to be due to an increase in suspended sediment concentration in the water column over the shellfish areas due the newly-available sediment material in the containment site.

As at Egg Island Point, the primary effect on shellfish will take place during storms when the greatest potential mobilization of sediment occurs. At Kelly Island, a review of the hindcasted storm simulations and calculations of transport rates yields the following:

Recurrence	Peak Bottom Current(cm/s)	Duration (hours)	Potential Transport Conc. (mg/l) Ambient (Silt)	Proposed Fill (Sand)
1yr	70	36-48	120	60
10yr	90	48-60	325	160
20yr	110	48-60	730	350
50yr	135	24-72	1650	800
100yr	150	24-48	2530	1215

617

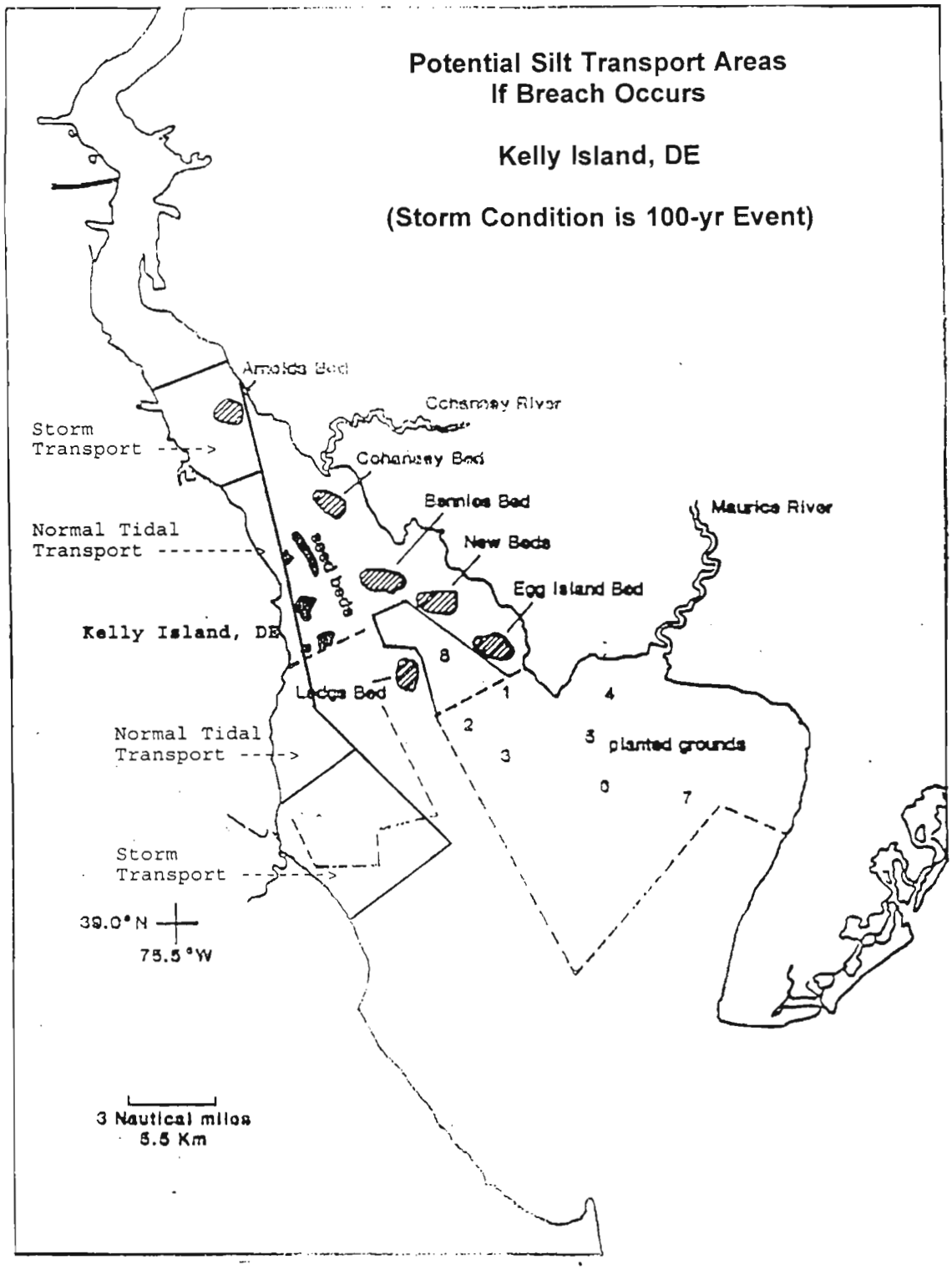

Figure 14: Anticipated Silt Dispersion Pattern, Kelly Island

618

In the table provided above, an estimate of extreme peak hourly storm bottom current speeds was estimated from the hindcasted population of storms which yielded 10 events exhibiting a storm-generated component over and above the normal astronomical tidal current. Also provided is a storm duration associated with each particular storm frequency as explained for Egg Island Point. Ambient sediment transport concentrations are presented for each storm frequency based upon the data provided by Haskins Shellfish Laboratory (see companion report). Again, scaling to more extreme conditions was performed for the listed recurrence levels. This is likely a conservative assumption given that the supply of sediment to the water column is not unlimited. Finally, an estimate of potential sediment transport concentrations is provided given an unlimited supply of material from the Kelly Island sand fill.

The table provided above indicates that storm-induced sediment transport of new material is again potentially significantly less than background levels of turbidity in the water column during most storm events. Again, the Haskins Shellfish Laboratory investigation of the conditions required for impact on oyster survivability indicates that only a 4-day event will have an observable effect on the shellfish and only if that event occurs in August. The longest extreme storm event found in the historical record was the March 1962 storm which lasted approximately 60 hours with a peak flow speed of about 100 cm/s. The peak current speed event was found to be the 1944 hurricane (139 cm/s) but that event caused increased current speeds for less that 24 hours which is typical of a summer/fall hurricane.

For the silt material (diameter of 0.05mm), the potential peak transport concentration during typical tide conditions adjacent to Kelly Island is calculated to be approximately 90 mg/l which is approximately 30% higher than the peak turbidity levels reported in historic data. During extreme events, the concentrations are calculated to be approximately the following:

Recurrence	Peak Bottom Current(cm/s)	Duration (hours)	Potential Transport Conc. (mg/l) Ambient (Silt)	Proposed Fill (Silt)
1yr	70	36-48	120	850
10yr	90	48-60	325	2300
20yr	110	48-60	730	5150
50yr	135	24-72	1650	11000
100yr	150	24-48	2530	18000

It should be noted that the extremely high concentrations during the

619

very extreme events are theoretical in nature and are probably beyond conditions for which sediment transport relationships are valid. However, the values indicate that during a long term leaching process (say 30 days), the concentrations of sediment in the water column may increase to the daily range of 90-100 mg/l, which is well-below levels modeled by Haskins Shellfish Laboratory that have an adverse effect on the oyster beds. However, at the 10yr events and higher, a catastrophic failure of the containment structures will bring concentrations above levels of adverse effect but the durations of the storms are relatively short and will limit or prevent adverse effects on the oyster beds.

4.3 LC-5 and MS-19 Stockpile Sites

The two stockpile sites MS-19 and LC-5 were modeled together in the same wave model and current model grids and simulations because of their proximity. In both cases, it was found that the sediment pathways were similar, i.e. net wave-driven mass transport is potentially onshore and the longshore potential net transport is to the northwest. Sediment pathways are illustrated in Figures 15 and 16. Net wave-driven potential transport is found to be approximately 15000 cubic yards per year in the onshore direction at MS-19 and 5000 cubic yards per year at LC-5. These values indicate that the stockpiles are expected to migrate slowly onshore; however, major 2- to 5-year storms can potentially transport 40,000 cubic yards in a single event in the onshore direction. Mean current-driven velocities along the coast due to astronomical tidal action were found to be about 30-40 cm/s flows at MS-19 and 40-60 cm/s at LC-5. The net transport potential due to these flows are calculated to be approximately 10,000 cubic yards per year at MS-19 and 5,000 cubic yards per year at LC-5 to the south. Again, these transports indicate slow movement of material to the northwest and southeast, forcing the stockpiles to spread laterally.

A significant transport component is the wave-induced longshore transport potential at these sites. At Broadkill Beach (LC-5) average net transport potential is calculated to be about 230,000 cubic yards per year to the northwest (left), and at Slaughter Beach (MS-19) net transport potential is calculated to be approximately 260,000 cubic yards per year in the same direction.

No change in longshore transport along the coast is calculated

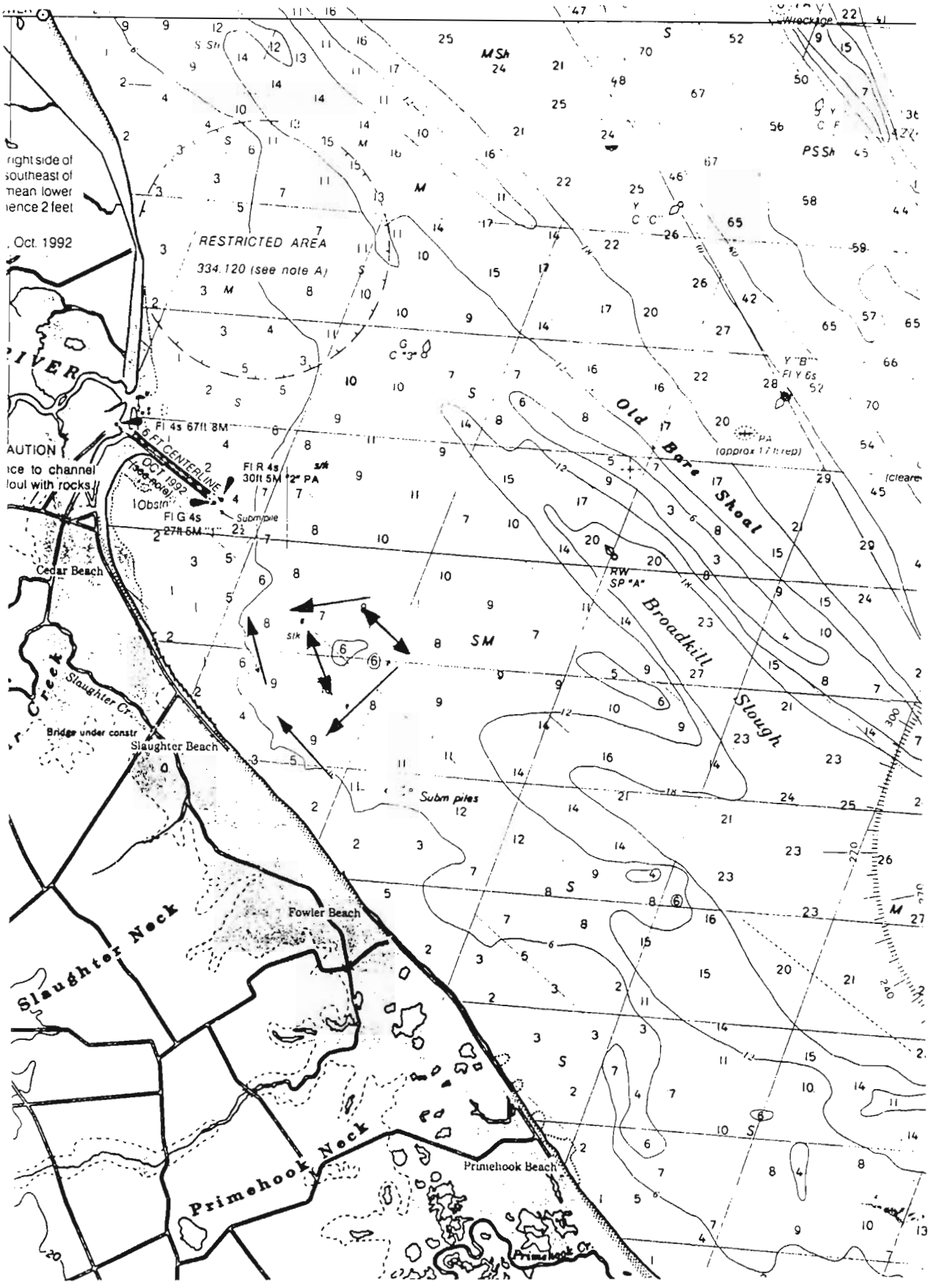

Figure 15: Sediment Pathways, Slaughter Beach

621

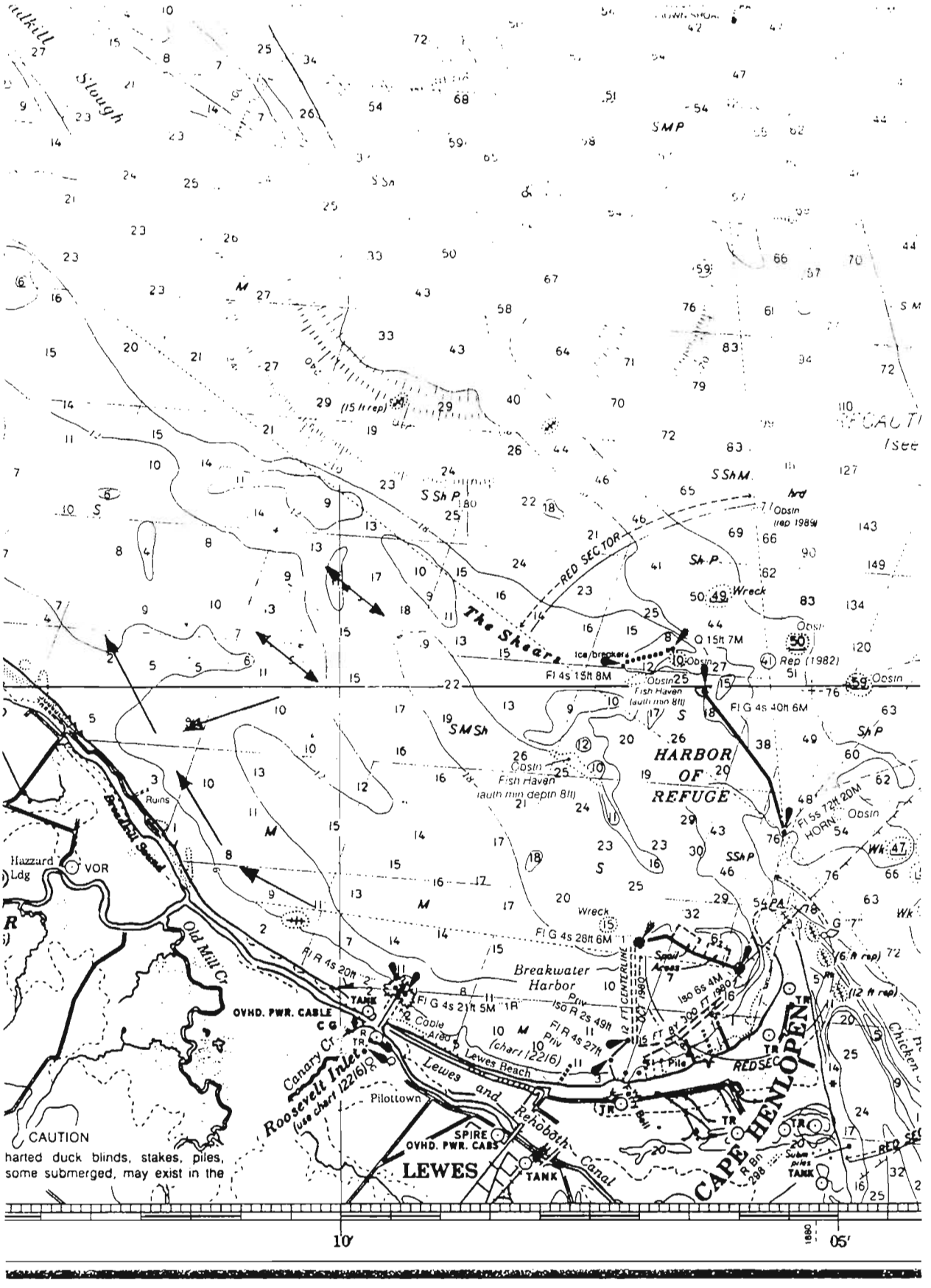

Figure 16: Sediment Pathways, Broadkill Beach

for the stockpiles with a crest elevation of -3 feet MLW or for either stockpile with a crest elevation of 0 feet MLW if the stockpiles are kept a minimum of 1500-2000 feet from shore.

5. CONCLUSIONS AND RECOMMENDATIONS

A sediment transport and shellfish survivability study was performed for four sites on the Delaware Bay. The objectives of the study were (1) to map potential sediment transport rates and pathways due to planned projects at Egg Island Point, Kelly Island, MS-19 and LC-5 and (2) to assess potential impacts on neighboring shellfish areas.

In order to perform the study, numerical current and wave models were employed to aid in defining sediment transport mechanisms. Tidal current data was collected in summer 1995 at each location during typical daily conditions to define ambient conditions and to provide some model calibration data. To aid in calibrating sediment transport estimates, suspended solids data collected over several years was supplied by the Haskin Shellfish Research Laboratory. Based upon the models and data, calculations of current-driven and wave-driven sediment transport were made for both storms and normal conditions which were then used in a shellfish survivability computer model to assess potential impacts on neighboring shellfish beds.

The modeling studies indicated sediment transport characteristics as shown in Table 1 for the wetland restoration sites and in Table 2 for the sand stockpile sites.

Shellfish survivability modeling was performed for the wetland restoration sites by examining the effect of a 4-day and a 30-day high-turbidity event in each season of the year with a turbidity level of 2 g/l, which was found to be approximately the maximum expected concentration during an extreme storm. The 4-day storm event was selected because it is longer than the extreme storms of record. The 30-day case was selected because it could be typical of the time required to detect and address a sediment leak from the containment areas and to provide information on the variation in impacts with the duration of turbidity.

The results of the shellfish survivability calculations show that there is no expected impacts on oyster survivability or growth due to the events considered except at Kelly Is. in August. Because August

623

Table 1

Sediment Transport Findings
for Wetland Restoration Sites (Sand 0.30 mm)

	Egg Island Point, NJ	Kelly Island, DE
Normal Current-Driven Transport Potential	5,000 cu yd/yr (net to southeast)	5,000 cu yd/yr (net to south)
Normal Wave-Driven Longshore Transport Potential	75-150,000 cu yd/yr (net to north)	25-50,000 cu yd/yr (net to north)
Storm Current-Driven Transport Potential	30-40,000 cu yd/yr (net to north)	30,000 cu yd/yr (net to south)
Dominant Sediment Pathways	Onshore and alongshore to the north on both sides of the point; slight easterly-driven sediment to the east of the point	Onshore and alongshore to the north and south; slight southeasterly-driven transport to the south of Port Mahon
Silt (0.05mm) Dispersion Potential	not applicable	Normal Tide Transport Potential: 45 cy/hr Normal Tide Travel Distance: 3.5 nm Mean Storm Transport Potential: 1500 cy/hr Storm Transport Travel Distance: 7 nm

624

Table 2

Sediment Transport Findings
for Sand Stockpile Sites (Sand 0.30mm)

	LC-5	MS-19
Net Wave-Driven Mass Transport Potential	Normal: 5,000 cy/yr (net onshore) Storm: 40,000 cy/yr (net onshore)	Normal: 15,000 cy/yr (net to onshore) Storm: 40,000 cy/yr (net onshore)
Net Current-Driven Transport Potential	5,000 cy/yr (net to south)	10,000 cy/yr (net to south)
Wave-Driven Longshore Transport Potential	175-300,000 cy/yr (net to north)	200-350,000 cy/yr (net to north)
Dominant Sediment Pathways	Onshore and alongshore to the north	Onshore and alongshore to the north
Impact of Stockpile Crest Elevation	Crest at -3'MLW appears to have minimal effect on nearshore transport processes	Crest at -3'MLW appears to have minimal effect on nearshore transport processes

625

storm events are much shorter than the 4-day event considered, insignificant impacts are expected on oysters during expected real storm events at that time of year. The 30-day event, although also potentially causing an impact at Kelly Island in August, is most likely to be prevented in August because that time of the year is best for performing repair work on the containment system. In addition, any 30-day event in August will exhibit turbidity concentrations that are much less than 2 g/l and more likely 150 mg/l. Similar 30-day simulations with turbidity levels of approximately 150 mg/l in August show much less impact, with the entire spawn not being lost and no increase in mortality over ambient conditions.

This study has incorporated a number of sophisticated models and data sets to aid in formulating results. In order to improve the accuracy of the results, it is recommended that site-specific wind, wave, current and sediment transport data be collected during storm conditions. On-site instruments could be installed for a short period during the winter months and during the critical month of August to collect such data. Concurrently, input parameters for the oyster survivability model should be collected so that the data set would be a consistent model validation tool for all modeling components of the study.

APPENDIX A

Coordinates of ADP Current Measurements

Broadkill Beach

STA.		DEG MIN	DEPTH, METERS MLLW
1A	N	38 49.545	3.1
	E	75 10.260	
3A	N	38 50.295	5.6
	E	75 09.433	
4A	N	38 50.312	3.8
	E	75 10.447	
5A	N	38 50.746	3.8
	E	75 10.043	
6A	N	38 50.385	2.2
	E	75 11.585	
8A	N	38 51.199	4.0
	E	75 10.728	

Egg Island Point

STA.		DEG MIN	DEPTH, METERS MLLW
1C	N	39 10.633	2.3
	E	75 07.437	
2C	N	39 10.263	3.0
	E	75 07.866	
3C	N	39 10.412	3.3
	E	75 08.729	
4C	N	39 11.018	3.3
	E	75 09.527	
5C	N	39 11.782	4.8
	E	75 10.605	
6C	N	39 11.882	2.9
	E	75 10.030	

Kelly Island

STA.		DEG MIN	DEPTH, METERS MLLW
1D	N	39 11.400	1.9
	E	75 23.301	
2D	N	39 11.072	2.5
	E	75 22.465	
3D	N	39 11.964	2.2
	E	75 23.104	
4D	N	39 12.074	2.5
	E	75 22.399	
5D	N	39 12.545	2.7
	E	75 23.370	
6D	N	39 12.765	1.4
	E	75 22.733	

Slaughter Beach

STA.		DEG MIN	DEPTH, METERS MLLW
1E	N	38 53.920	2.6
	E	75 16.327	
2E	N	38 54.293	3.3
	E	75 15.685	
3E	N	38 54.537	3.0
	E	75 16.559	
4E	N	38 54.921	2.5
	E	75 16.080	
5E	N	38 54.802	2.4
	E	75 17.458	
6E	N	38 55.193	2.5
	E	75 16.959	

APPENDIX B
ADP Specifications

ADP

A new Current Profiler for rivers, estuaries, and coastal regions.

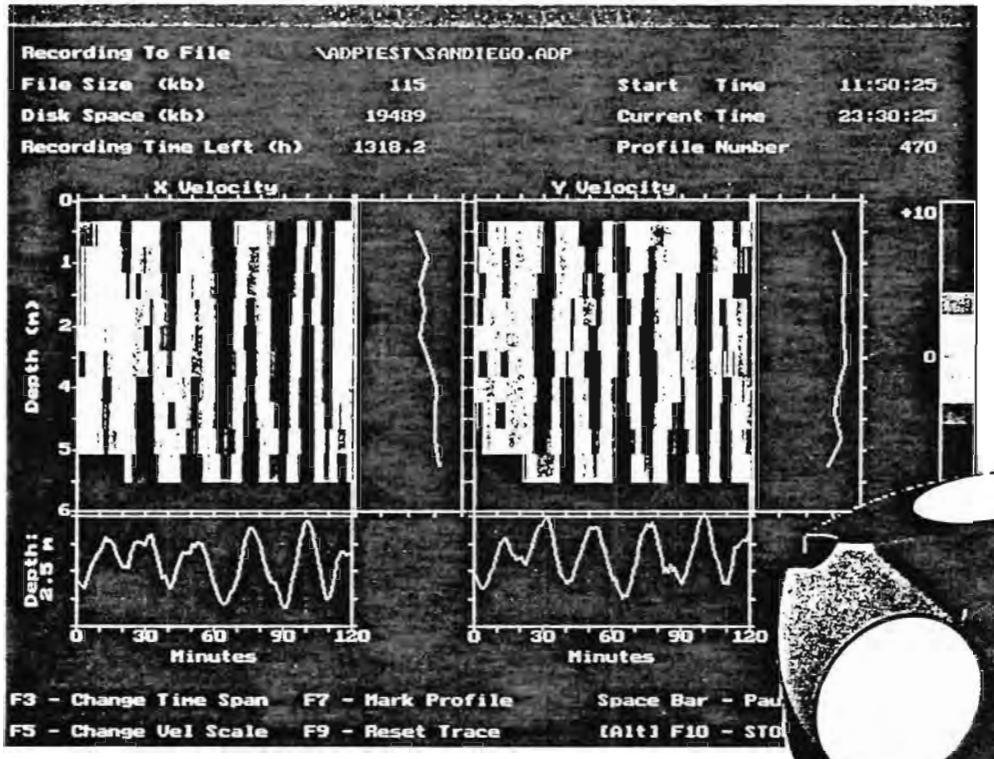

The ADP real-time data acquisition software displays color contour plots of the velocity profiles, time series of the horizontal components at a user-selected depth, and the last velocity profile. Data are stored to the hard disk.

The ADP transducer module generates three acoustic beams that are slanted 25 from the vertical. From the along-beam velocities the software calculates the three dimensional velocity profile.

The ADP (Acoustic Doppler Profiler) is an affordable current profiler that is simple and easy to use. It measures the three dimensional velocity in a number of vertical cells over a range of up to 60 meters and with a vertical resolution as fine as 0.25 meters. The ADP is ideal for applications that require precise, non-intrusive measurements of the mean current away from flow interference generated by bridge piers, observation towers, etc. The three dimensional profiling capability and rugged low profile housing makes the ADP suitable for bottom mounting to avoid damage from boat traffic or fishing activity. Immune to zero-drift and resistant to biological fouling, the ADP is well suited for low-flow applications in estuaries.

The SonTek ADP is a breakthrough in price/performance for water current meters. By taking advantage of state-of-the-art electronic design methods and efficient manufacturing processes, the SonTek ADP provides current profiling measurement at a price similar to many single-point current meters.

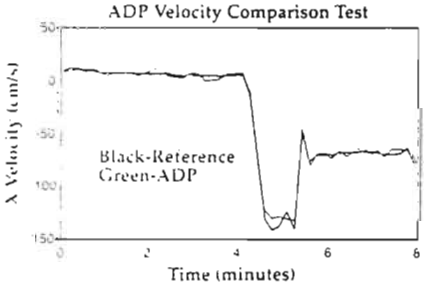

Time series plot from Miramar lake

The ADP compares quite well with a calibrated single-point current meter during lake tests with a moving boat. The comparison is equally good for all range cells.

SonTek

ADP
SPECIFICATIONS

Acoustic Frequency:	3 MHz	1.5 MHz	0.75 MHz
Profiling Range:	3-5 m	10-15 m	40-60 m
Maximum Resolution:*	0.25 m	0.5 m	1 m
Zone of no measurements (Blanking)	0.2 m	0.4 m	0.8 m
Mid-point of first range cell:	0.45 m	0.9 m	1.8 m

*For even finer resolution, please call.

Number of Range Cells:	Programmable up to 128
Velocity Components:	When used with the optional internal compass, the ADP provides East-West, North-South, and vertical velocity components. Without a compass, the data are reported in the coordinate system of the transducer module.
Velocity Range:	±5 m/s (standard), ±10 m/s (optional)
Maximum Operating Depth:	75 m
Velocity Resolution:	0.01 cm/s
Velocity Accuracy:	± 1%, ± 0.5 cm/s
Sampling Rate:	Maximum 1 Hz (data averaged internally at higher rates)

	Transducer Module:	Electronics:
Operating Temperature:	0 to 40 C°	-5 to 45 C°
Storage Temperature:	-10 to 50 C°	-20 to 60 C°

Dimensional Drawings

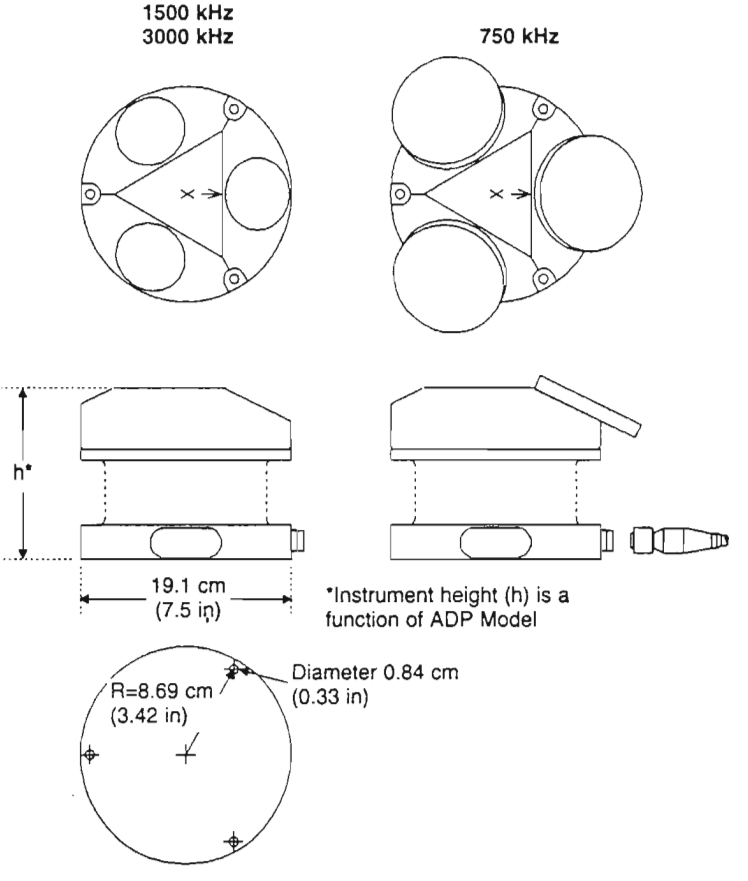

For more information about the ADP or to receive news about other water velocity meters, please call 619-695-8327, fax us at 619-695-8131, or send an e-mail to inquiry@sontek.com

SonTek

7966 Arjons Drive, Suite D
San Diego, CA 92126
Tel: (619) 695-8327
Fax: (619) 695-8131

630

Specifications subject to change without notice
© Sontek 1995

ADP/Ver 2.0/Q1000/Feb 1/95

High-quality test results from Tampa Bay

A SonTek Acoustic Doppler Profiler (ADP) was deployed for two days of testing in Tampa Bay. The test, part of a public-private partnership program organized by NOAA's National Ocean Service with logistic support from the University of South Florida, compared SonTek's ADP with the Acoustic Doppler Current Profiler used in the Tampa Port Project. The tests produced exceptionally good results with mean velocity differences of about 1 cm/s and clearly show the low-cost ADP to be comparable to the high-priced Current Profiler presently used. The ADP recorded the velocity data from 1 m above the bottom to 1 m below the surface, showing no sign of data loss in the so-called surface sidelobe layer. SonTek is very satisfied with the results, and we are pleased that the ADP provides both great value and cutting-edge performance.

The PC-based ADP was deployed with a small boat near the Port Tampa Current Profiler (PTCP) on April 3 and April 4, 1995. The 1.5 MHz ADP was configured for 1 m range cells and velocity profiles were averaged and recorded every minute. The PTCP recorded data every six minutes.

On Day 1 (see map), the ADP was deployed about 20 m from the shore station and about 25 m from the PTCP. During increasing flood, the position of the ADP was such that eddies from a nearby structure were visibly shedding into the acoustic beams. Reasonable agreement was obtained during the peak currents, but the effect of the land-based structures was still considerable, and the ADP measured lower currents than the PTCP.

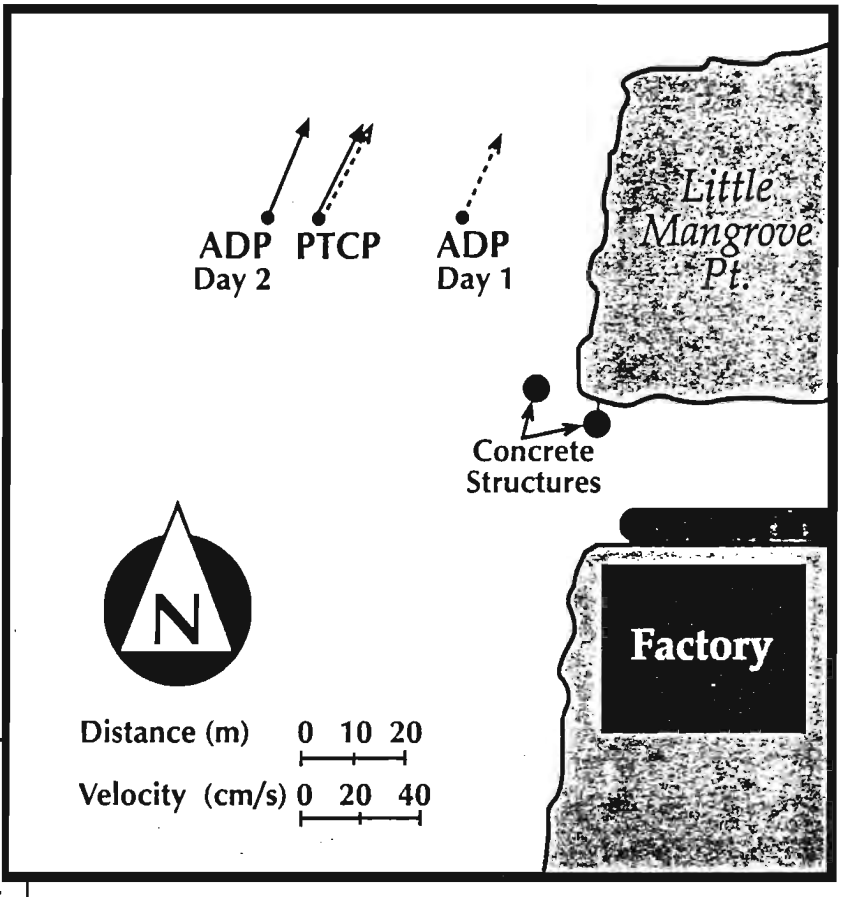

The arrows show the magnitude and direction of the three-hour mean current in a 1-m range cell located 5 m below the surface.

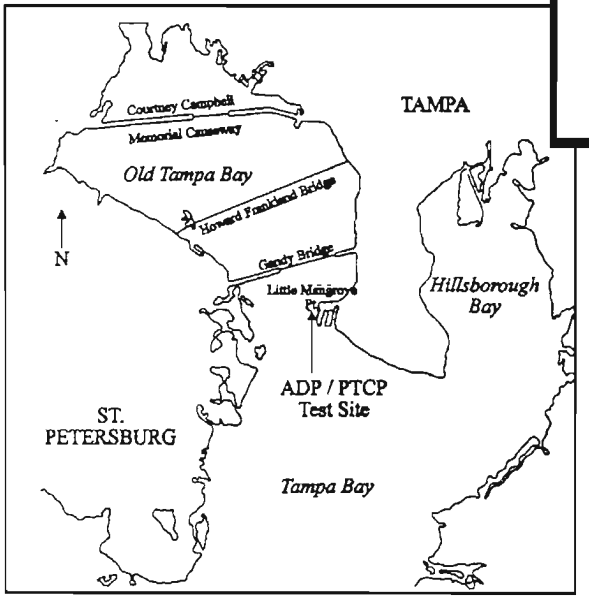

631

NOAA Tests — continued

On Day 2, the ADP was deployed within 15 m of the PTCP in the middle of the channel and cabled to an anchored boat. Data were accumulated in a PC for approximately three hours. Results were exceptionally good for a field intercomparison considering spatial, timing, and sampling differences. Comparing six-minute averages (see below), the difference in mean current speed is about 1 cm/s. Differences in the mean direction are equally small, with a maximum difference of 3° in the range cells located 4-5 m below the surface. The pronounced sidelobe effect in the PTCP (2 m below the surface) is not visible in the profile from the ADP. In the bottom boundary layer, the ADP measures a stronger shear than the PTCP. This is believed to be a positive result of the robust ADP-design, where the velocity at each level is measured independently to ensure superb resolution of velocity gradients.

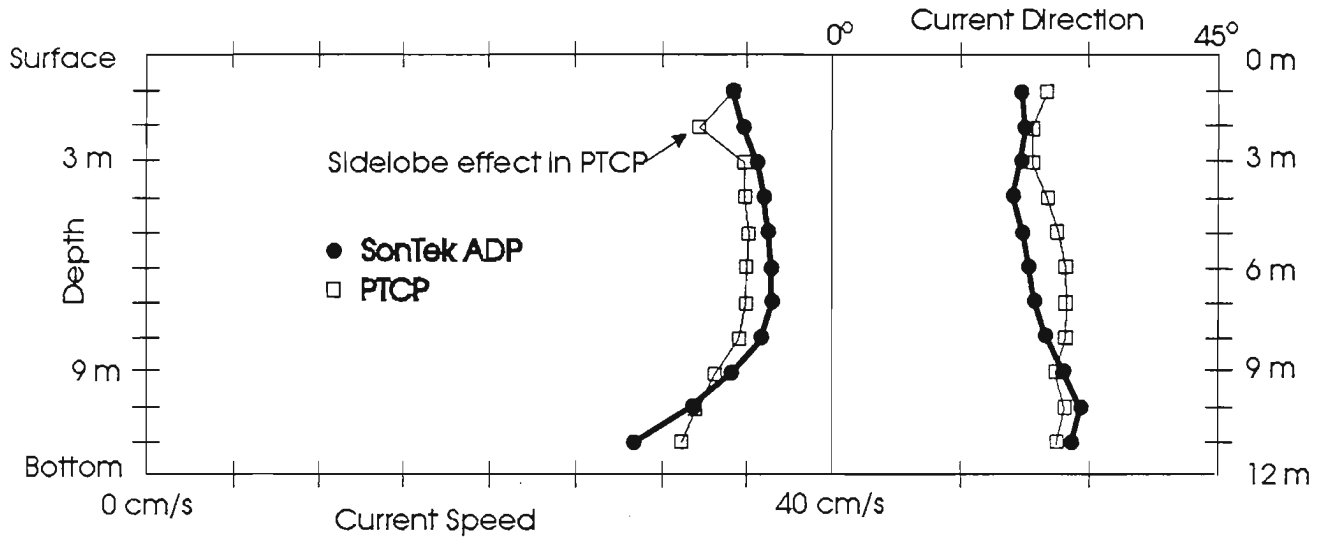

Both instruments were deployed at a depth of approximately 12 m. The profiles show the mean horizontal velocity over a period of 2.7 hours of increasing flood.

Calibration Test

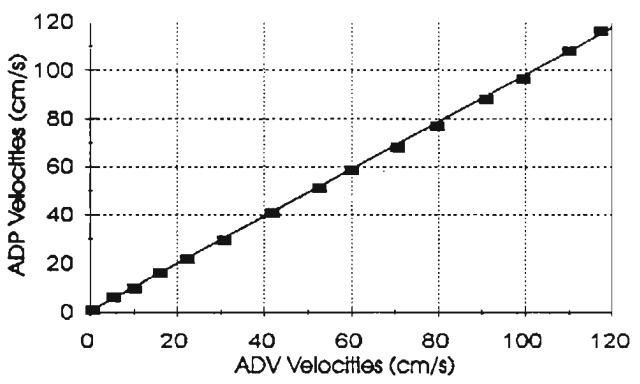

Flume testing at Scripps:

Before the test at Tampa Bay, a one-beam ADP was checked against a calibrated Acoustic Doppler Velocimeter (ADV) in a current flume at Scripps Institution of Oceanography. The one-beam ADP was oriented horizontally into the flow, and the ADV measured the water velocity at the same level as the ADP and to the side of the beam. A least-square fit of the data shows the slope to be 0.98 and the correlation to be better than 0.999.

For more information about the ADP or to learn more about other water velocity meters, please call 619-695-8327, fax us at 619-695-8131, or send an e-mail to inquiry@sontek.com

SonTek

7966 Arjons Drive, Suite D
San Diego, CA 92126
Tel: (619) 695-8327
Fax: (619) 695-8131
inquiry@sontek.com

632

PC-Based Model

SONTEK ADP

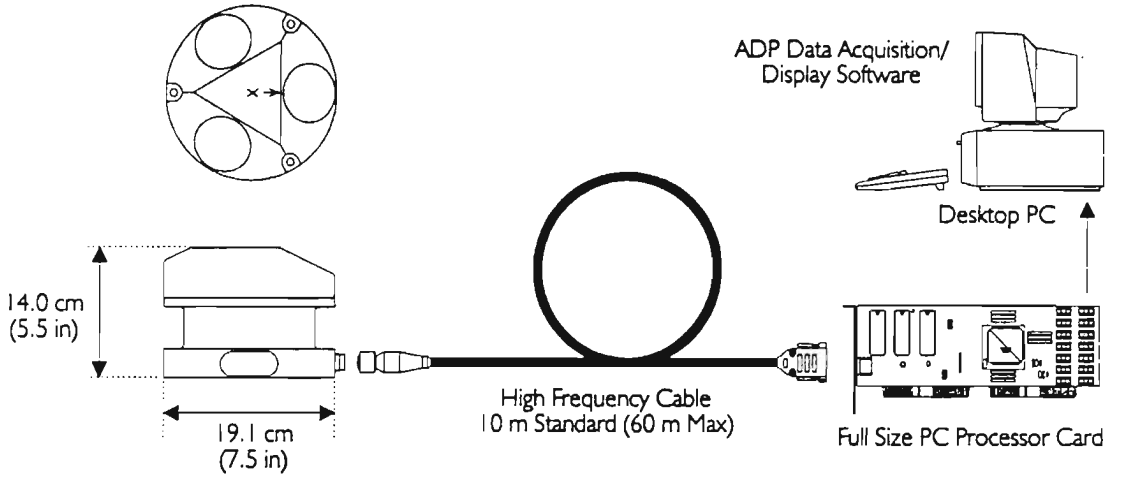

ADP specifications:

- Low profile transducer module easily mounts for profiling up, down or sideways.
- Supports cable lengths to 60 m (200 ft).
- Operates from the PC power supply. Voltages in the cable do not exceed ±12 VDC (50 mA) and 20 Vrms AC (200 mA).

Software:

- Automatically configures full-size PC card for system operation.
- Displays real-time data contour plots, time series at user selected depth and last vertical velocity profile.
- Data stored to computer hard disk.

Optional Sensor:
Compass/tilt: accurate to ±0.5° heading, ±0.2° tilt.

User-supplied computer for use with ADP:
Minimum 386 with co-processor, VGA graphics, hard disk, space for full-sized board (ISA-bus).

SonTek's ADP is a high-performance, cost-effective Acoustic Doppler Current Profiler. The PC-based version of the ADP provides an affordable and user friendly solution for current measurements in environments with access to AC power. Applications include surveys from piers, bridges, offshore platforms and stationary vessels.

The PC-based system includes transducer module with front end electronics, processor card, and standard 10 m cable.

For more information, call our technical sales group to discuss how SonTek can meet your current measurement needs.

SonTek

7966 Arjons Drive, Suite D
San Diego, CA 92126
Tel.: (619) 695-8327
Fax : (619) 695-8131
Internet: inquiry@sontek.com

633

APPENDIX C
Representative Current Profile Plots

635

Delaware Bay Current Measurements

Profile 1A, Peak Ebb

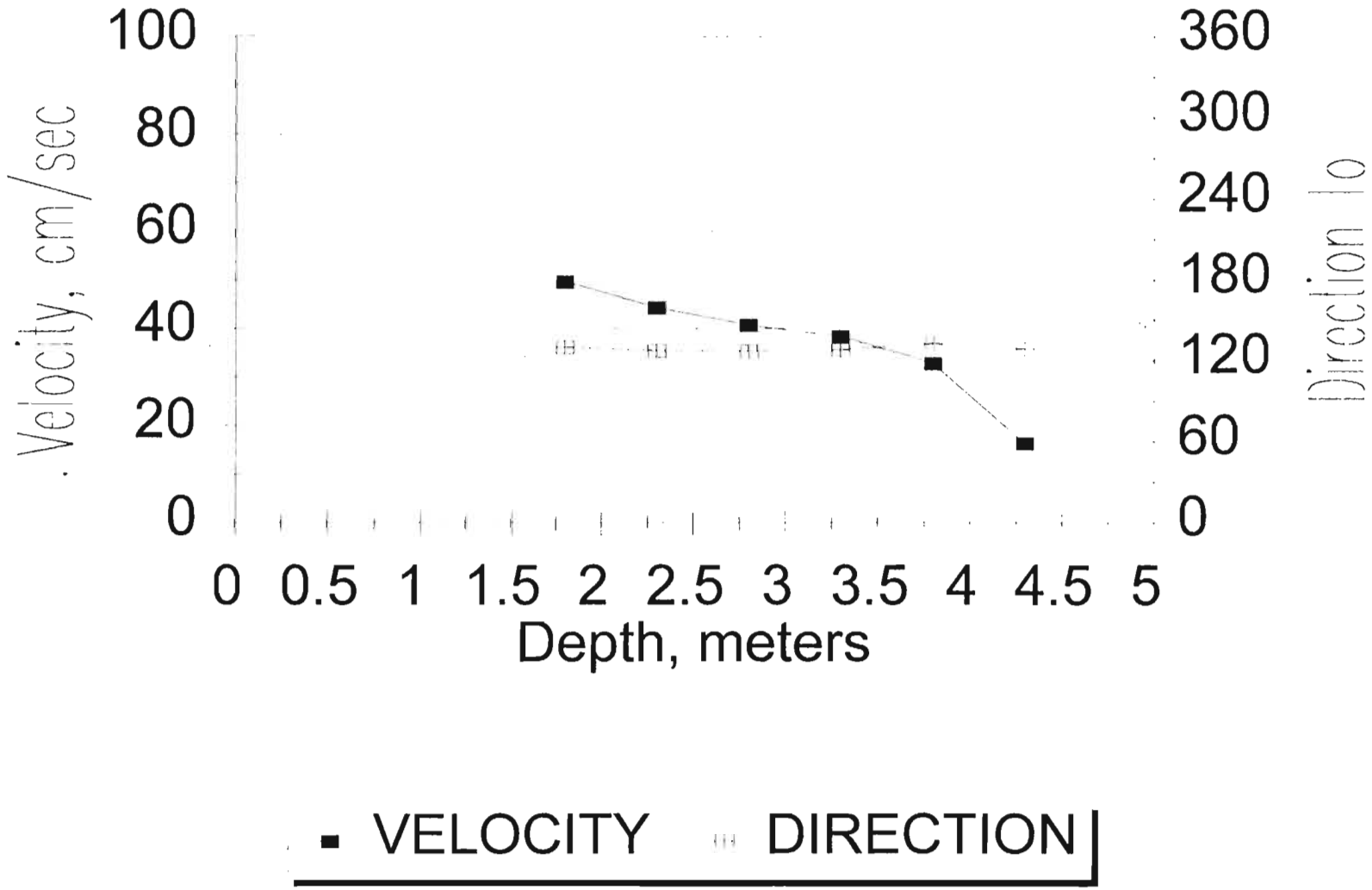

Delaware Bay Current Measurements

Profile 1A, Peak Flood

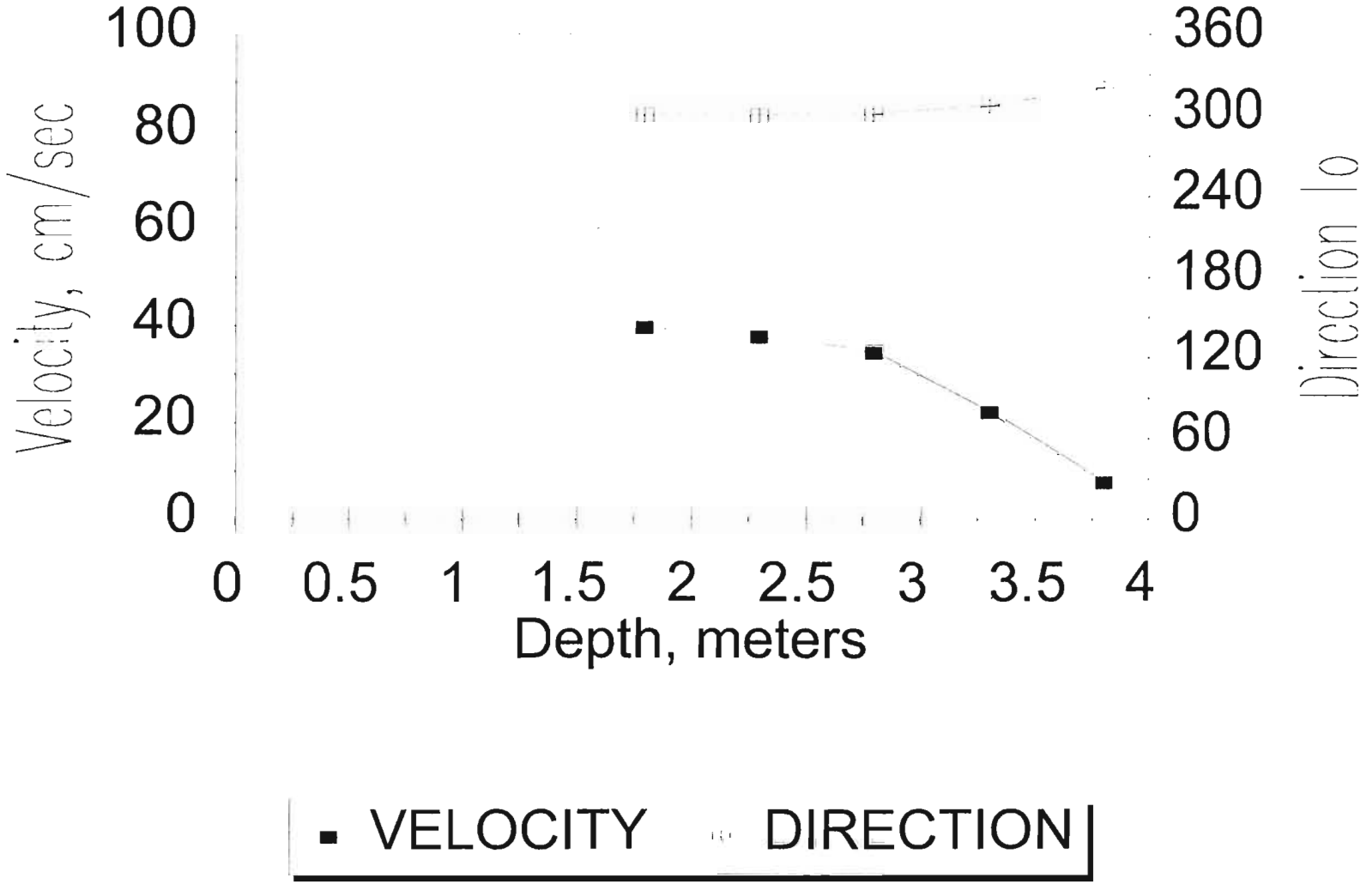

637

Delaware Bay Current Measurements

Profile 3A, Peak Ebb

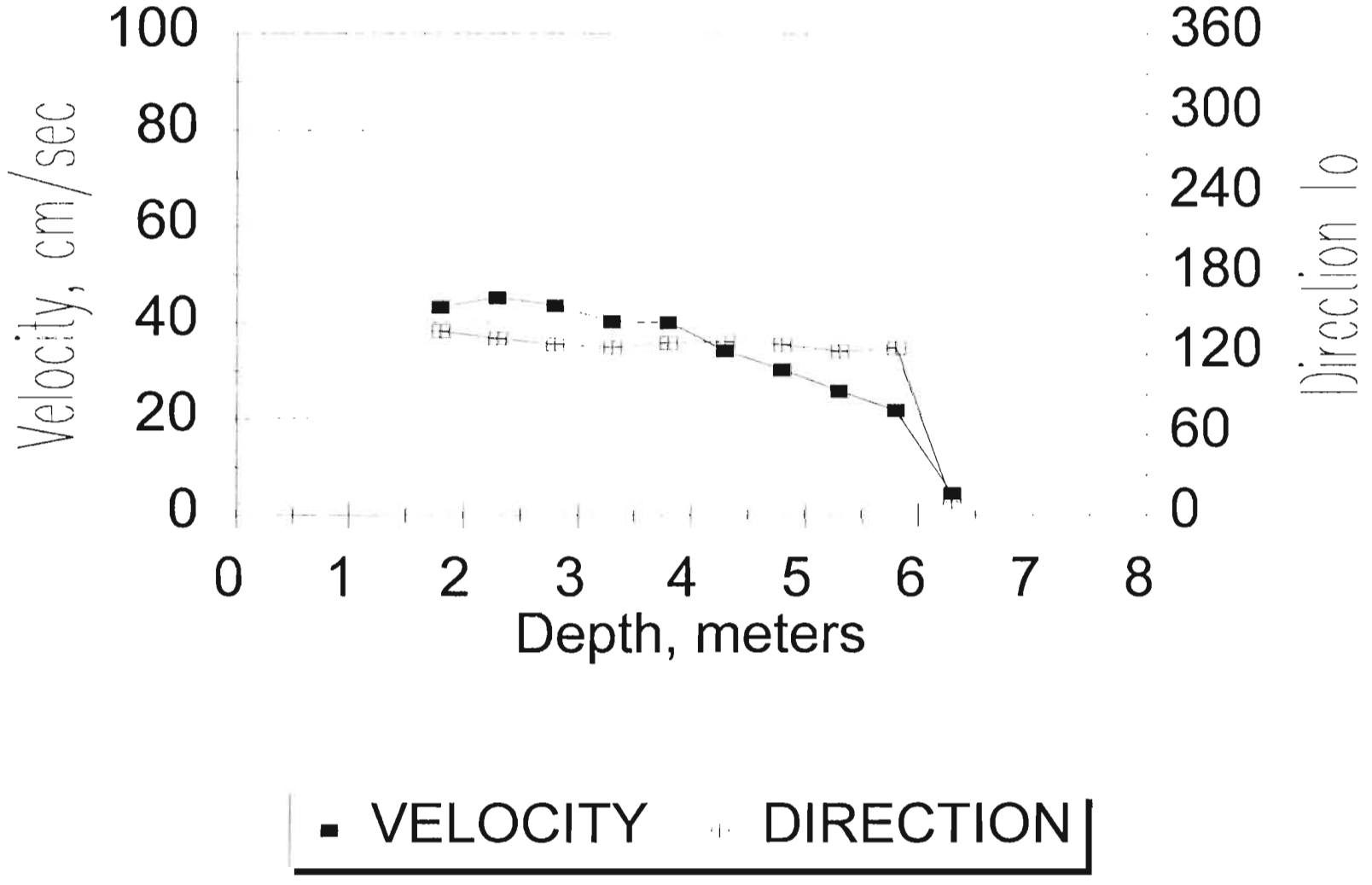

Delaware Bay Current Measurements

Profile 3A, Peak Flood

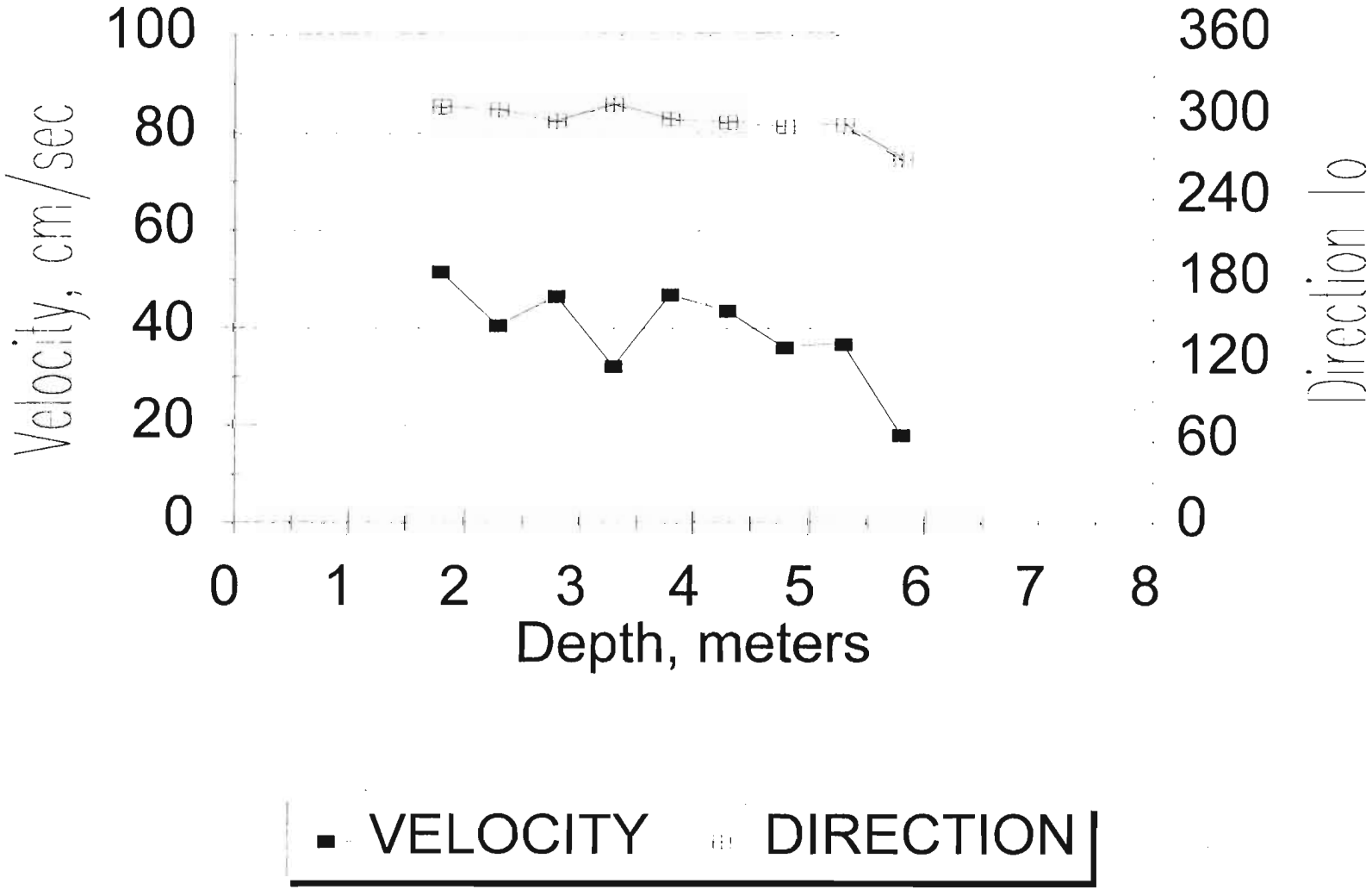

Delaware Bay Current Measurements

Profile 5A, Peak Flood

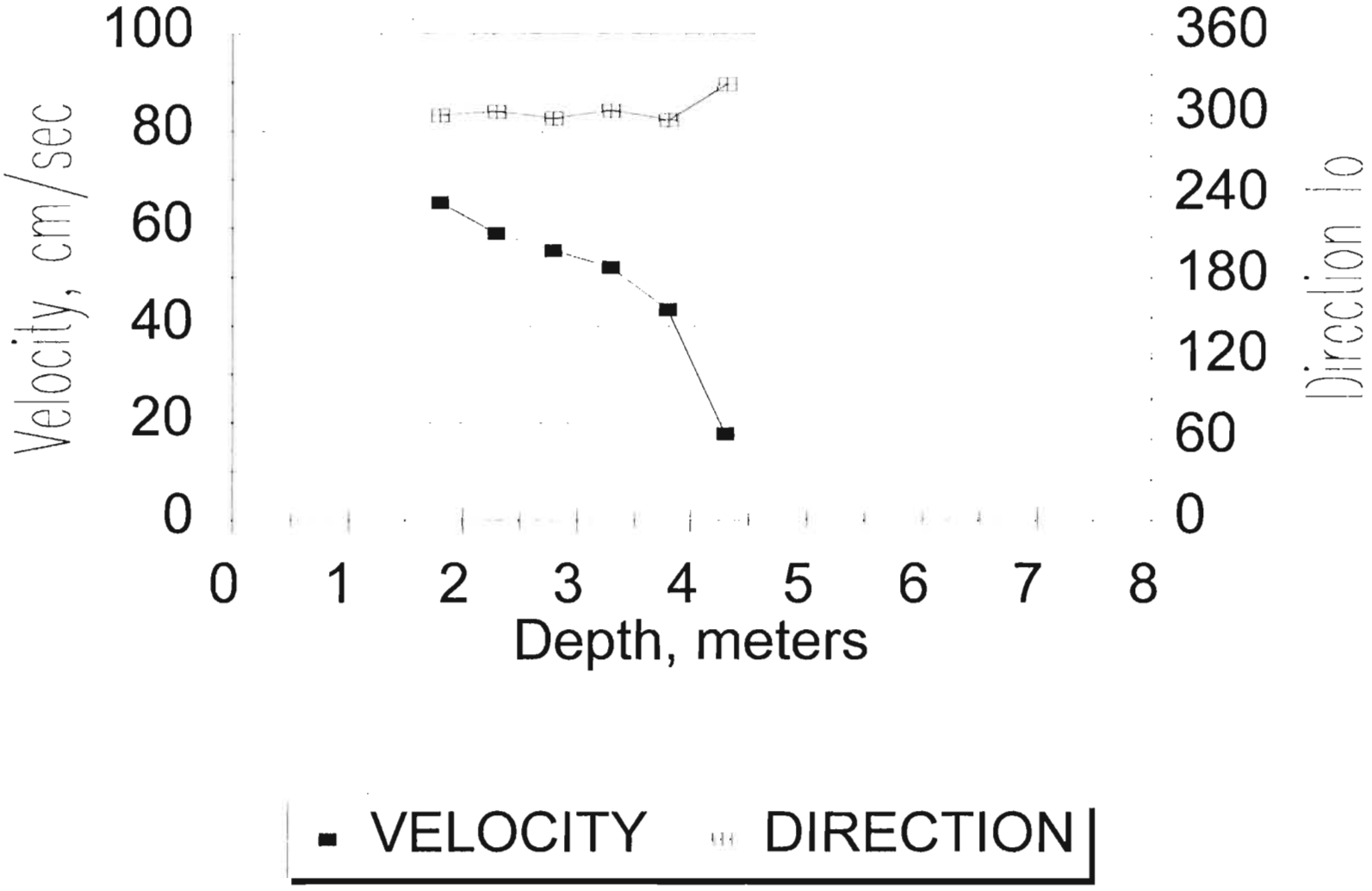

Delaware Bay Current Measurements

Profile 5A, Peak Ebb

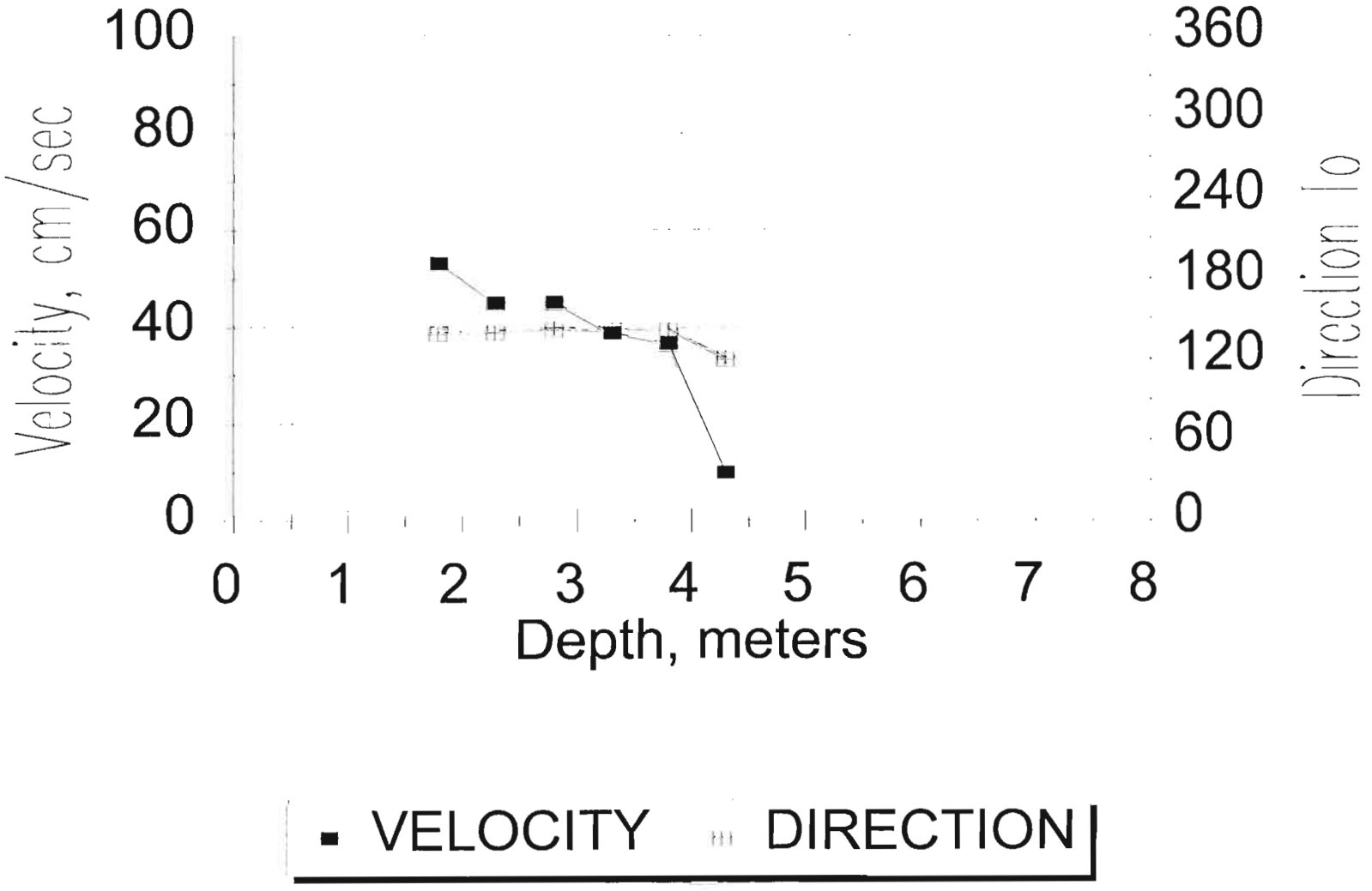

Delaware Bay Current Measurements

Profile 1C, Peak Ebb

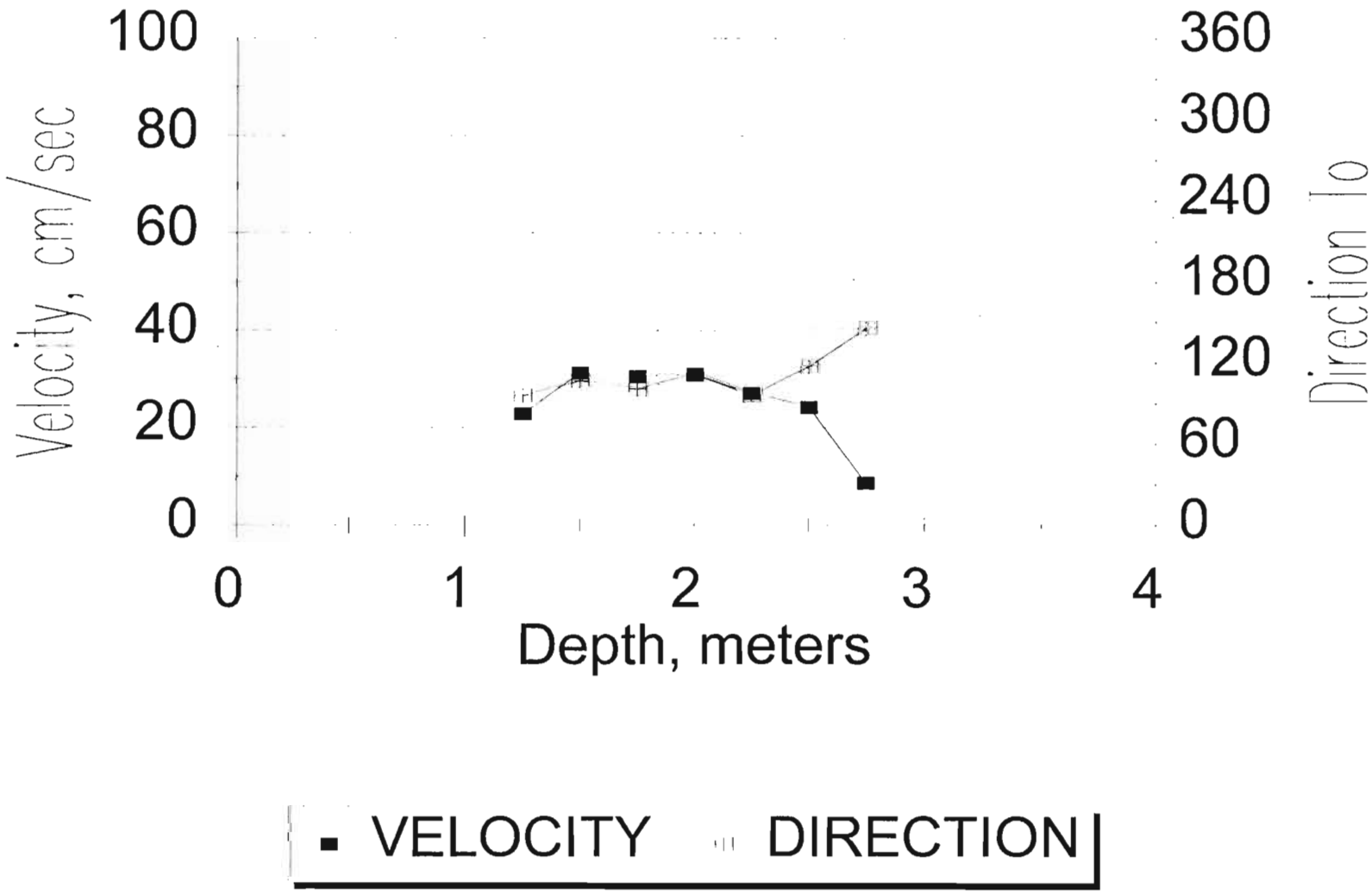

Delaware Bay Current Measurements

Profile 1C, Peak Flood

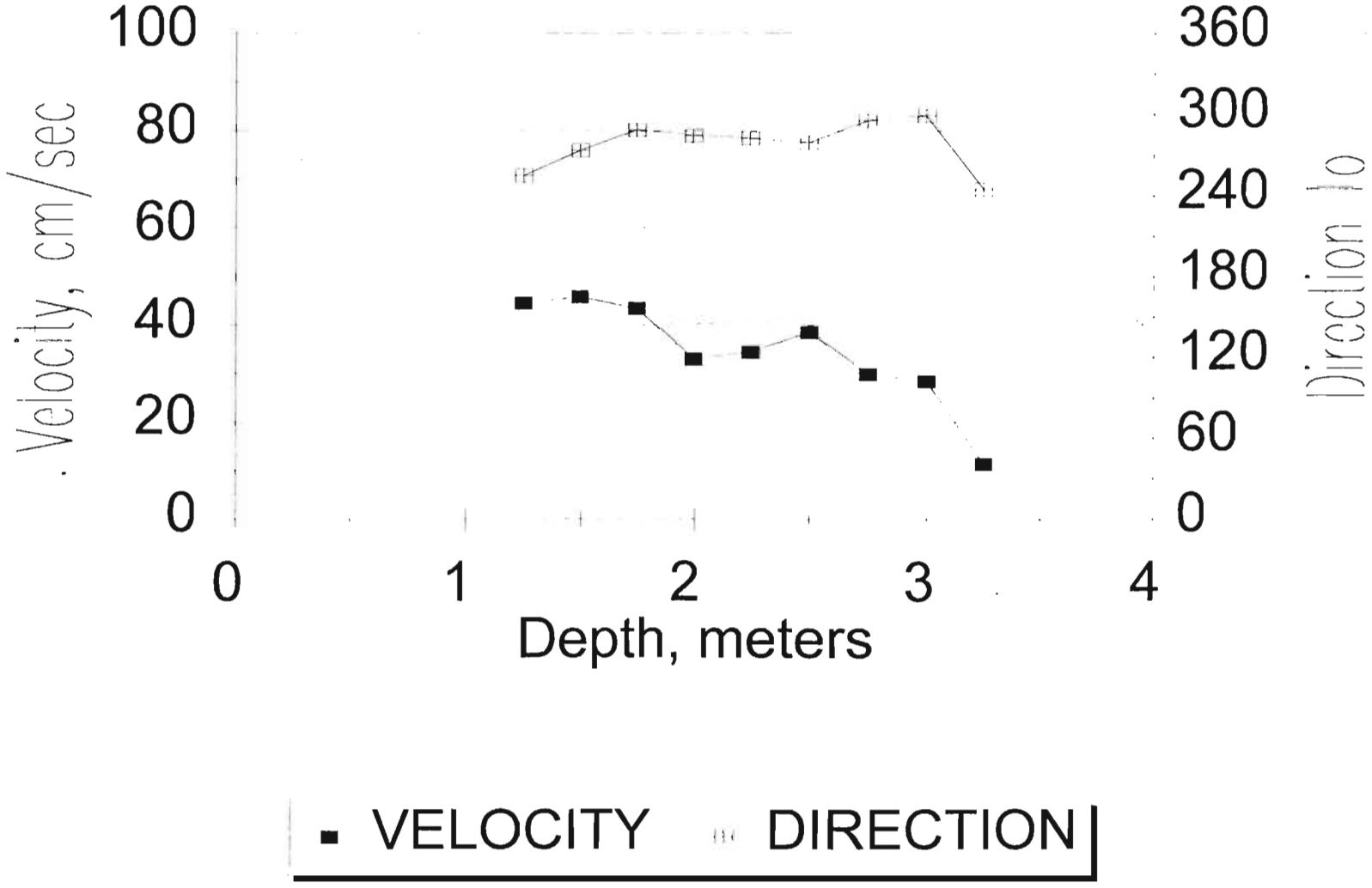

Delaware Bay Current Measurements

Profile 3C, Peak Ebb

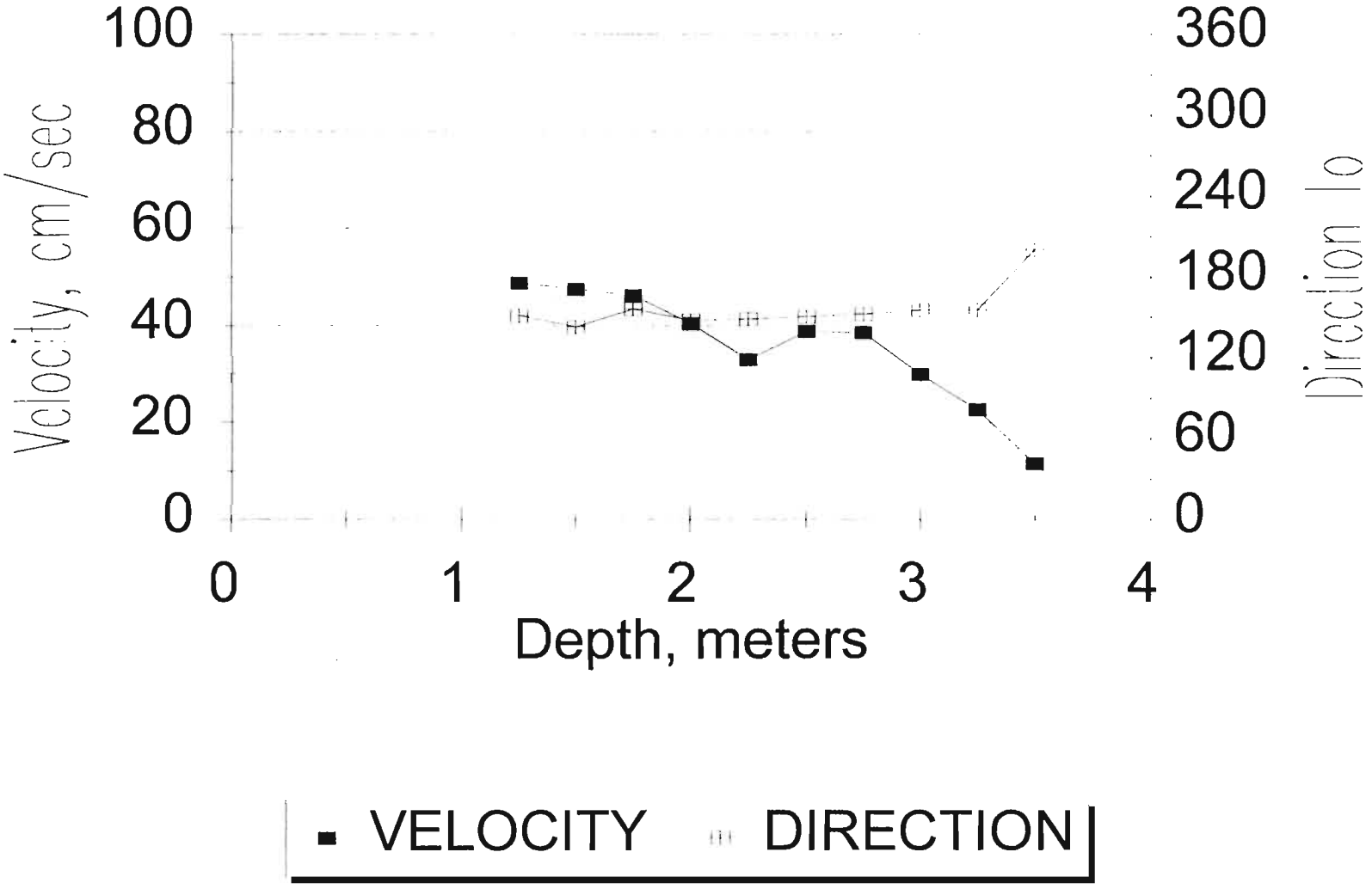

Delaware Bay Current Measurements

Profile 3C, Peak Flood

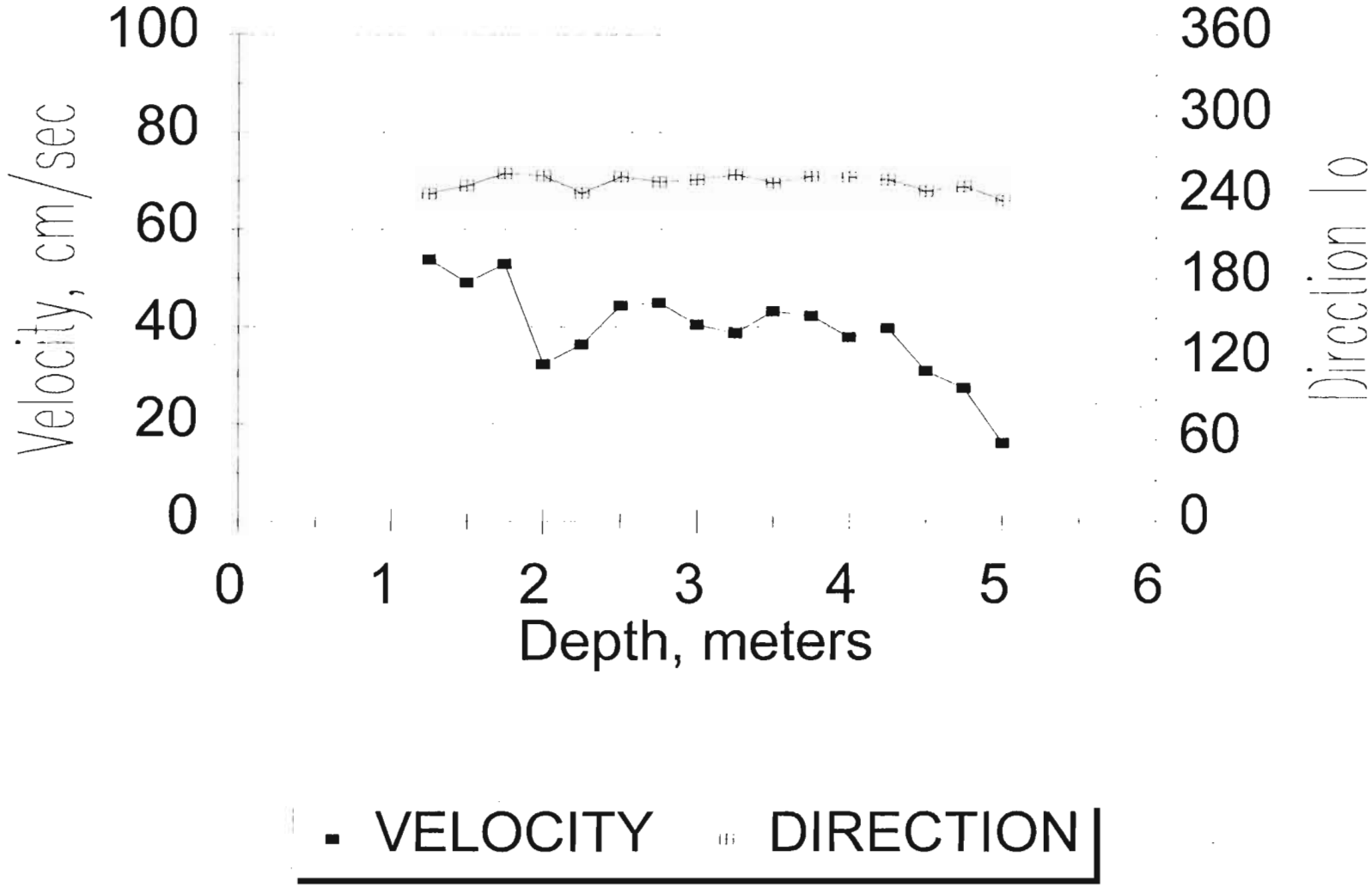

Delaware Bay Current Measurements

Profile 5C, Peak Ebb

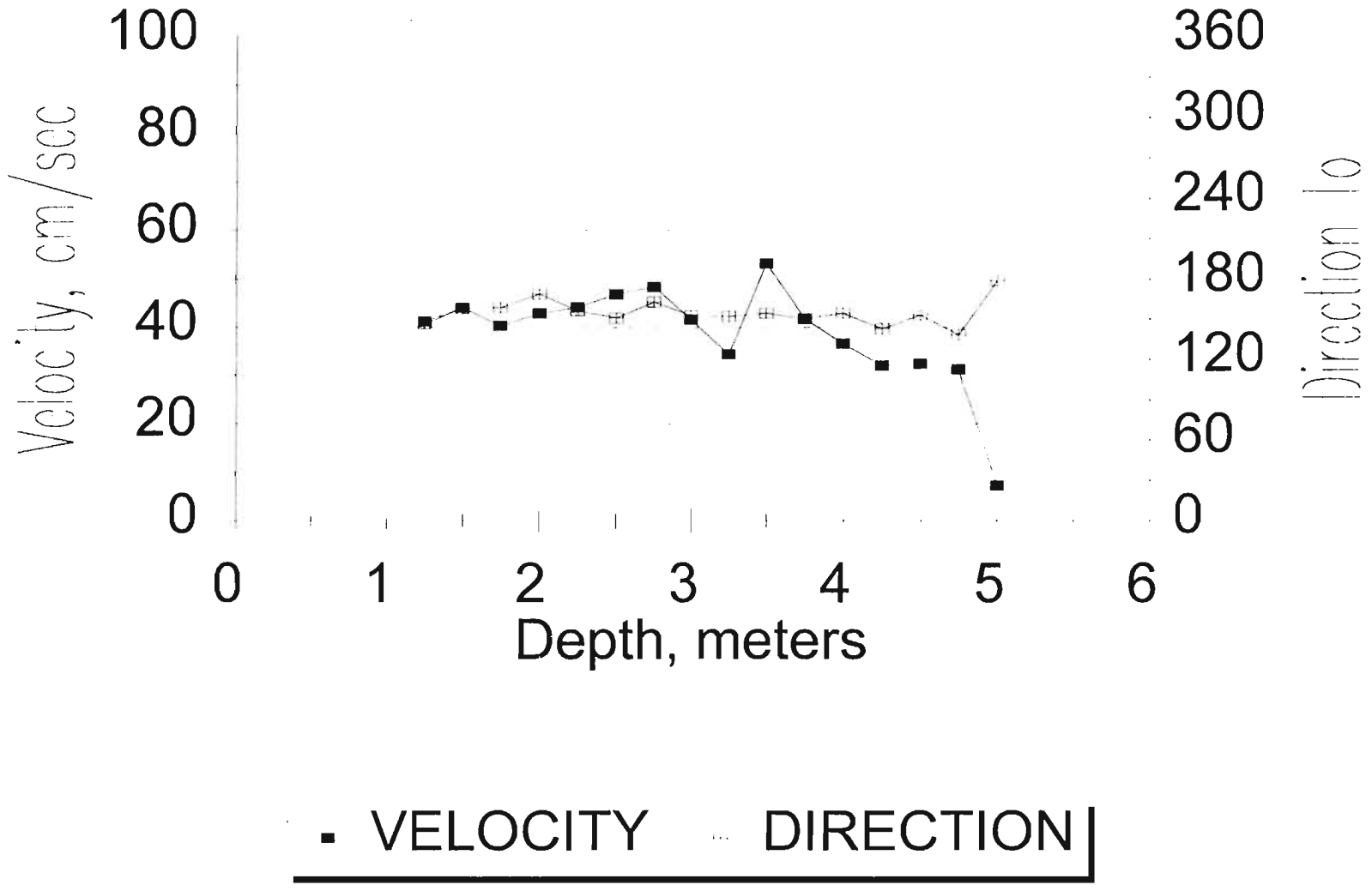

Delaware Bay Current Measurements

Profile 5C, Peak Flood

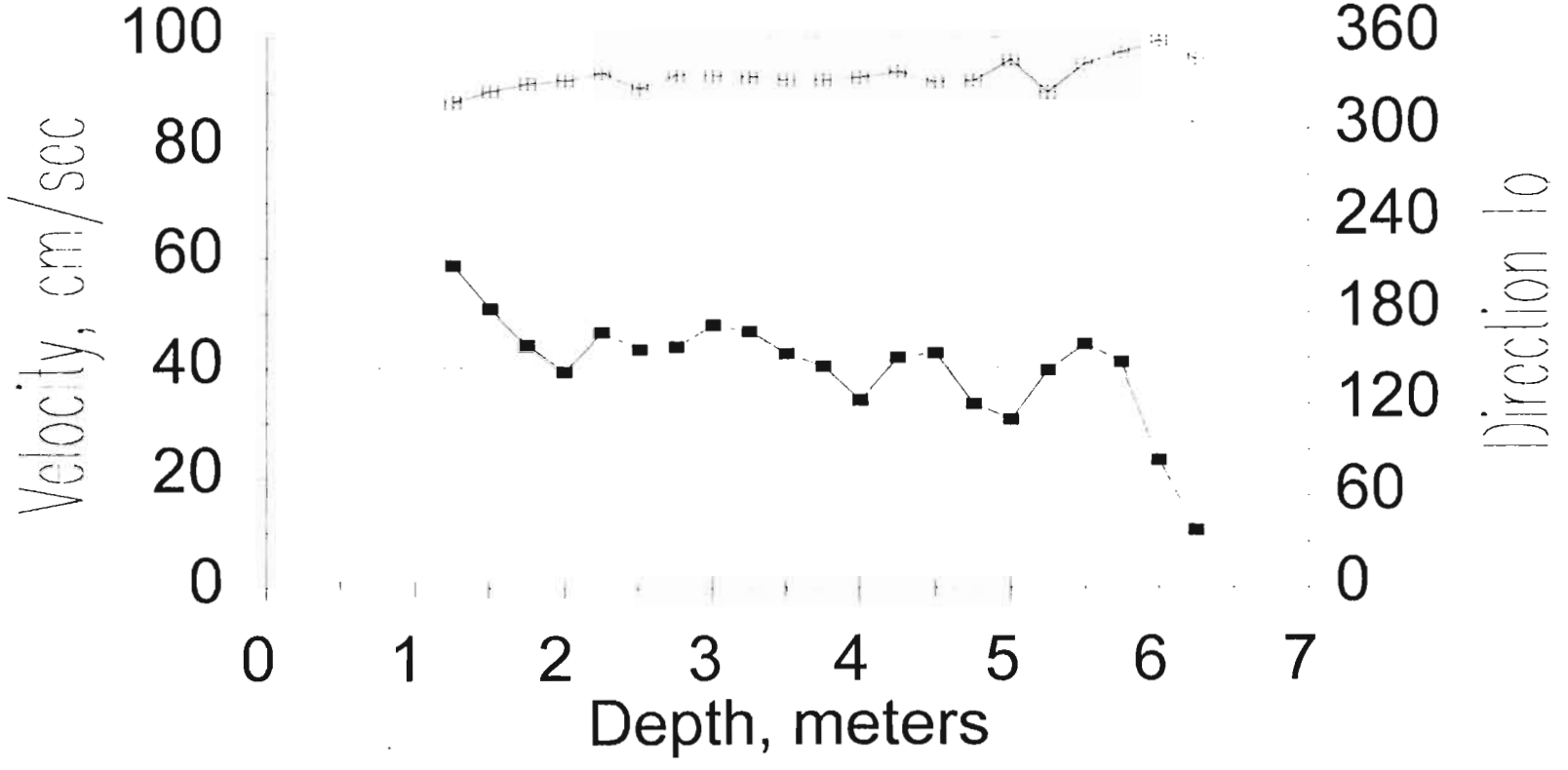

▪ VELOCITY ⁘ DIRECTION

Delaware Bay Current Measurements

Profile 1D, Peak Ebb

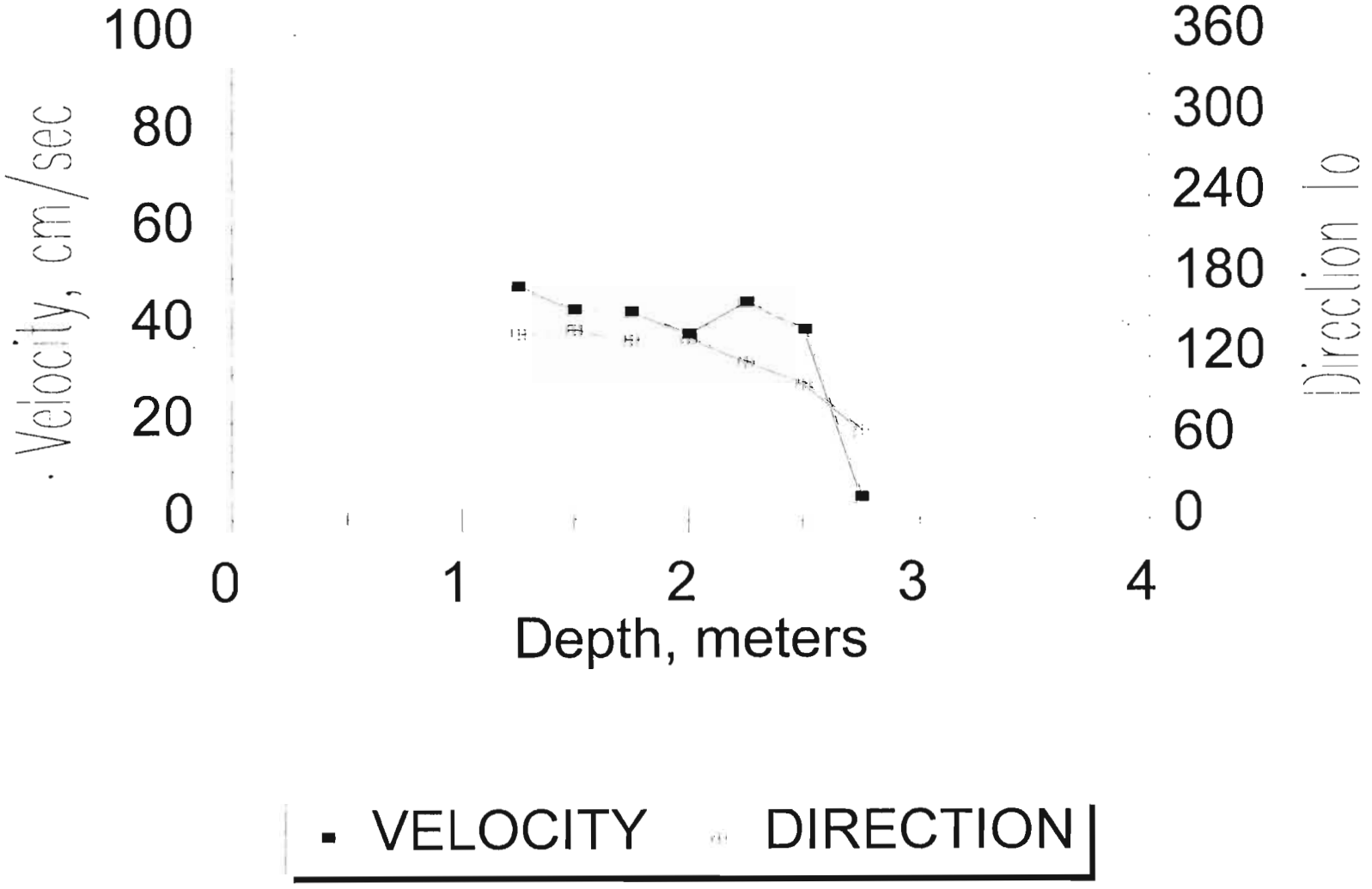

Delaware Bay Current Measurements

Profile 1D, Peak Flood

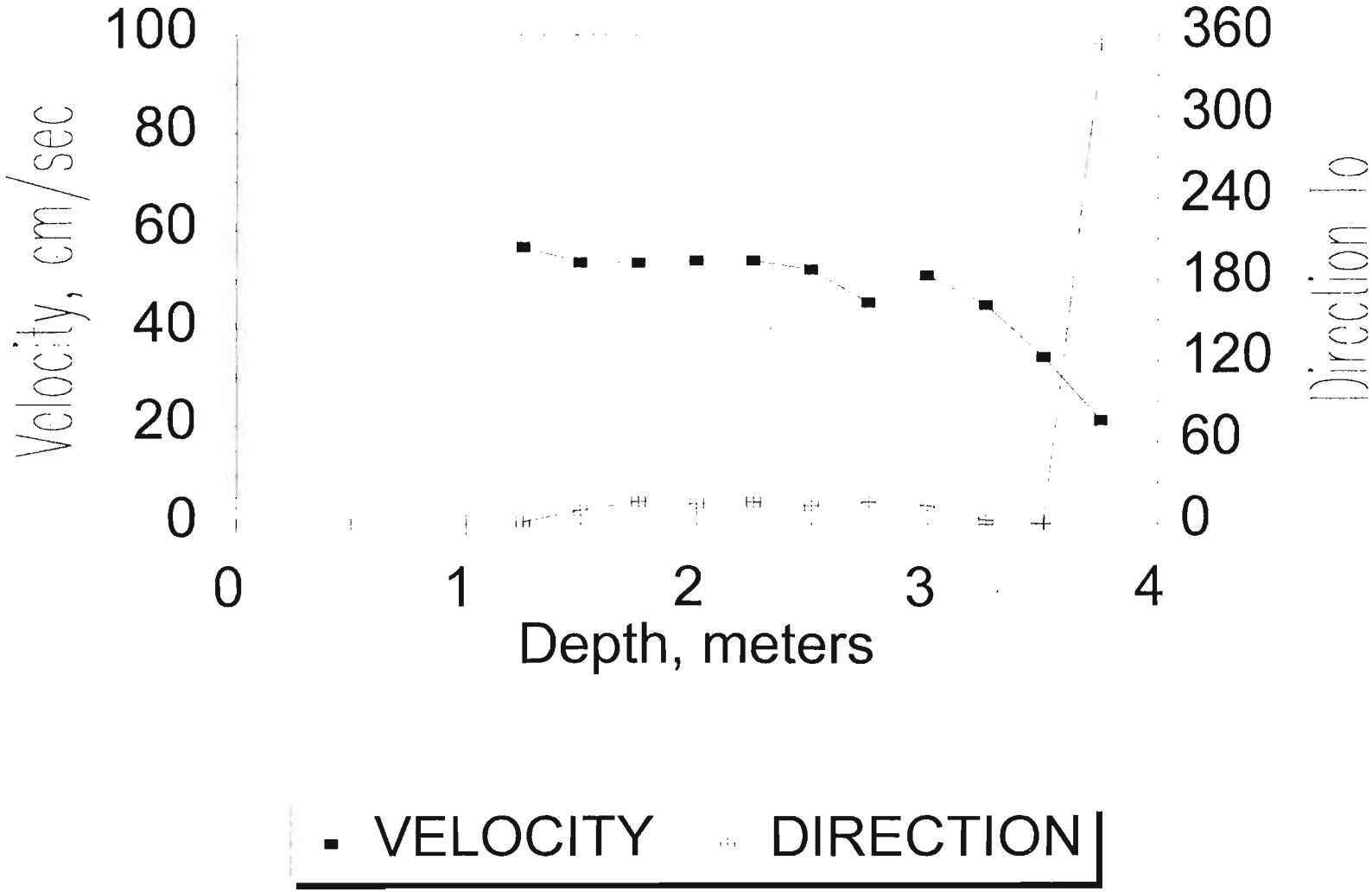

Delaware Bay Current Measurements

Profile 4D, Peak Ebb

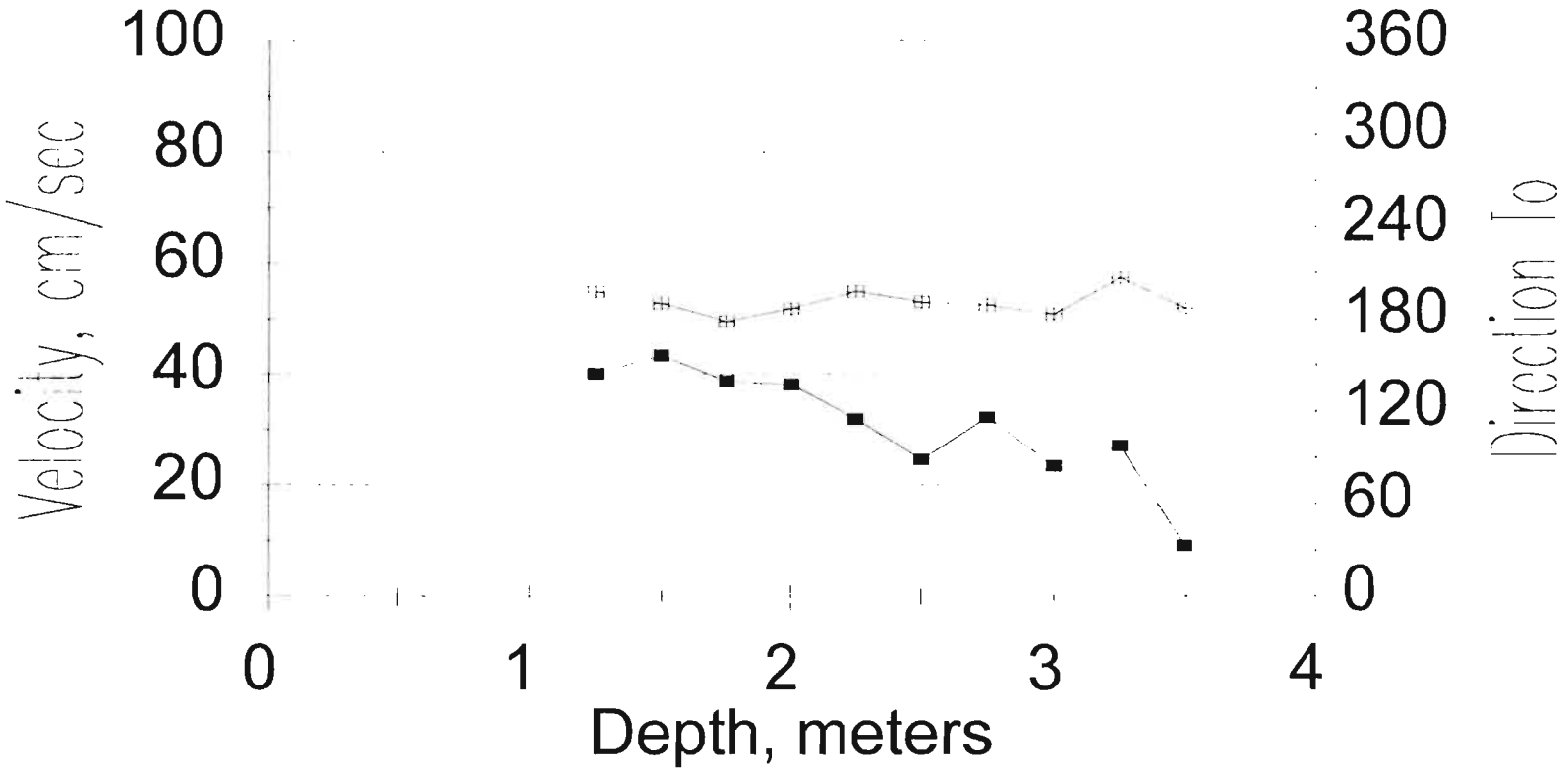

▪ VELOCITY ▫ DIRECTION

Delaware Bay Current Measurements

Profile 4D, Peak Flood

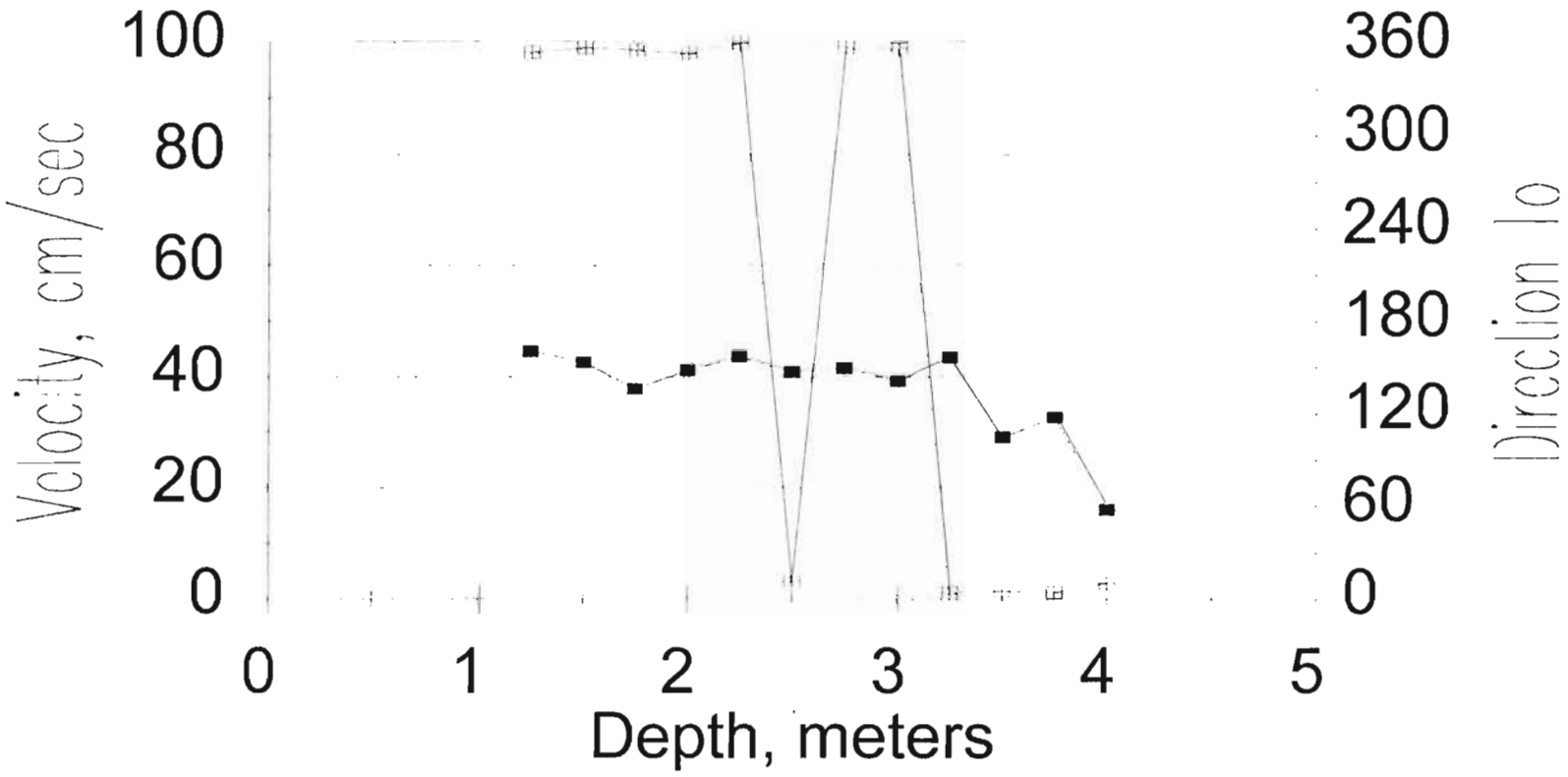

▪ VELOCITY ⁘ DIRECTION

Delaware Bay Current Measurements

Profile 5D, Peak Ebb

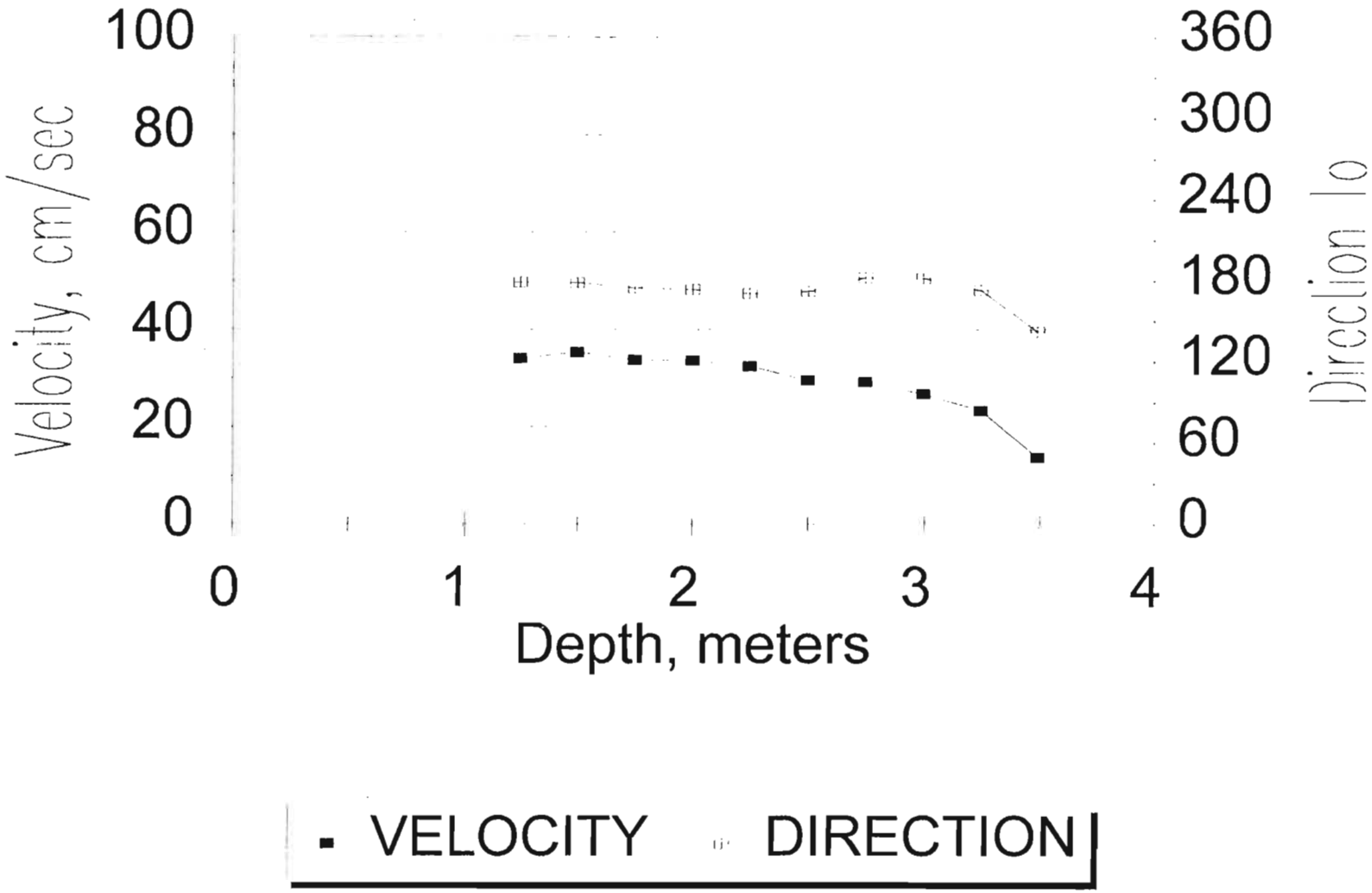

Delaware Bay Current Measurements

Profile 5D, Peak Flood

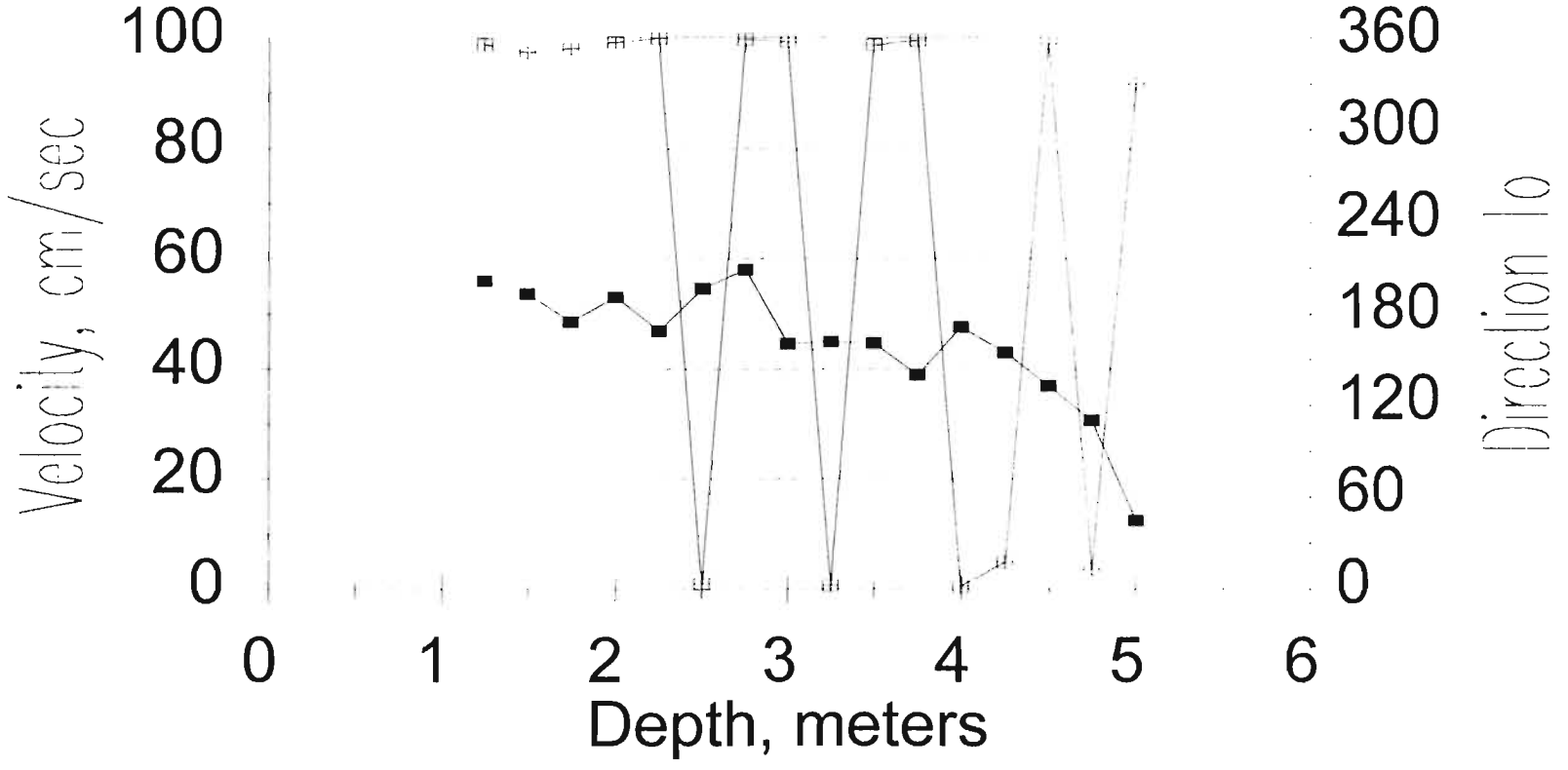

▪ VELOCITY ▫ DIRECTION

Delaware Bay Current Measurements

Profile 1E, Peak Ebb

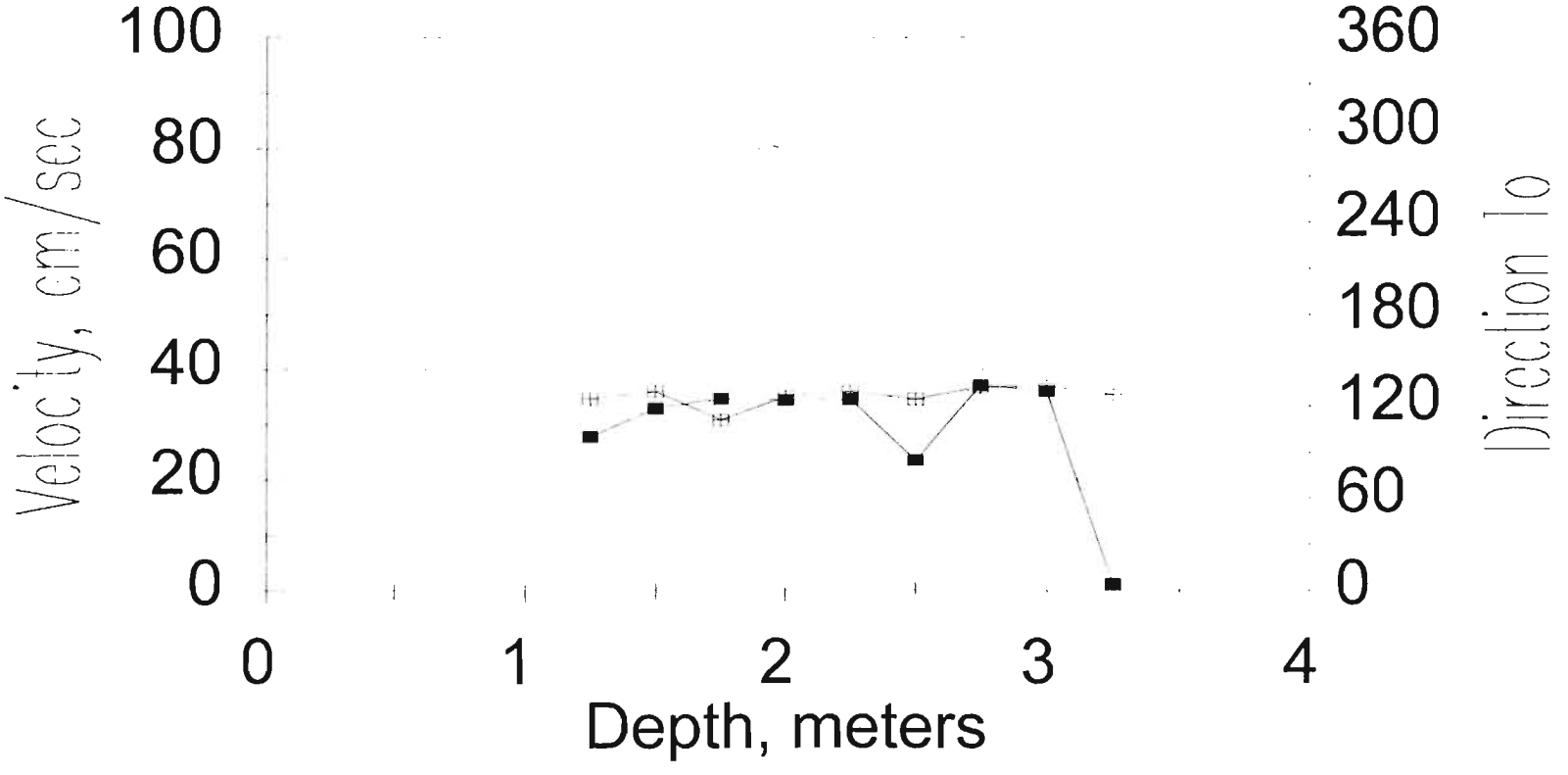

▪ VELOCITY ⋯ DIRECTION

Delaware Bay Current Measurements

Profile 1E, Peak Flood

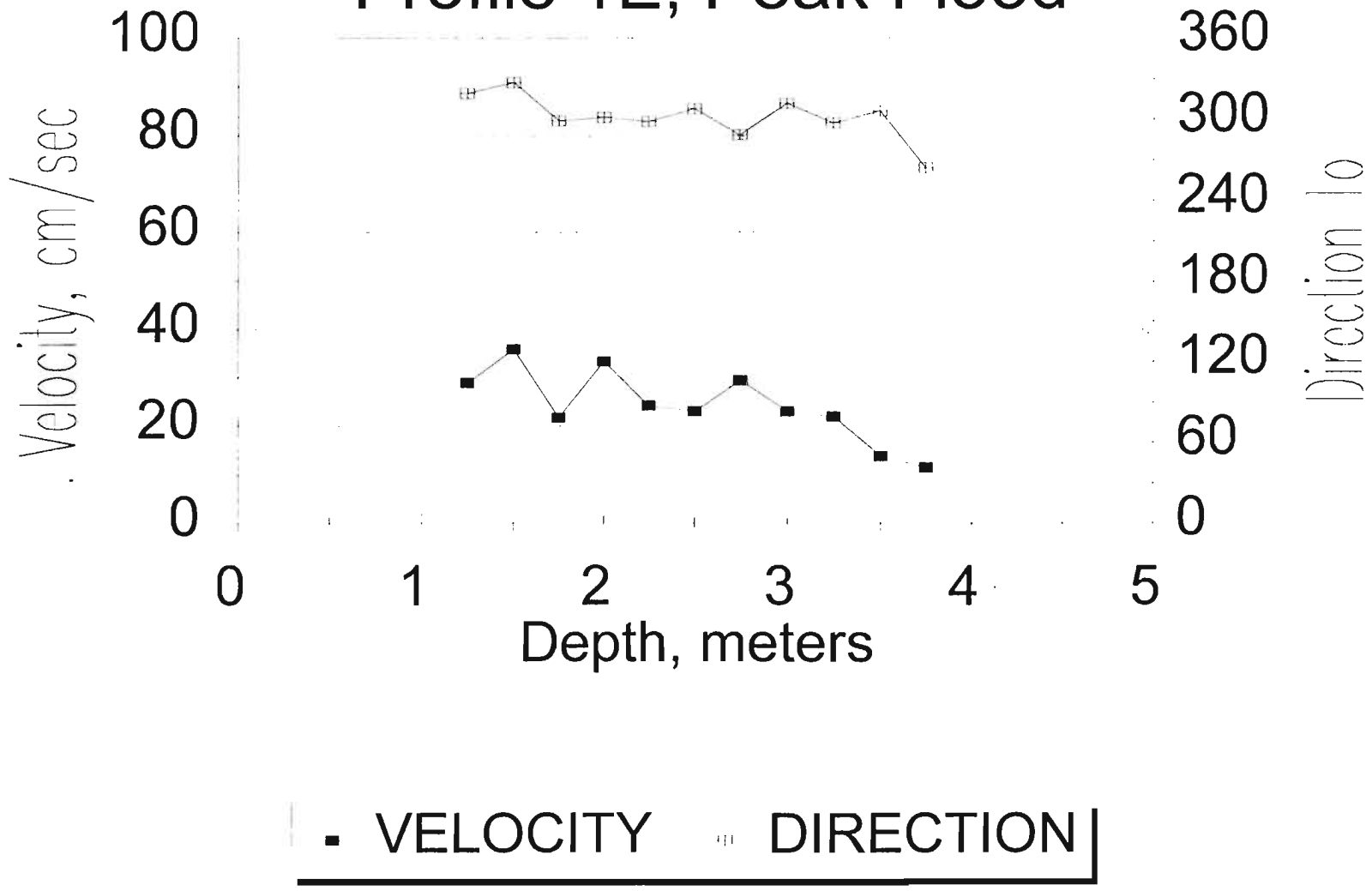

Delaware Bay Current Measurements

Profile 3E, Peak Ebb

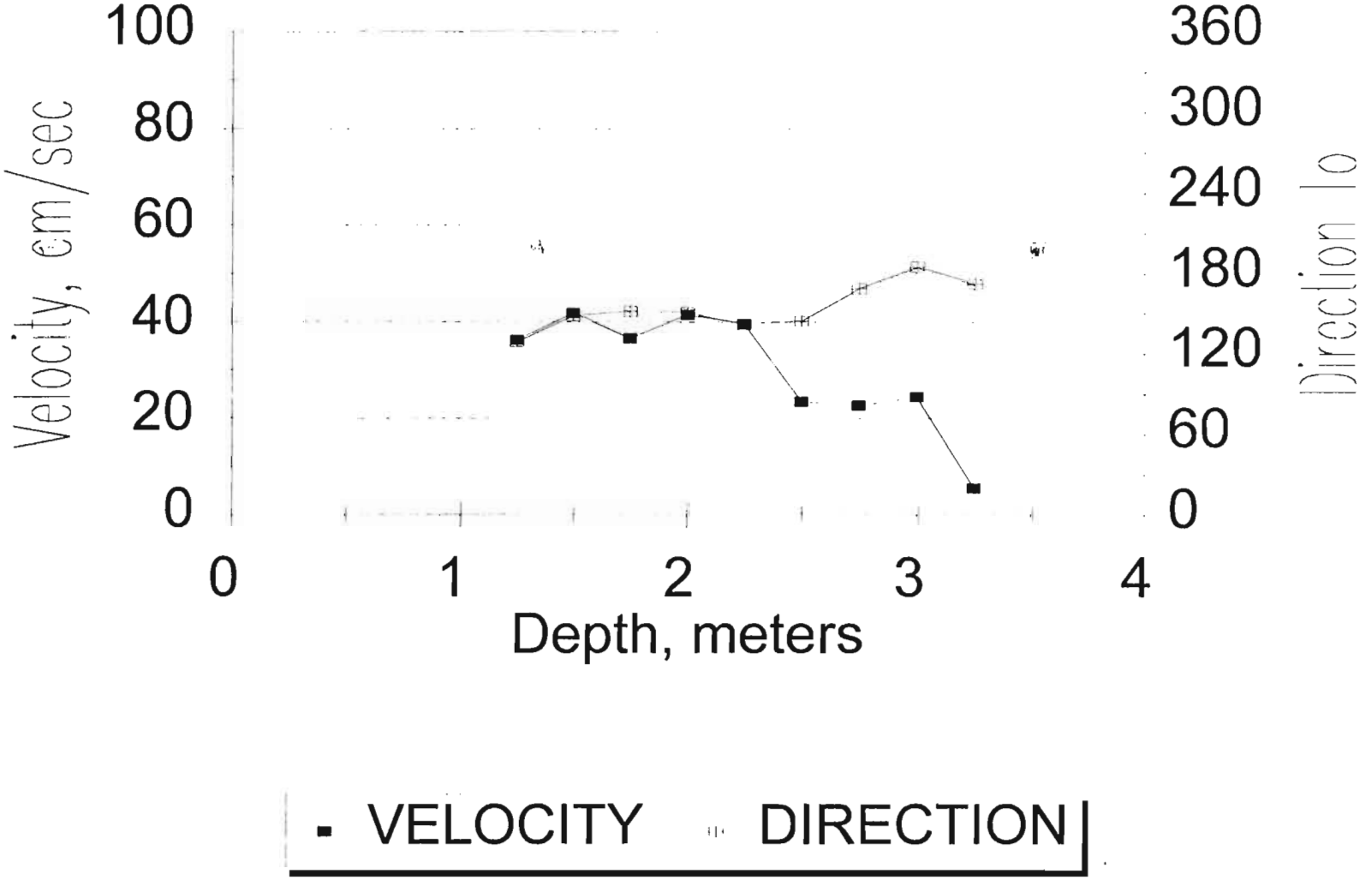

Delaware Bay Current Measurements

Profile 3E, Peak Flood

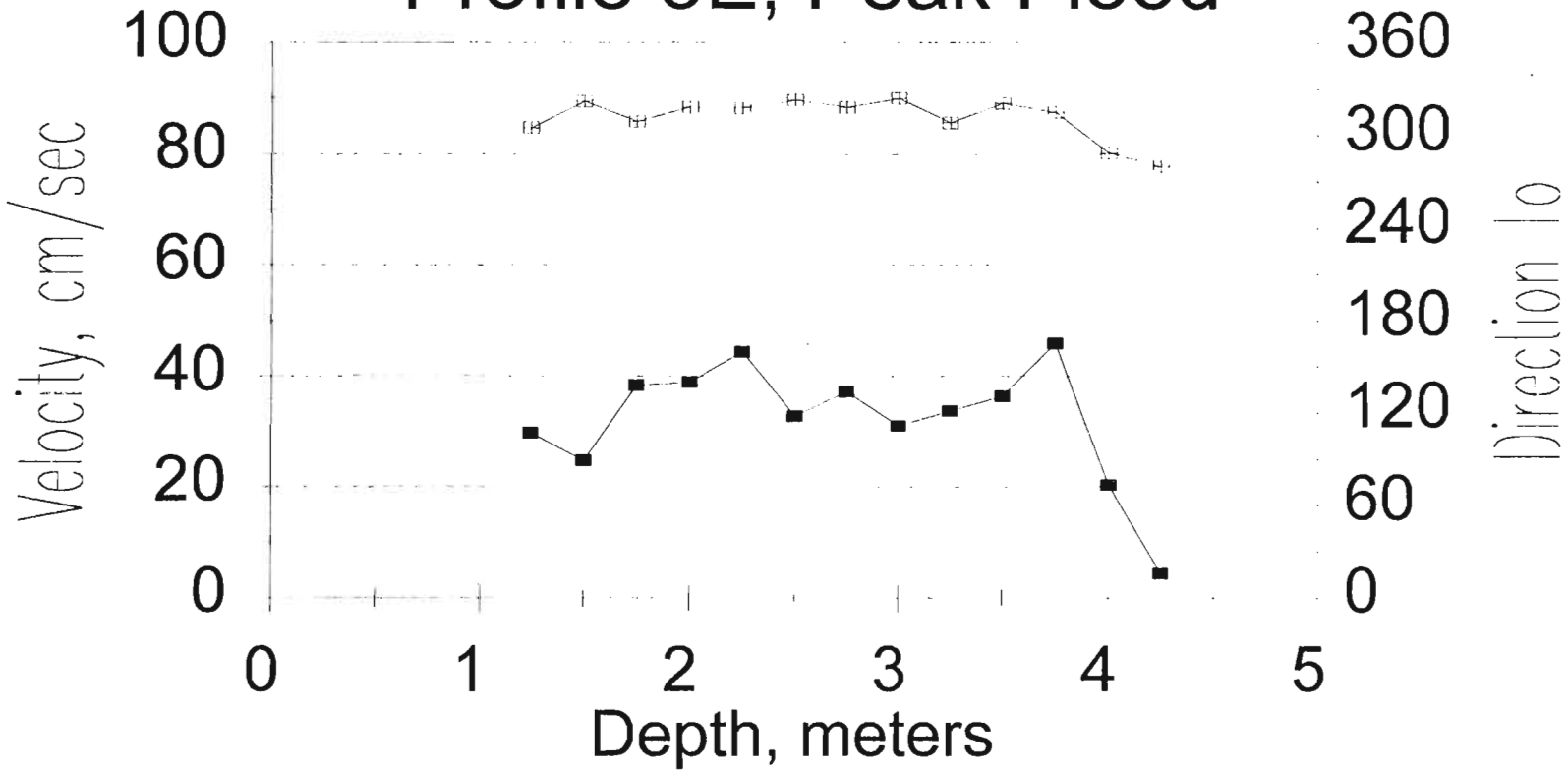

▪ VELOCITY ⁘ DIRECTION

259

Delaware Bay Current Measurements

Profile 6E, Peak Ebb

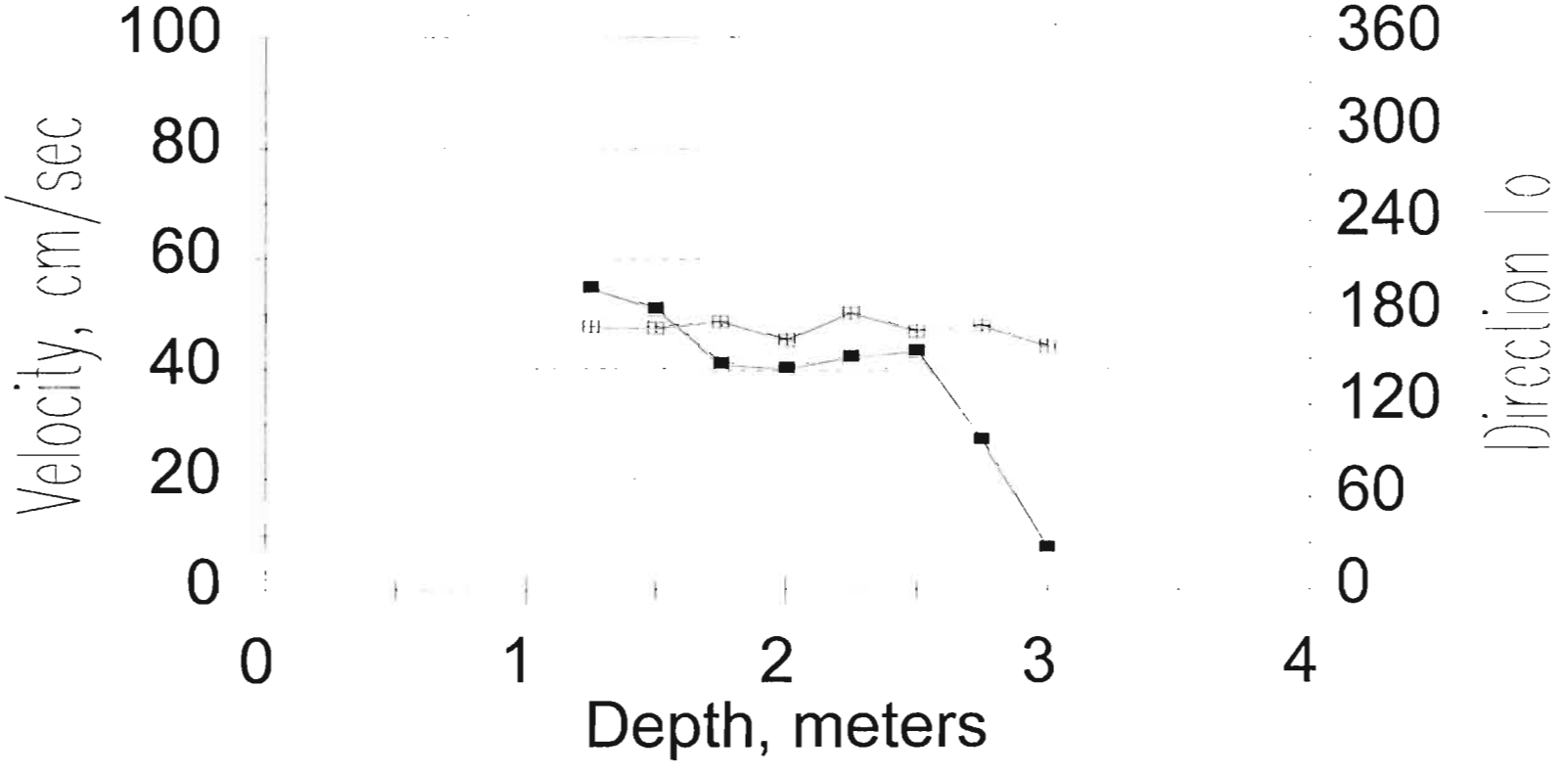

▪ VELOCITY ⁞ DIRECTION

Delaware Bay Current Measurements

Profile 6E, Peak Flood

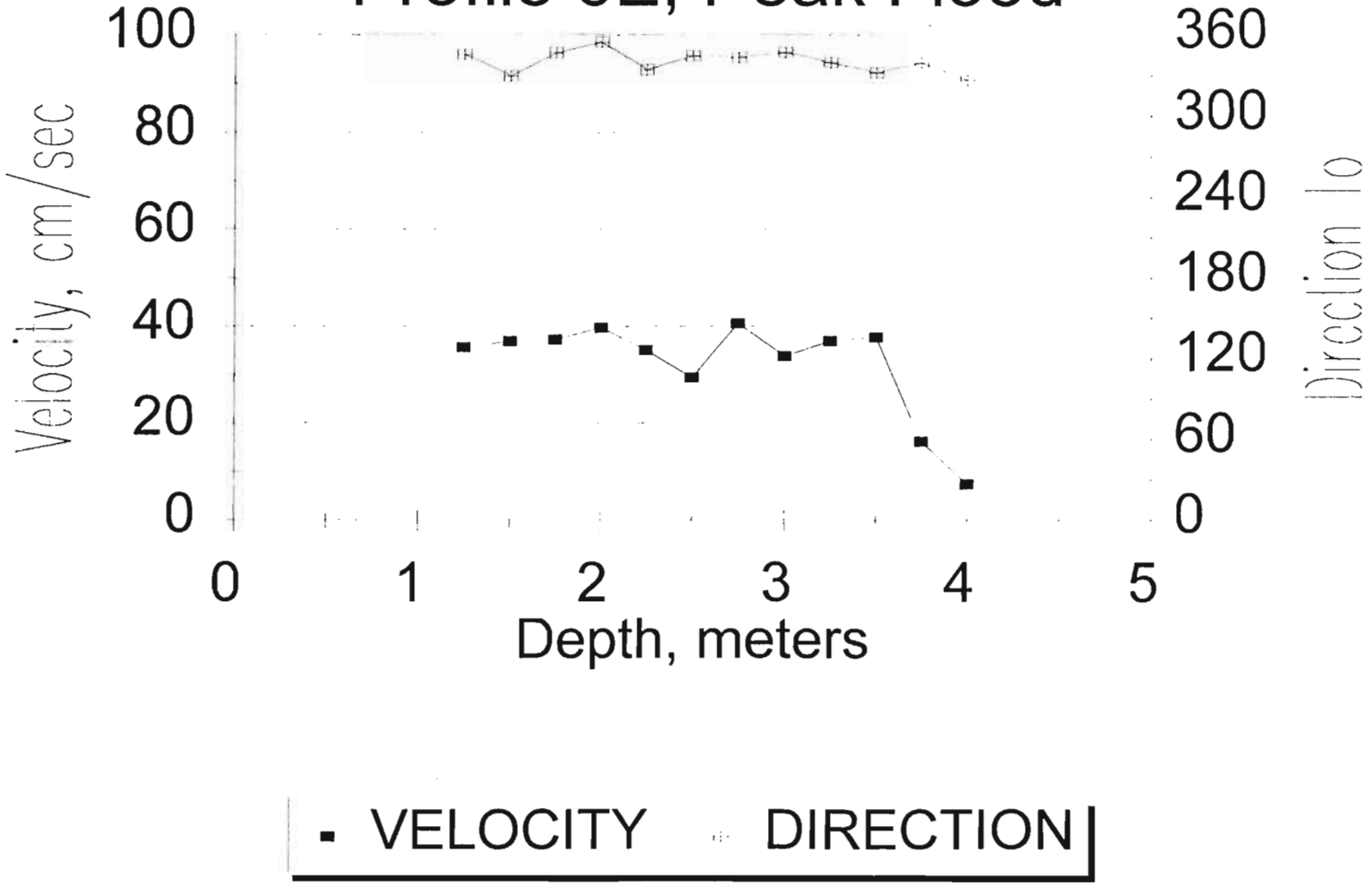

APPENDIX D
Current Velocity and Direction Time History Plots

Delaware Bay Current Measurements

Station 1A

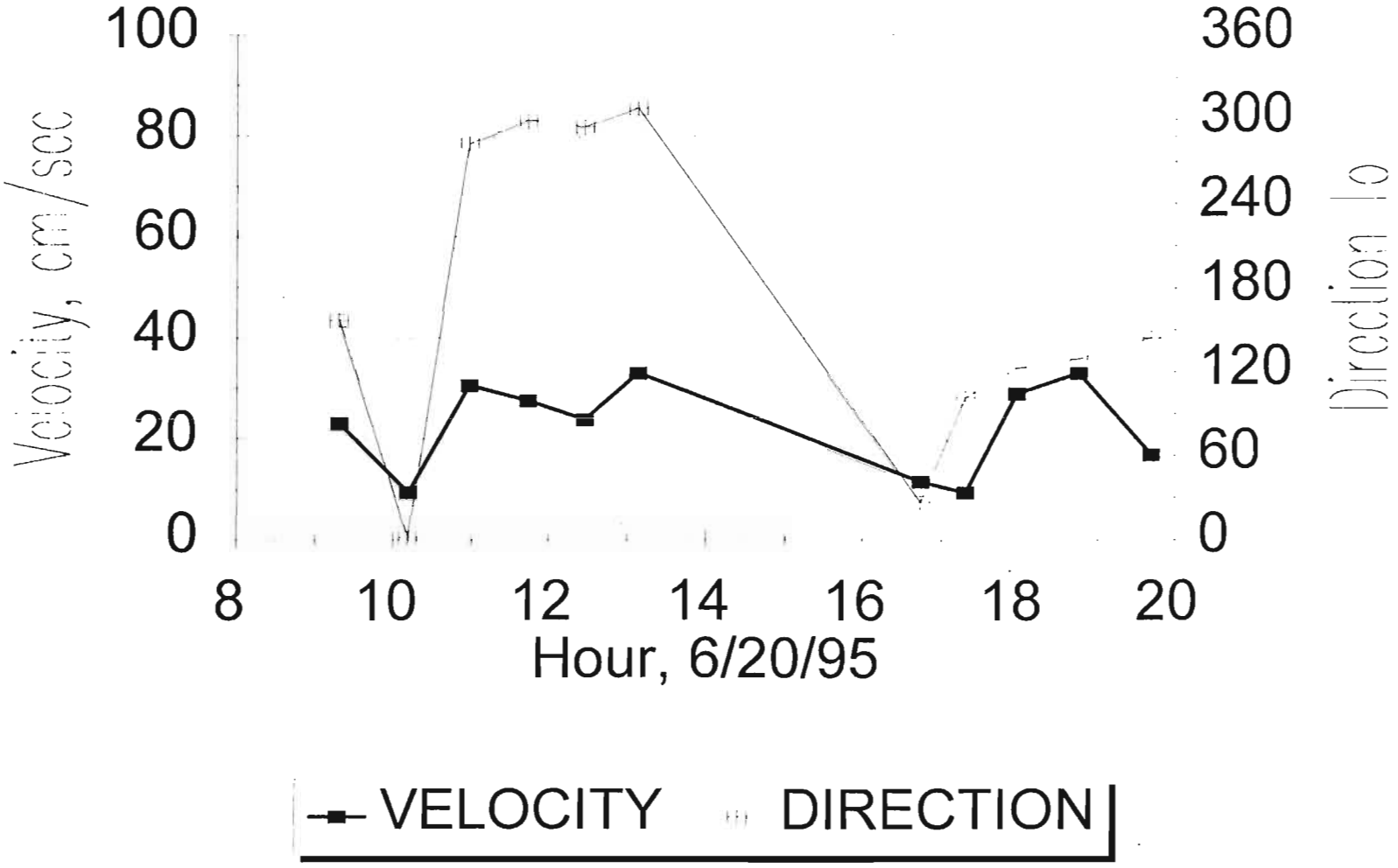

660

Delaware Bay Current Measurements

Station 3A

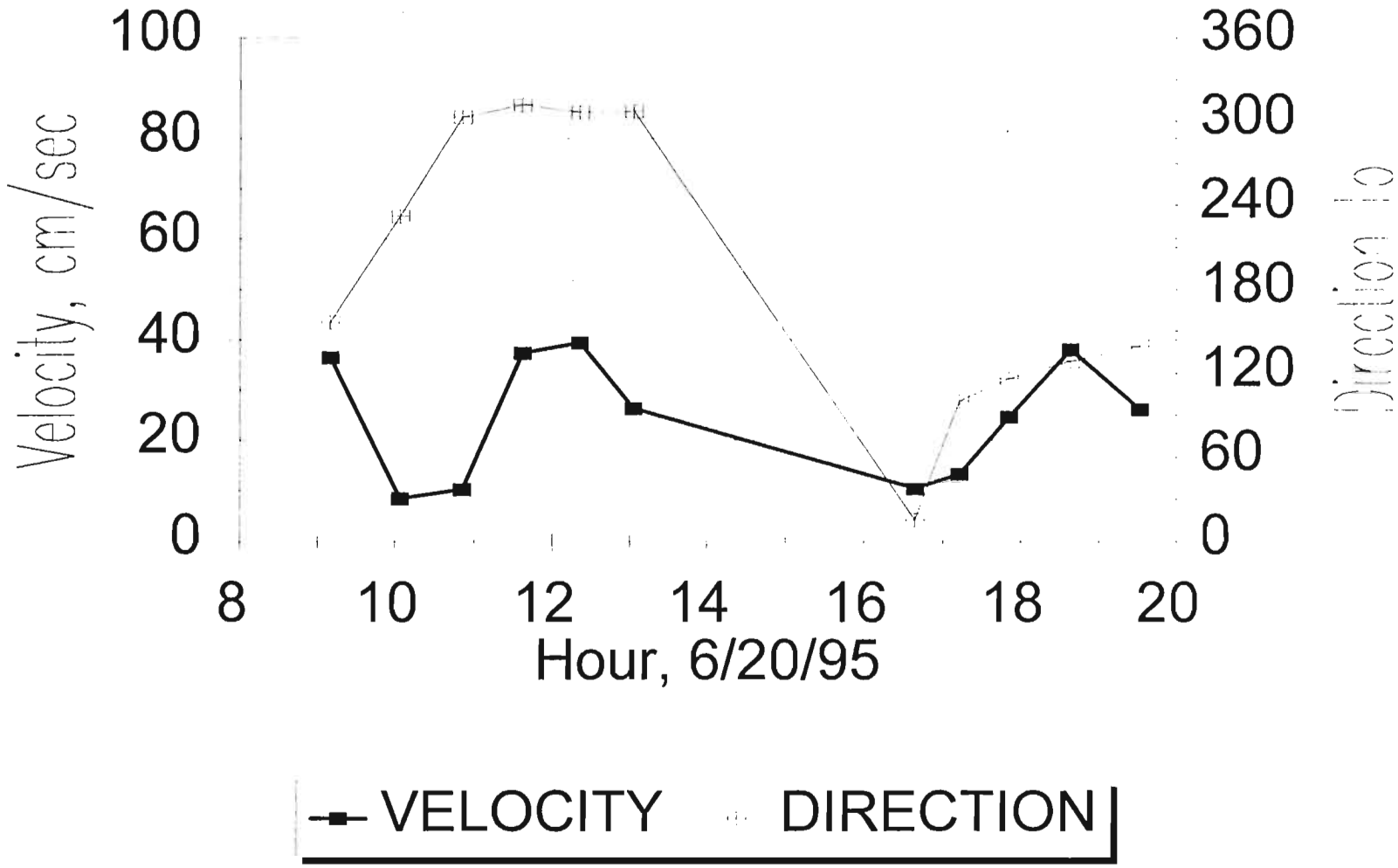

Delaware Bay Current Measurements

Station 4A

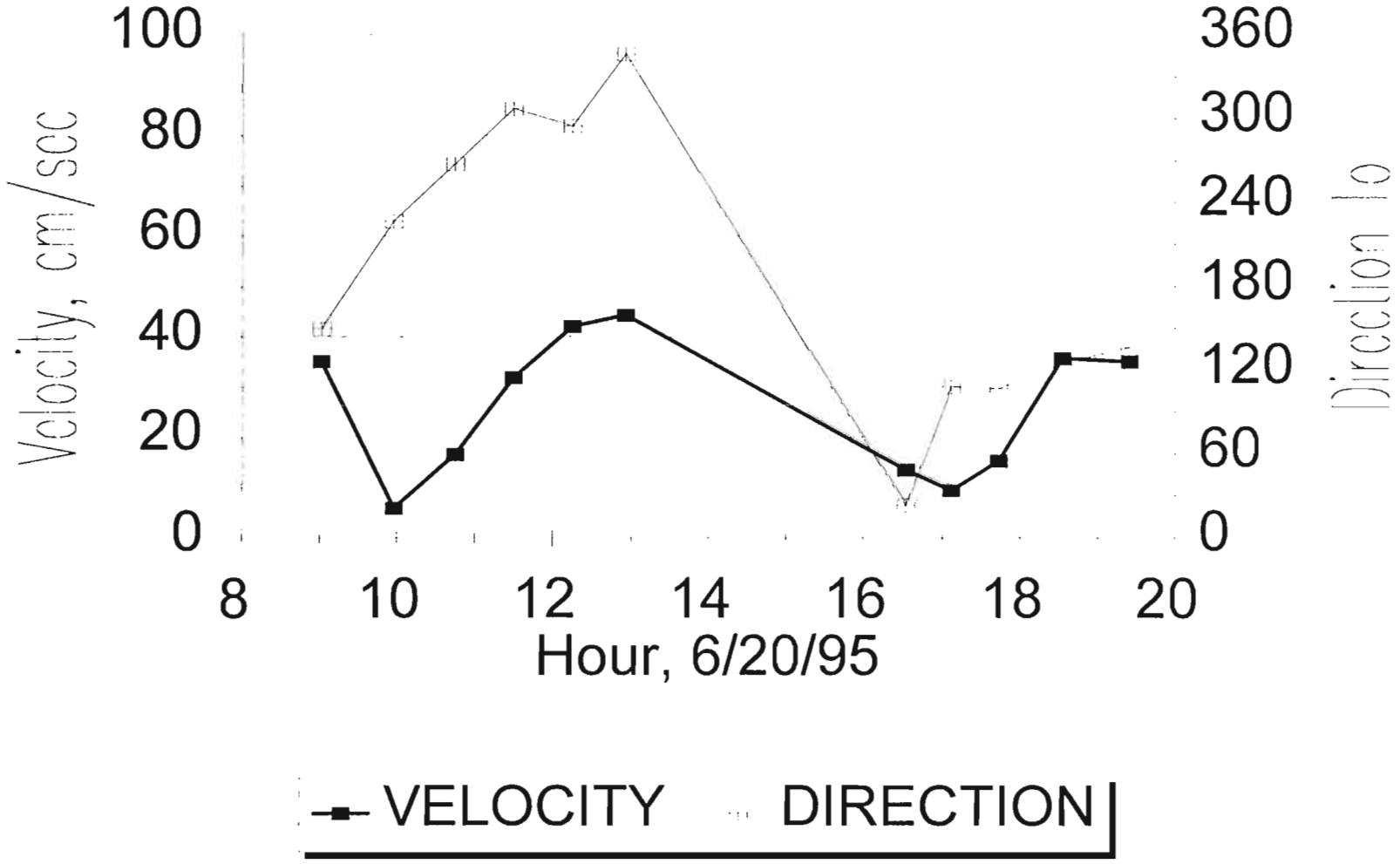

627

Delaware Bay Current Measurements

Station 5A

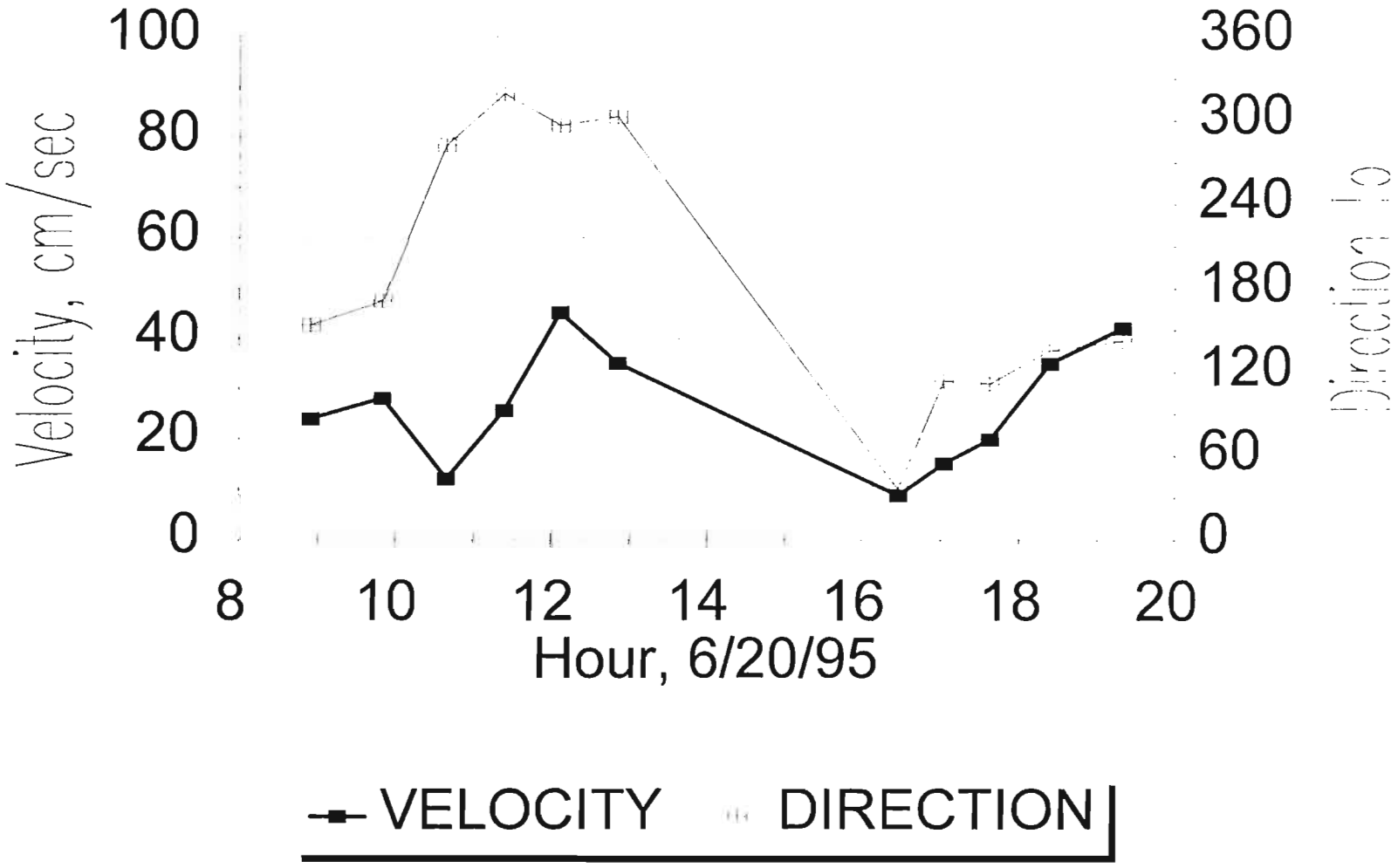

Delaware Bay Current Measurements

Station 6A

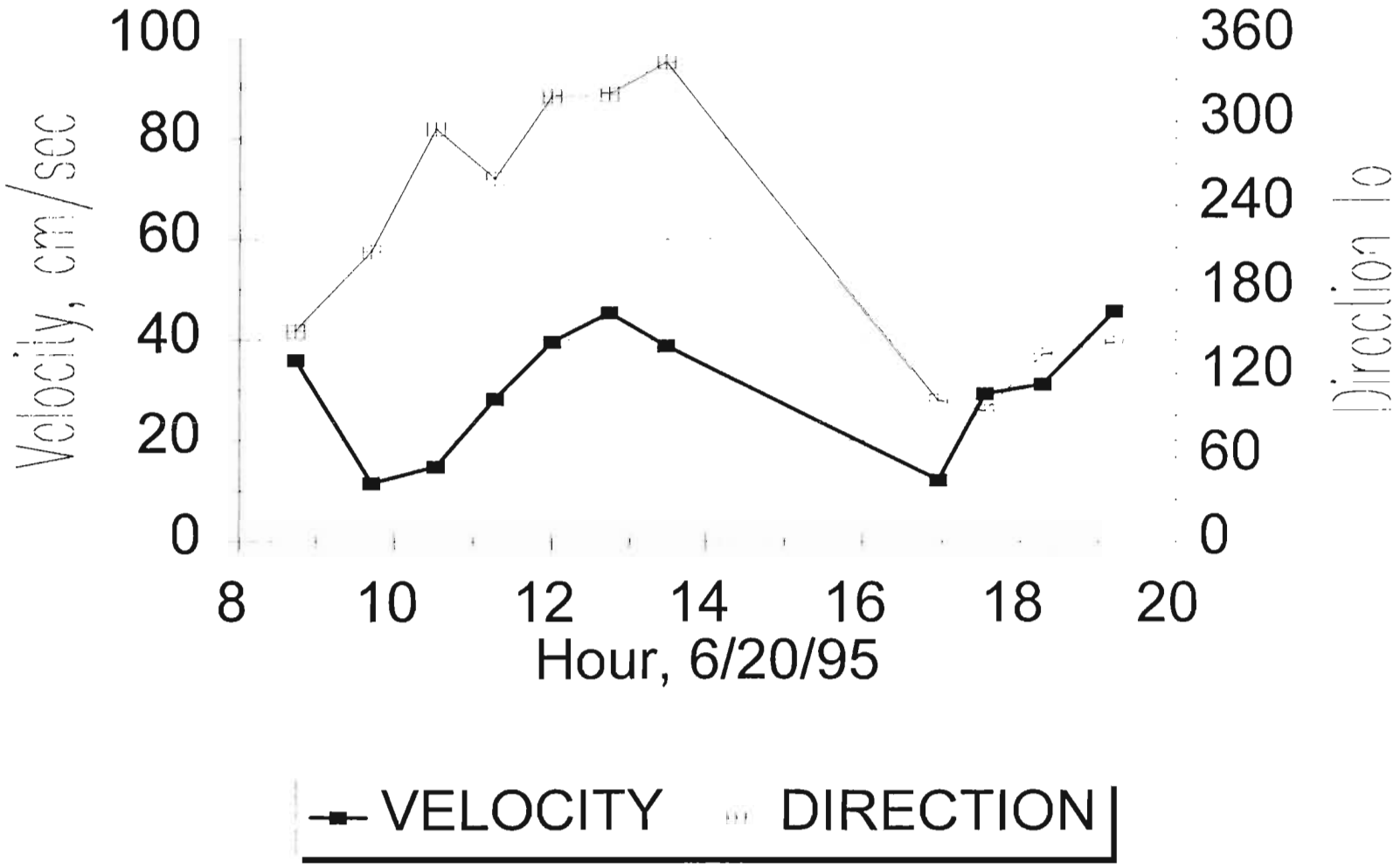

Delaware Bay Current Measurements

Station 8A

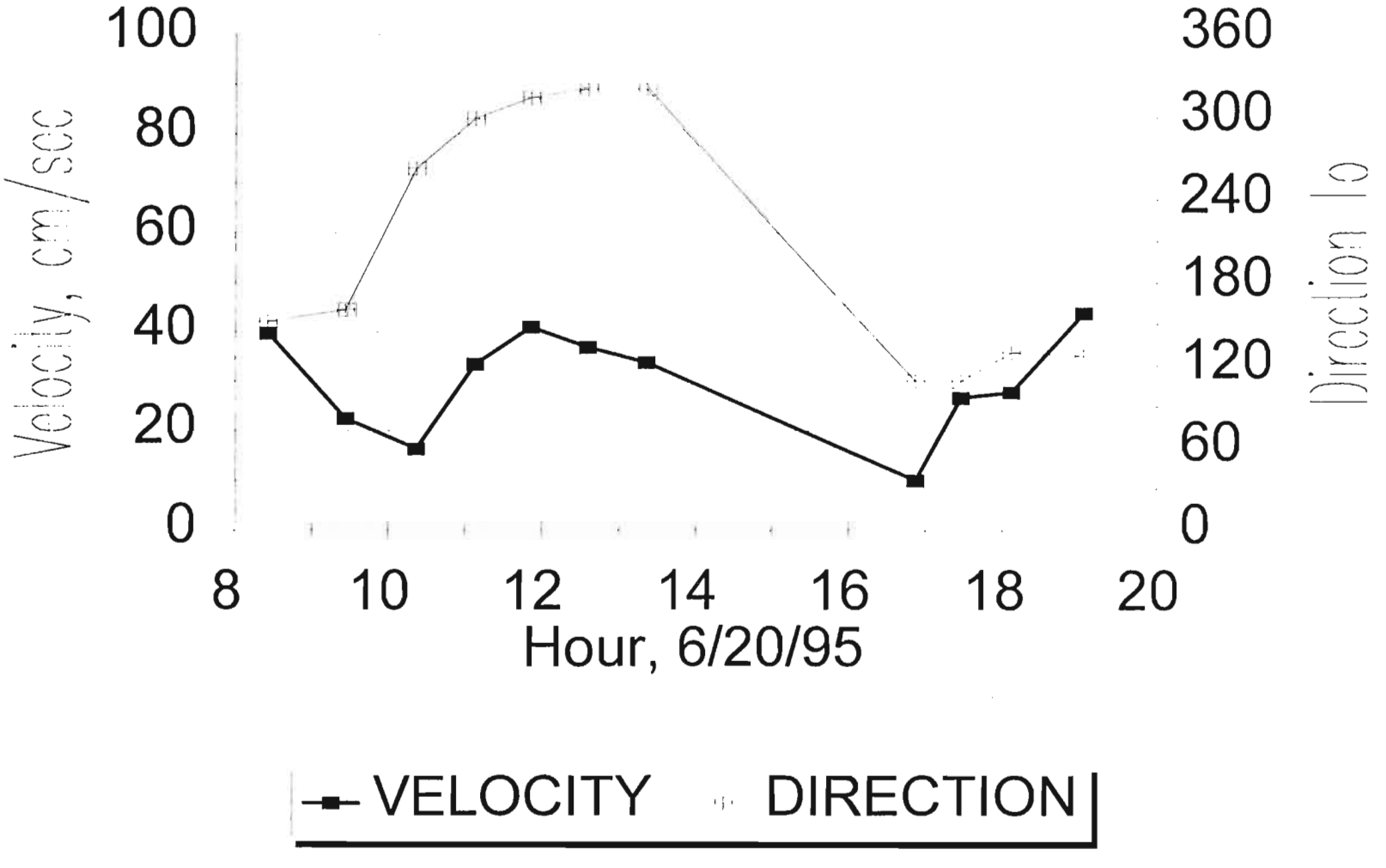

Delaware Bay Current Measurements

Station 1C

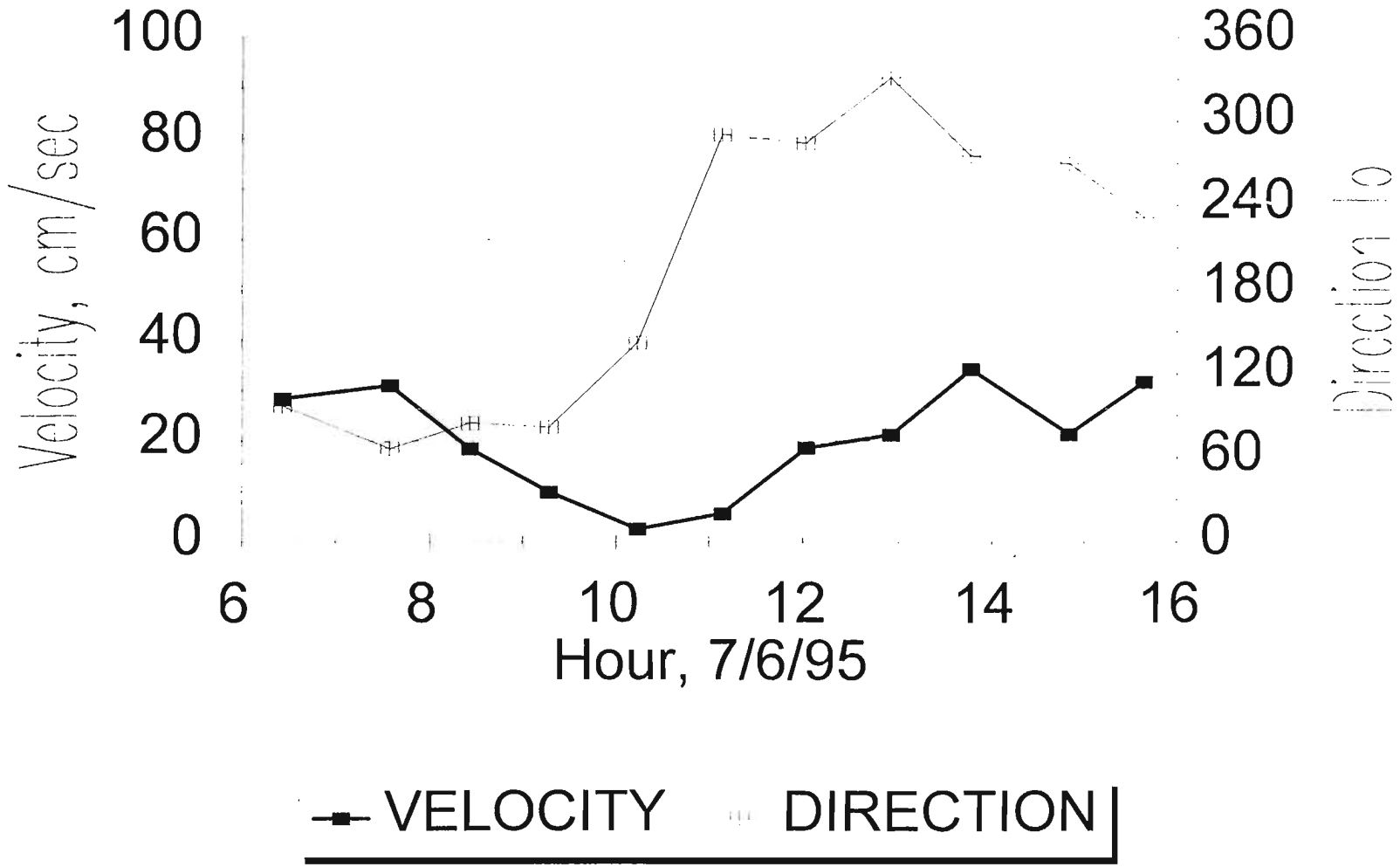

666

Delaware Bay Current Measurements

Station 2C

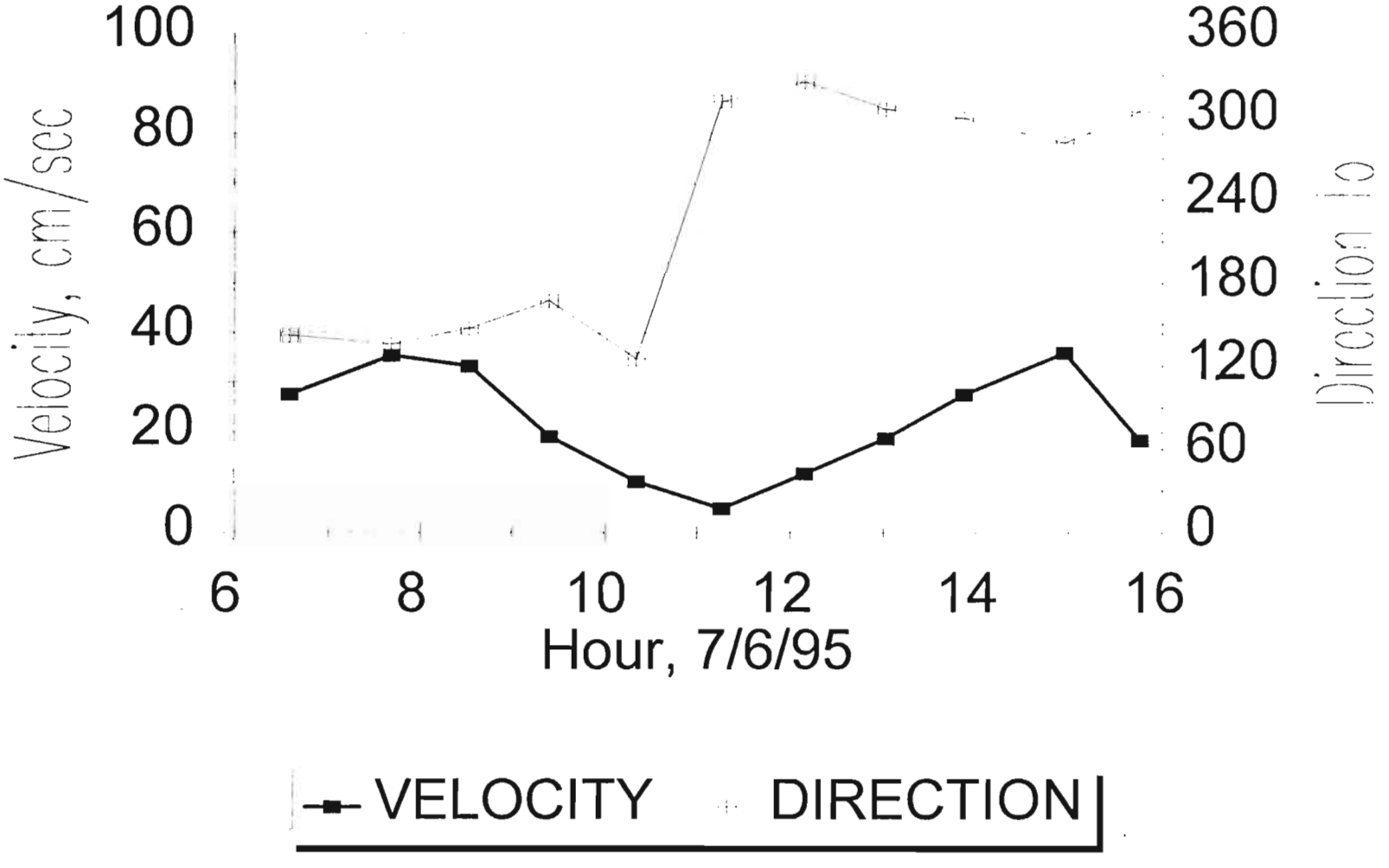

Delaware Bay Current Measurements

Station 3C

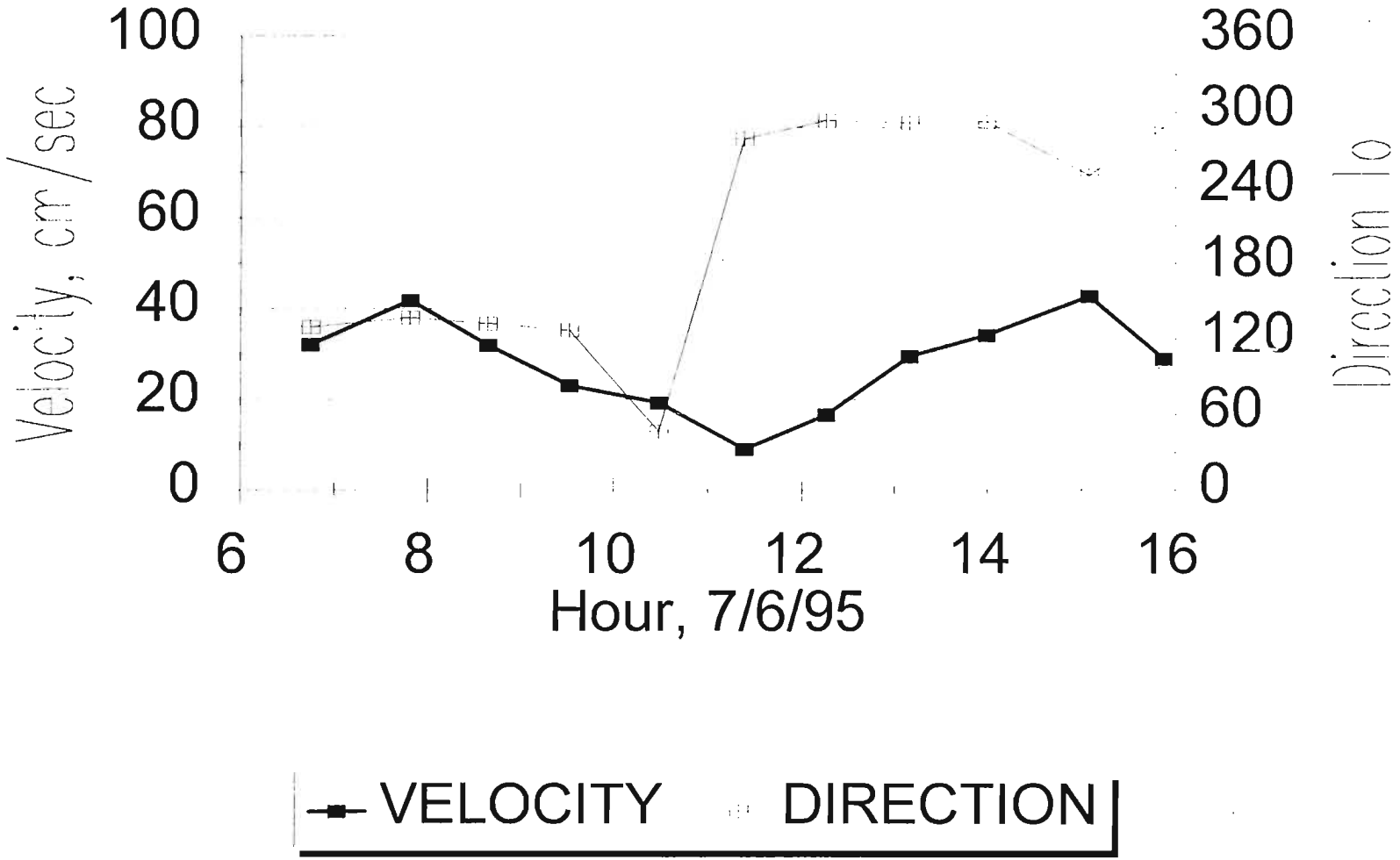

6 of 9

Delaware Bay Current Measurements

Station 4C

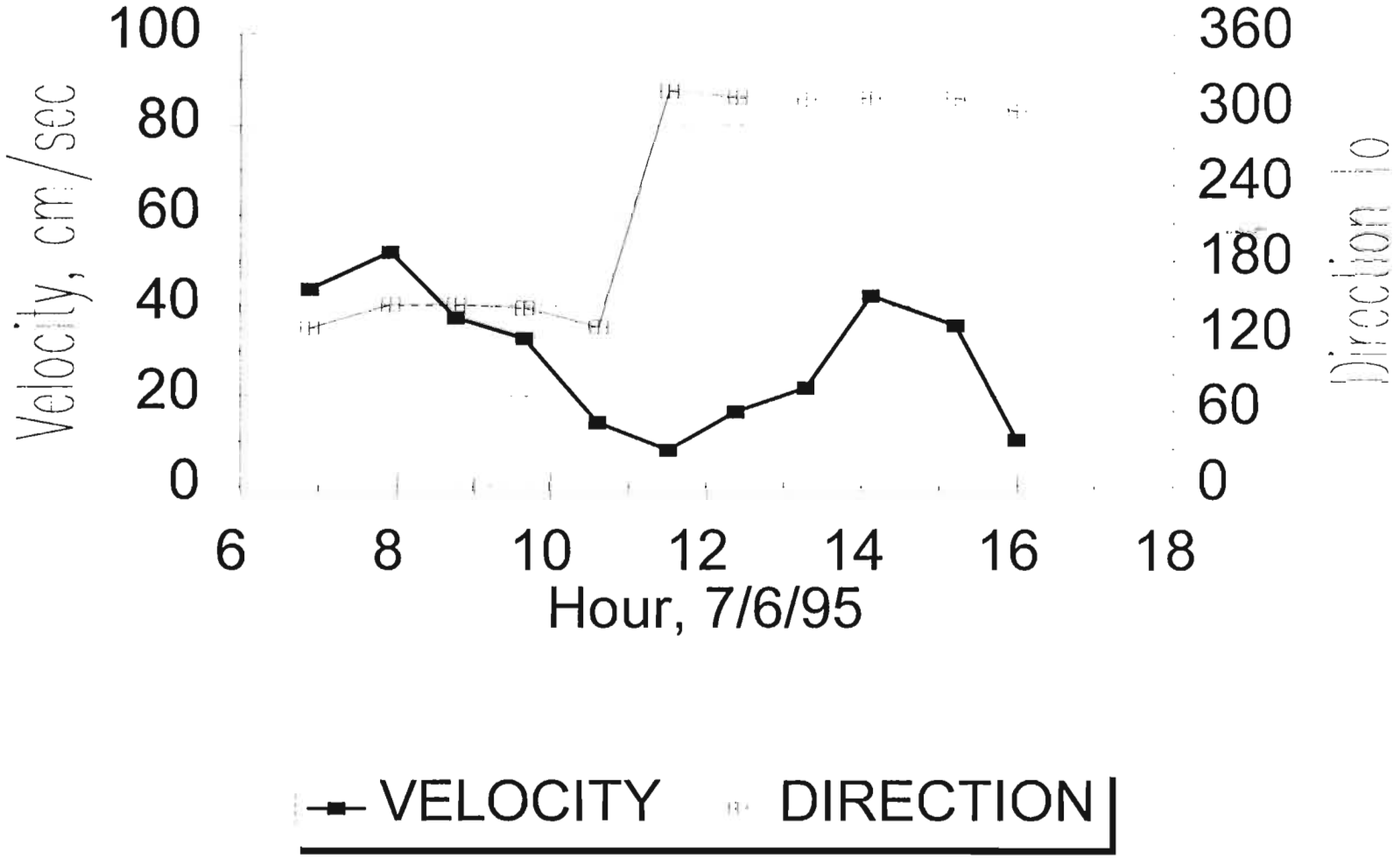

Delaware Bay Current Measurements

Station 5C

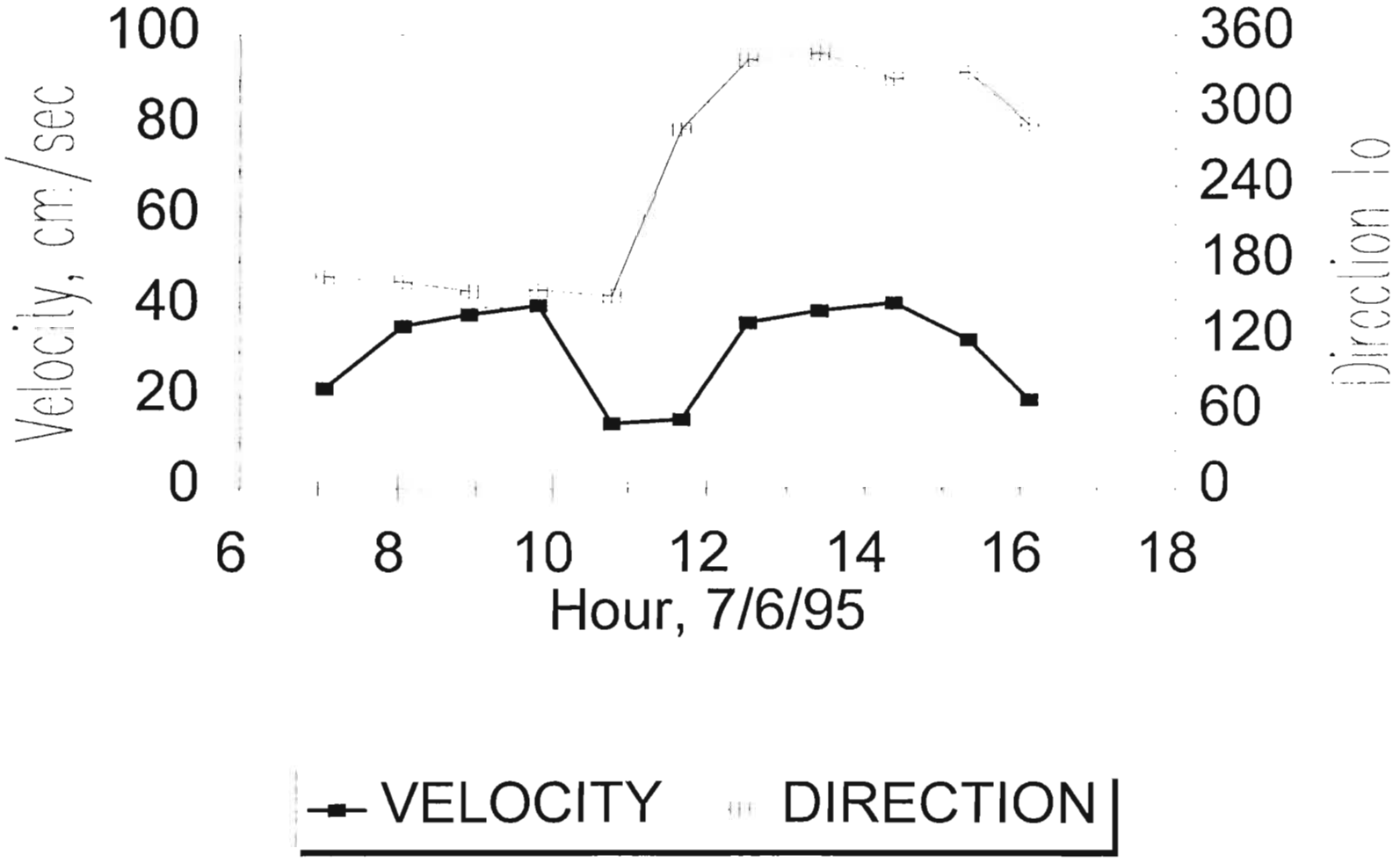

C70

Delaware Bay Current Measurements

Station 6C

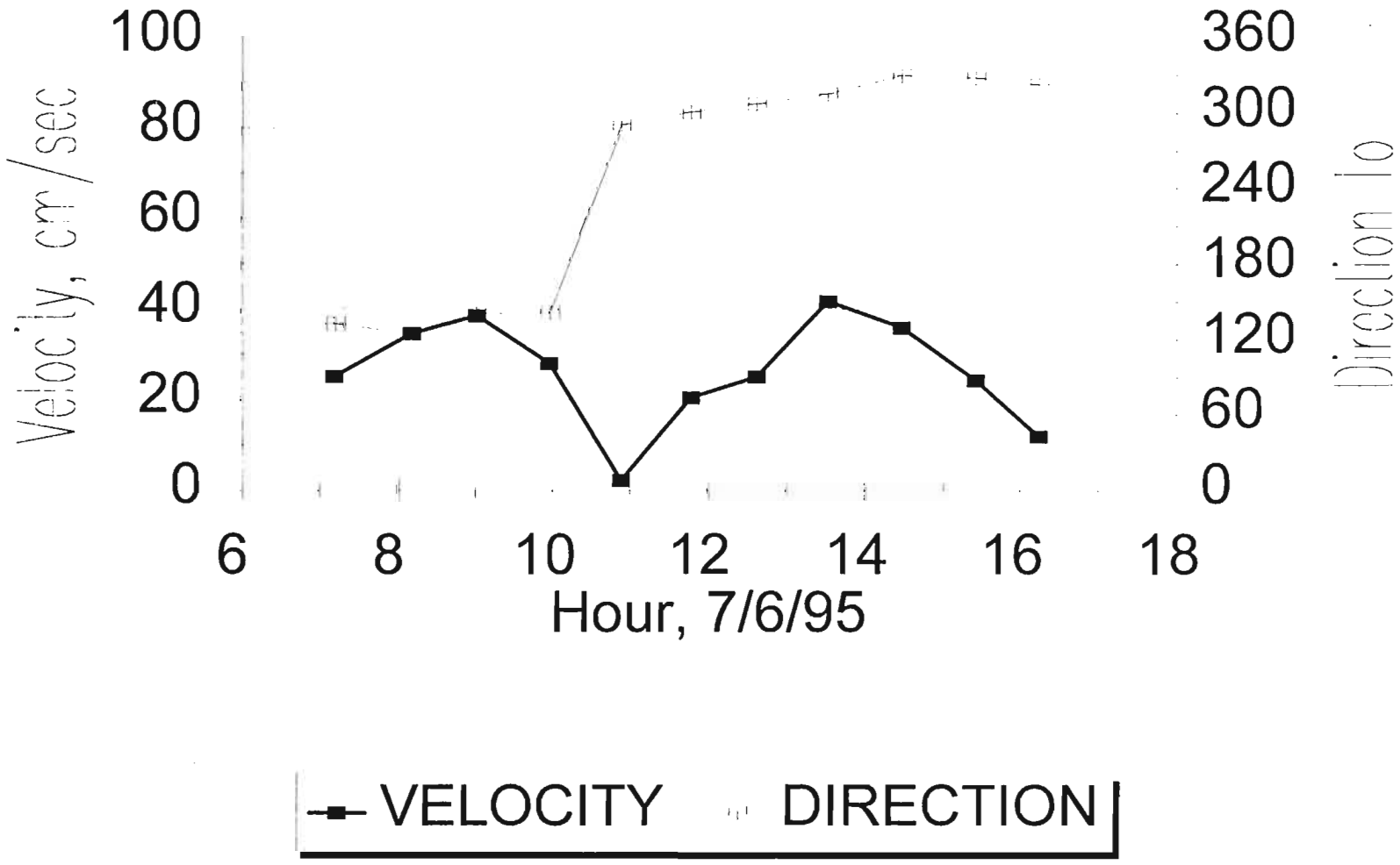

Delaware Bay Current Measurements

Station 1D

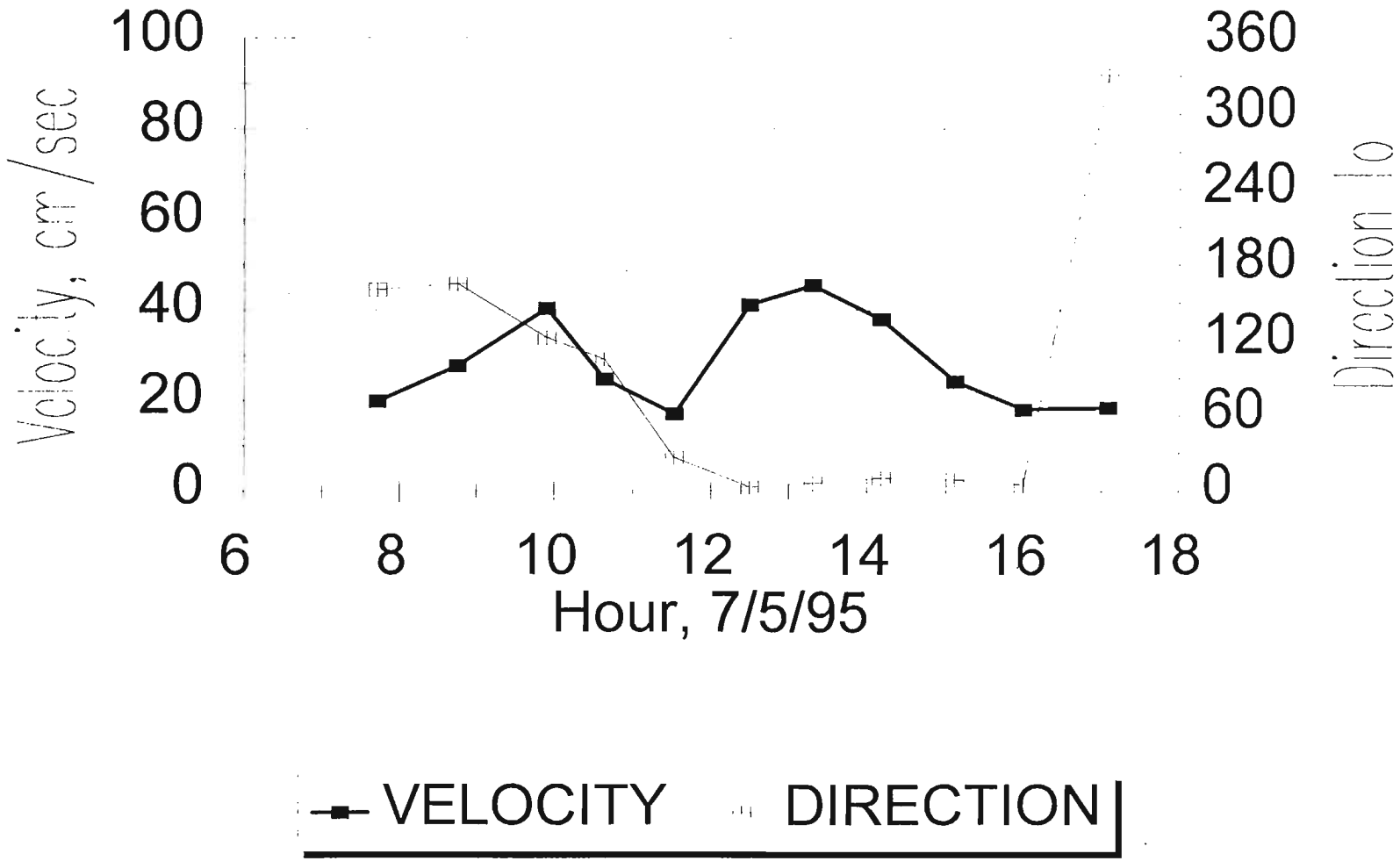

Delaware Bay Current Measurements

Station 2D

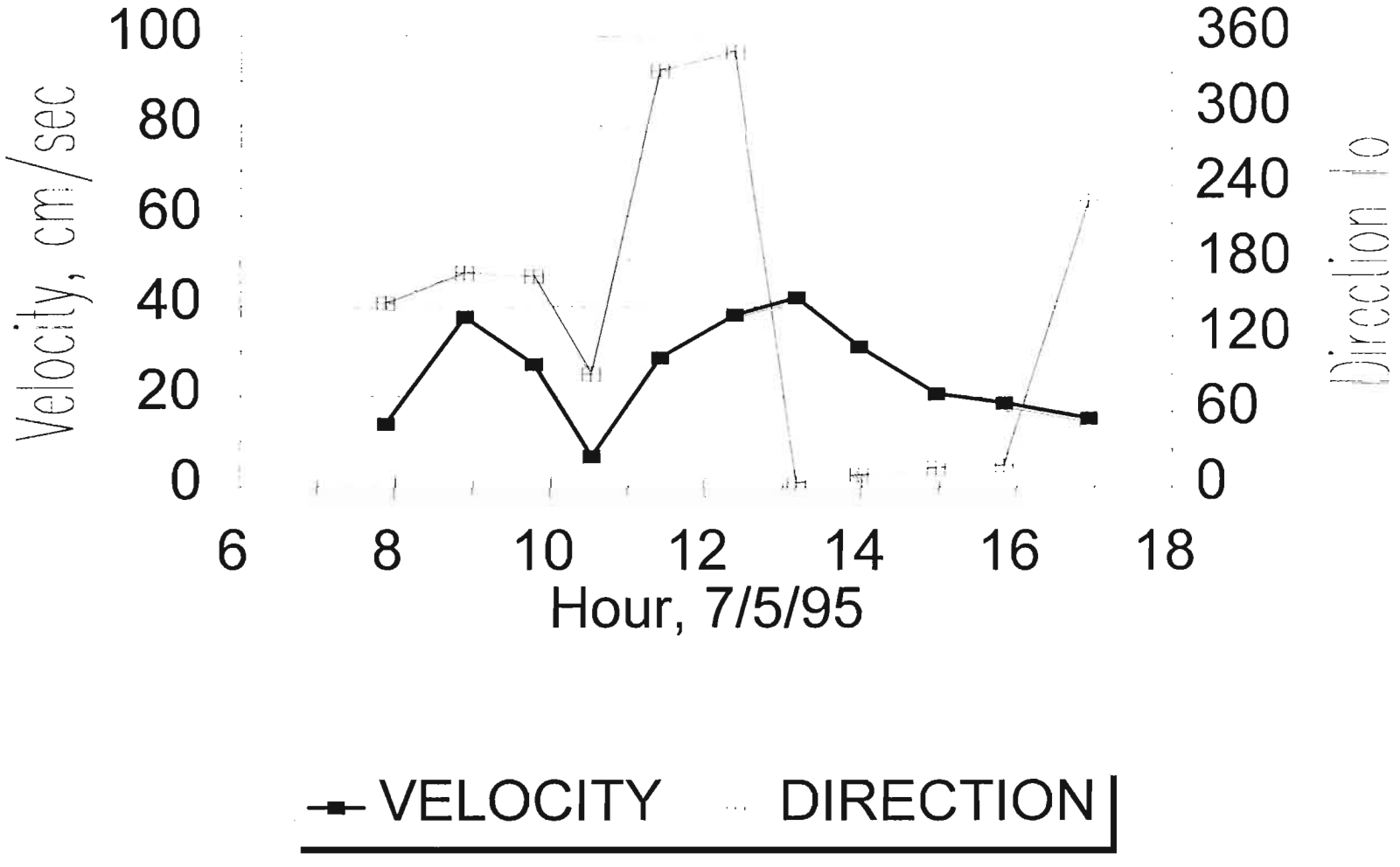

Delaware Bay Current Measurements

Station 3D

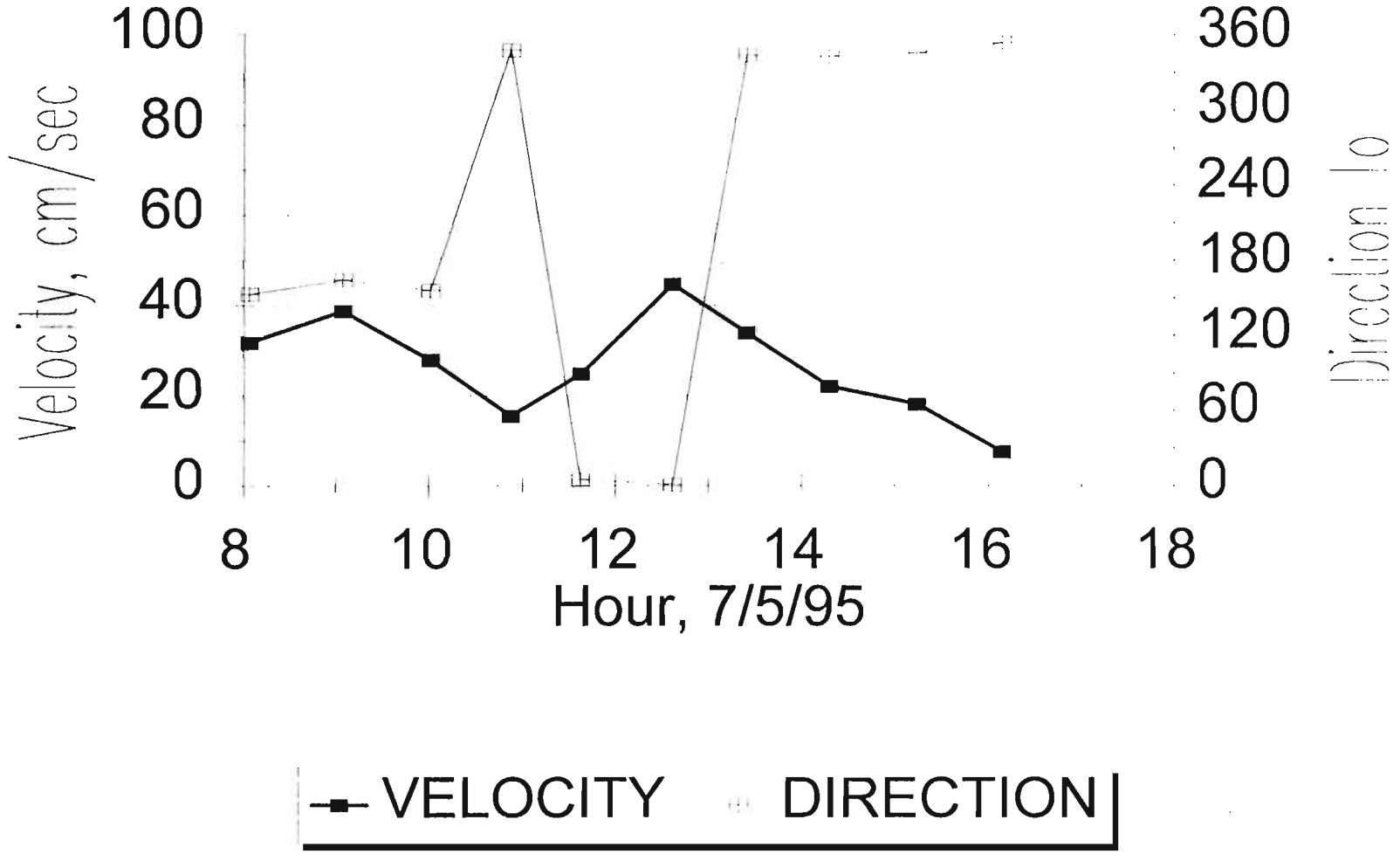

Delaware Bay Current Measurements

Station 4D

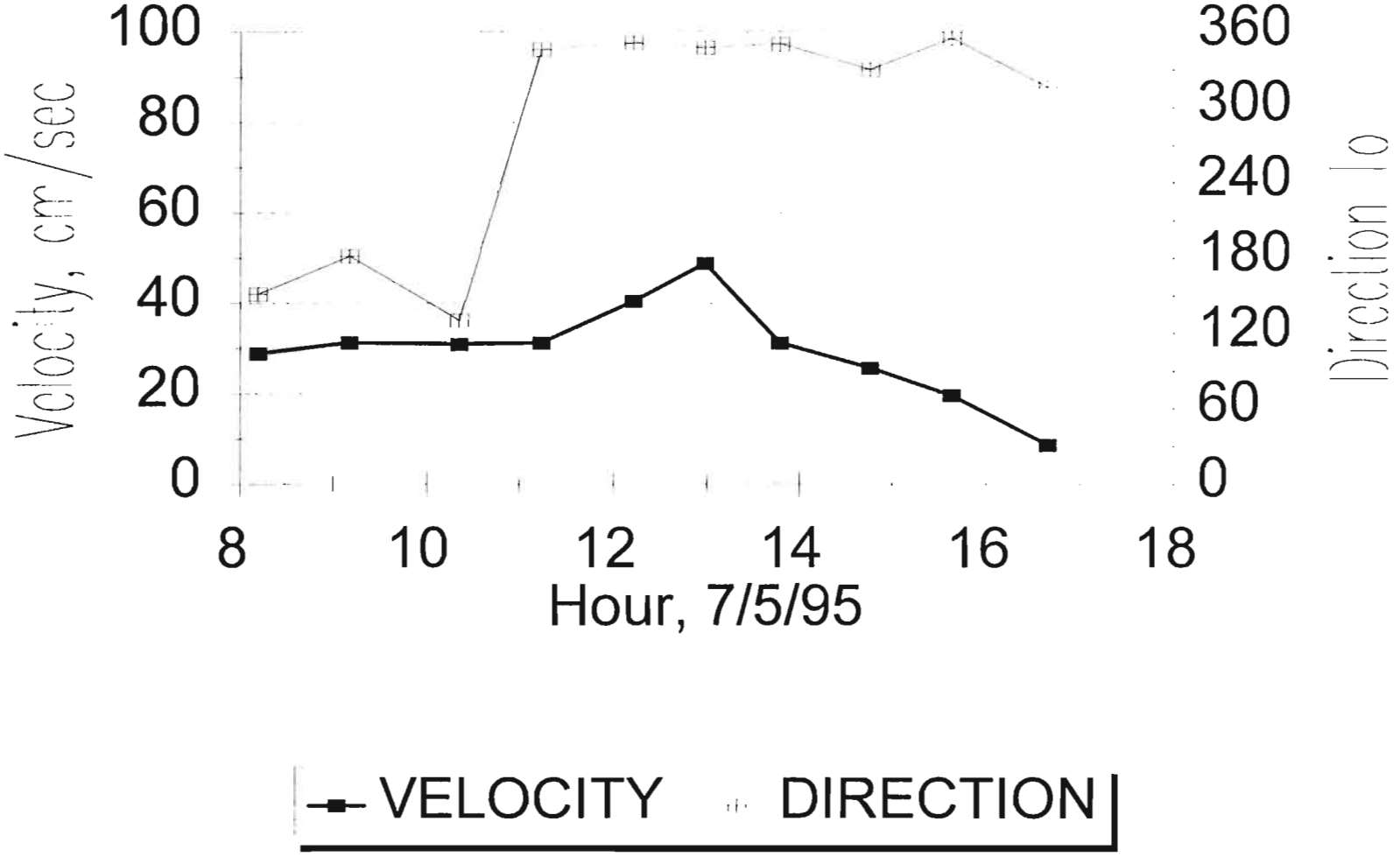

Delaware Bay Current Measurements

Station 5D

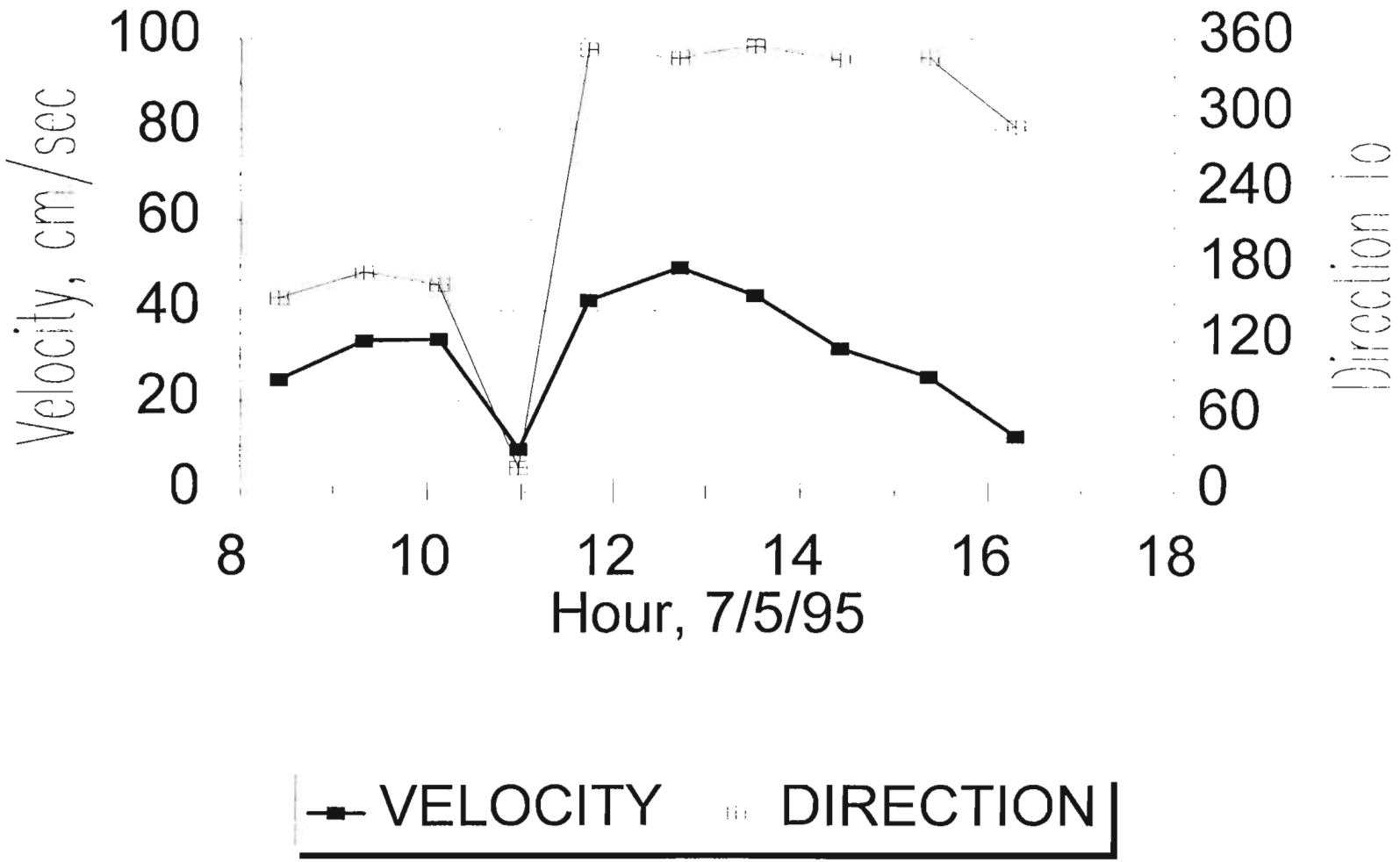

019

Delaware Bay Current Measurements

Station 6D

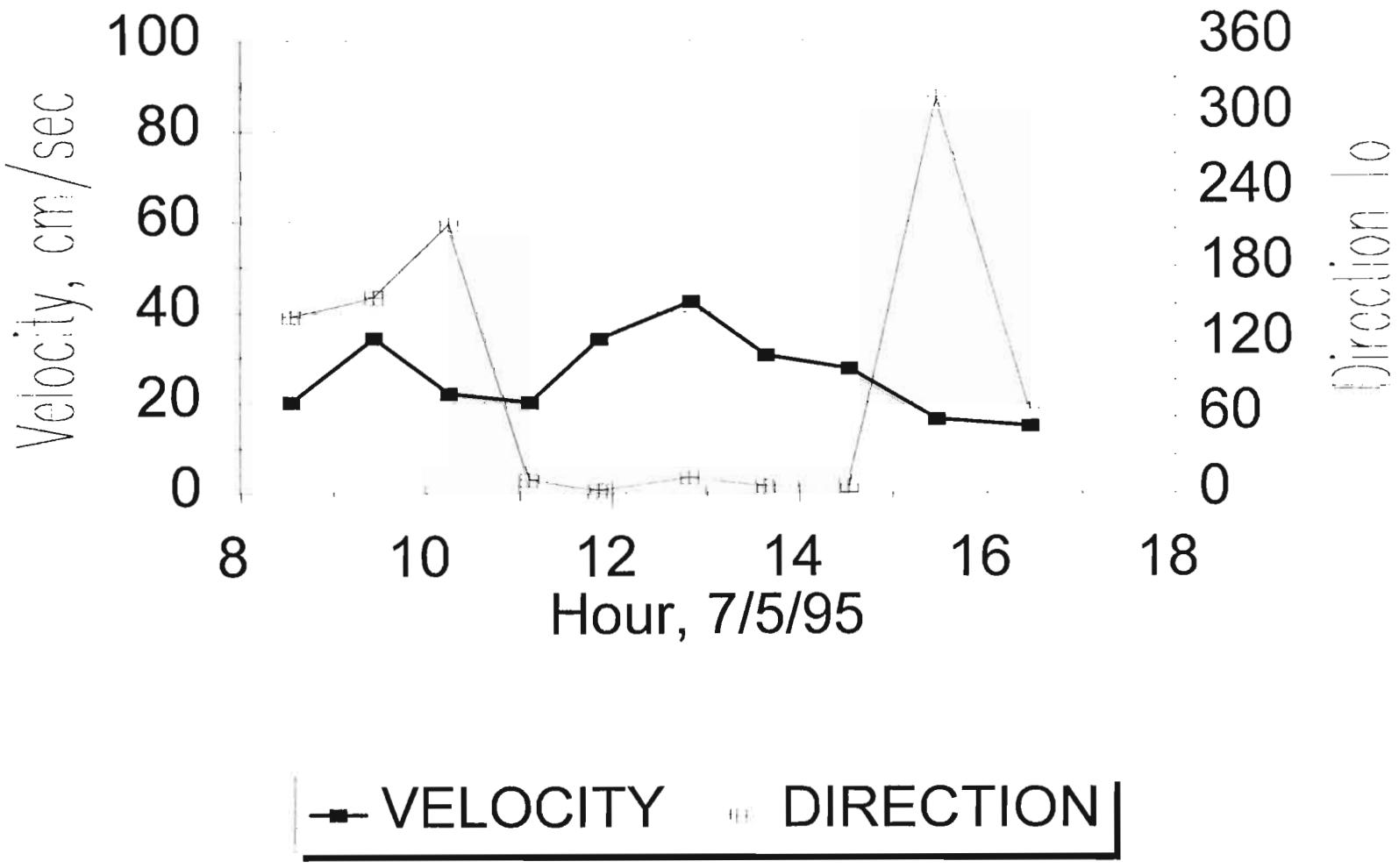

Delaware Bay Current Measurements

Station 1E

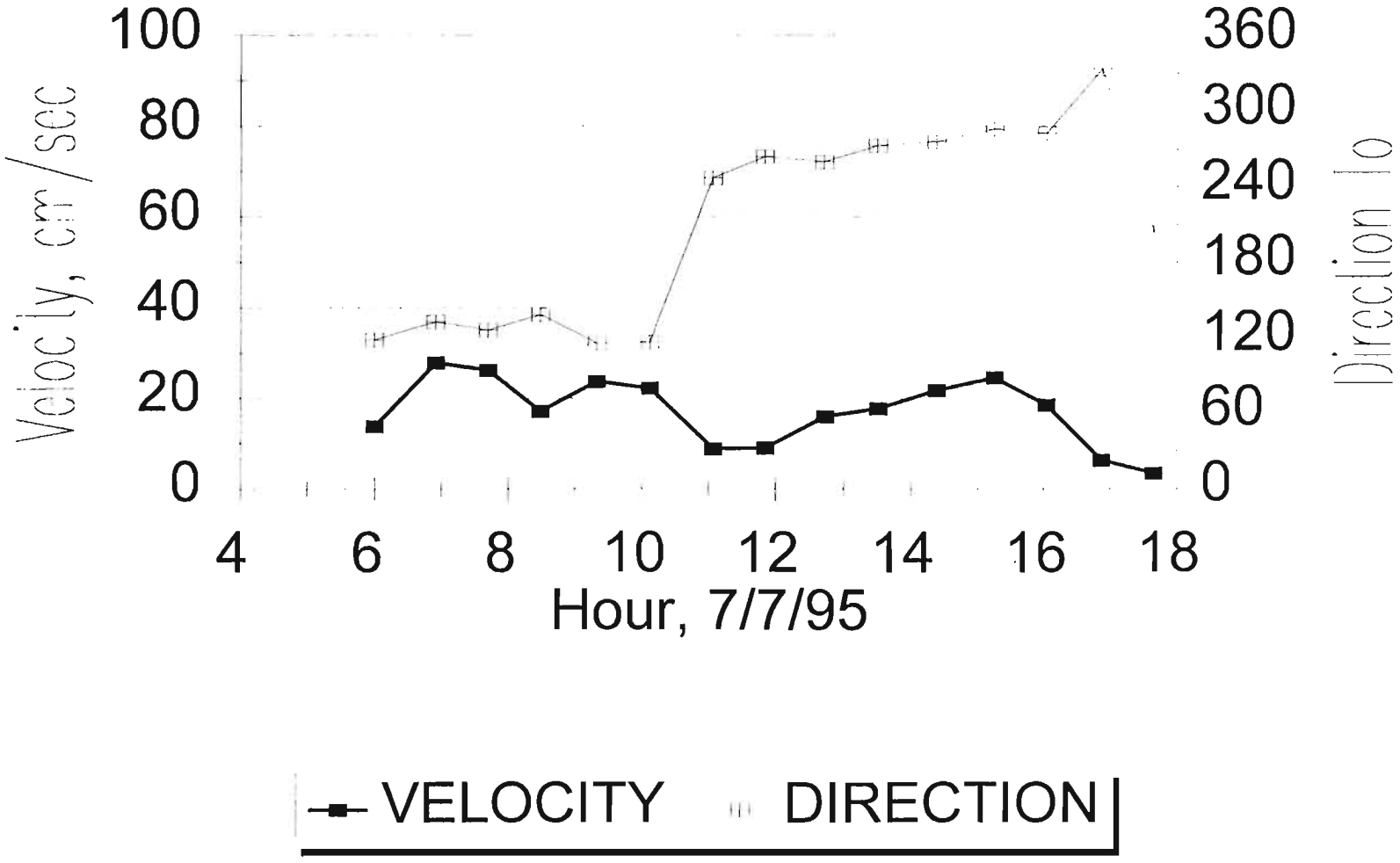

Delaware Bay Current Measurements

Station 2E

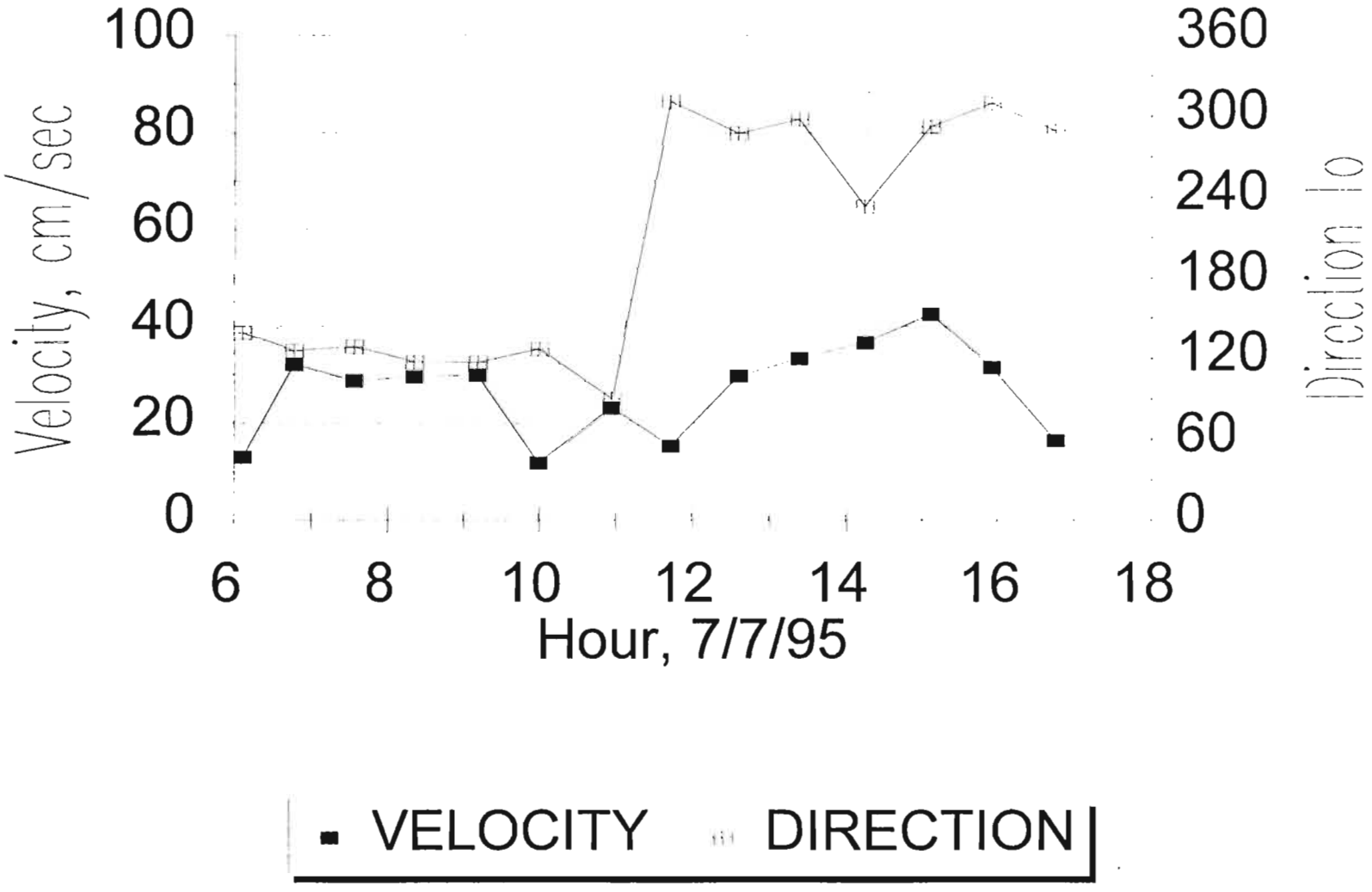

Delaware Bay Current Measurements

Station 3E

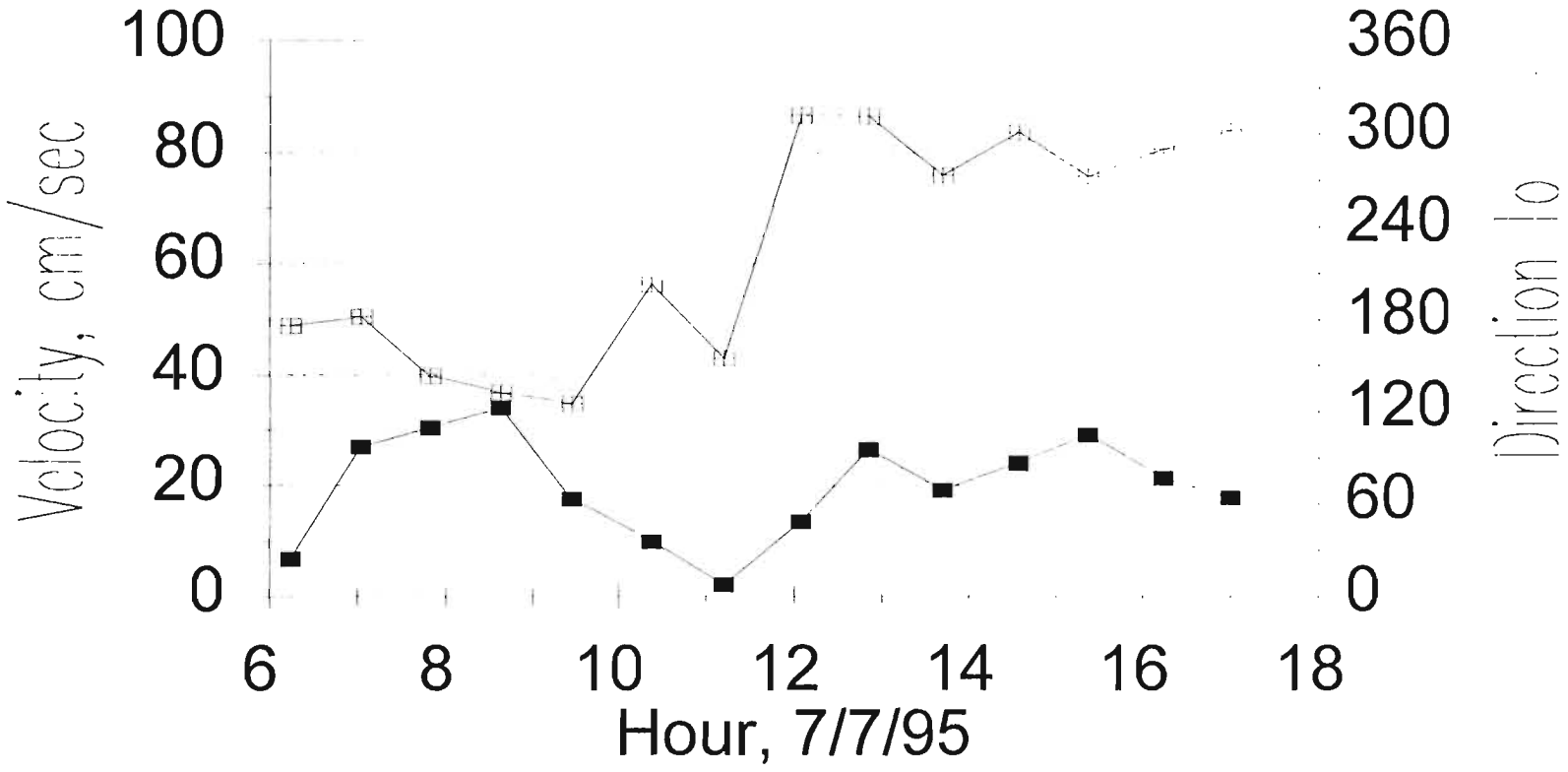

▪ VELOCITY ⁞⁞ DIRECTION

Delaware Bay Current Measurements

Station 4E

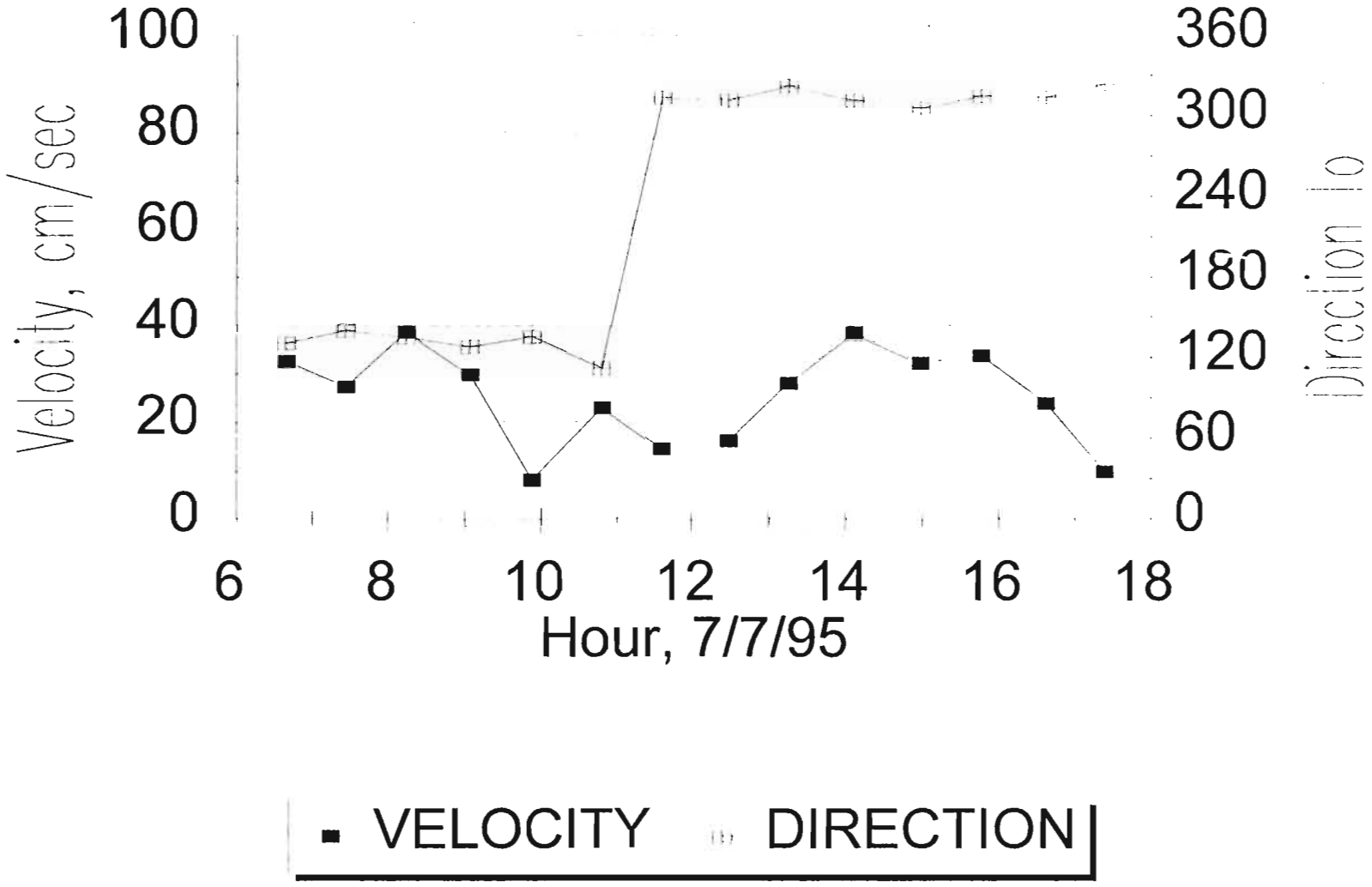

Delaware Bay Current Measurements

Station 5E

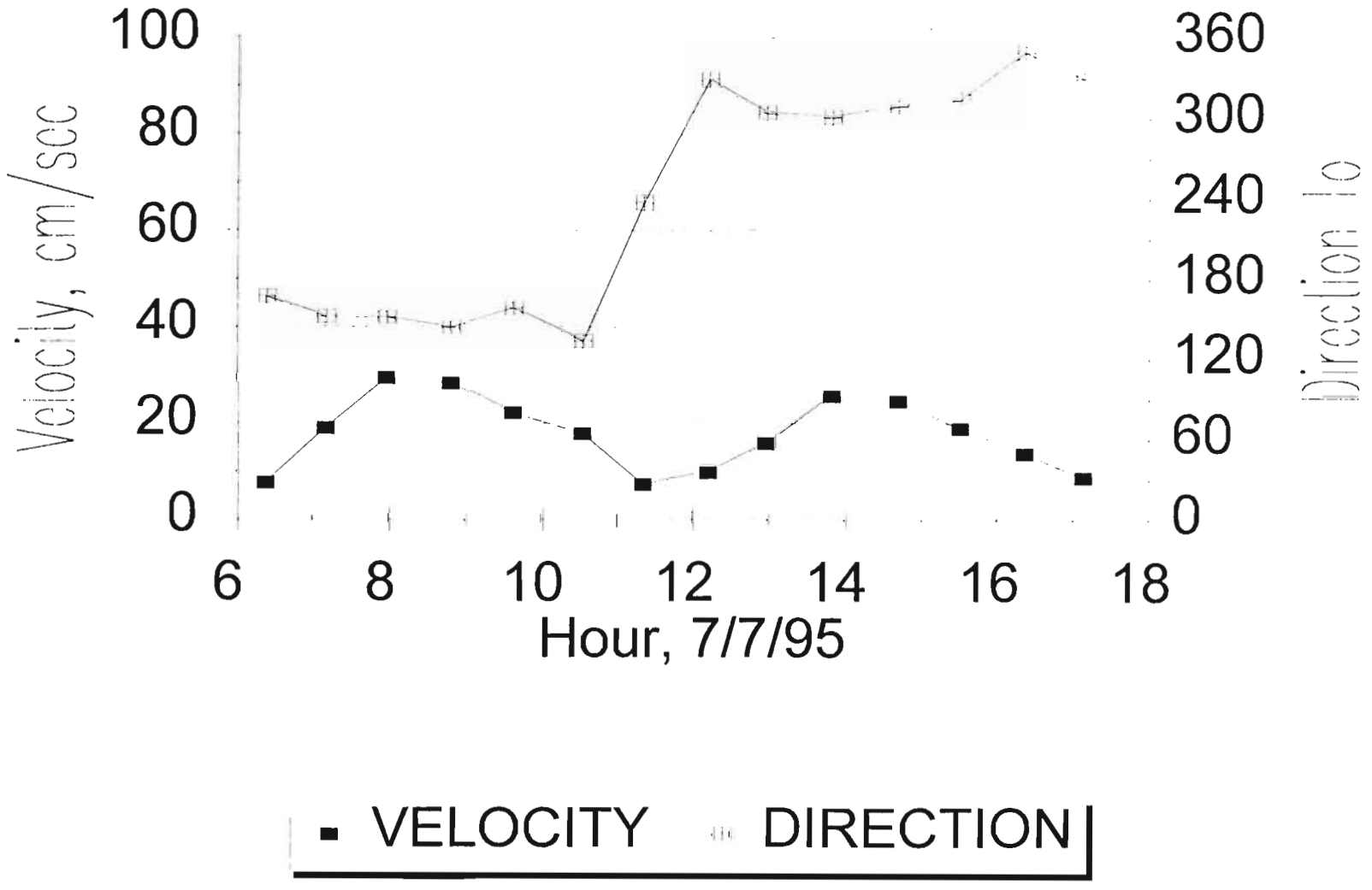

280

Delaware Bay Current Measurements

Station 6E

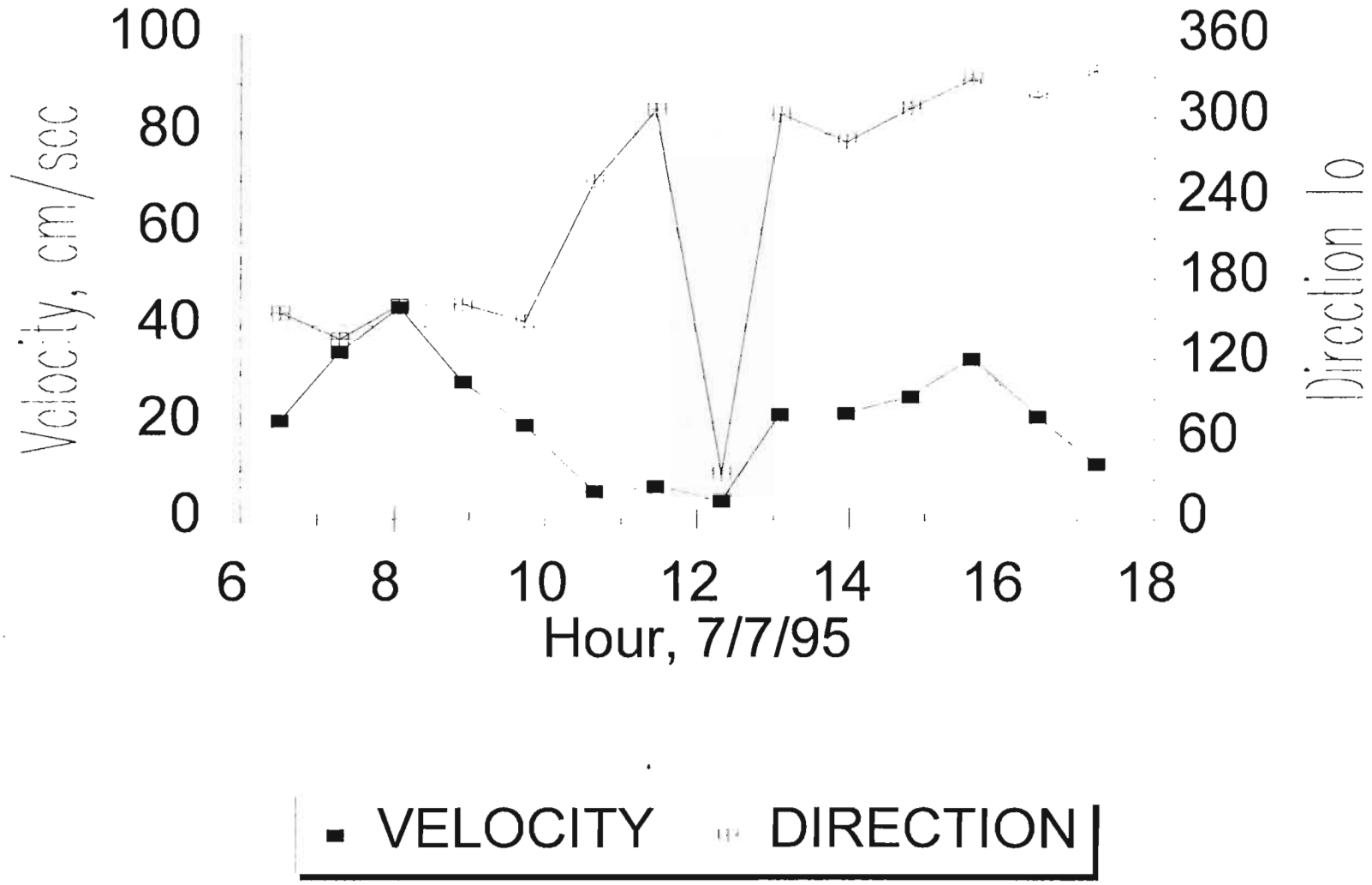

APPENDIX E
Shellfish Survivability Modeling

The effect of increased turbidity on selected Delaware Bay oyster populations
Report on simulation modeling

Eric N. Powell
Rutgers University, Haskin Shellfish Research Laboratory

John Klinck and Eileen Hofmann
Center of Coastal Physical Oceanography, Old Dominion University

685

INTRODUCTION

The proposed deepening of the Delaware Bay Ship Channel includes the necessity of disposing of the dredge material. Present plans involve sequestering the dredge material in two locations, adjacent to Egg Island, New Jersey and Kelly Island, Delaware. Questions have been raised concerning the effect of increased turbidity associated either with catastrophic failure of the containment structures or with the effect of major storms resuspending sediment on nearby oyster populations. The former scenario would raise turbidity for an indefinitely long period, perhaps as long as a month. The latter scenario, a major storm, could be expected to raise turbidity levels for 2 to 4 days.

Turbidity affects post-settlement oysters (spat, sub-adults, and adults) by decreasing filtration rate. Decreased filtration rate limits ingestion which results in decreased growth and fecundity. Decreased growth can be expected to also increase mortality from disease, since slower growing oysters are more susceptible to disease-produced mortality. The present study uses a computer model of post-settlement oyster populations to examine the effect of turbidity on oyster populations from the two selected areas.

OYSTER POPULATION DYNAMICS MODEL - DESCRIPTION

The host-parasite model consists of separate components for the dynamics of the post-settlement oyster population and the growth of *Perkinsus marinus*. The model components are coupled by relationships that describe the removal of oyster energy by the parasite to support its metabolic requirements, relationships that relate the rates of parasite cell division and mortality to host mortality, and relationships that produce mortality in the oyster population by *Perkinsus marinus*. The oyster population model is described in detail by Hofmann et al. (1992, 1995) and Powell et al. (1994). These references are attached as Appendices. Only brief reviews of these components will be given here.

The post-settlement oyster component consists of a size-structured model that considers the processes regulating the growth and death of the oyster from newly settled juveniles to adults. The time change in oyster standing stock ($O_{j,k}$) in each oyster size class (j) and *P. marinus* infection level (k) is the result of changes in net production ($NP_{j,k}$), which is the sum of the production of somatic ($Pg_{j,k}$) and reproductive ($Pr_{j,k}$) tissue, and the addition of individuals from the previous size class or loss to the next largest size class by growth. Oyster net production is assumed to be the difference between assimilation ($A_{j,k}$) and respiration ($R_{j,k}$), and losses to *P. marinus* ($E_{j,k}$) as:

$$NP_{j,k} = Pg_{j,k} + Pr_{j,k} = A_{j,k} - R_{j,k} - E_{j,k}. \quad (1)$$

The governing equation for the oyster population is then:

$$\frac{dO_{j,k}}{dt} = Pg_{j,k} + Pr_{j,k} + (\text{gain from } j-1) - (\text{loss to } j+1) \tag{2}$$

where $j = 1, 11$, which represents the size class partitioning of the oyster life history. Reproductive tissue formation is zero for the first three size classes, which represent juveniles.

During suboptimal conditions, oysters can resorb gonadal or somatic tissue and hence lose biomass ($NP_{j,k} < 0$) and transfer into the next lower size class. Thus biomass can change during periods of negative scope for growth. To allow for this, equation (2) is modified as:

$$\begin{aligned}\frac{dO_{j,k}}{dt} =& Pg_{j,k} + Pr_{j,k} \\ &+(\text{gain from } j-1) - (\text{loss to } j+1) \\ &+(\text{gain from } j+1) - (\text{loss to } j-1).\end{aligned} \tag{3}$$

The right-hand two terms on the right side of equation (3) represent the individuals losing biomass and, thus, moving to the next lower size class.

The final modification to the oyster governing equation allows oysters in any size class to increase or decrease in *P. marinus* infection intensity:

$$\begin{aligned}\frac{dO_{j,k}}{dt} =& Pg_{j,k} + Pr_{j,k} \\ &+(\text{gain from } j-1) - (\text{loss to } j+1) \\ &+(\text{gain from } j+1) - (\text{loss to } j-1) \\ &+(\text{gain from } k-1) - (\text{loss to } k+1) \\ &+(\text{gain from } k+1) - (\text{loss to } k-1).\end{aligned} \tag{4}$$

The bottom four terms in equation (4) represent changes in infection intensity of the oyster population as the *P. marinus* population increases or decreases in cell number. The model includes twenty-eight predefined infection levels. Level one consists of uninfected oysters. The remaining 27 levels represent degrees of infection that correspond to the number of cell doublings of the *P. marinus* population beginning with one cell in level 2.

Three aspects of the model given by equation (4) deserve note. First, settlement of juvenile oysters (as spat) occurs exclusively in the first size class and first infection level. These newly recruited individuals are uninfected by *P. marinus*. Second, movement of oysters from the uninfected to the newly infected stage occurs by the acquisition of one infective cell (infection level 2) and occurs only in the positive direction, a gain of infection. Infections, once acquired by oysters, are never lost. Finally, once the oysters have reached the infection level defined as lethal, they are classified as dead and both the *P. marinus* cells and the oyster biomass are permanently lost from the population.

The gain, loss or transfer of energy (or biomass) between size classes or across infection levels in equation (4) is expressed in terms of specific rates (d^{-1}) which are multiplied by the caloric quantity in the size or infection class. Transfers of oysters between size classes were scaled by the ratio of the average weight of the current size class (in g dry wt or cal) to that of the size class from which energy was gained or to which energy was lost. This scaling is necessary because the oyster size classes were unevenly distributed across the size-frequency spectrum. This ensured that the total number of oyster individuals in the model was conserved, in the absence of recruitment and mortality. A similar scaling is used for transfers between infection levels because these are are not equivalent in dimension. Thus, each specific rate for each transfer was scaled by:

for transfers up: $W_j/(W_{j+1} - W_j)$

for transfers down: $W_j/(W_j - W_{j-1})$

where W is the median value for biomass ($g.AFDW$) in the size class, or by the ratio of cell numbers between infection classes

for transfers up: $C_k/(C_{k+1} - C_k)$

for transfers down: $C_k/(C_k - C_{k-1})$

where C is the number of cells per individual. For simplicity, these scalings are not explicitly stated in the equations given here.

The model includes parameterizations for the processes that determine the production of somatic and reproductive tissue and thus the transfer between size classes. Specifically included are formulations for: assimilated ingestion as it depends on filtration rate, ambient food supply and assimilation efficiency; filtration rate as a function of oyster size, temperature, salinity, turbidity and current flow; respiration as it depends upon oyster size, temperature and salinity; the apportionment of net production into somatic and reproductive growth as a function of temperature and time of year; the preferential resorption of gonadal tissue when

$NP_{j,k} < O$; and spawning as a function of the total cumulative reproductive biomass and the male/female ratio. The relationships used for these processes are given in the aforementioned references.

The *P. marinus* component includes processes that govern cell growth and mortality, those that determine the energy demand of the parasite on the host, and those that affect the physiology of the host. Cell division time is the time between one cell division and the next for an individual cell. The population doubling time, however, depends upon the balance between the rate of cell division and the rate of cell mortality. For *P. marinus*, cell mortality is likely mediated in some way by the defense system of the oyster. In the *P. marinus* model component, the biology of the parasite and the processes determining the rate of cell division are treated separately from those that describe the oyster's defense system and the rate of cell mortality.

Cell division time for *P. marinus* depends upon temperature, salinity and cell density. Given the limited observations on *P. marinus* growth *in vivo*, this process was modeled using standard relationships for temperature and salinity dependencies which were calibrated by comparing the simulated growth of *P. marinus* to data sets that provide observations of the time dependency of parasite infection intensity. Simulations of *P. marinus* using just temperature and salinity dependencies resulted in cell growth rates and cell densities that were too high relative to those suggested by field measurements. Most measurements of protozoa in culture show that cell division rate decreases at high population densities as food becomes limiting. An empirical relationship that modifies the specific cell division rate at high cell density was obtained experimentally. Mortality of *P. marinus* cells is presumably a result of the oyster defense system and is temperature and salinity dependent. As with cell division, cell mortality is dependent on cell density.

Examination of the combined effect of the specific growth and mortality relationships on the specific rate of *P. marinus* population growth shows that no net population growth occurs at 20°C and 20‰. The population growth rate becomes negative at low temperature regardless of salinity and at low salinity regardless of temperature. Therefore, when subjected to these environmental extremes, the *P. marinus* population decreases in concentration and infection level in an individual oyster. At high salinity and temperature, the specific population growth rate is positive and the population density increases.

The *P. marinus* population depends on the oyster host to provide sufficient energy to support cell respiration and cell growth. Thus, the energy requirement of the parasite population, Ec, can be expressed as:

$$Ec = Eg + Er - El \tag{5}$$

where Eg is the energy required to increase the population biomass through cell division and Er is the energy requirement for population respiration. The last term on the right of equation (5), El, represents the return of energy to the host from the parasite which occurs through cell mortality. The energy requirement for population growth is defined by $Eg - El$ and is determined by the net change in cell number ($C_{j,k}$) in the *P. marinus* population in a specific time interval. The respiratory energy required by the *P. marinus* population is obtained from measurements made for protozoa using a Q_{10} of 2.

The primary effects of *P. marinus* infection on oysters are to reduce oyster filtration rate and eventually cause host mortality. Measurements of the effect of *P. marinus* on oyster filtration rate show an exponential decrease in oyster filtration rate that depends on the ratio of the number of cells of the parasite to the size (weight) of the host. A relationship between host mortality, host size and *P. marinus* cell number can be obtained assuming that host mortality occurs when the energy demand of the *P. marinus* cell population is some fraction of the host's net production. The specific relationship was obtained by comparing the results of simulations with data on oyster populations reported in the field studies. The final relationship relating lethal cell density to oyster size is a regression of the form:

$$C_{L_j} = 10^{(\nu \log_{10}((\frac{W_j}{z})^q + \sigma)} \tag{6}$$

and yields lethal cell densities equivalent to a Mackin's level of 5 for all oyster size classes, as required by the literature. Values for the coefficients can be found in the Appendices.

The specific rate of infection of uninfected oyster individuals, $r(\eta)$, was assumed to be the result of an interpopulation transmission rate, $r(\eta)_b$, and an intrapopulation specific transmission rate, $r(\eta)_0$ as:

$$r(\eta)_{(k=0)} = r(\eta)_b + r(\eta)_0 (\frac{P_1 + P_2 + P_3}{3}) \tag{7}$$

where P_1, P_2 and P_3 are factors that modify the intrapopulation transmission rate and represent oyster density, *P. marinus* prevalence and *P. marinus* infection intensity, respectively.

ENVIRONMENTAL TIME SERIES AND PARAMETERIZATION

The oyster model requires environmental time series for food, salinity, temperature, turbidity, and flow speed. Data for temperature, salinity, chlorophyll and

turbidity (total seston) were obtained from data collected by HSRL (Haskin Shellfish Research Laboratory) scientists during 1981-1986, with the most time-intensive collections made between 1982 and 1984. Data for Egg Island simulations were taken from a site just south of Egg Island in Delaware Bay (39°10.46' N 75°5.05' W. This site is representative of the inshore leased grounds used by the oyster industry. The second site, used for the Kelly Island simulations, was located just east of the Delaware Bay Ship Channel opposite of Kelly Island (39°14.44' N 75°16.47' W). HSRL collected no data from the Delaware side of the bay and no closer data could be obtained. This site is representative of the seed beds that supply the oysters transplanted to leased grounds by the industry each spring.

The six-year time series showed very similar yearly trends. Examples of temperature, salinity, total suspended solids, and chlorophyll appear as Figures 1-7. The largest fraction of the data plotted came from years 1982-1984 when sampling was most intensive. In these figures, W represents a seven-day running average, F, a fortnightly running average, and M, a monthly running average. Values at the bottom of the graph (mostly values of the seven-day running average) indicate occasions when missing observations prevented the calculation of a running-mean. Fortnightly running averages were used for the simulations reported upon here. In all cases, bottom data were used. In cases where bottom data were less complete than surface data, missing bottom data were estimated by the relationship of surface to bottom values in other points of the time series. Chlorophyll data were converted to food supply (mg AFDW l^{-1}) using the following equation:

$$Food = 0.088 * chlorophyll + 0.26. \tag{8}$$

This equation recognizes that oyster food can include a significant non-chlorophyll explained component.

During verification studies in Galveston Bay, simulated oyster populations were found to better agree with observation if a non-chlorophyll explained component was added to obtain total food supply. To do this, a relationship between chlorophyll and total available food obtained by Thomas Soniat (now at Nicholls State Univ.) was used. This relationship was

$$Food = 0.088 * chlorophyll + 0.52. \tag{9}$$

In verification studies for Delaware Bay, conducted during the course of this study and discussed in a later section, we found that chlorophyll alone did not provide an adequate food supply, as was also found for Galveston Bay. Unfortunately, a relationship of the type provided by Soniat was not available for Delaware Bay. The

relationship used (equation 8) was derived iteratively by comparing model output to observations collected by HSRL scientists. Equation (8) differs from equation (9) by the value assumed for the non-chlorophyll explained food.

Velocity values for a typical tidal cycle were obtained from Offshore & Coastal Technologies, Inc. These values were repeated each tidal cycle throughout the simulation.

MODEL CONFIGURATION AND APPROACH

Simulations used the post-settlement oyster population dynamics model. Larval settlement was prohibited and predators were not included. The chief oyster disease, *Perkinsus marinus*, however, was included, as previously discussed. The rationale for simplifying the model by removing the effect of predators and larval settlement is as follows.

Predators are not affected by turbidity. Their presence in the simulation would have added complexity to population mortality, making the effect of *P. marinus* more difficult to discern. *P. marinus* was included because disease intensity is related to the relative rates of growth of the disease organisms and the oyster and oyster growth rates are directly affected by turbidity.

Larvae are affected by turbidity. Growth rates decline and mortality rates increase. However, larvae are also distributed widely by water motion and spend a significant portion of the time in the upper, less turbid portion of the water column. Generally, long-term point source pollution effects are observed principally in the benthos immediately downstream rather than in the plankton. In addition, the removal of larval settlement made examination of the effects on juveniles and market-size adults more clear. Finally, initial simulations indicated that populations opposite Kelly Island probably are not self-supporting. Larvae settling in these areas are derived from populations located elsewhere, because food supplies in summer and fall in this reach are not adequate for larval growth; thus most larvae, exposed only to these conditions, do not survive to settlement size.

As *P. marinus* mortality exerted a steady drain on population abundance, an early September settlement event was stipulated in each simulated year to stabilize total population abundance. This settlement, 25% of initial population abundance, was independent of yearly fecundity and its value was chosen based on the expectation that *P. marinus* mortality would account for 20% to 50% of the population yearly.

Each simulation was run for 6 yr, beginning on January 1 of year 1 (Julian day 1). The time step used was 1 hr. The model was initialized with a size-frequency distribution representative of that found in the Egg Island area. Initial *P. marinus*

prevalence was set at 50%. Experience with this type of simulation has indicated that *P. marinus* prevalence and infection intensity take about 1 year of simulation to reach equilibrium with environmental conditions. Thus, results in year 1 were not used for subsequent interpretation and all manipulations of time series were introduced in year 2.

Storms were introduced into the simulation only once per simulation, in year two. We examined storms in the months of May, August, October, and December. Besides choosing one simulation in each of the four seasons, the specific timing was chosen as follows. The May event occurred late in the spring bloom when water temperatures were high enough to produce the highest oyster growth rates. The August event occurred during the hottest, driest period when disease intensity was near its zenith. Population mortality normally peaks in August and September. October's storm took place during the height of the fall harvest. December was a typical winter month.

Storm events were of 4 days duration and used bottom turbidity values of 2 g l^{-1} obtained as a representative mean value from simulations of the sediment transport model by Offshore & Coastal Technologies, Inc. In addition, 30 day turbidity events were examined. These simulations were used to clarify the effects of turbidity in comparison to the 4-day and baseline (no storm) cases. They also simulated the conditions that might occur during catastrophic failure of the containment structures. Each simulation was run for 6 yr to identify long-term effects, if they existed.

VERIFICATION

We relied on the following key population attributes for verification: biomass-frequency distribution, spawning season, *P. marinus* prevalence and infection intensity, and population mortality from disease. Each of these attributes accrues from a complex interaction of the oyster's (and disease organisms') life cycle and the environment. Thus, they are robust indicators of model accuracy. Moreover, these are measures for which significant information is available from past studies in Delaware Bay. Data for comparison were made available by HSRL scientists and included measurements made during the 1982-1984 time period from whence the largest fraction of the data that produced the environmental time series were also derived.

Results of verification studies for both localities showed that biomass-frequency, *P. marinus* prevalence, spawning season, and population mortality fell within the range of measured values. *P. marinus* infection intensity was somewhat overestimated during summer months; however, we describe in an Appendix (Hofmann et al., 1995) that this result is often produced by differences between the fraction of the population sampled by field biologists and the fraction of

the population censused during the simulation, so that this overestimate can be expected in comparing simulations of this sort with field data. Accordingly, the model adequately simulates the normal population dynamics of oysters in both locales.

RESULTS

Egg Island

The baseline case (no storms) shows a broad, stable biomass-frequency distribution with most individuals between size classes 5 and 9 in early summer (Figure 8). In this and all other figures, the x-axis is time in Julian days and the large and small tics are year, half-year, and month markers. Contours in this case are log(individuals). Size classes 1-3 are juveniles and size class 6 is a market-size adult, so most individuals reach market size in this simulation, as would be expected for oysters not succumbing to predators on the leased grounds. (Recall that predation is not included so that juvenile mortality, mostly due to predation, is not a component of these simulations.) Growth to market size takes more than one year, also as expected. Spawning begins in June and peaks in July and August (Figure 9). The dashed line in Figure 9 records the presence of gonadal material; the solid line records actual spawns, both in units of log(joules). The solid line in Figure 10 shows total abundance during the simulation as log(individuals) (left-hand y axis). Larval settlement was set in this simulation to about equal *P. marinus* mortality, as stated earlier.

P. marinus prevalence reaches near 100% each summer as documented by field sampling and infection intensity peaks at 4 (a moderately-heavy infection on the 0-to-5-point scale of Mackin) (Figures 11,12). In Figure 11, the market-size population is indicated by -=- and the total population by a solid line. In Figure 12, a -o- indicates the market-size population. (These figures are explained in more detail in the Appendices.) Mortalities are primarily in the market-size fraction of the population, a distribution typical of *P. marinus* mortality. (Recall that predator mortality, normally skewed towards the smaller size classes, was not included, there being no direct connection between predation and turbidity). *P. marinus*-produced mortality peaks in September at about 20% of the population (Figure 10; -.-, right-hand y-axis), about 40% of the market-size individuals, but epizootic conditions do not occur. (Although *P.marinus* may not have been present in Delaware Bay during 1981-1986, certainly epizootic conditions did not occur in those years.)

An 4-day increase in turbidity in any of the 4 months examined had no observable effect. A 30-day increase in turbidity reduced juvenile growth when the increase occurred in October, December or May, however the population recovered within one-half year. Slower growth could have exposed these juveniles to predation

for a longer time period, however predation rates are normally low during the cooler months, so no long term effects should have accrued. The effect of a 30-day rise in turbidity was more intense when the increase occurred in August. Spawning ceased early (solid line in Figure 13) and mortality from *P. marinus* rose (-.-, Figure 14). Nearly two years were required for the population to recover to the baseline state.

Kelly Island

The baseline case (no storms) shows a broad, stable biomass-frequency distribution with most individuals between size classes 3 and 6 in early summer (Figure 15). Size class 6 is a market-size adult, so most individuals do not reach market size, as is typical for the seed beds. *P. marinus* prevalence reaches near 100% each summer as documented by field sampling and infection intensity peaks at 4.3 (a moderately-heavy infection on the 0-to-5-point scale of Mackin) and a slight overestimate of field values (Figure 16). Mortalities are distributed over most adult size classes; individuals less than market size are several years old because growth rates are slow and these older individuals succumb to the disease. Spawning begins in June and peaks in July and August (Figure 17). *P. marinus*-produced mortality peaks in September at about 20% of the population, but epizootic conditions do not occur (Figure 18).

A 4-day increase in turbidity had no observable effect except in August. Fecundity fell after a 4-day increase in turbidity in August (Figure 19, solid line). A 30-day increase in turbidity produced reduced juvenile growth in May, however this decrease disappeared within one-half year. The total number of market-size individuals declined during year 2, but recovered in year 3. *P. marinus*-induced mortality increased when increased turbidity occurred in December, May and August. Once again, the effect of a 30-day rise in turbidity was most intense when the increase occurred in August. Spawning ceased completely (solid line, Figure 20) and mortality from *P. marinus* rose significantly (-.-, Figure 21) The population required nearly two years to recover to the baseline state, assuming an external supply of larvae as modeled in these simulations. A 30-day turbidity episode in August, but at a order of magnitude lower level (0.2 g l^{-1} rather than 2.0 g l^{-1}), resulted in decreased fecundity, however the entire spawn was not lost and no increase in *P. marinus*-induced mortality was observed. No effects occurred if this lower-intensity turbidity episode occurred in May.

Simulations with larval settlement added

An equivalent series of simulations was run with larval settlement added. For ease of presentation, the turbidity event was introduced into year 3 rather than year 2 in these simulations. The same trends were present as described earlier. Figures 22 through 25 show examples of these simulations for the month of August. At the

Egg Island site, a 30-day turbidity event causes a cessation of spawning (Figure 22, solid line). This loss produces an increase in Dermo infection intensity (Figure 23, solid line) because reduced fecundity reduces the number of uninfected individuals added by larval settlement. The increase in infection intensity about doubles the rate of mortality produced by Dermo (Figure 24, -.-). A 4-day turbidity event has only a minor effect. At Kelly Island, a 30-day turbidity event in August significantly restricts spawning (Figure 24, solid line). A 4-day turbidity event produces a lesser, but still noticeable reduction in fecundity (Figure 25, solid line). Lesser effects were noted in all other months. Thus, general trends and the critical physiological processes affected are the same in this simulation type as in those without larval settlement discussed in more detail earlier.

DISCUSSION

The effects of channel deepening include the possibility of increased salinity intrusion into Delaware Bay and the possible increase in turbidity associated with the beneficial use of dredge material at disposal sites. Simulations of Delaware Bay using a hydrodynamics model developed and run by the Waterways Experiment Station has indicated that salinity would normally rise in Delaware Bay by <1‰. A salinity rise of this magnitude is unlikely to produce any significant impacts on oyster populations. Simulations of salinity changes of this order, in other applications, have consistently shown no effect over most of the salinity range experienced by oyster populations. Accordingly, no additional simulations were run to investigate the effect of salinity change.

The simulations run for this report were designed to assess the impact of increased turbidity as a result of the disposal plan that includes containment at Kelly Island and Egg Island. Under certain circumstances, a 30-day rise in turbidity produced decreased growth rates, increased mortality, and decreased fecundity. Each is related to a decrease in food supply which directly limits growth and fecundity and, because *P marinus* growth is not equivalently inhibited, permits increased infection intensities and subsequent mortalities. Effects produced by high-turbidity events in October and December were limited; filtration rates decline during these months as temperature declines, so ingestion rates are normally low and a further reduction is of little consequence. Effects are somewhat greater from a high turbidity event in May, however the size of the spring bloom dampens the overall impact. In effect, even with the higher turbidity and lower filtration rate, enough food is present to sustain reasonable growth and reproductive development.

In contrast, a high turbidity event in August consistently produces the most serious impact. A much reduced or failed spawn occurred, commonly coupled with an increase in population mortality due to *P. marinus*. Conditions in late summer exacerbate the effects of a drop in food supply. Food supply is already low, high temperatures have increased metabolic rate, thus reducing scope for growth

even further, most energy is being allocated to reproduction so reproduction is most sensitive to a decline in food, and environmental conditions promote rapid proliferation of *P. marinus*. Thus, in Delaware Bay, a summer increase in turbidity is likely to be, by far, the most damaging.

Oysters from the Kelly Island locale (actually directly across the Delaware Bay Ship Channel) were more greatly affected by increased turbidity than oysters from the Egg Island locale. Food supply was significantly lower in the Kelly Island time series, during and after the spring bloom. Decreased food supply exacerbated the effects of increased turbidity. Although other data sets would need to be examined for confirmation, these simulations suggest that, in Delaware Bay, food concentration in the late summer and early fall is likely to be a good predictor of the sensitivity of populations to increased turbidity.

A 4-day storm produced no noticeable effects in any month except August, and only then at the Kelly Island locale where food supply was particularly low. A 4-day storm, at this locale, significantly reduced fecundity. The environmental time series used came from the Delaware Bay seed grounds. This simulation emphasizes the sensitivity of the seed beds to increased turbidity during the summer months.

Overall, the simulations suggest that increased turbidity in the Egg Island area is unlikely to have a major impact, as long as direct smothering does not occur. Only late summer events of substantial duration should have any significant impact. Most populations recover from impacts over the next 12 to 24 months. The upestuary site, Kelly Island, is much more sensitive to turbidity, especially long-term exposures that might occur following catastrophic failure of containment structures, and especially in late summer. The greater sensitivity of the upestuary site to increased turbidity should be taken into account in developing disposal plans for dredge materials at Kelly Island or elsewhere in the bay reach supporting the oyster seed beds. These seed beds, existing under inherently low food supplies, do not have the reserves required to easily withstand increased turbidity levels.

In light of the sensitivity of the Kelly Island area, certain mitigation measures might be planned for in case a catastrophic containment failure did occur. These measures might include monitoring to determine impacts and replacement or rehabilitation of damaged oyster bottom. Inherent in any monitoring approach to assess damage is the need for data obtained prior to the containment failure. Routine sampling, minimally twice a year (winter and summer), would be necessary to assure that the required data were available. Possible effects of containment failure include mortality due to smothering, and reduced growth and reproduction due to lowered rates of filtration. Measurements, both of the status quo ante and to assess possible effects subsequent to containment failure, must include methods to assess these three likely impacts and, thus, should include abundance, size (biomass) frequency, disease *Perkinsus marinus* infection intensity, reproductive

state (gonadal index by histological examination or immunological probe), and recent mortality (by number of new boxes).

Measures might be considered designed to replace or rehabilitate oyster bottom damaged by containment failure. The Army Corps of Engineers Galveston District Office has recently built oyster reefs in Matagorda Bay and the applicability of their approach for Delaware Bay might be assessed. A study of artificial reefs in Galveston Bay showed that artificial reefs did as well as natural reefs in the same area. Thus success was determined by environment rather than origin. Studies in Louisiana have shown that most forms of $CaCO_3$ are more or less equivalent as clutch (e.g. oyster shell, clam shell, crushed limestone), however their long-term stability on various bottom types may vary considerably. In addition, regardless of carbonate type, success is dependent on sediment chemical and physical conditions. Softer sediments will require larger quantities of shell. Sediments that generate acid (through sulfate reduction and subsequent sulfide oxidation) will gradually destroy shell. Models are available to help assess the impact of the latter, however examination of local chemical conditions is required. Thus the development of a plan for oyster bottom creation or rehabilitation should include a chemical and physical assessment of the bottom, identification of the quantities and costs of available shell or shell substitute for substrate, a trial planting to directly assess stability of the emplaced material, and the use of a model to assess its long-term survival.

RESEARCH NEEDS

The modeling exercise has identified a number of weaknesses in the Delaware Bay data that might affect the accuracy of model simulations. Chief among these are uncertainties with regard to food supply and the detail of the environmental time series.

Available food can be divided into phytoplankton, measured by chlorophyll, and non-phytoplankton. Data for the latter are presently lacking. Verification simulations indicated that this latter source of food, not estimable from chlorophyll measurements, must be crucial, particularly in late summer and fall, for oysters in Delaware Bay. In the simulations reported upon here, we borrowed a general relationship that has proven adequate in Texas and Louisiana bays to add this non-chlorophyll-containing food to total food supply. The accuracy of this relationship for higher latitude systems remains unaddressed.

Generally, the more intensive the time series, the more accurate the simulation. In verification studies in Louisiana, in collaboration with Thomas Soniat at Nicholls State University, we observed that data collected at least weekly was necessary to obtain the best simulations. A large modeling study of Galveston Bay, using the oyster population dynamics model used here, showed that time series of one day provided much improved results over weekly or monthly values. The reason

that increased time resolution improves simulation accuracy is that many of the hourly and daily variations in the environment significantly vary ingestion rate and the rate of cell division of parasites. Thus, as an example, current velocity may, on the average, exceed the value needed to prevent overfiltration; however, if velocity is reduced for 25% of the time, ingestion will be significantly reduced for this period, even though the mean value is adequate. Basically, at some point, higher velocities do not impact ingestion, but low values do. A mean value calculated from velocities of both types will, then, normally overestimate food availability. Many physiological processes have analogous thresholds typically controlled by salinity, turbidity, or current velocity; thus more temporal resolution in the time series better approximates the environment actually responded to by the oyster population. The data presently available are weekly or less frequent measurements. Improved accuracy would accrue from a more time-intensive data set.

In addition to weaknesses in the input time series, the development of the model has permitted the identification of certain deficiencies in the data available on oyster physiology. One of these involves the process of filtration in which food is preferentially sorted from inorganic seston. The influence of turbidity on this process is not well understood. A single data set exists, in fact, relating filtration rate to turbidity and that study did not address the relationship of sorting efficiency with turbidity. Our model assumes a relatively high sorting efficiency at seston concentrations above 10 mg l^{-1}. This relationship is required to generate the appropriate growth rates and adult sizes using the known food supply and the presently available relationships between filtration rate and seston content. Although literature data are inadequate, the presently available data suggests a lower sorting efficiency because pseudofeces normally have a relatively high caloric value. For this to be true would require that the turbidity relationship be in error or that the measures of available food be incorrectly derived from chlorophyll data. Clearly, improving the estimation of the impact of turbidity above that which can presently be obtained requires a better understanding of the influence of turbidity on oyster filtration rate and sorting efficiency.

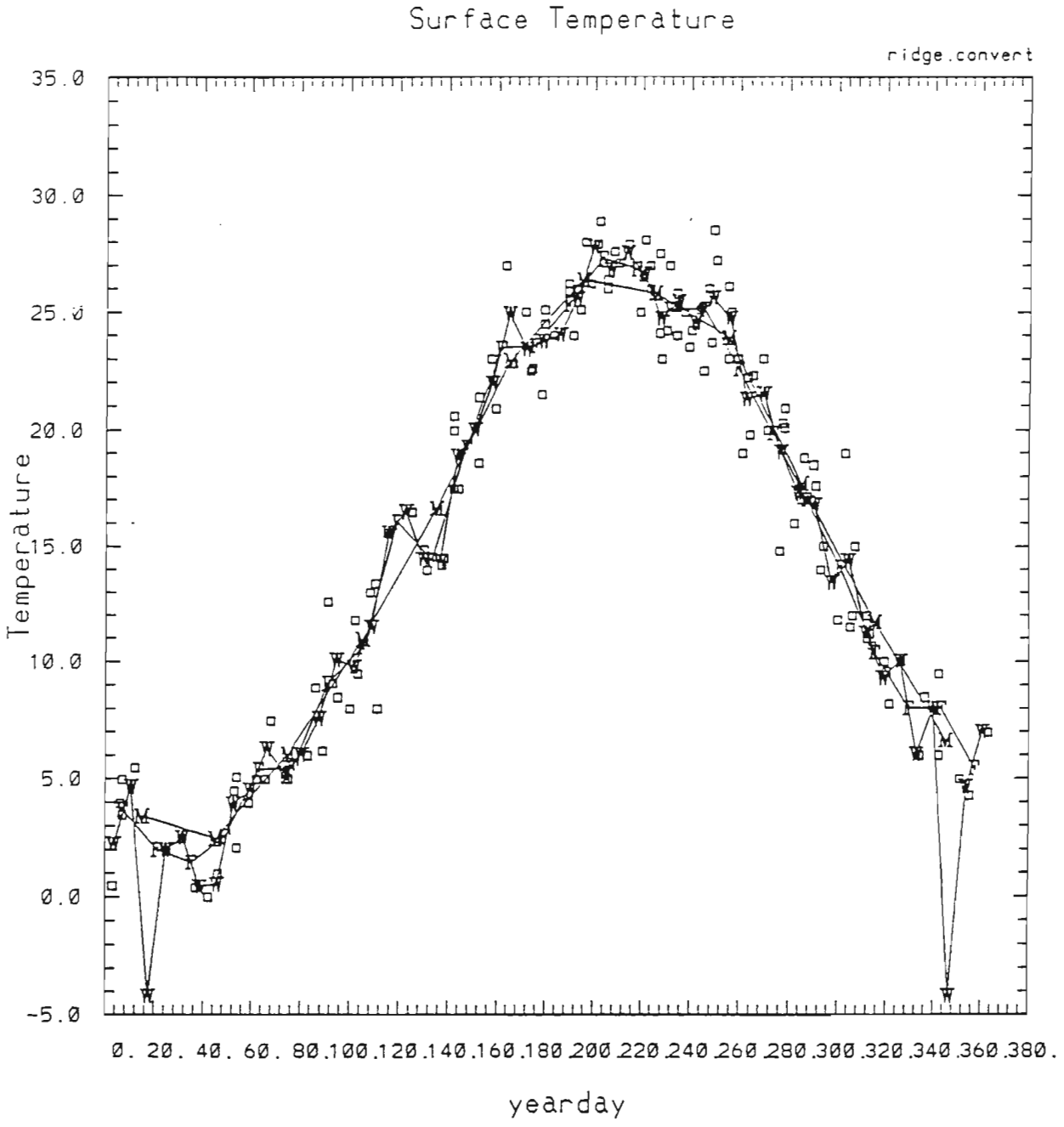
Surface Temperature
ridge.convert
35.0
30.0
25.0
20.0
15.0
10.0
5.0
0.0
-5.0
Temperature
0. 20. 40. 60. 80.100.120.140.160.180.200.220.240.260.280.300.320.340.360.380.
yearday

Figure 1

700

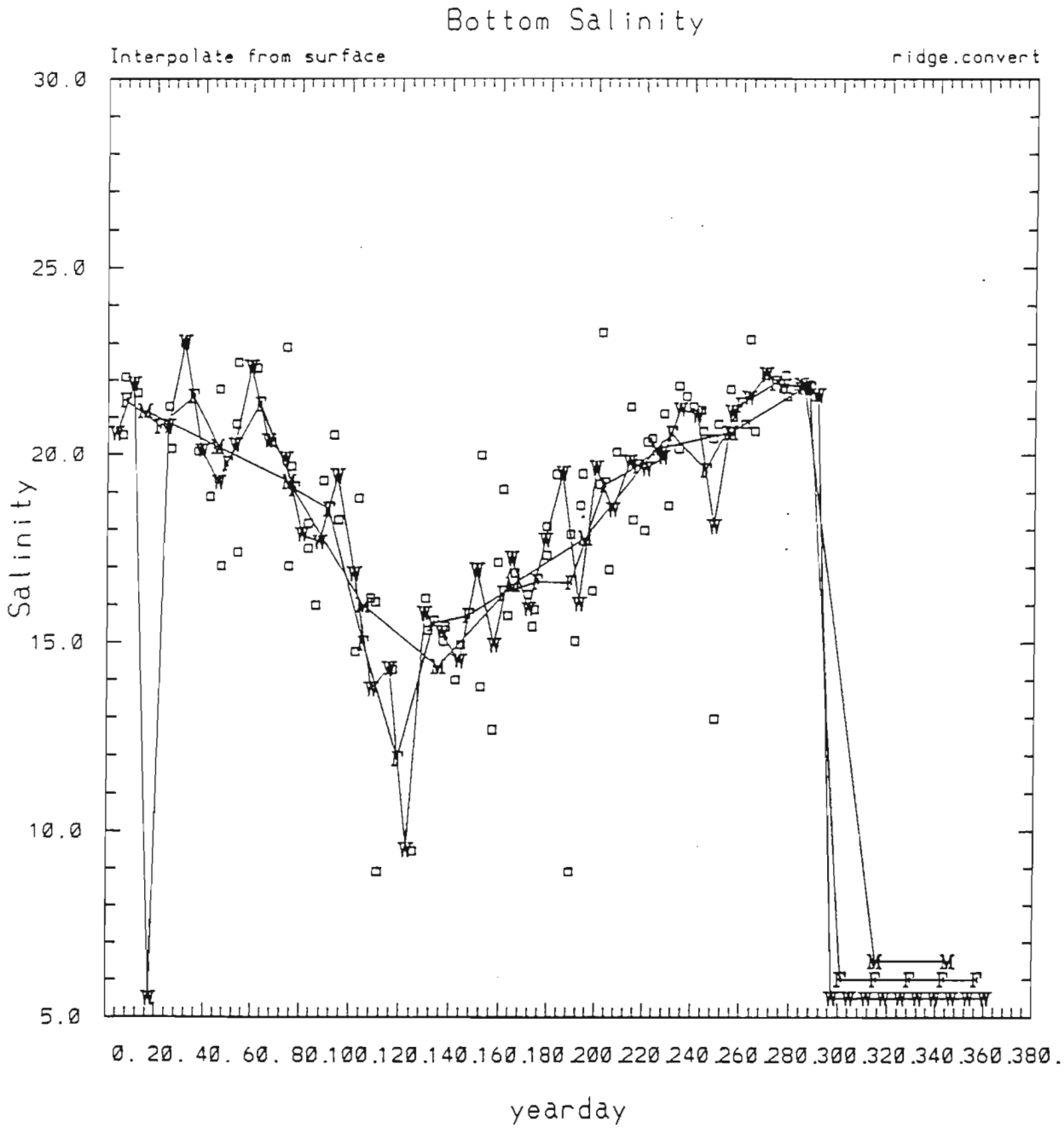
Bottom Salinity
Interpolate from surface
ridge.convert
30.0
25.0
20.0
15.0
10.0
5.0
Salinity
0. 20. 40. 60. 80.100.120.140.160.180.200.220.240.260.280.300.320.340.360.380.
yearday

Figure 2

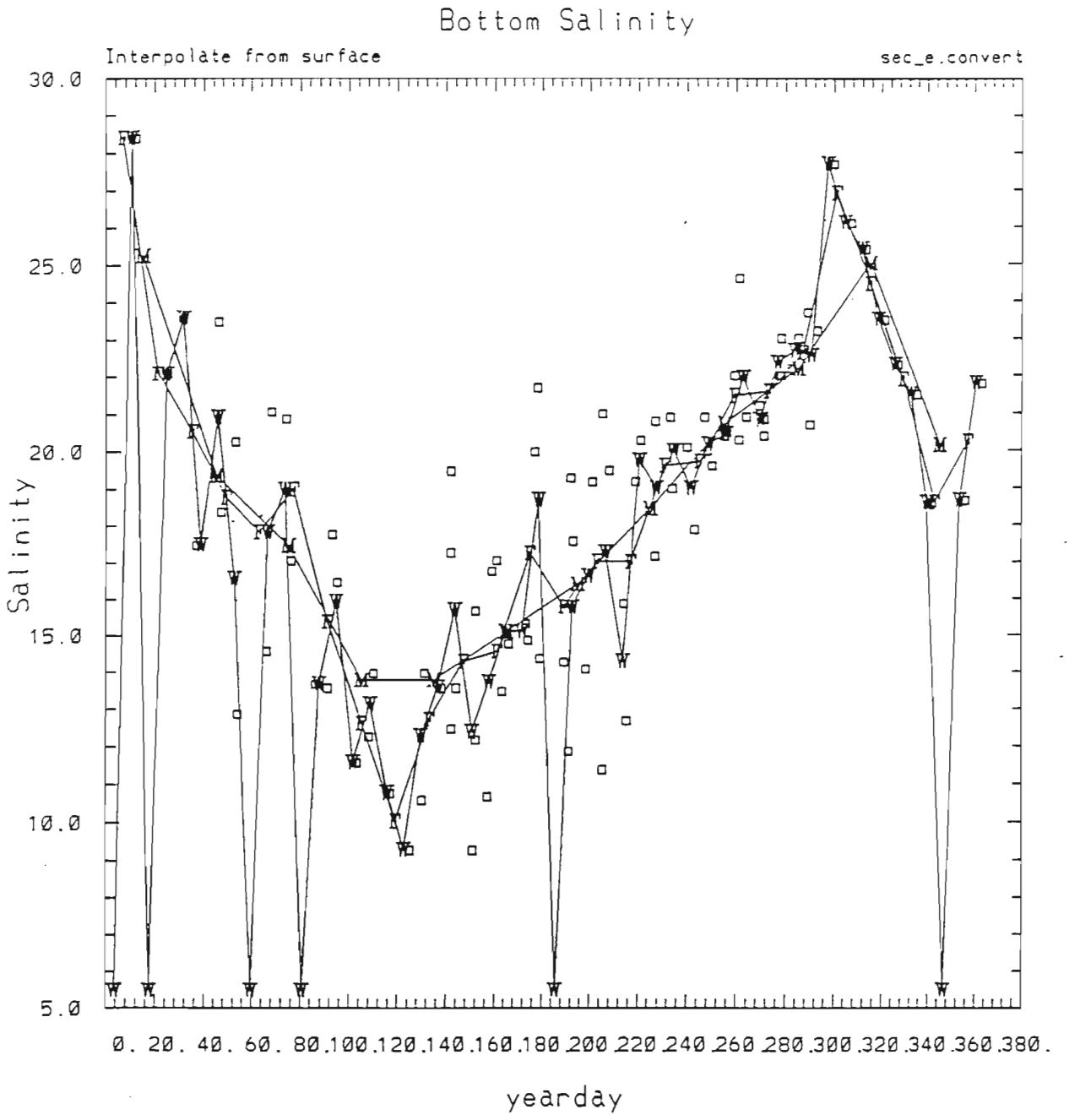
Bottom Salinity
Interpolate from surface
sec_e.convert
30.0
25.0
20.0
15.0
10.0
5.0
Salinity
0. 20. 40. 60. 80.100.120.140.160.180.200.220.240.260.280.300.320.340.360.380.
yearday

Figure 3

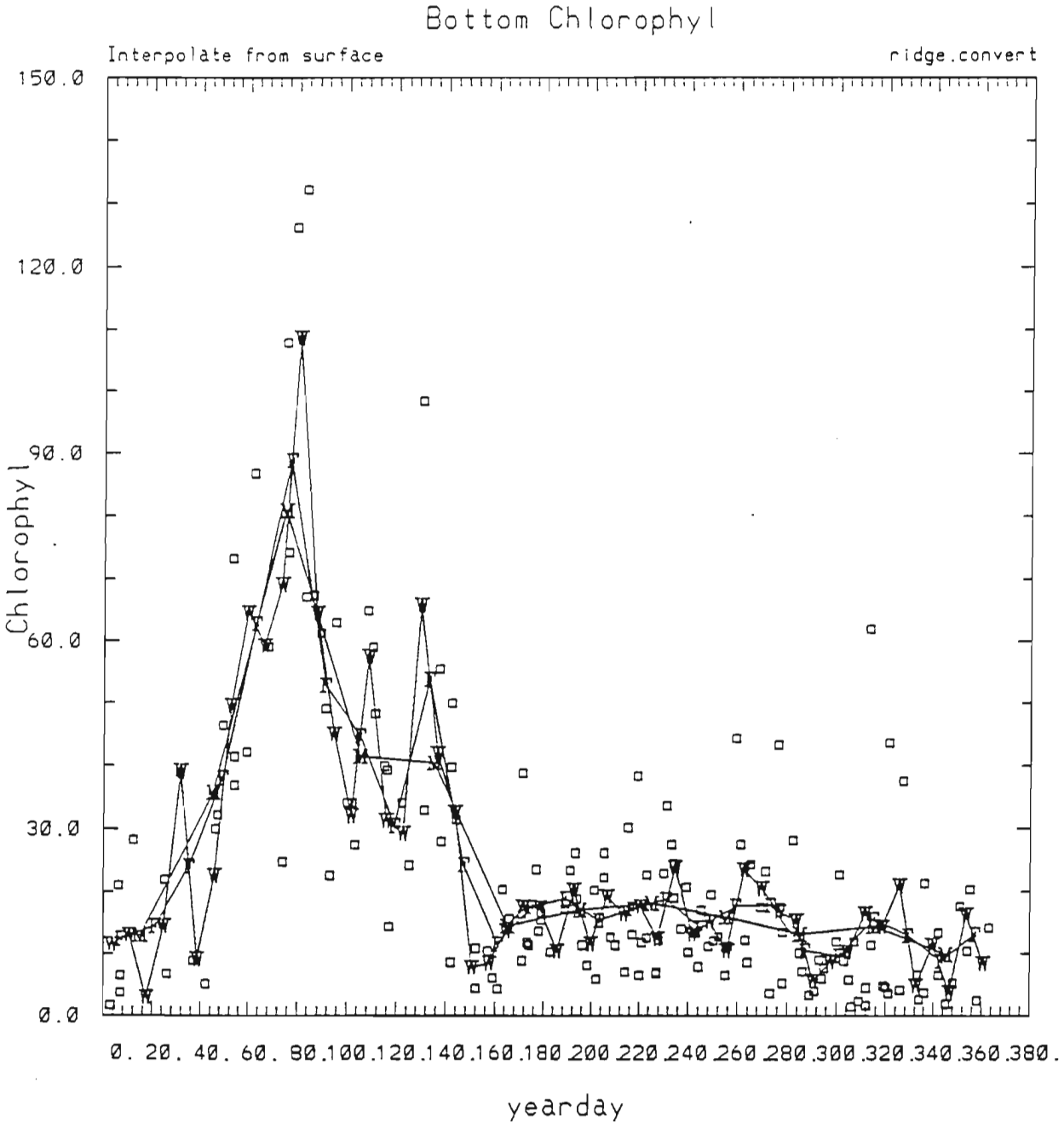
Bottom Chlorophyl
Interpolate from surface
ridge.convert
150.0
120.0
90.0
60.0
30.0
0.0
Chlorophyl
0. 20. 40. 60. 80.100.120.140.160.180.200.220.240.260.280.300.320.340.360.380.
yearday

Figure 4

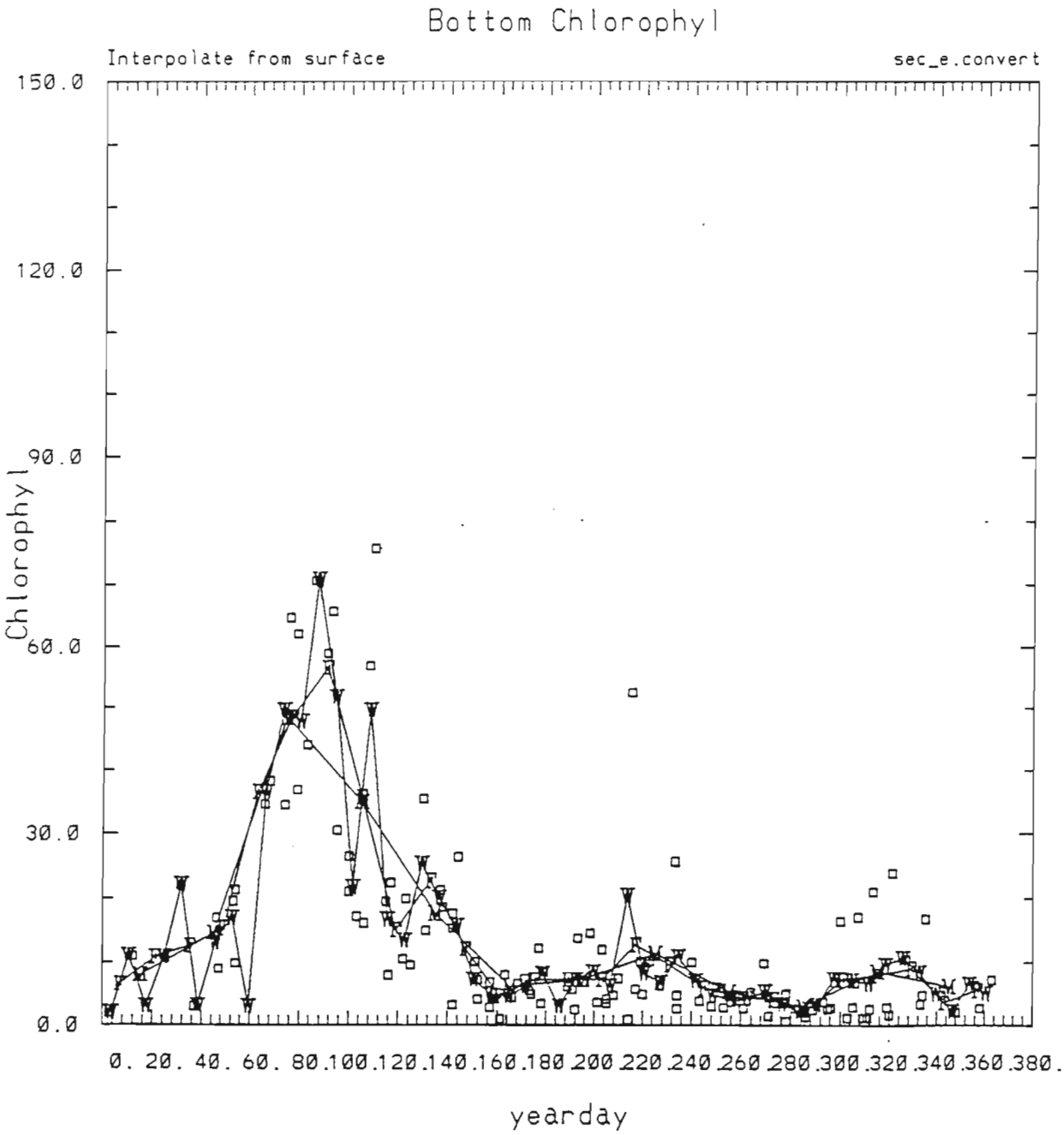
Bottom Chlorophyl
Interpolate from surface
sec_e.convert
150.0
120.0
90.0
60.0
30.0
0.0
Chlorophyl
0. 20. 40. 60. 80.100.120.140.160.180.200.220.240.260.280.300.320.340.360.380.
yearday

Figure 5

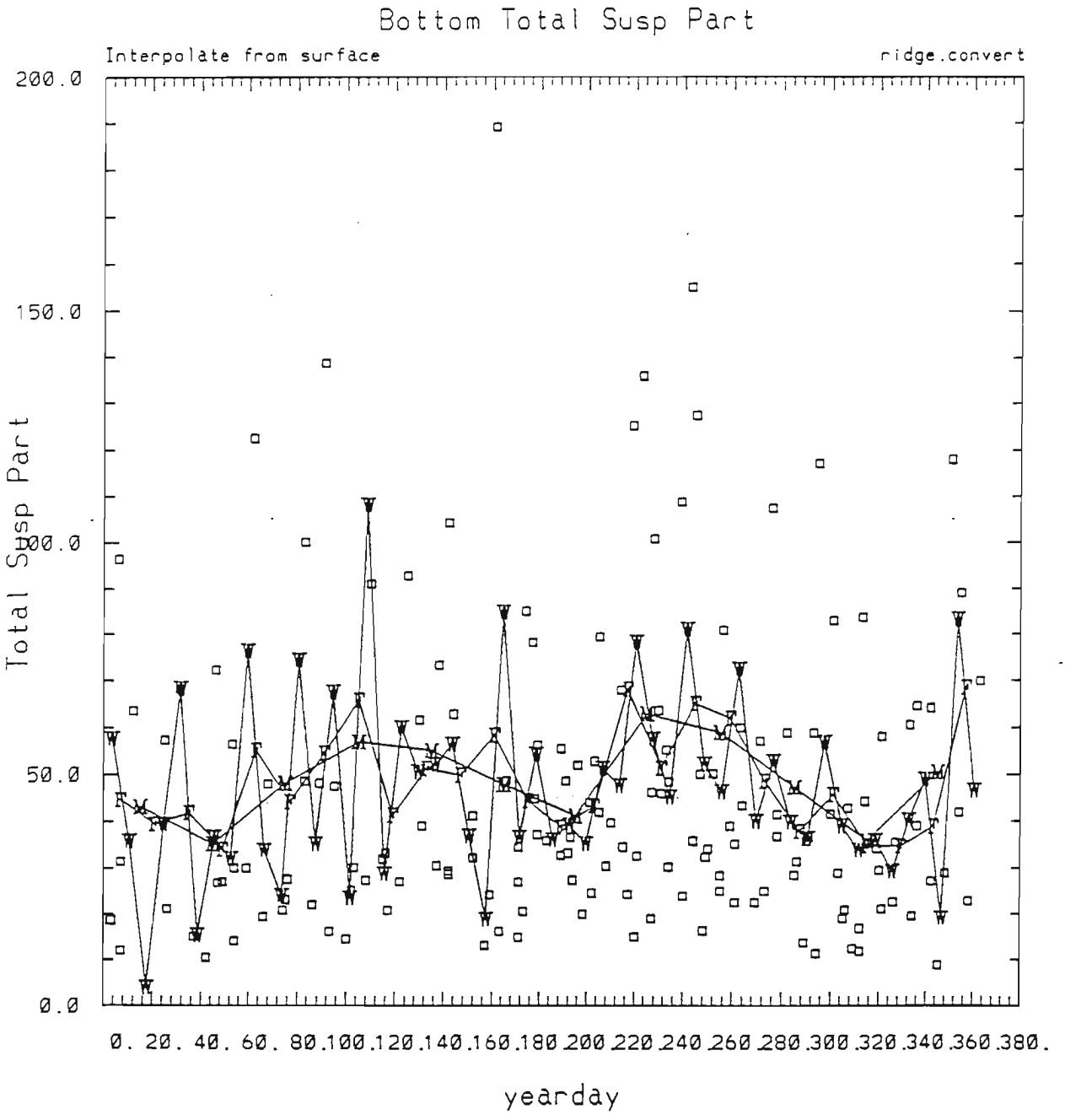
Bottom Total Susp Part
Interpolate from surface
ridge.convert
200.0
150.0
100.0
50.0
0.0
Total Susp Part
0. 20. 40. 60. 80.100.120.140.160.180.200.220.240.260.280.300.320.340.360.380.
yearday

Figure 6

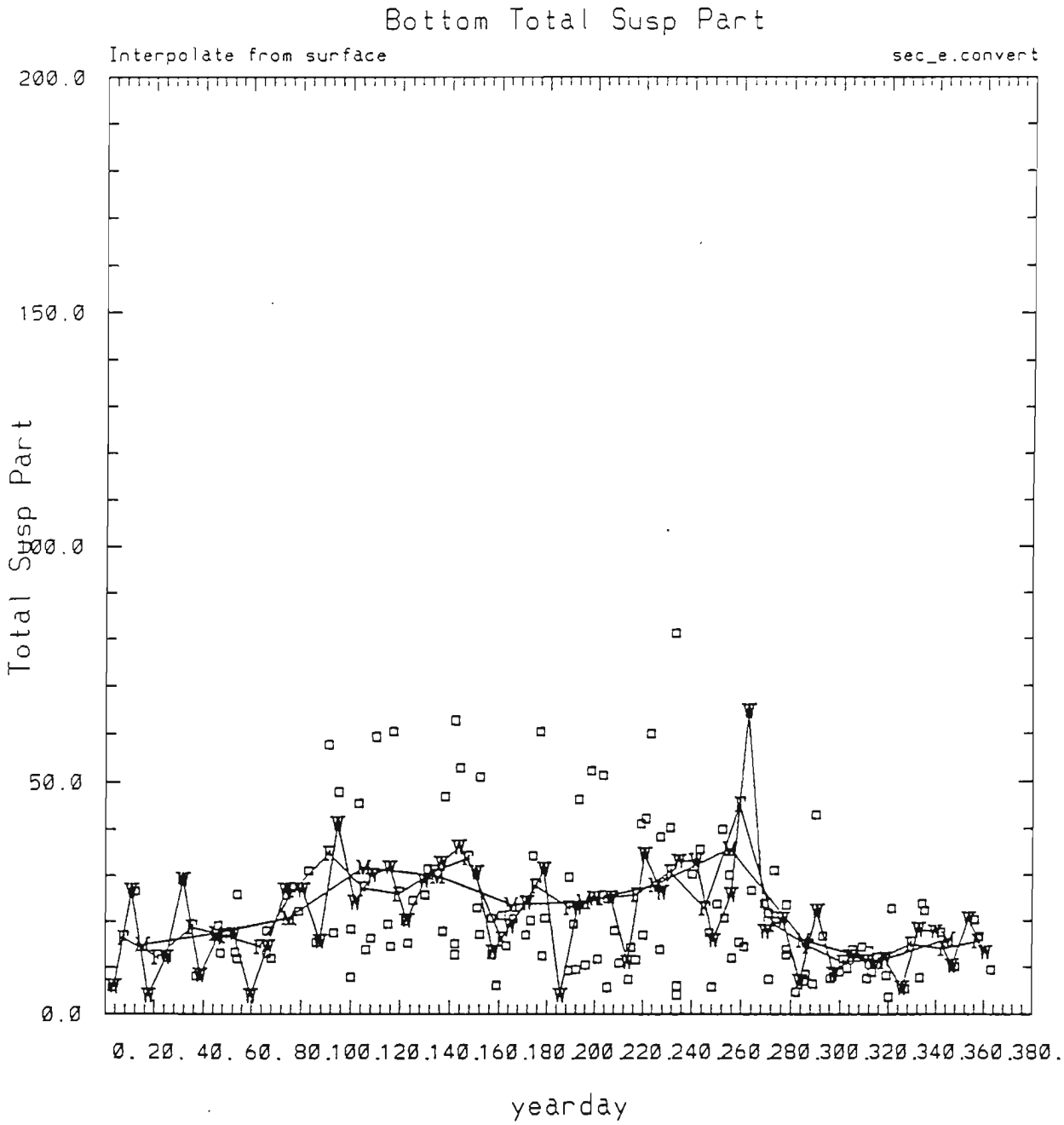
Bottom Total Susp Part
Interpolate from surface
sec_e.convert
200.0
150.0
100.0
50.0
0.0
Total Susp Part
0. 20. 40. 60. 80.100.120.140.160.180.200.220.240.260.280.300.320.340.360.380.
yearday

Figure 7

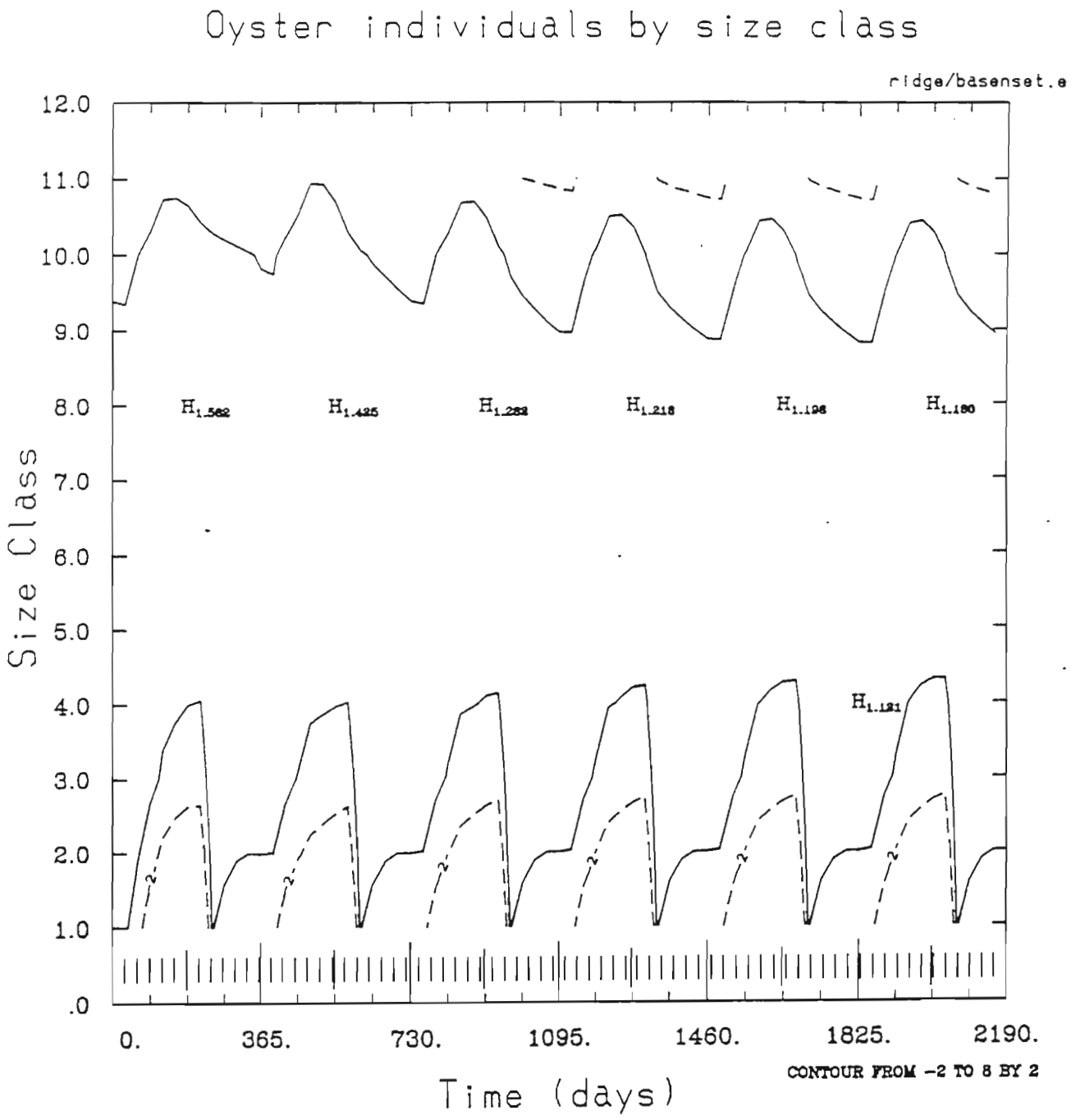
Oyster individuals by size class
ridge/basenset.e
12.0
11.0
10.0
9.0
8.0
7.0
6.0
5.0
4.0
3.0
2.0
1.0
.0
Size Class
H1.562
H1.425
H1.283
H1.218
H1.196
H1.180
H1.121
0.
365.
730.
1095.
1460.
1825.
2190.
Time (days)
CONTOUR FROM -2 TO 8 BY 2

Figure 8

707

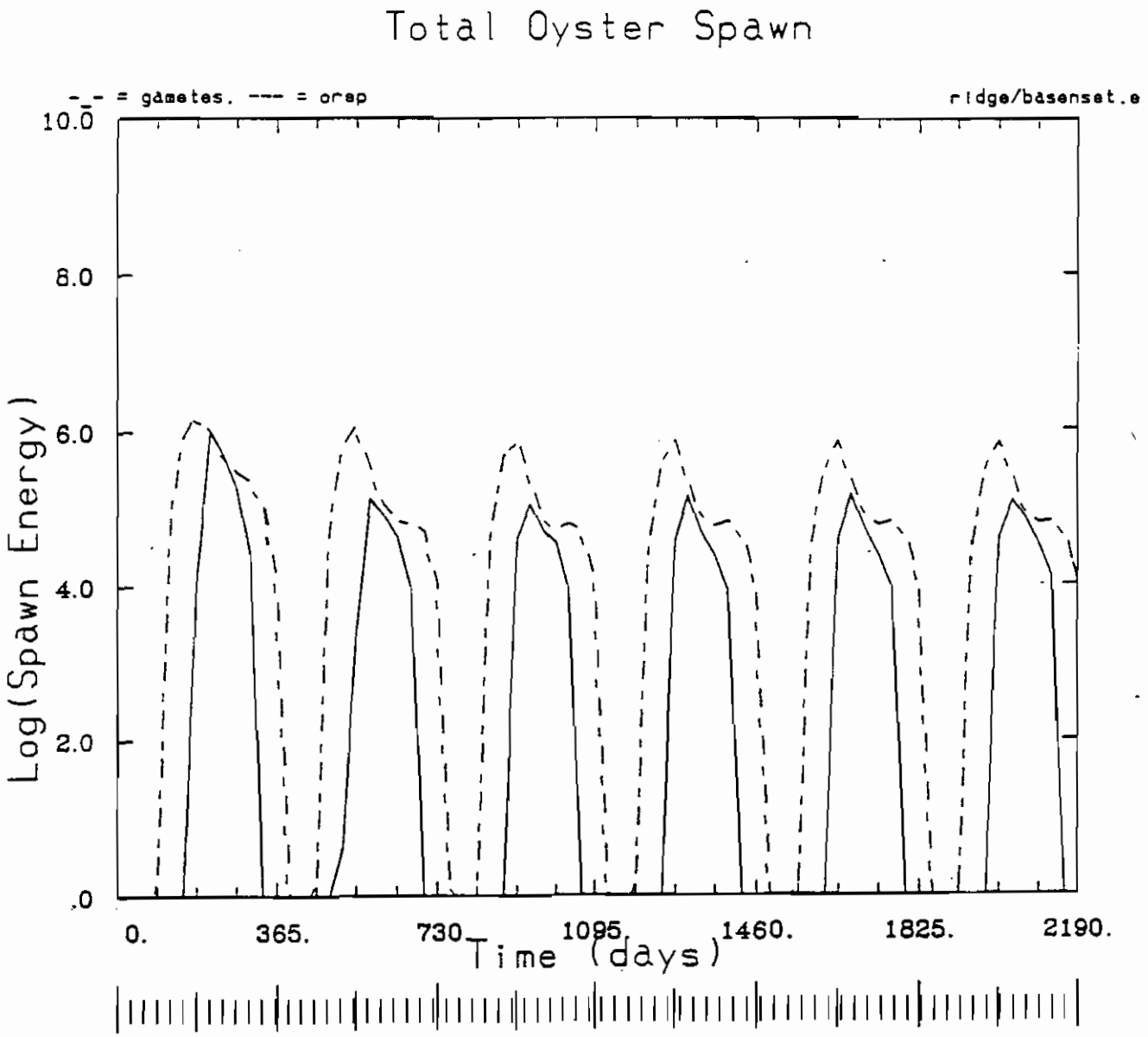
Total Oyster Spawn
-_- = gametes, --- = orep
ridge/basenset.e
10.0
8.0
6.0
4.0
2.0
.0
Log(Spawn Energy)
0.
365.
730.
1095.
1460.
1825.
2190.
Time (days)

Figure 9

708

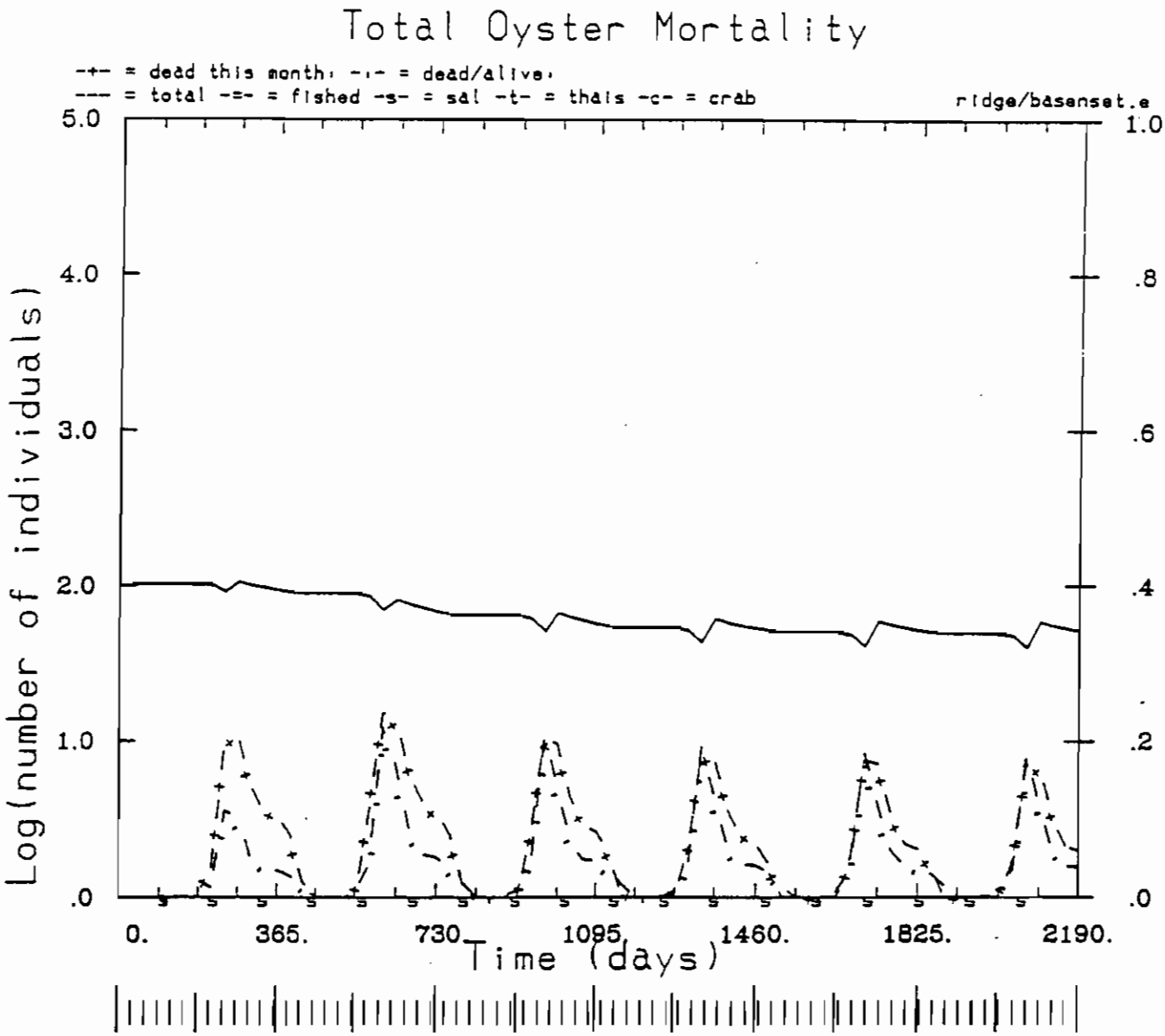

Figure 10

709

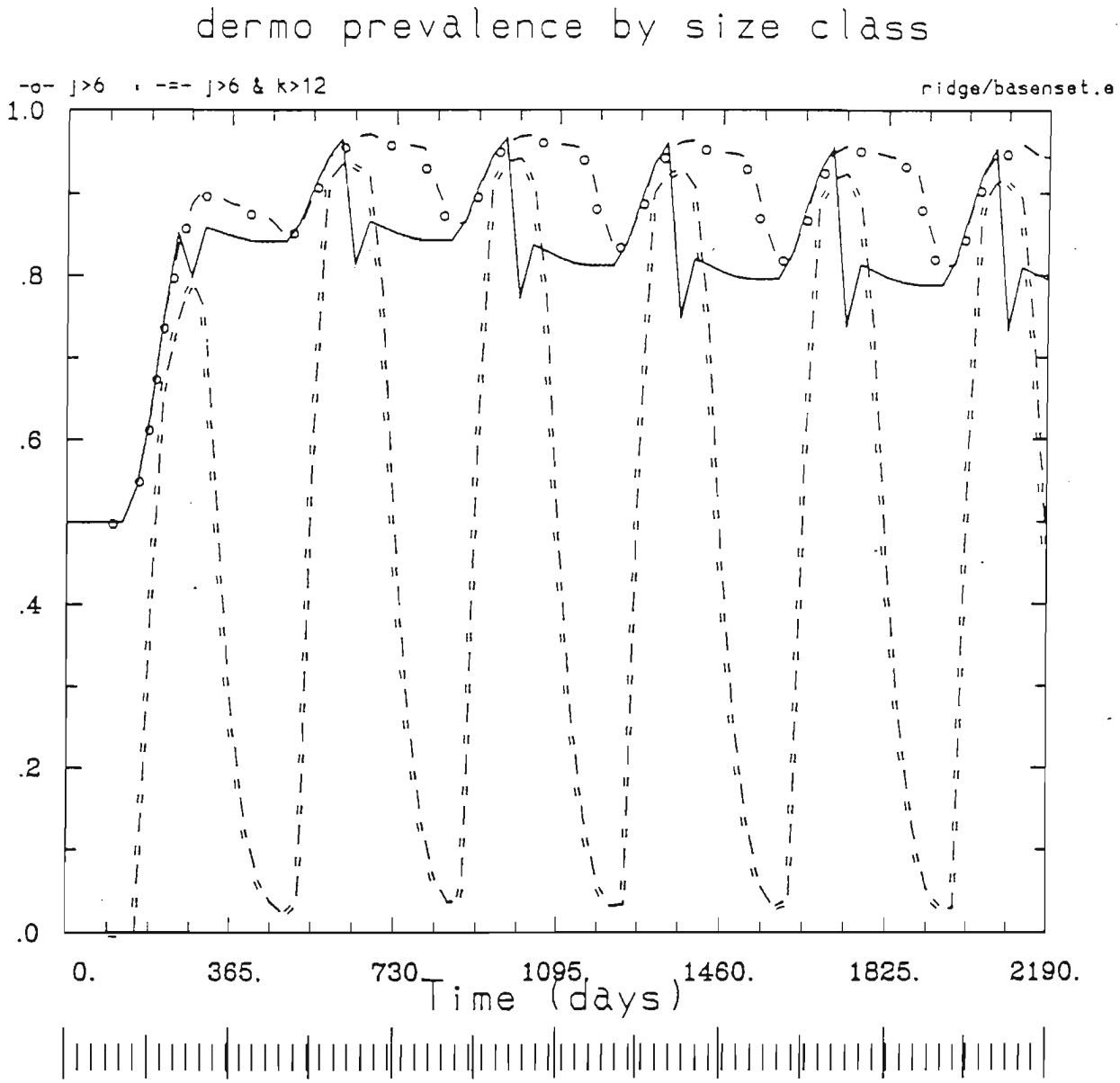

Figure 11

710

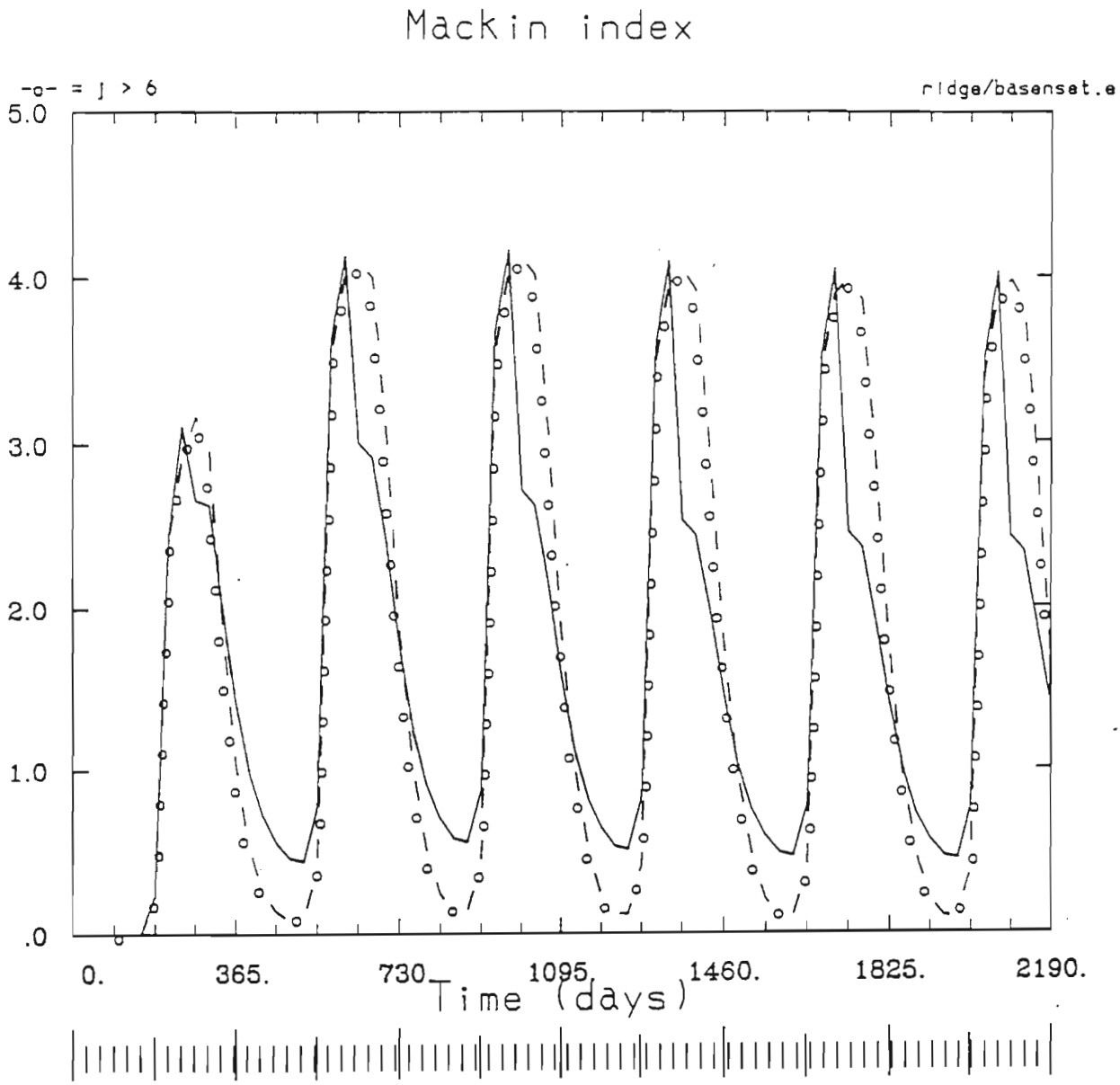
Mackin index
-o- = j > 6
ridge/basenset.e
5.0
4.0
3.0
2.0
1.0
.0
0.
365.
730.
1095.
1460.
1825.
2190.
Time (days)

Figure 12

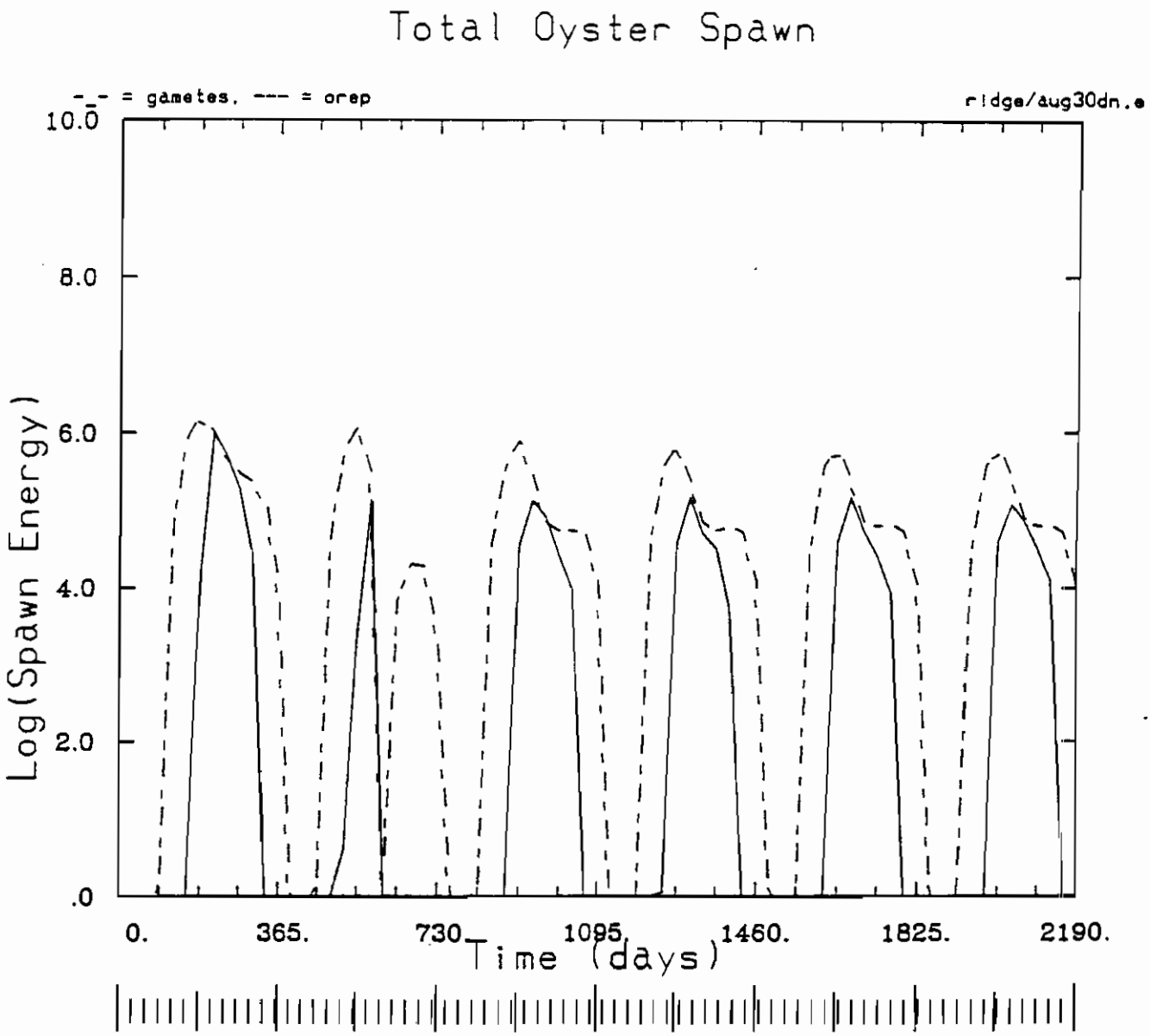
Total Oyster Spawn
-_- = gametes, --- = orep
ridge/aug30dn.e
10.0
8.0
6.0
4.0
2.0
.0
Log(Spawn Energy)
0.
365.
730.
1095.
1460.
1825.
2190.
Time (days)

Figure 13

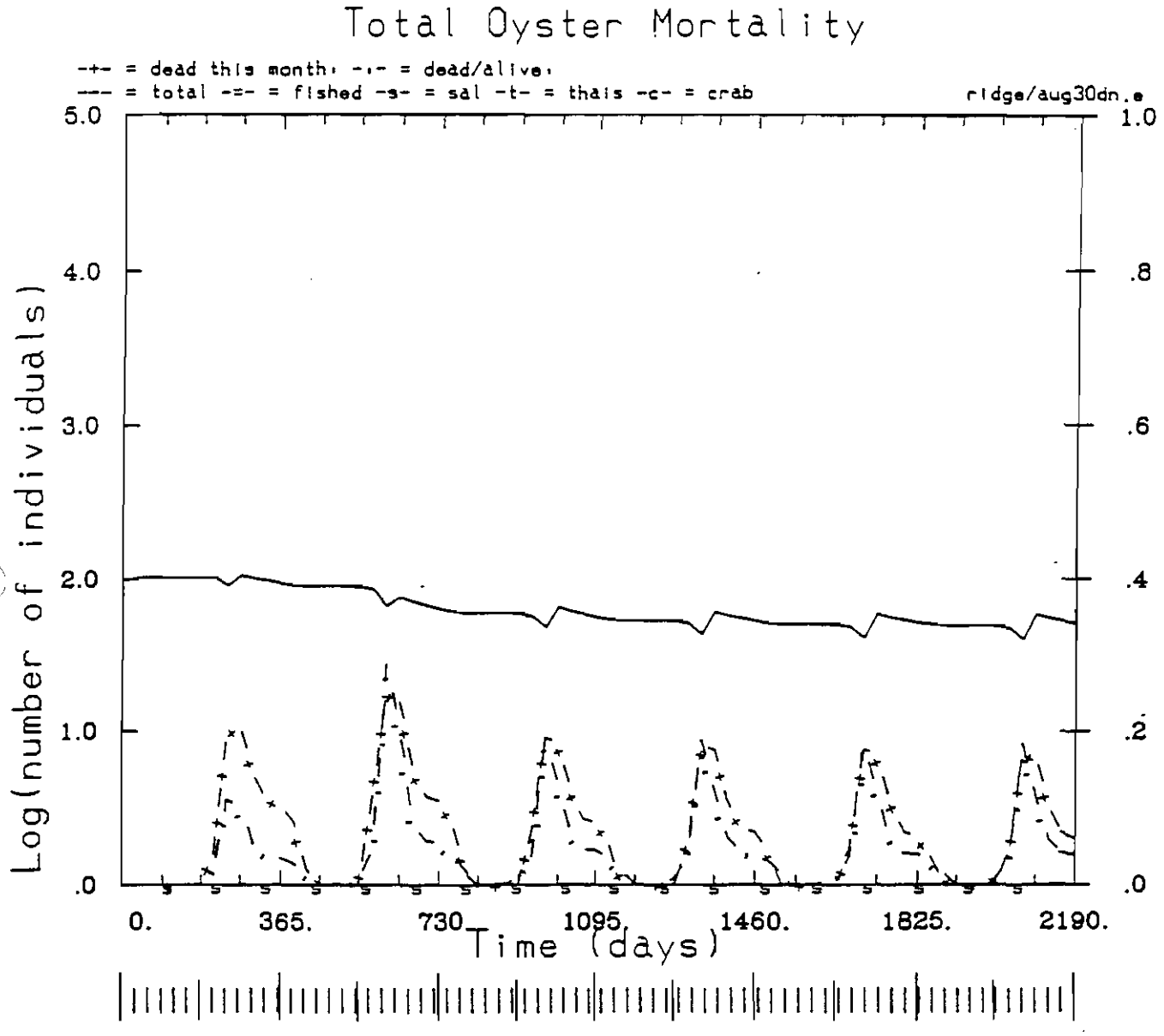
Total Oyster Mortality
-+- = dead this month, -.- = dead/alive,
--- = total -=- = fished -s- = sal -t- = thais -c- = crab
ridge/aug30dn.e
5.0
4.0
3.0
2.0
1.0
.0
1.0
.8
.6
.4
.2
.0
Log(number of individuals)
0.
365.
730.
1095.
1460.
1825.
2190.
Time (days)

Figure 14

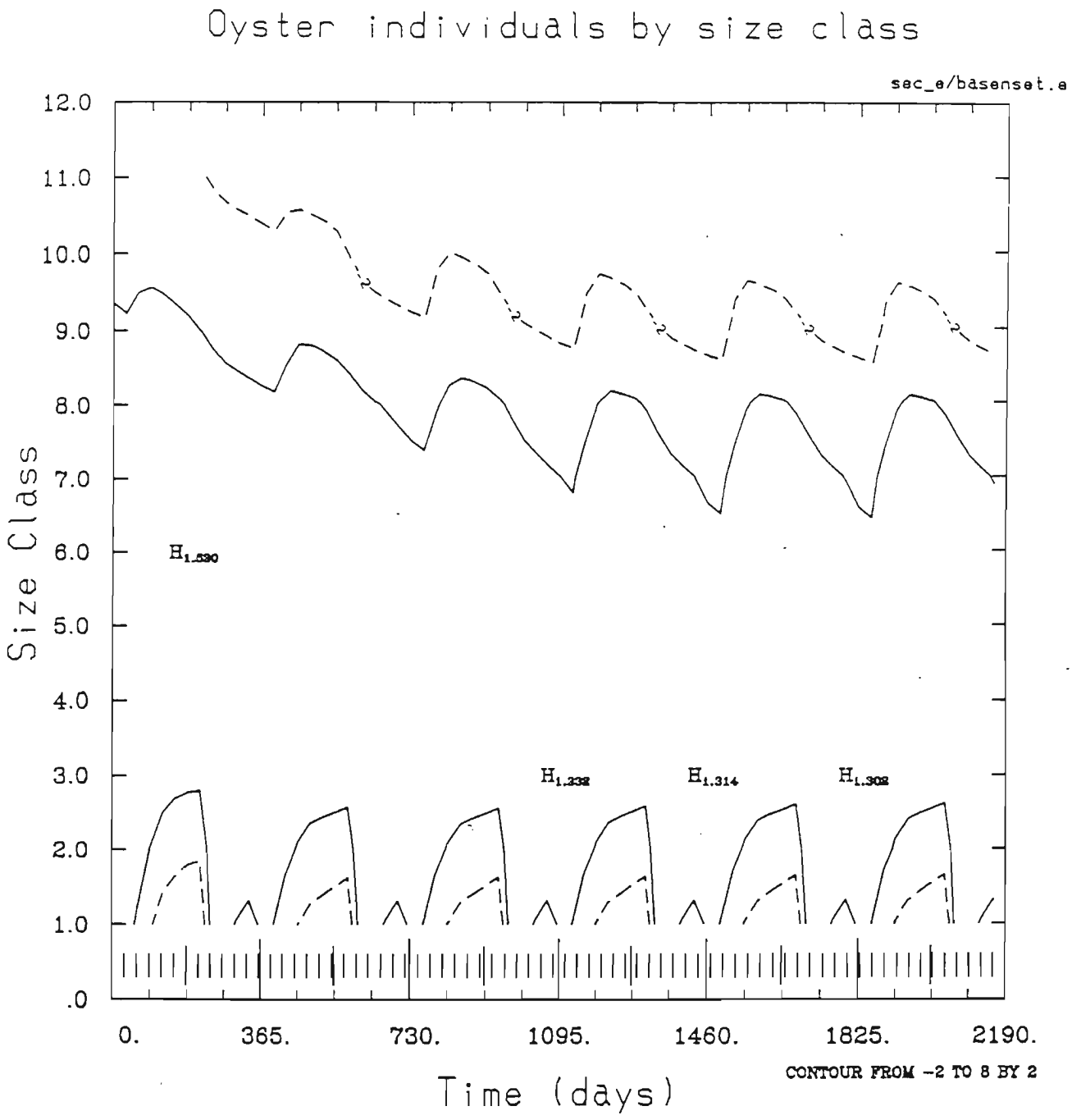
Oyster individuals by size class
sec_e/basenset.e
12.0
11.0
10.0
9.0
8.0
7.0
6.0
5.0
4.0
3.0
2.0
1.0
.0
Size Class
H1.530
H1.332
H1.314
H1.302
0.
365.
730.
1095.
1460.
1825.
2190.
Time (days)
CONTOUR FROM -2 TO 8 BY 2

Figure 15

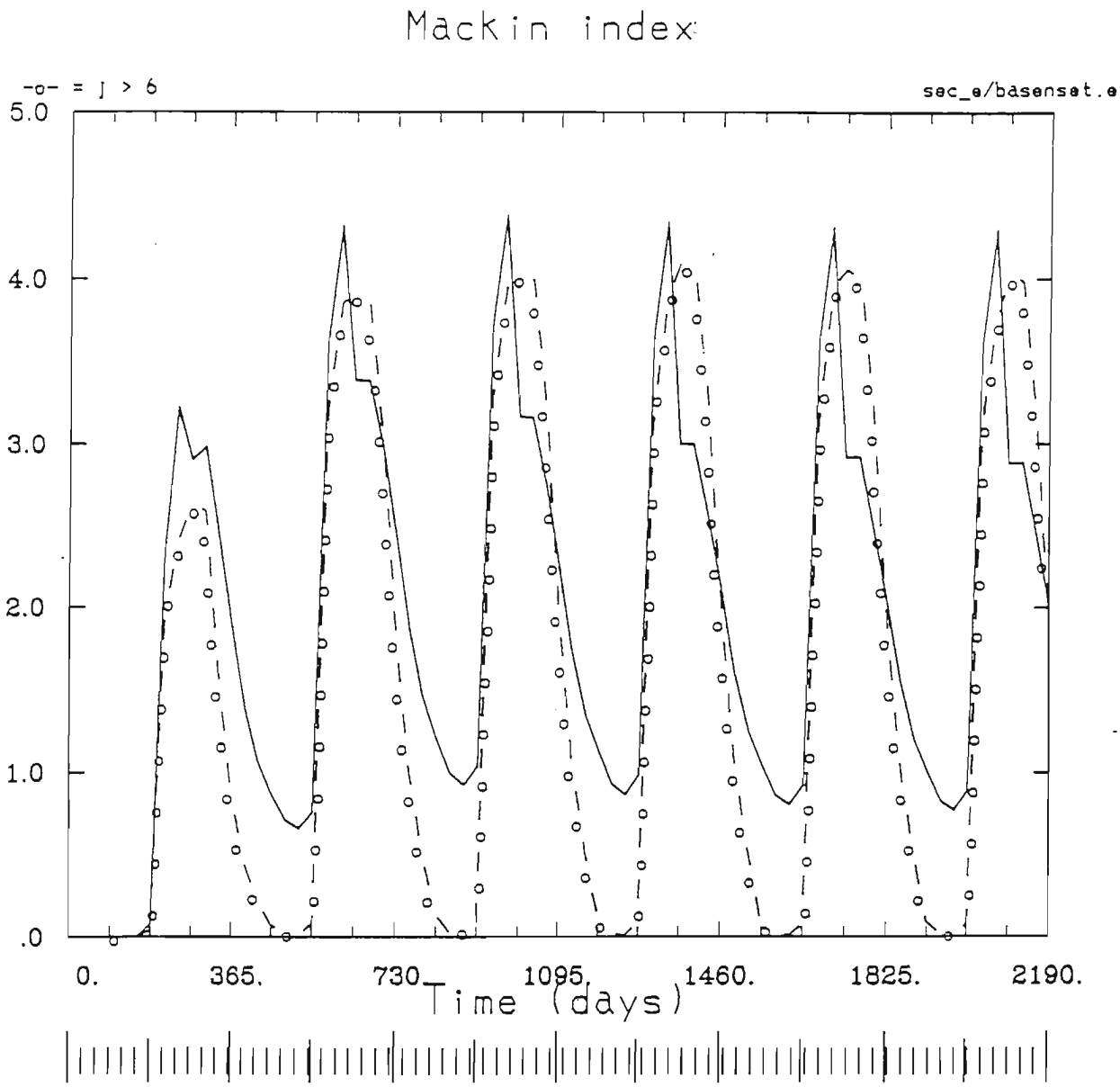

Figure 16

215

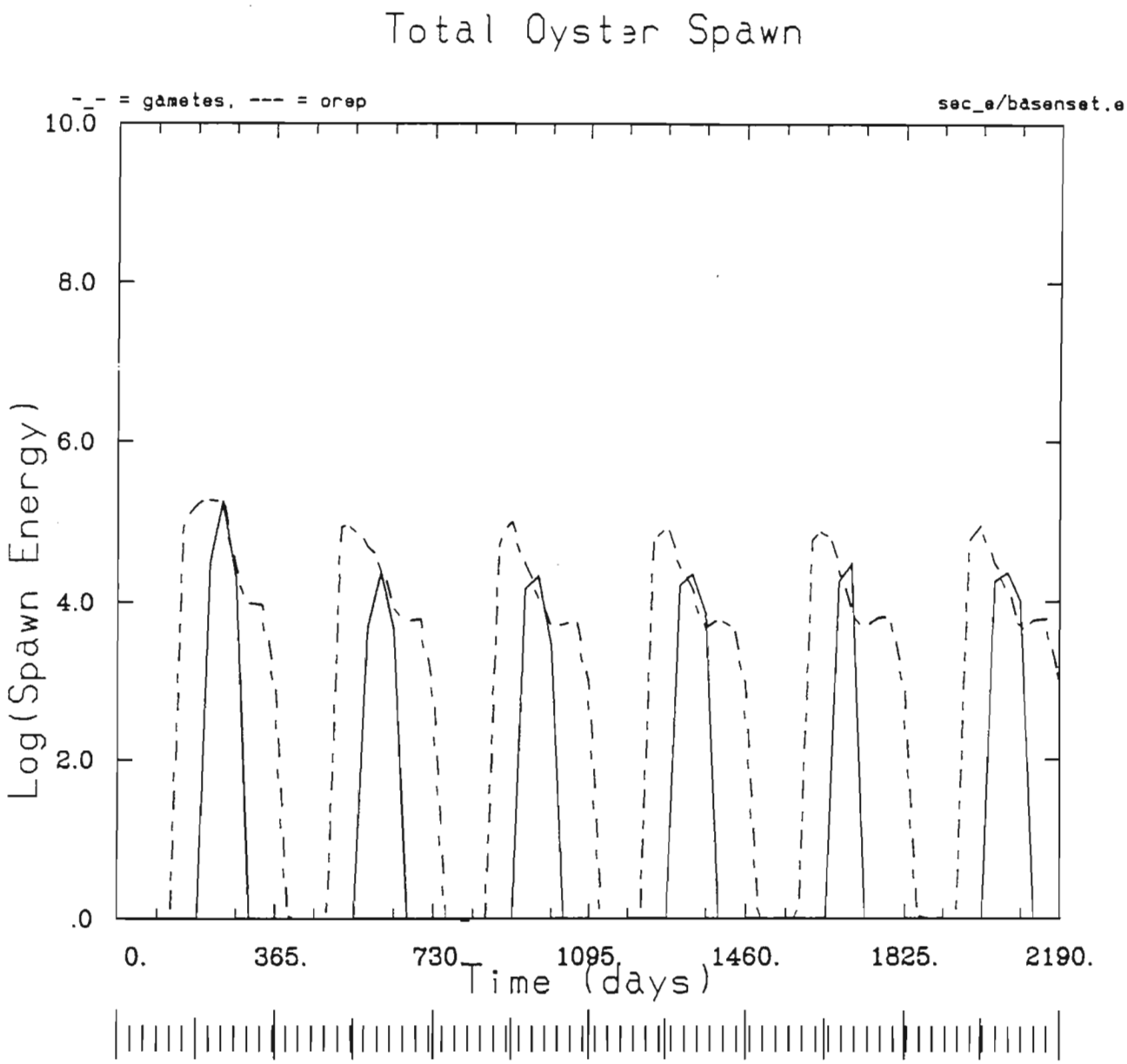
Total Oyster Spawn
-_- = gametes, --- = orep
sec_e/basenset.e
10.0
8.0
6.0
4.0
2.0
.0
Log(Spawn Energy)
0.
365.
730.
1095.
1460.
1825.
2190.
Time (days)

Figure 17

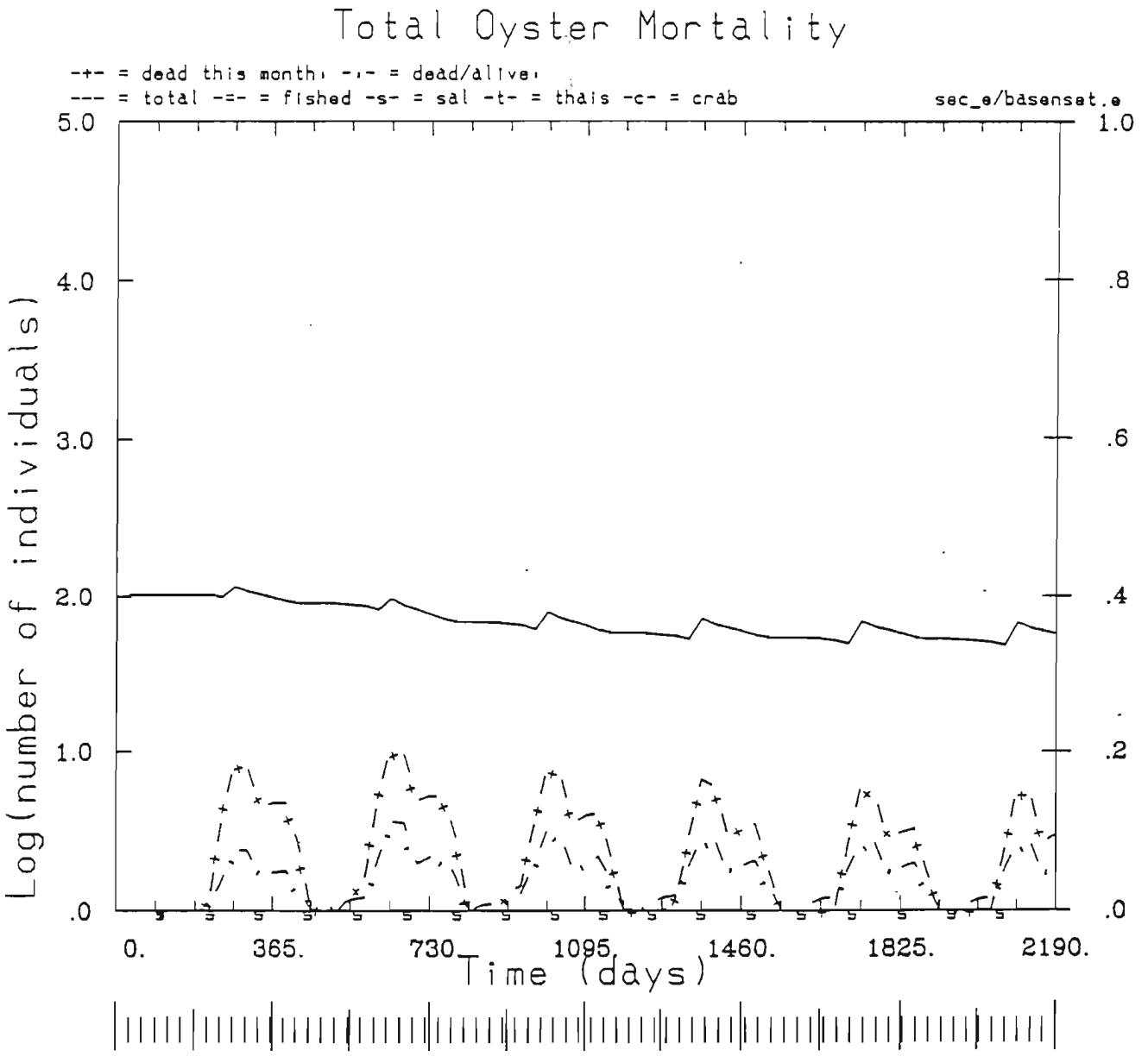
Total Oyster Mortality
-+- = dead this month; -;- = dead/alive;
--- = total -=- = fished -s- = sal -t- = thais -c- = crab
sec_e/basensat.e
Log(number of individuals)
5.0
4.0
3.0
2.0
1.0
.0
1.0
.8
.6
.4
.2
.0
0.
365.
730.
1095.
1460.
1825.
2190.
Time (days)

Figure 18

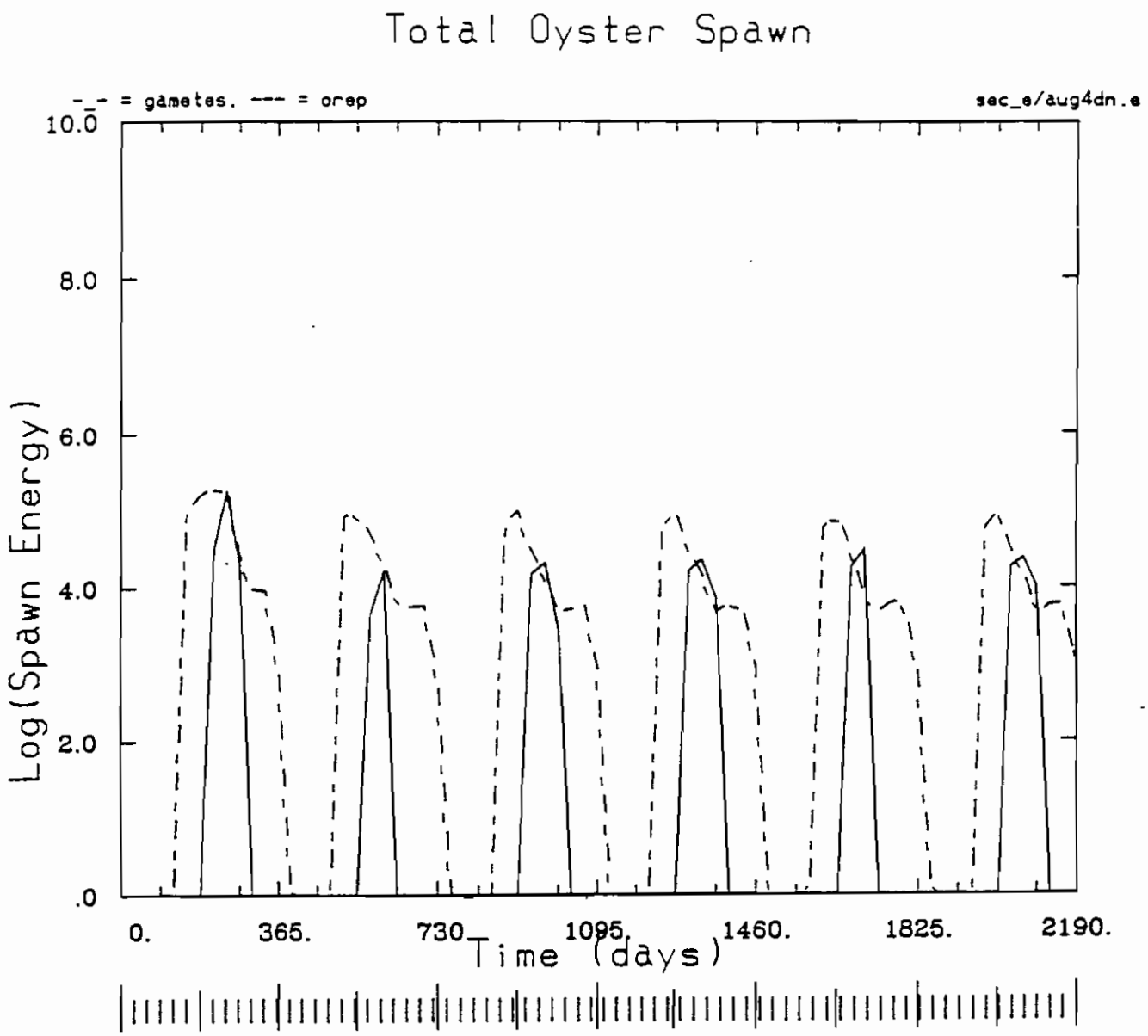
Total Oyster Spawn
-_- = gametes. --- = orep
sec_e/aug4dn.e
10.0
8.0
6.0
4.0
2.0
.0
Log(Spawn Energy)
0.
365.
730.
1095.
1460.
1825.
2190.
Time (days)

Figure 19

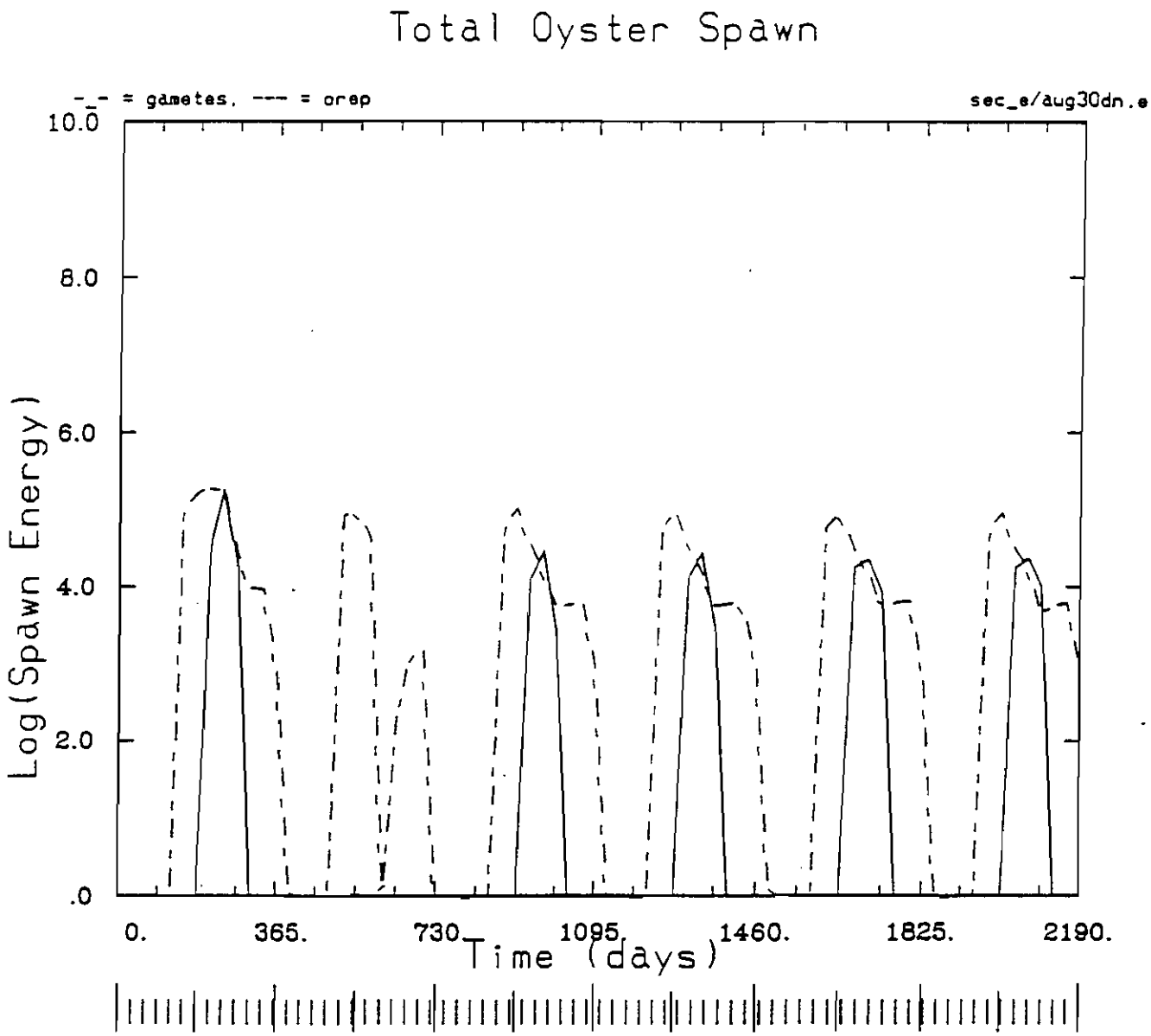
Total Oyster Spawn
-_- = gametes, --- = orep
sec_e/aug30dn.e
10.0
8.0
6.0
4.0
2.0
.0
Log(Spawn Energy)
0.
365.
730.
1095.
1460.
1825.
2190.
Time (days)

Figure 20

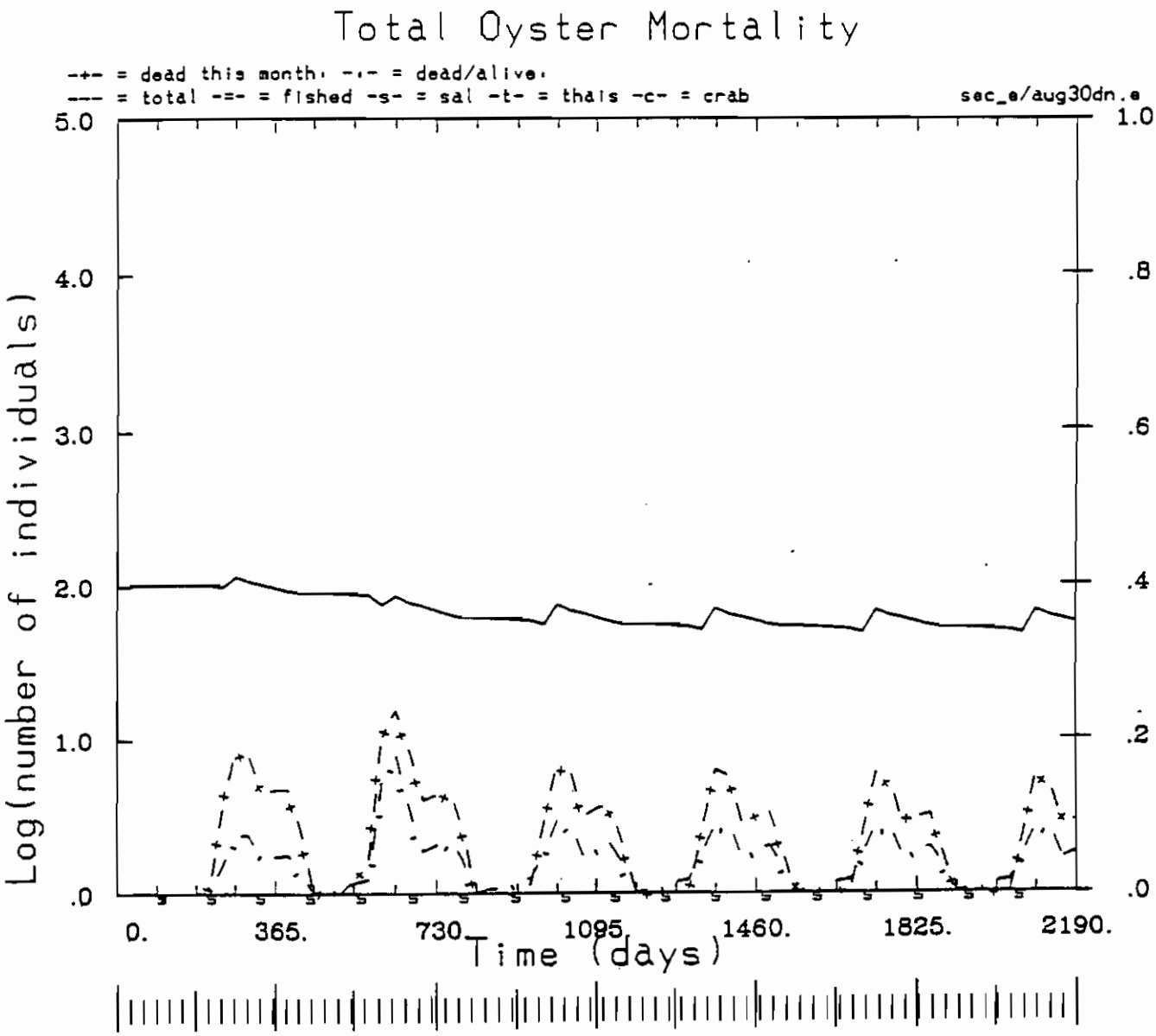
Total Oyster Mortality
-+- = dead this month, -.- = dead/alive,
--- = total -=- = fished -s- = sal -t- = thais -c- = crab
sec_e/aug30dn.e
5.0
4.0
3.0
2.0
1.0
.0
1.0
.8
.6
.4
.2
.0
Log(number of individuals)
0.
365.
730.
1095.
1460.
1825.
2190.
Time (days)

Figure 21

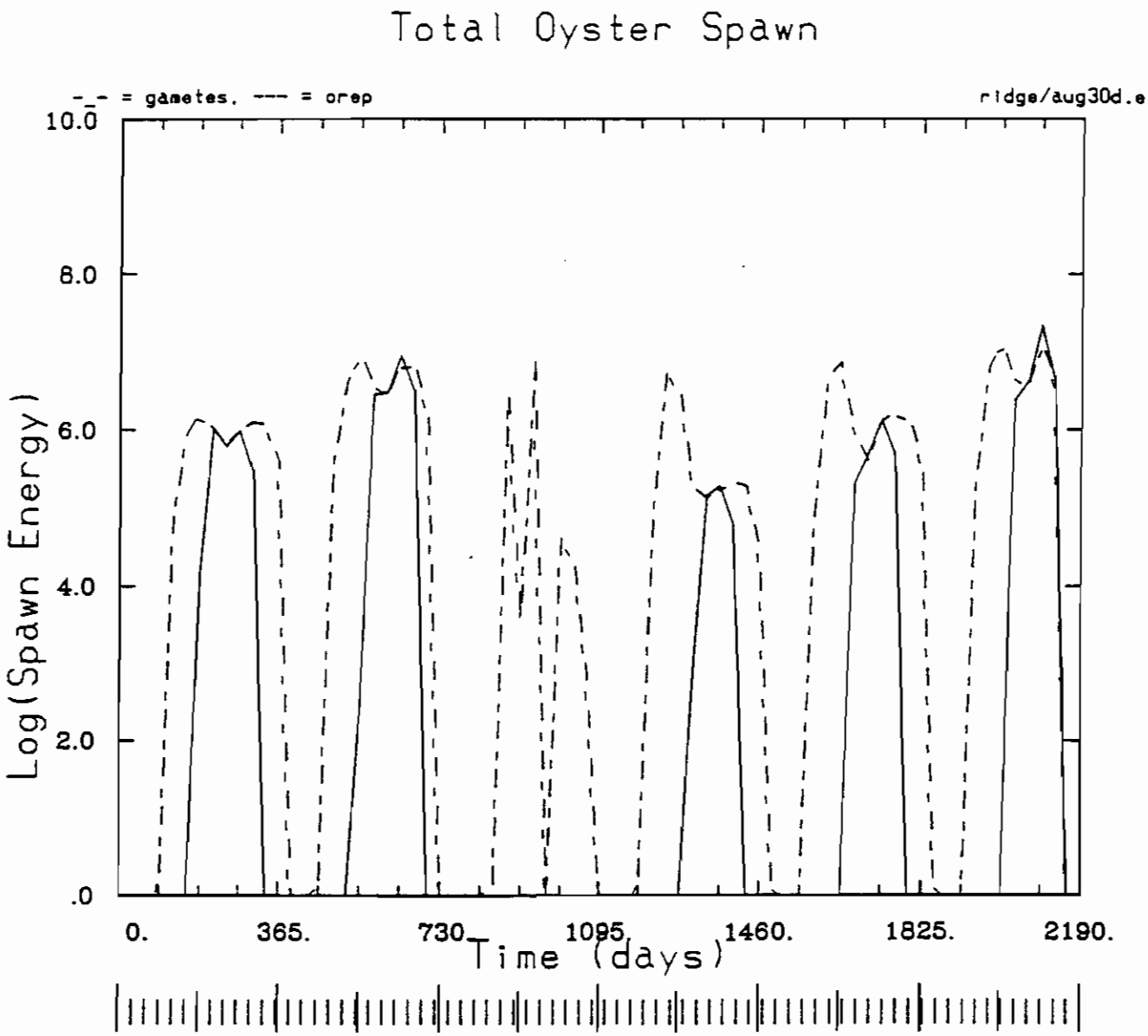

Figure 22

721

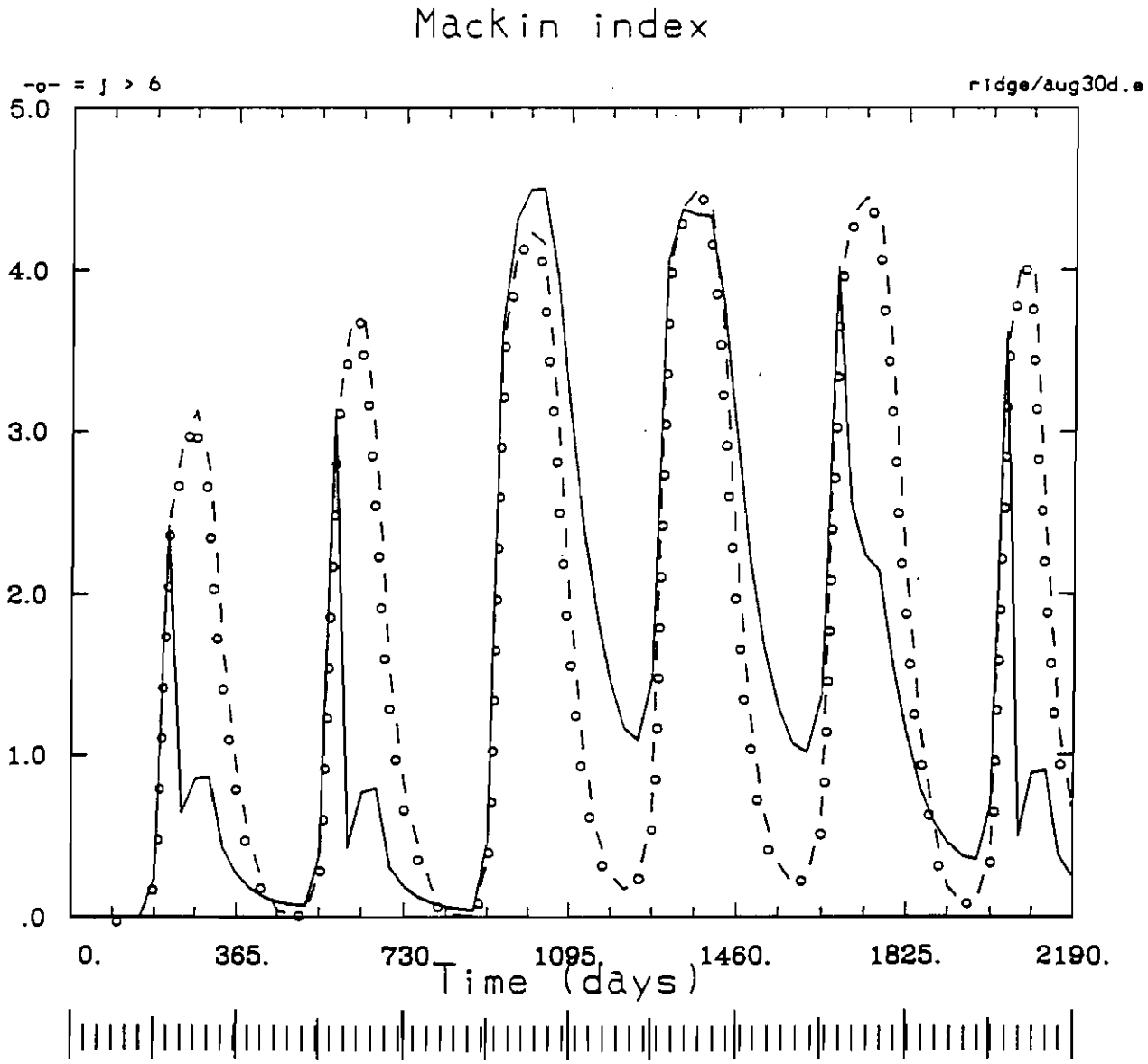
Mackin index
-o- = j > 6
ridge/aug30d.e
5.0
4.0
3.0
2.0
1.0
.0
0.
365.
730.
1095.
1460.
1825.
2190.
Time (days)

Figure 23

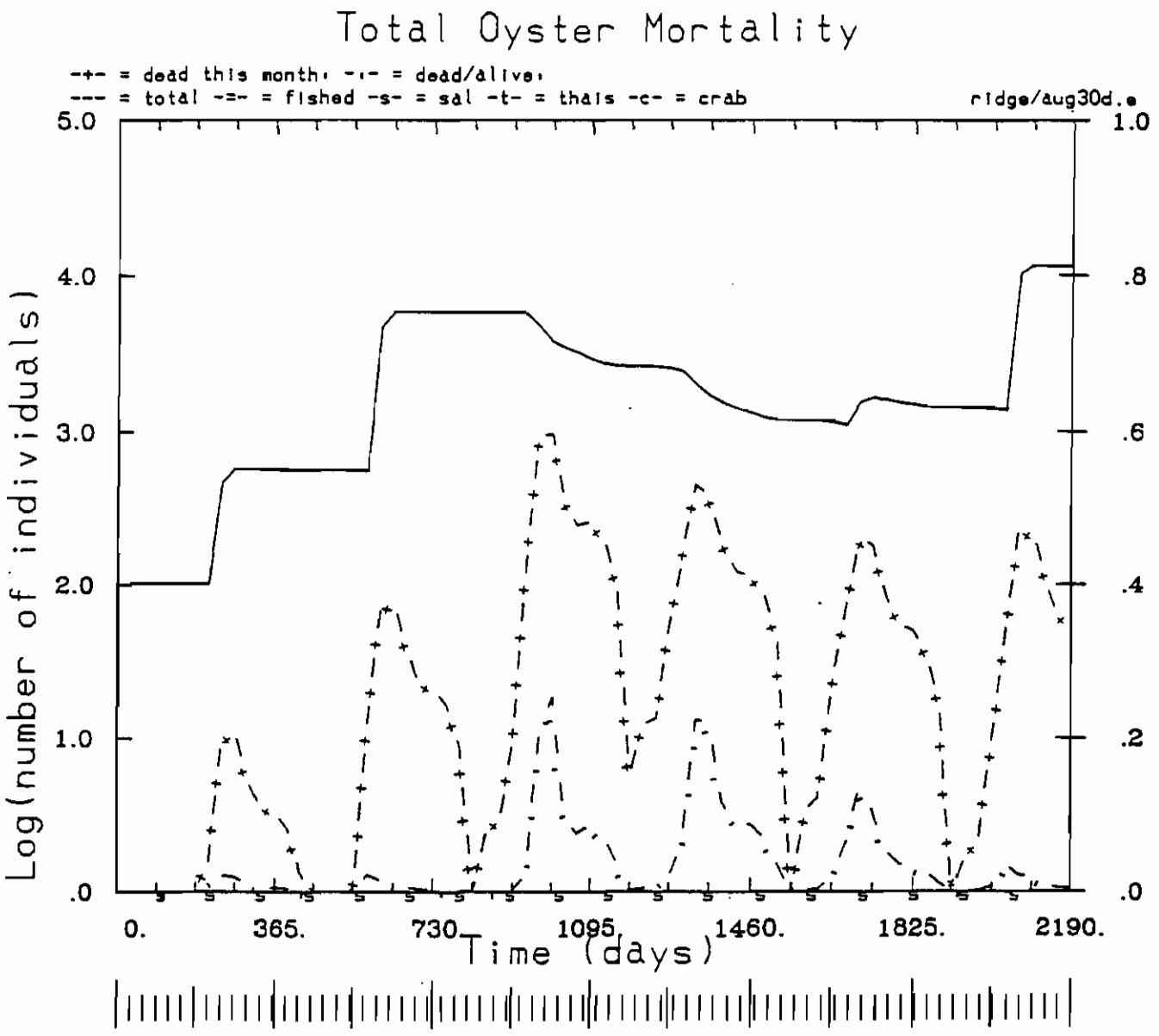

Figure 24

723

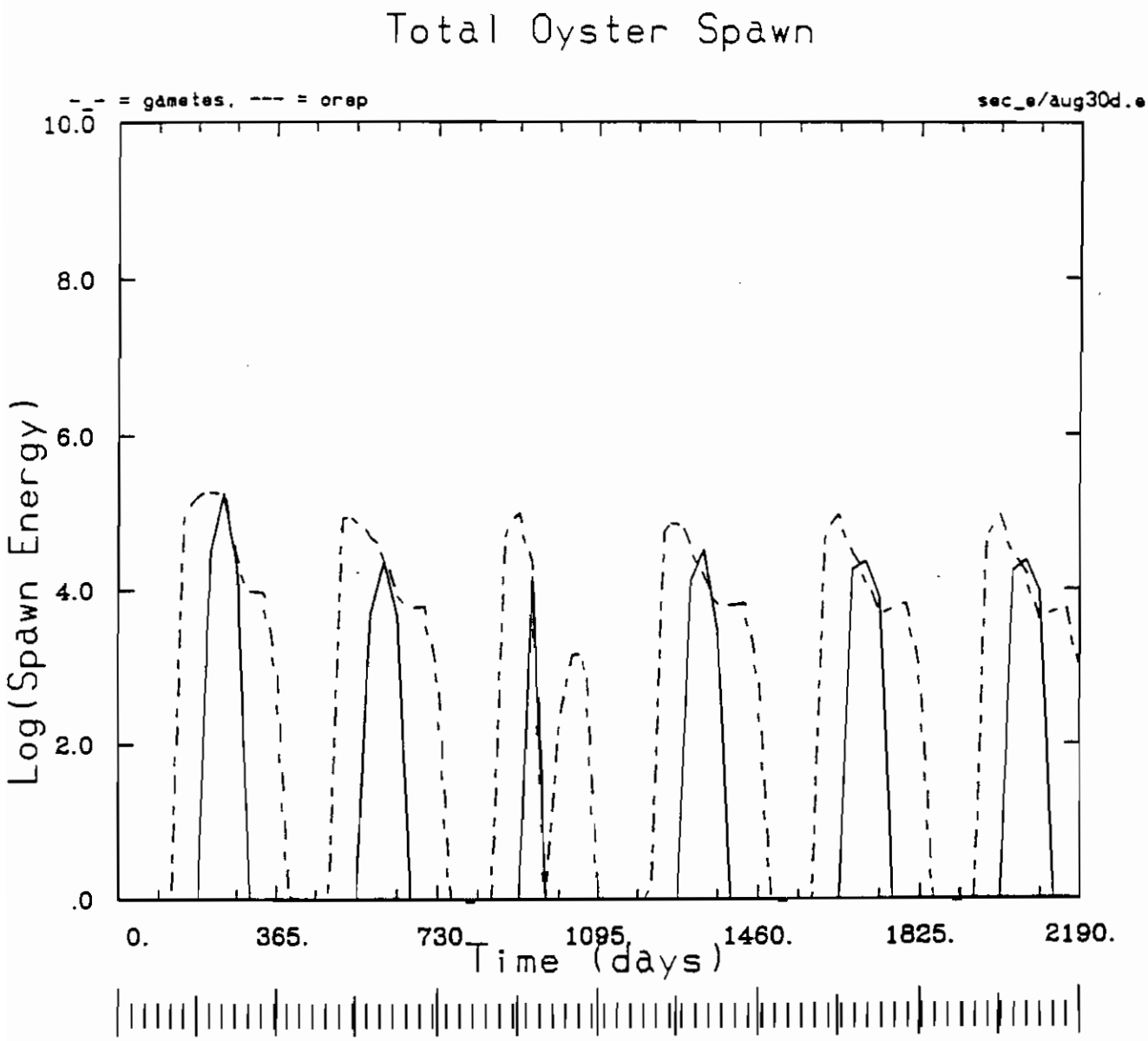
Total Oyster Spawn
-_- = gametes, --- = orep
sec_e/aug30d.e
10.0
8.0
6.0
4.0
2.0
.0
Log(Spawn Energy)
0.
365.
730.
1095.
1460.
1825.
2190.
Time (days)

Figure 25

Delaware River Deepening
Hydraulics Appendices

APPENDIX B-5B

EMPIRICAL ASSESSMENT OF DELAWARE BAY (SAND) STOCKPILES.

725

DEPARTMENT OF THE ARMY
WATERWAYS EXPERIMENT STATION, CORPS OF ENGINEERS
3909 HALLS FERRY ROAD
VICKSBURG, MISSISSIPPI 39180-6199

REPLY TO
ATTENTION OF

CEWES-CD-SE (1110) 11 October 1995

MEMORANDUM FOR Commander, U.S. Army Engineer District, Philadelphia, ATTN: CENAP-EN-H (Mr. Jeffery A. Gebert), Wanamaker Building, 100 Penn Square East, Philadelphia, PA 20314-1000

SUBJECT: Transmittal of Final Report, MIPR CENAP-EN-95-721, "Empirical Assessment of Delaware Bay, Stockpiles, A Phase II Report on the Bay Deepening Project"

1. The enclosed report completes the stockpile stability portion of Phase II investigations.

2. Should any questions arise concerning this report or study, please contact Mr. Edward Hands (601/634-2088) directly.

FOR THE DIRECTOR:

James R. Houston

Encl

JAMES R. HOUSTON, PhD
Director
Coastal Engineering Research Center

CF (w/encl):
CERD-C (Mr. David B. Mathis)

727

Empirical Assessment of Delaware Bay Stockpiles
A Phase II Report on the Bay Deepening Project

Edward B. Hands
U.S. Army Engineer Waterways Experiment Station
3909 Halls Ferry Road
Vicksburg, MS 39180

EXECUTIVE SUMMARY

Comparing two proposed Delaware Bay stockpile sites to carefully monitored mounds indicates significant sediment dispersion is likely in the bay. Transport rates will be slow, however, so most of the placed material will remain in the stockpiles for decades. The stockpile sand that does leave will move predominately landward, then spread laterally along the shore, thereby contributing to the stockpile objective, which is to provide fill material for nourishment of sand-starved bay beaches.

INTRODUCTION

Background.

The Delaware Estuary Main Channel Deepening Project requires removing about 10 million cubic yards (mcy) of sediments from channel reaches within the Delaware Bay Estuary. The U.S. Army Engineer District, Philadelphia (NAP) has worked with various Federal and state agencies to develop plans for beneficial uses of this material. The U.S. Army Engineer Waterways Experiment Station (WES) Environmental Laboratory (EL) and Coastal Engineering Research Center (CERC) assisted in evaluating feasibility and designs for beach nourishment, wetland restoration, and submerged sand stockpiles as beneficial uses for the materials to be dredged.

Of the 10 mcy to be dredged, about 9 mcy will be sand and 1 mcy will be silt or clay. All of the material from the finer-grained dredging areas and some from sandy reaches will be used for wetland restorations at Kelly Island and Egg Island Point (LC-9 and PN-1A, respectively, in Figure 1). The remainder of the sandy material will go into two stockpiles near the Delaware shore: one off Slaughter Beach, the other off Broadkill Beach (LC-5 and MS-19 in Figure 2).

In Phase I, EL and CERC evaluated wetland restoration and underwater berm stockpile potential to determine if any other field tests were needed, and to help optimize

728

beneficial applications for the dredged material. The Phase I report evaluated alternatives and recommended design approaches (Landin, Davis, and Hands 1995).

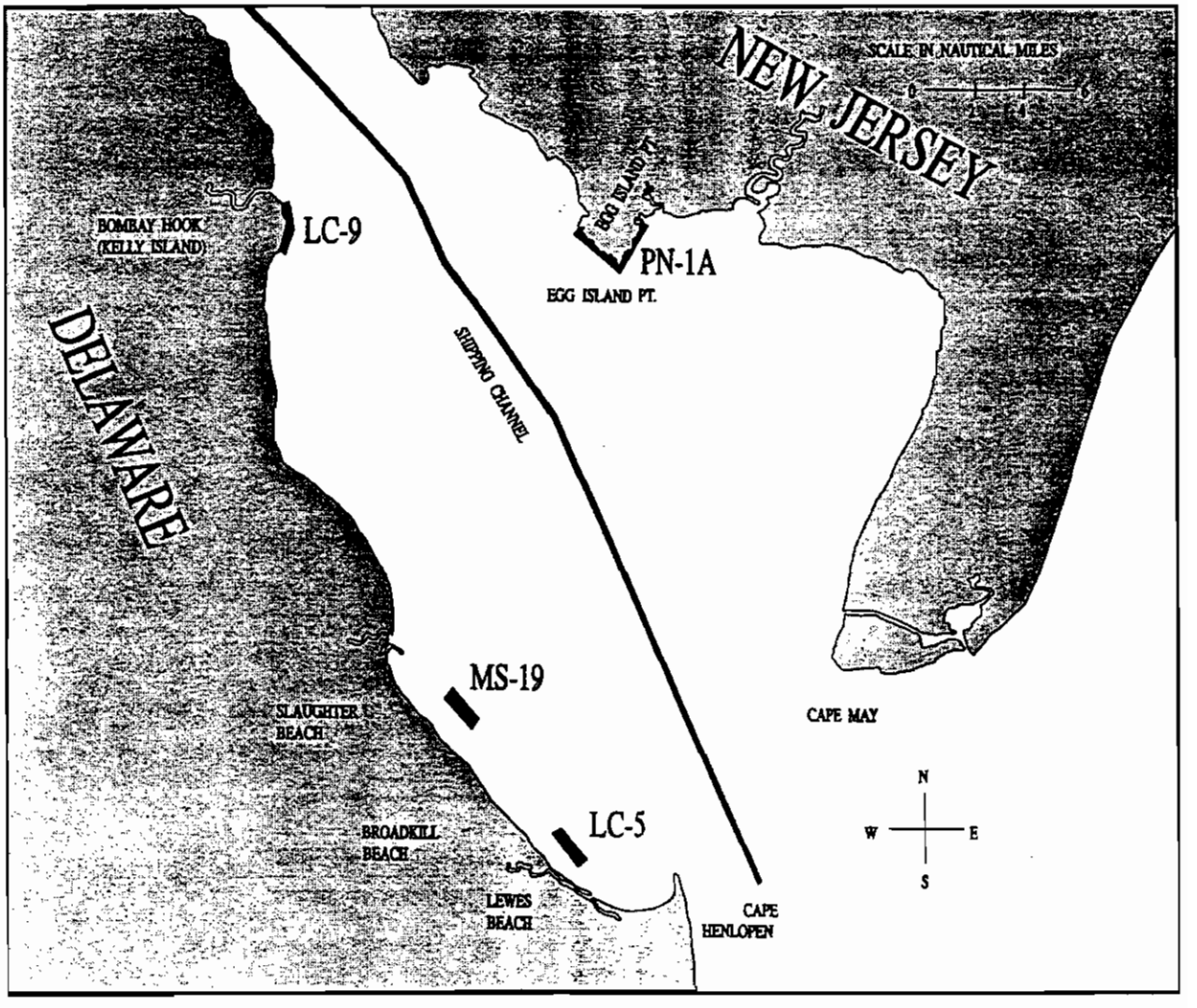

Figure 1. Four beneficial use sites in Delaware Bay

Phase II Objectives.

In Phase II, three coordinated reports were prepared simultaneously:

o "Wave and Sediment Transport . . . " by Grosskopf (in preparation) presents waves and current databases for all four project sites, calculates sand transport rates, and estimates the effects that dredged material placement will have on wave and currents.

229

- "Wetland Restoration Design . . . " by Landin and Davis addresses wetland restoration.
- "Empirical Assessment of Delaware Bay Stockpiles . . . " focuses on sand stockpile stability.

Authority.

MIPR CENAP-EN-95-721 dated 10 May 1995 authorized preparation of this report.

Scope of This Report.

This report evaluates the long-term (multiple-year) stability of the sand stockpiles based on grain size, placement depths, and wave climates at the two chosen sites. Comparisons are made to the fate of other dredged material mounds that have been monitored at sites in the Gulf of Mexico and in the Atlantic and Pacific Oceans.

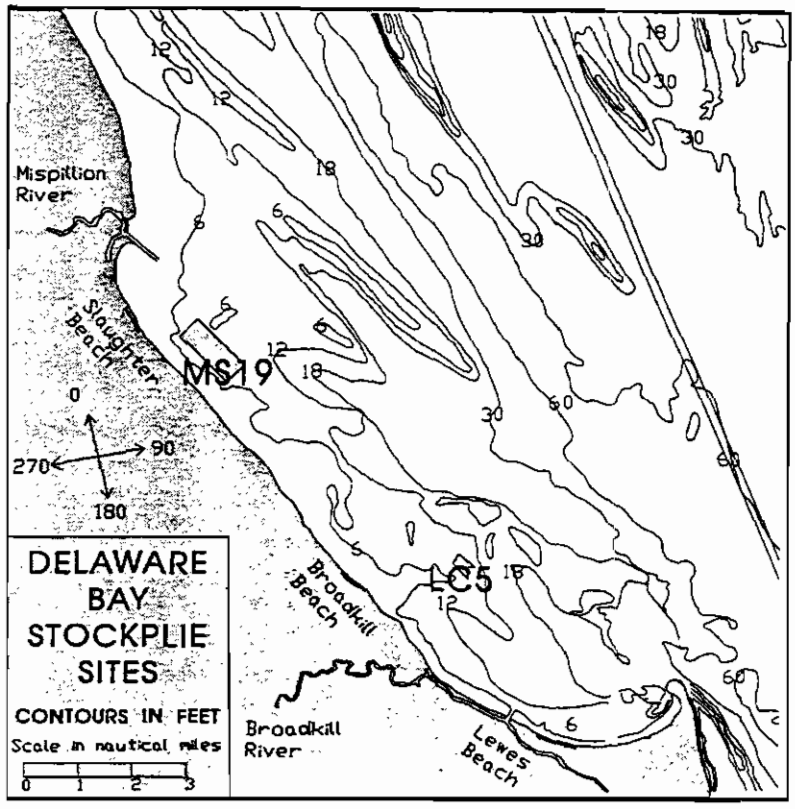

Figure 2. Bay stockpiles

Organization of This Report.

The Executive Summary briefly states the major conclusion of this study. The Introduction describes report objectives, authority, and the relevance of this and previous studies to the planned Delaware Estuary Channel Deepening Project. Reasons for choosing the adopted methodology and data are given in the Approach section. The Approach section ends with a narrative description of steps in preparing and analyzing the data. Basic data and calculated results are described under Data Analysis, where algorithms are given for each component of the empirical assessment. The Interpretation section compares the Bay sites to reference sites in terms of climatic processes and, consequently, relative mound stabilities. Conclusions, Acknowledgements, References, and a Notation conclude this report.

730

APPROACH

EBERM Criteria.

Because potentially large cost savings are achievable by coupling channel maintenance with shore protection needs, dredged material mounds have been built world-wide (e.g., Uda et. al. (1991) in Japan; deLange and Healy (1991) in New Zealand; Mikkelsin (1977) in Denmark; Vera-Cruz (1972) in Brazil; Zwamborn et. al. (1970) in South Africa). Some mounds were designed to be wave attenuator, others to be feeder deposits. More than a dozen field tests have attempted to place dredged material where natural currents would carry sand shoreward to mitigate coastal erosion problems. These nearshore feeder experiments met with a mixture of successes and disappointments. The U.S. Army Corps of Engineers (CE) has completed such tests at 11 locations. Periodic hydrographic surveys document the long-term fate of these mounds for up to 12 years as reviewed in Hands 1991. Taken together, these results provide a coherent database for comparing and interpreting the considerable variations in observed movements of sand mounds. This database serves as a useful calibration set for numeric models that simulate long-term sediment fate (Scheffner 1991, Johnson et al. 1994). Moreover, the data also serve as a reference standard for direct empirical comparisons (Hands and Resio 1994).

A PC system EBERM (Empirical **BERM** fate) incorporates various fate criteria to rank potential placement sites with reference standards in terms of expected and documented mound movement. EBERM algorithms and databases facilitate site comparisons. Unfortunately, as presently configured, EBERM bathymetric, wind, wave, and current databases cover only the Gulf of Mexico. The EBERM criteria, however, can be evaluated using other programs and databases. This report presents results of such an evaluation for bay stockpiles.

Nonlinear Criteria.

In linear wave theory, symmetry requires that water particle velocities and accelerations under the wave crest have the same magnitude and duration as under the trough. Directions of flow, however, reverse from crest to trough so that water particles complete closed orbits each wave period. In real water waves, speeds are fastest under crests, shorter in duration, and associated with mass transport in the direction of wave propagation. If particle speeds differ enough, this skewness affects sediment transport. Ongoing studies indicate that a simple expression of this nonlinear wave effect can be used to predict cross-shore transport not only at offshore mounds, but at the shoreline as well (Ahrens and Hands, in preparation). Nonlinear criteria will be applied to Bay stockpile sites.

731

Bay Wave Climate.

Wave agitation is a primary criterion for assessing stockpile stability (Hands and Resio 1994; Douglass, Resio, and Hands 1995). Ocean and Coastal Technology, Inc. (OCTI) applied a directional spectral wave model to generate waves on a 1-min grid throughout Delaware Bay at 3-hr intervals from 1987 to 1993. The methodology and resulting data are discussed in the companion report (Grosskopf, in preparation). Maurmeyer (1978) summarized a decade of ship observations at latitude 38° 55.9' N and longitude 75° 10.3' W which is close to the more northerly stockpile site (MS-19). Maurmeyer's data were used in WES's Phase I report (Landin, Davis, and Hands 1995) because hindcast data were not available then. OCTI's new time series is used here because it should provide better, more consistent representation of future wave conditions. The hindcast avoids problems with observer accuracy and bias, provides a fairly long and detailed record that is transformable to the depths and coordinates of each stockpile, and is compatible with the Wave Information Study (WIS) hindcasts that characterize the reference ocean berm sites with which the bay will be compared.

Sequence of Steps in Present Assessment.

Grosskopf's 6-year hindcasts, transformed to the stockpile sites, characterize the potential for wave agitation of placed sediments. The entire time series were ordered in terms of wave height. The median and 99.863-percentile wave heights were calculated, $H_{s\,50}$ and $H_{s\,99.86}$ respectively. Using D_{50} = 0.30 mm (the estimated median grain size of the material to be placed)[1] and the specific gravity of quartz as nominal sediment parameters, Hallermeier's coastal profile zonation limits were calculated (Hallermeier 1980). Nondimensional expressions of these two depth limits (*HIL* and *HOL)* form the first two empirical criteria. The third criterion uses near-bed oscillatory peak speeds (*NOPS*). Each of the 17,534 pairs of wave height and period were used to calculate 17,534 *NOPS* at a depth d_B of 3.7 m (the base of both stockpiles). The resulting distributions for each site were compared to similarly calculated distributions for reference sites. Lastly, differences in wave crest and trough peak speeds were calculated and plotted to determine cross-shore transport directional tendencies.

---

[1] Personal communication, 1995, Richard McGee, U.S. Army Engineer Waterways Experiment Station, Hydraulics Laboratory, Vicksburg, MS.

DATA ANALYSIS

Input Data.

The EBERM PC system standardizes application of previously described empirical criteria for discriminating *active* and *stable* berm sites. Besides increasing site selection objectivity, EBERM increases the speed and consistency of site evaluation by providing built-in standardized wave transformations as well as extensive databases on:

a. Bathymetry.
b. Winds.
c. Waves.
d. Performance of reference mounds.

For the present bay application, similar analyses were done independent of EBERM due to lack of bay or even Atlantic coast databases in the present version.

Algorithms for Fate Criteria.

Three empirical fate criteria are based on the following parameters:

Hallermeier's Inner Limit.

$$HIL \equiv 2.28\ H_{S_{99.863}} - \frac{68.5 H_{S_{99.863}}{}^{2}}{g \overline{T}_a^2} \tag{1}$$

where $H_{S_{99.863}}$ is the 12-hr exceedance significant wave height, g is the acceleration of gravity, and $\overline{T}_a$ is the average period of all waves with height $H_{S_{99.863}} \pm 0.05$ m.

Hallermeier's Outer Limit.

$$HOL \equiv H_{S_{50}}\ \overline{T}_a \sqrt{\frac{g}{5D_{50}}} \tag{2}$$

733

where H_{S50} and T_a are defined similarly with respect to the median wave height, and D_{50} is the representative grain size of the placed material in millimeters.

The *Shore Protection Manual* (SPM 1984) uses Hallermeier's (1981) profile zonation limits as guidance on depths of coastal sediment transport and profile variation. Hallermeier (1981) describes these two limits as bounding a "shoal or buffer" zone in which "surface waves have neither strong nor negligible effects on the sand bottom during a typical year." *HIL* is usually less than *HOL* and between these two limits the fate of material is uncertain and probably subject to larger interannual differences.

Distribution of Near-bed Oscillatory Peak Speeds (NOPS).

Peak oscillatory speed for each 3-hr wave condition can be estimated from linear wave theory

$$u_{\max_d} = \pi \frac{H}{T} \div \sinh \frac{2\pi d}{L} \tag{3}$$

where the peak wave period is substituted for T, and L is the equivalent wave length

$$L = \frac{gT^2}{2\pi} \tanh \frac{2\pi d}{L} \tag{4}$$

at the berm depth d. The iterations in Equation 4 can be time-consuming when run for the entire WIS time series. Fenton and McKee (1990) offer the following simple explicit solution which is exact at the shallow- and deepwater limits and better than 1.7 percent accurate everywhere:

$$L \approx \frac{gT^2}{2\pi} \left(\tanh \left(2\pi \frac{\sqrt{d/g}}{T} \right)^{3/2} \right)^{2/3} \tag{5}$$

Nonlinearity Criteria to Categorize Cross-shore Transport.

Nonlinear criteria are being proposed in a yet unpublished paper (Ahrens and Hands, in preparation) as predictors of cross-shore transport. These criteria combine work on nonlinear waves by Dean (1974) with work on sediment movement initiation by Komar and Miller (1974) and Hallermeier (1980). Ahrens developed a method for explicitly

-73-

estimating the peak near-bed oscillatory speeds under the crest (u_{dc}) and under the trough (u_{dt}) using Dean's Stream Function Wave Theory. Equation 6 expresses the tendency for onshore sediment movement under wave crests, while Equation 7 expresses the tendency for offshore directed movement under the trough.

$$U_c' \equiv \frac{u_{dc\ \max}}{u_{crit}} \tag{6}$$

$$U_t' \equiv \frac{u_{dt\ \max}}{u_{crit}} \tag{7}$$

where $u_{d\ \max}$ is the near-be speed due to nonlinear waves estimated from Stream Function Theory and u_{crit} is the critical speed required to initiate sediment movement:

$$u_{crit} \equiv \sqrt{8\, g\, \gamma\, D_{50}} \qquad for\ D_{50} \leq 2\ mm \tag{8}$$

$$u_{crit} \equiv \{0.46\, \gamma\, g\, T^{1/4}\, (\pi D_{50})^{3/4}\}^{4/7} \qquad for\ D_{50} \geq 2.0\ mm \tag{9}$$

where $\gamma = (\rho_s - \rho)/\rho$
ρ_s = density of the sediment
ρ = density of water

Ahrens and Hands (in preparation) evaluate real and synthetic data to show Equations 6 and 7 are applicable over wide ranges of wave conditions, sediment sizes, and cross-shore locations. Moreover, the trends expressed by these equations are consistent with our present understanding of onshore and offshore sediment movement based on decades of testing both in the field and large wave tanks (many reviewed and cited in Kraus, Larson, and Kriebel 1991).

735

Application of Empirical Criteria to stockpiles.

Table 1 lists bay and reference sites, their plotting symbols, placement depths, grain sizes, and the fates at reference sites. Grain sizes, depths, and wave parameters constitute the input values for all empirical fate criteria. Though bay sites are close to the shallowest reference conditions, all bay input values fall within the range of calibration.

Table 1 Conditions on Reference and Test Mounds

Symbol	Location	Berm depth	Grain size	Fate class
STABLE or *active*[2]		d_B m	D_{50} mm	
li	Fire Island Inlet, NY	4.6	0.40	*active*
LB	Long Branch, NJ	11.6	0.23	*STABLE*
AC	Atlantic City, NJ	5.8	0.35	*STABLE*
DN_C	Dam Neck, VA	7.6	0.08	*STABLE*
DN_B	Dam Neck, VA	10.4	0.08	*STABLE*
nr	New River, NC	2.1	0.50	*active*
sib	Dauphin Is, AL	5.8	0.20	*active*
sim	Dauphin Is, AL	5.6	0.22	*active*
bb	Brownsville, TX	8.1	0.13	*active*
ag	Imperial Beach, CA	5.8	0.22	*active*
SB	Santa Barbara ,CA	9.1	0.20	*STABLE*
hbns	Humboldt, CA	15.8	0.23	*active*
MD-65	Capped MD, NY	19.8	0.42	*STABLE*
lc-5	Broadkill Beach, DE	3.7	0.30	*being tested*
ms19	Slaughter Beach, DE	3.7	0.30	*being tested*

[2] Upper case symbols refer to *stable* mounds and lower case to *active* ones.

736

INTERPRETATION

Nondimensionalized Hallermeier Criteria.

Figure 3 compares bay stockpiles to calibration mounds in terms of two of the empirical fate criteria. Corps of Engineers practice is to avoid placing dredged material above the Hallermeier outer limit (*HOL*) if material is intended to remain in place. In terms of Figure 3, this means not above zero on the vertical axis. Conditions at *stable* sites are indicated by the first letter in the symbol for each reference mound (upper case symbols column 1 of Table 1). Note that none of the *stable* mounds are significantly above zero while all of the *active* ones (lower case symbols in Table 1 and the following figures) are above zero. The bay stockpiles (numerals *5* and *9* in Figure 3) plot well above this limit and thus provide no assurance of stability.

Where sediment dispersion is desirable, site selection should consider Hallermeier's Inner Limit (*HIL*). The recommendation is to locate intended dispersive sites above local *HIL*. Note that the seven calibration berms were all near or above this criterion (i.e., to the right of zero). Dispersion of the two calibration berms slightly below *HIL* would be expected because they were so close to the *HIL* and so far above their *HOL* (Figure 3).

Both of the bay sites are far above *HIL*. In fact only New River is the only reference site with a nondimensional inner limit above that of the bay sites. Shallow placement of dredged material at New River was the first demonstration of inexpensive feeder placement. About 60 percent of the New River channel maintenance material migrated out of the nearshore placement zone in the first 28 days. The berm at the next lower limit just below both bay sites completely disappeared before its first postplacement survey. On the basis of these two Hallermeier limits, some placed material should disperse promptly from both bay sites.

737

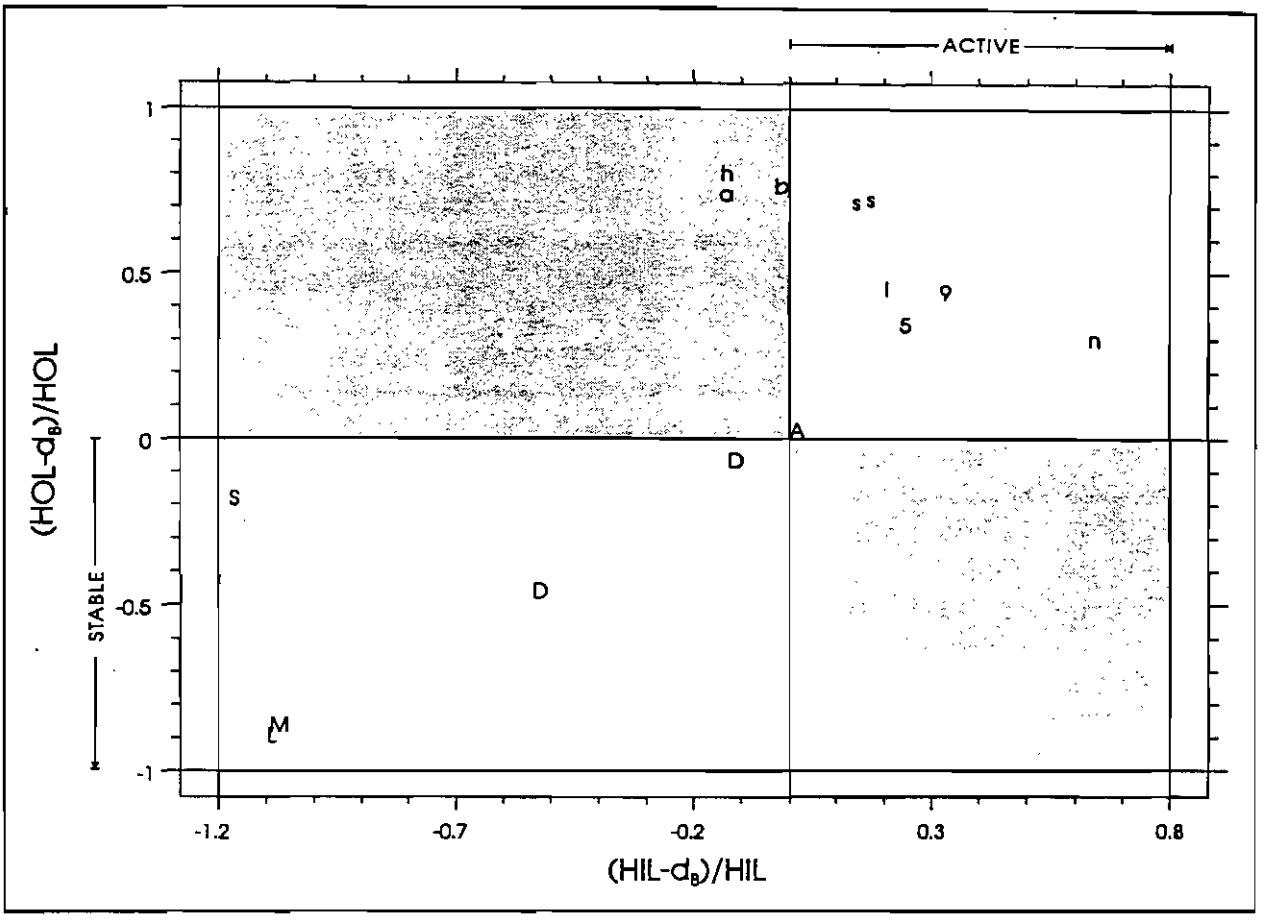

Figure 3. First two EBERM criteria

NOPS Criterion.

Figure 4 shows the cumulative distribution of NOPS determined for ever 3-hr observation using Equation 3. Relatively frequent mild conditions, with speeds below about their 75th percentile, may not stir sediment at *active* sites. Yet more energetic waves are still frequent enough at these sites to cause bathymetric changes detectable in less than a year. Rarer storms, beyond the 95th percentile, contribute to the highest bottom speeds (extending off the scale in Figure 3), but occur too infrequently to explain changes observed at the reference sites. To predict a 1- to 5-year mound response, the most relevant portion of the distribution seems to be in a zone from the 75th to 95th percentiles. Because NOPS values in this frequency band are higher at dispersive berm sites, Figure 4 is divided into *stable* and *active* regions separated by an intermediate zone of uncertainty.

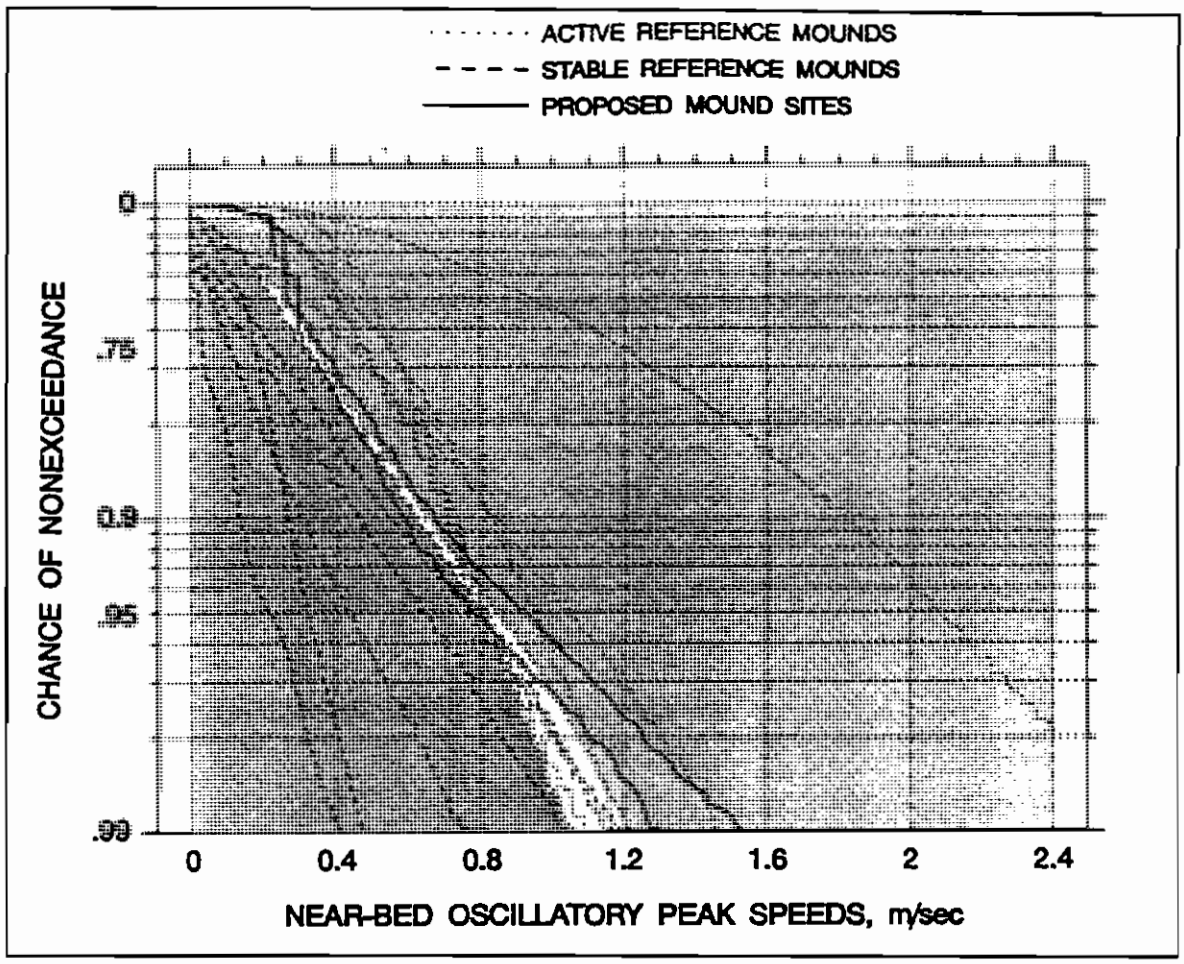

Figure 4. Third EBERM Criterion

The more energetic of two bay sites, MS-19, is in the lower portion of the *active* region (Figure 4). Beyond the 95th percentile, extreme storms push the NOPS index above all but two of the *active* reference sites. MS-19 is thus expected to be dispersive. The distribution of NOPS for LC-5 is, however, more intermediate — slower than known *active* sites, but faster than almost *stable* standards. In the present context, even this less energetic bay site is interpreted as probably dispersive because all but one of the *stable* reference sites have distinctly slower NOPS; the only *stable* site with similar NOPS may have migrated ashore subsequent to its 12-year monitoring period (Hands 1991); tidal velocities (neglected in the present empirical approach) are stronger and more phase-dominate at the bay sites than at the open-ocean reference sites; time periods of interest in the bay may extend beyond the duration of monitoring at most reference sites;

739

and in the region of extreme events (above 98th percentile) LC-5 is more *active* than all but the two most *active* reference sites (Figure 4).

Nonlinearity Criteria.

Because bay stockpiles are judged dispersive on the basis of all three empirical criteria and because stockpiles are intended to retain sand for future use, it is important to understand more about this expected dispersion. When and how will sediment disperse? Where will it go?

All but one of the *active* reference berms moved landward carrying most of the placed material toward beaches. If dredged material leaves the stockpiles and moves to bay beaches, stockpile losses will actually benefit beaches and do so without the extra expense of planned redredging and artificial transport to the beaches at some later date. If, on the other hand, stockpiled sand moves offshore or disperses widely and mixes with bay muds, such dispersion would have an adverse effect on planned benefits; and the rates of dispersion would determine the severity of the loss.

New empirical criteria for assessing directions of cross-shore transport will be examined next. The paper proposing this approach has been submitted for journal publication; however, there has been no independent evaluation. The new approach is based on well-known nonlinear aspects of real water waves. Linear equations for wave motion (e.g., Equation 3) have been widely compared to flume and field measurements. Measurements were surprisingly close to linear predictions even in regard to kinematics of particle motions including peak bottom velocities under wave crests. For larger wave heights and shallow water depths, however, nonlinear effects increase. Wave crests peak while the intervening troughs get wider and shallower. As nonlinearities increase, so do differences in orbital speeds under crests as compared to troughs.

Differences in orbital speeds are especially important in cross-shore transport beyond the surf zone and in cases of larger grain sands, which do not even move below certain thresholds. The following analysis attempts to exploit a simple measure of nonlinearity and threshold to distinguish onshore and offshore transport situations.

Ahrens and Hands (in preparation) show that the skill of these nonlinear criteria for discrimination of shore erosion and accretion events is very high and almost identical when tested against the field and large wave flume data compiled by Kraus and Mason 1991. If a storm is large enough to move appreciable sediment, the shore recedes when $U'_t < -2$ and otherwise progrades. The response of dredged material mounds is not so simply characterized, but stronger nonlinearities are definitely associated with increased landward mound migration as indicated in Figure 5.

740

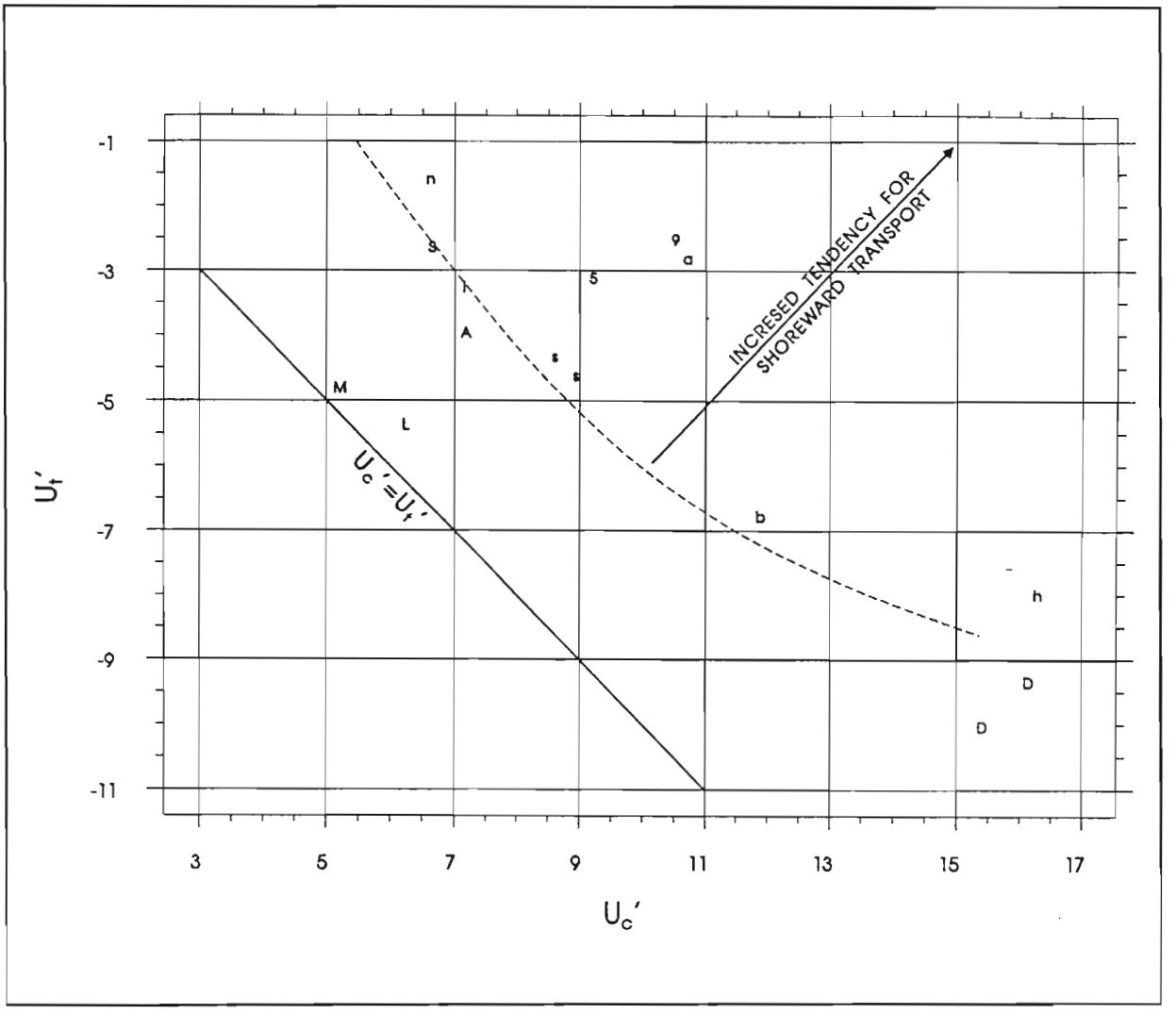

Figure 5. Nonlinear criteria

The line in Figure 5 is a lower bound where orbital speeds under the crest and trough are the same. During representative storm conditions chosen for mound comparisons, both speeds were well above sediment threshold speeds. At all sites, waves were strongly nonlinear, but more so for the *active* berms that migrated landward. Stable berms plot closer to the linear boundary, $U'_c = U'_t$. Furthermore, note that the single *active* berm that did <u>not</u> move landward lies closer to the linear boundary than any other *active* mound. This intended feeder berm disappeared with time rather than migrate shoreward as the other six did. No tendency for landward transport would have been predicted for that dispersive site. Importantly, grain size on that particular mound was much finer than planned for the bay stockpiles. The bay sites (*5* and *9* in Figure 5) plot well away from the linear,

741

Nonlinear criteria thus indicate that when sand disperses from both bay sites, wave asymmetries will be strongly onshore and the sand will naturally nourish the adjacent beaches. More information on directions and rates of transport can be found in the companion report by Grosskopf (in preparation).

Limitations of Empirical Criteria for Stockpiles.

Comparisons presented here do not explicitly account for any erosive forces other than oscillatory wave motion. Effects of steady currents (e.g., wind- and surge-driven) may be quasi-implicit in this approach because they correlate strongly with wave amplitudes. Tidal currents, however, are totally neglected and higher in the bay than at reference sites. Stockpile sites are so close to shore that no significant cross-shore component should be expected, but longshore tidal currents nevertheless contribute to bottom stresses and promote sediment resuspension. For this reason, the present analysis tends to underestimate dispersion. On the other hand, increases in water depths due to storm setup will tend to reduce bottom stress. Estimation of surge, tidal, and wind effects, which are thought to have a insignificant net effect, would be contrary to the direct and simple comparison intended in this report. Grosskopf's report considers include these factors. The LTFATE model (Scheffner 1991) and a model by Ockenden and Delo (1990) are additional approaches that specifically evaluate storm surge and tidal-dominate transport.

Caution should be exercised not to extrapolate from this study's intended long-term prediction backwards to the effect of any single storm. Monitoring periods for reference sites typically extended over several years and included the net effects of numerous storms with varying intensities. Observed responses at the reference sites and inferred movements on bay stockpiles do not apply to individual extreme events. The likelihood of a single rare storm occurring increases with project life; however, its impact on the cumulative net change does not necessarily increase.

CONCLUSIONS

Known and proposed mounds have been ranked in terms of their potential wave-agitation. All four empirical criteria are in basic agreement. Both stockpiles will experience persistent loss of placed sands. The rate of loss will, however, be slow relative to total volumes placed. Furthermore, sand leaving the stockpiles will move predominately landward. Nonlinear criteria indicate that wave asymmetries will be strongly onshore at both sites. Furthermore, these criteria indicate that the relatively coarse placed sands will eventually migrate all the way to shore where it will contribute to subaerial beach accretion without the planned extra effort of redredging and pumping. Longshore transport inside the breaker zone will spread the nourishment benefits widely alongshore.

By illustrating similarities between proposed bay stockpiles and previously monitored mounds, figures in this report graphically express the degree of confidence appropriate for these conclusions. The relative closeness of bay sites to known *active* mounds, together with the relative spread among those *active* mounds as contrasted with their separation from the group of *stable* mounds strongly supports the expected gradual landward transport. Most of the placed material will, however, remain right where it is placed for decades.

ACKNOWLEDGMENTS

This is one of several studies being managed at the U.S. Army Corps of Engineers, Philadelphia District, by Mr. Stan Lulewicz in support of the Delaware Estuary Main Channel Deepening Project. This report benefits from cooperation and information exchange among other investigators working simultaneously on related studies; Drs. Mary Landin (CEWES-ER-W) and Lisa Roig (CEWES-HE-S), Messrs. Jack Davis (CEWES-CD-SE), Richard McGee (CEWES-HS-H), and W. G. Grosskopf (OCTI). Messrs. Tony DePasquel (CENAP-EN-DG) and Robert Griggs (CENAP-) provided GIS and geotechnical input. Mr. John Brady (CENAP-PL-E) provided background information, conducted workshops, and conducted valuable field trips. Mr. Jeff Gebert (CENAP-EN-H) coordinated this and other sediment-physical processes studies.

The approach used here was developed in the recently completed dredging program managed by Mr. Clark McNair (CEWES-CP). The author of this report worked under the direct supervision of Mr. Thomas W. Richardson, Chief, Engineering Development Division; Ms. Joan Pope, Chief, CS&E Branch; Dr. Yen-hsi Chu, Chief, Engineering Applications Unit. The input of all of these persons is gratefully acknowledged.

REFERENCES

Ahrens, J. P., and Hands, E. B. (in preparation). "Velocity Parameters, Application to Cross Shore Sediment Movement," submitted to the American Society of Civil Engineers, NY.

de Lange, W., and Healy, T. (1991). "Assessment of the Suitability of Inner Shelf Dredge Spoil Mounds for Indirect Bypassing at Tidal Inlets," Proceedings of the Hilton Head Island International Coastal Symposium, ed. P. Bruun, Hilton Head, SC, 291-296.

Dean, R. G. (1974). "Evaluation and Development of Water Wave Theories for Engineering Application," Volumes I and II, Coastal Engineering Research Center Special Report No. 1, U.S. Army Engineer Waterways Experiment Station, Vicksburg, MS.

743

Douglass, S. L., Resio, D. T., and Hands, E. B. (1995). "Impact of Near-Bottom Currents on Dredged Material Mounds Near Mobile Bay," Dredging Research Program Technical Report DRP-95-6, U.S. Army Engineer Waterways Experiment Station, Vicksburg, MS.

Fenton, J. D., and McKee, W. D. (1990). "On Calculating the Lengths of Water Waves," Coastal Engineering, 14, 499-513.

Grosskopf, W. G. (in preparation) "Wave and Sediment Transport, A Phase I Report on the Delaware Bay Deepening Project," U.S. Army Engineer District, Philadelphia, PA.

Hallermeier, R. J. (1980). "Sand Motion Initiation by Water Waves: Two Asymptotes," Jour. of Waterway, Port, Coastal, and Ocean Engineering, Vol. 106, No. WW3, 299-318.

Hallermeier, R. J. (1981). "A Profile Zonation for Seasonal Sand Beaches from Wave Climate," Journal of Coastal Engineering, Vol. 4, No. 3, 253 - 277.

Hands, E. B. (1991). "Unprecedented Migration of a Submerged Mound off the Alabama Coast," Proceedings of the Western Dredging Association Conference, Las Vegas, NV, Center for Dredging Studies, College Station, TX, 245-269.

Hands, E. B., and Resio, D. T. (1994 Nov). "Empirical Guidance for Siting Berms to Promote Stability or Nourishment Benefits," Proceedings of the 2nd International Conference on dredging and Dredged Material Placement, Buena Vista, FL, American Society of Civil Engineers, New York, NY, 220-228.

Johnson, B. H., Scheffner, N. W., Teeter, A. M., Hands, E. B., and Moritz, H. R. (1994). "Analysis of Dredged Material Placed in Open Water," Proceedings of Dredging '94, Buena Vista, FL, American Society of Civil Engineers, NY.

Kajima, R., Shimizu, T., Maruyama, K., and Saito, S. (1982). "Experiments of Beach Profile Change with a Large Wave Flume," Proceedings of the 18th Coastal Engineering Conference, ASCE, Cape Town, South Africa, 1385-1404.

Komar, P. D., and Miller, M. C. (1974). "Sediment Threshold under Oscillatory Waves," Proceedings of the 14th Coastal Engineering Conference, Copenhagen, Denmark, 756-775.

Kraus, N. C., Larson, M., and Kriebel, D. L. (1991). "Evaluation of Beach Erosion and Accretion Predictors," Proceedings of Coastal Sediments '91, Seattle, WA, American Association of Civil Engineers, NY, 572-587.

Kraus N.C., and Mason, J. M.(1991). "Field Data Set for Testing Beach Erosion and Accretion Predictive Criteria," Memorandum for Record, Coastal Engineering Research Center, U.S. Army Engineer Waterways Experiment Station, Vicksburg, MS, 28 May 1991.

Landin, M. C., Davis, J. E., and Hands, E. B. (Jan 1995). "Wetland Restoration, Underwater Features, and Other Beneficial Uses, A Phase I Report on the Delaware Bay Deepening Project," U.S. Army Engineer District, Philadelphia, PA.

Landin, M. C., and Davis, J. E. (in preparation) "Wave and Sediment Transport, A Phase II Report on the Delaware Bay Deepening Project," U.S. Army Engineer District, Philadelphia, PA.

Maurmeyer, E. M. (1978). "Geomorphology and Evolution of Transgressive Estuarine Washover Barriers Along the Western Shore of Delaware Bay," Ph.D diss., University of Delaware, Newark.

Mikkelsin, S. C. (1977). "The Effects of Groins on Beach Erosion and Channel Stability at the Limfjord Barriers, Denmark," Proceedings of the Fifth Symposium on Coastal Sediments 1977, American Society of Civil Engineers, 17-32.

Ockenden, M. A., and Delo, E. A. (1990). "Dispersal of Dredged Material, Long Term Predictive Models," Report SR 228, Hydraulics Research, Wallingford, Oxfordshire, England.

Scheffner, N. W. (1991). "A Systematic Analysis of Disposal Site Stability," Proceedings, Coastal Sediments '91, Seattle, WA.

Shore Protection Manual. (1984. 4th ed., 2 Vols, U.S. Army Engineer Waterways Experiment Station, Coastal Engineering Research Center, U.S. Government Printing Office, Washington, DC.

Uda, T., Naito, K., and Kanda, Y. (1990). "Field Experiment on Sand Bypass Off the Iioka Coast," Coastal Engineering in Japan, 34, 2, 205-220.

Vera-Cruz, D. (1972). "Artificial Nourishment of Copacabana Beach," Proceedings, 13th Coastal Engineering Conferences, American Society of Civil Engineers, Vol II, 1451-1463.

Zwamborn, J. A., Fromme, G. A. W., and Fitzpatrick, J. B. (1970). "Underwater Mound for Protection of Durban's Beaches," Proceedings 12th Coastal Engineering Conference, American Society of Civil Engineers, II, 975-994.

245

NOTATION

d	=	water depth
d_b	=	wave breaking
d_B	=	water depth at base of berm
D_{50}	=	median grain diameter
g	=	acceleration of gravity
H	=	wave height
H_o	=	deepwater monochromatic wave height or significant deep=water wave height for field wave conditions, depending on context
H_b	=	maximum or breaking wave height
L_o	=	deepwater wave length = $gT^2/2\pi$
T	=	monochromatic wave period or characteristic wave period for field wave conditions, depending on context
$u_{d\ max}$	=	maximum near-bed speed due to waves
u_{crit}	=	critical speed required to initiate sediment movement
U'	=	ratio $u_{=d\ max}/u_{crit}$, in general
U'_c	=	value of U' under crest
U'_t	=	value of U' under trough
ρ_s	=	density of sediment
ρ	=	density of water
γ	=	$(\rho_s=\rho)/\rho$

746